THE UNIVERSITY *of* EDINBURGH

Identification and Characterisation of the Restorative Hepatic Macrophage

Prakash Ramachandran

Submitted for the degree:

Doctor of Philosophy

University of Edinburgh 2014

Table of Contents

Table of Figures

Abbreviations

ALT: Alanine aminotransferase

ANIT: α-naphthylisothiocyanate

APC: Antigen Presenting Cell

Arg-1: Arginase-1

AST: Aspartate aminotransferase

ATP: Adenosine Triphosphate

BDL: Bile duct ligation

BMDM: Bone Marrow Derived Macrophage

CCL2: Chemokine (C-C Motif) Ligand 2 (MCP-1)

CCL3: Chemokine (C-C Motif) Ligand 2 (MIP-1α)

CCl_4: Carbon tetrachloride

CCR2: Chemokine (C-C Motif) Receptor 2

CD115: Colony stimulating factor 1 receptor (CSF1-R, M-CSFR)

CD11b: Integrin α_m

CD11c: Integrin α_x

CD169: sialic acid binding Ig-like lectin 1 (sialoadhesin)

CD62L: CD62 antigen-like family member L (L-selectin)

CD68: macrosialin

CD74: invariant polypeptide of major histocompatibility complex, class II antigen-associated

cDNA: complementary DNA

CEBP/β: CCAAT/enhancer binding protein (C/EBP), beta

Chi3l3: chitinase 3-like 3 (YM-1)

Csf1r: See CD115

CX3CR1: chemokine (C-X3-C motif) receptor 1 (fractalkine receptor)

CXCL2: chemokine (C-X-C motif) ligand 2 (MIP-2)

CXCL10: chemokine (C-X-C motif) ligand 10 (IP-10)

CXCR2: chemokine (C-X-C motif) receptor 2

Cyp2E1: cytochrome P450, family 2, subfamily e, polypeptide 1

DAPI: 4', 6-diamidino-2-phenylindole

DC: Dendritic Cell

DMSO: Dimethyl suphoxide

DT: Diphtheria Toxin

DTR: human diphtheria toxin receptor (DTR) gene also known as the membrane anchored form of heparin-binding epidermal growth factor-like growth factor (hbEGF)

ECM: Extracellular Matrix

EMT: Epithelial Mesenchymal Transition

ERK: extracellular-signal-regulated kinase

F4/80: EGF-like module containing, mucin-like, hormone receptor-like sequence 1

FACS: Flow Cytometry Assisted Cell sorting

FSC: Forward Scatter

FSP-1: Fibroblast-specific protein 1

G2A: G protein-coupled receptor G2A

GPNMB: glycoprotein (transmembrane) nmb (osteoactivin)

HSC: Hepatic Stellate Cell

IFN-γ: interferon gamma

IGF-1: insulin-like growth factor 1

IL-1β: interleukin 1 beta

IP: Intraperitoneal

ITGAV: integrin alpha V

IV: Intravenous

IVC: Inferior Vena Cava

Ki-67: antigen identified by monoclonal antibody Ki 67

LDL: low density lipoprotein

LPS: Lipopolysaccharide

Ly-6C: lymphocyte antigen 6 complex, locus C1

MAPK: Mitogen-activated protein kinase

M-CSF: Macrophage colony-stimulating factor

MCP-1: Monocyte chemotactic protein-1 also known as Chemokine (C-C motif 2) ligand 2 (CCL2)

MEK1/2: mitogen-activated protein kinase kinase 1 and 2

MFG-E8: milk fat globule-EGF factor 8 protein

MHCII: Major histocompatibility complex class II

MIF: Macrophage migration inhibitory factor

MMP: Matrix metalloproteinase

MPS: Mononuclear Phagocyte System

MRC-1: mannose receptor, C type 1

NAFLD: Non-alcoholic fatty liver disease

NASH: Non-alcoholic steatohepatitis

NF-κB: Nuclear factor of kappa light polypeptide gene enhancer in B-cells

NK Cell: Natural Killer Cell

NPC: Non-parenchymal cells

PBC: Primary Biliary Cirrhosis

PBS: Phosphate buffered saline

PDGF: platelet-derived growth factor

pERK: phosphorylated ERK

PPAR: Peroxisome proliferator-activated receptor

PS: Phosphatidylserine

PSC: Primary Sclerosing Cholangitis

PSR: Picrosirius Red

qPCR: quantitative polymerase chain reaction

Retnla: resistin like alpha (FIZZ-1)

SAM: Scar Associated Macrophage

SMA: Smooth muscle actin

SSC: Side scatter

TAA: Thioacetamide

TGF-β: transforming growth factor, beta

Thbs1: thrombospondin 1

TIMP: Tissue Inhibitor of Metalloproteinase

TLR: Toll-like receptor

TNF-α: Tumour Necrosis Factor alpha

TRAIL: tumor necrosis factor (ligand) superfamily, member 10 (Tnfsf10)

UTP: Uridine triphosphate

YM-1: see chi3l3

Declaration

I declare that this thesis is composed by me and that the work presented herein is my own. Some experiments were carried out in collaboration with colleagues in my research group. Where this is the case, I have acknowledged it in the appropriate figure legends. I can confirm that this work has not been submitted for any other degree or professional qualification.

Prakash Ramachandran

Acknowledgements

I'd like to thank my supervisors John Iredale, Stuart Forbes and David Kluth for their excellent support and advice throughout this work. Their input and enthusiasm has been invaluable. I'd also like to thank all the members of the Iredale and Forbes research groups with whom I enjoyed working so closely.

Particular thanks go to Professor Steve Anderton and Dr Andrew MacDonald, who kindly provided some of the animals provided for the studies presented. I'd also like to acknowledge the expertise in bioinformatics and data analysis offered by Donald Dunbar and Jonathan Manning to assist with interpretation of microarray findings. I am also extremely appreciative for the experimental suggestions offered by Professor Sir John Savill.

This research was funded by the Wellcome Trust.

Finally I'd like to dedicate this thesis to my dad and late mum, who are the most supportive and generous parents one could hope for, and whose ability to face lifes' adversity with a positive outlook is a constant source of inspiration to me.

Abstract

Long thought to be irreversible, it is now clear that liver fibrogenesis is a dynamic process, with scar tissue capable of being remodelled as well as deposited. Macrophages have been shown to have a critical role in both liver fibrogenesis and fibrosis resolution. Whilst previous work has identified a Ly-6C^{hi} hepatic macrophage population, derived from recruitment of inflammatory monocytes, as being the main pro-fibrogenic population, the nature and phenotype of the pro-resolution macrophage subset is unknown. In this thesis, I sought to identify and characterise this restorative hepatic macrophage. I established a reversible murine model of liver fibrosis using CCl_4. At the time of initiation of fibrosis regression, Ly-6C^{lo} CD11b^{hi} F4/80^{int} hepatic macrophages represented the most numerous macrophage population and the principal expresser of matrix degrading MMP enzymes. Depletion of this population in CD11b-diphtheria toxin (DTR) mice prevented fibrosis resolution. Subsequent, adoptive transfer and *in situ* labelling experiments, demonstrated that this restorative macrophage population derives from inflammatory monocytes, a common origin to the pro-fibrotic Ly-6C^{hi} hepatic macrophage subset, indicating a switch in macrophage phenotype *in situ* to form the restorative phenotype. Characterisation of FACS-sorted restorative and pro-fibrogenic liver macrophage subsets using gene expression profiling demonstrated higher expression of pro-resolution genes and lower expression of pro-fibrotic genes in restorative macrophages, which also upregulated a number of genes involved in phagocytosis. Confocal microscopy confirmed that restorative macrophages showed evidence of prior phagocytosis. This could be replicated i*n vitro*, where feeding macrophages with cellular debris resulted in matrix-degrading properties analogous to those seen *in vivo*, which was dependent on activation of the ERK signalling cascade. This effect was also demonstrated with the phagocytosis of liposomes *in vitro*. Finally, the administration of liposomes to CCl_4-injured mice *in vivo* induced phagocytosis, causing an increase in hepatic restorative macrophage number and accelerating fibrosis regression. Hence, I have been able to identify and characterise the restorative hepatic macrophage and have utilised these data to develop a novel method to alter macrophage phenotype *in vivo* and accelerate the resolution of liver fibrosis and restoration of normal tissue architecture.

CHAPTER 1 - INTRODUCTION

The Clinical Burden of Liver Disease

Chronic liver disease results from a range of conditions including chronic alcohol excess, chronic viral infection with hepatitis C or B, non-alcoholic fatty liver disease (NAFLD) in association with obesity and the metabolic syndrome, parasitic infection and numerous other immune and metabolic conditions. Ultimately, if left untreated, these diseases cause chronic liver damage resulting liver cirrhosis with the pathological hallmarks of advanced fibrosis, nodular hepatocyte regeneration and significant liver architectural disruption. Patients with chronic liver disease are then at risk of a number of clinical sequelae including portal hypertension, hepatocellular carcinoma and liver failure, all of which are major causes of morbidity and mortality worldwide. In the UK, chronic liver disease ranks as the 5th commonest cause of death, and unlike the other members of the top 5, the incidence is increasing (Leon and McCambridge, 2006). This worrying trend most likely represents the growing burden of alcohol problems in addition to the epidemic of obesity and the metabolic syndrome in the Western world.

Despite this concerning epidemiological data, our treatment options remain limited. Clearly, removal of the causative agent or management of the underlying disease can be an effective strategy if done at an early stage. However, this is not always possible and due to the lack of preceding symptoms, many patients present with cirrhosis-related complications, at which juncture our therapeutic options are often restricted to management of these or potentially liver transplantation for a select few. With an already severe shortage of donor organs and an increasing demand predicted in forthcoming years, this is clearly not the optimum long-term solution. What are badly needed are disease modifying therapies, which can prevent liver disease progression or indeed induce regression of established liver disease.

Central to the development of such therapies is an in depth understanding of the pathogenic mechanisms of liver disease. Given, that hepatic fibrosis is the key hallmark of all chronic liver disease and precedes the other clinical features of cirrhosis, knowledge of the molecular and cellular processes underlying this could be fruitful in yielding novel therapeutic strategies. Indeed, tissue fibrosis in all organs has been associated with up to 45% of deaths in the Western World (Hayden, 2011), and therefore anti-fibrotic strategies used in the liver may have a more generic role in other organ disease, whilst we can potentially utilise therapies developed for other organs in patients with chronic liver disease (Mehal et al., 2011).

Liver Architecture in Health

In order to understand the key mechanisms in the pathogenesis of liver fibrosis it is first important to have knowledge of the basic anatomy of the liver in health. The liver is the largest internal organ in the adult body and has a number of key functions including carbohydrate, lipid and protein metabolism, synthesis of proteins such as coagulation factors, drug metabolism, storage of a range of compounds and immunoregulation. The main metabolic factory of the liver is the parenchymal hepatocytes. These pallisades of hepatocytes are surrounded by a heavily fenestrated endothelial layer, called the hepatic sinusoidal endothelium (**Fig 1.1**). Separating the hepatocyte sheets and the hepatic sinusoidal endothelium is the Space of Disse, which normally contains extracellular matrix (ECM) components and vitamin A-containing hepatic stellate cells (HSCs). On the other side of the sinusoidal endothelial cells, within the hepatic sinusoid, are numerous tissue-resident macrophages, innate immune cells of the mononuclear-phagocyte system, which in the liver are called Kupffer cells (**Fig 1.1**). The other principal parenchymal cell type in the undamaged liver is the cholangiocyte. Cholangiocytes are polarised epithelial cells which line the large network of bile ducts. These networks begin at small vessels between sheets of hepatocytes known as bile canaliculi, which filter into canals of Herring and ultimately into larger bile ducts for drainage into the duodenum. This biliary epithelium mediates both bile salt and water transport and is responsible for the flow of bile in the biliary tree.

Functionally, the liver is divided into acini, containing a central hepatic vein surrounded by pallisades of hepatocytes and portal triads. These portal triads contain branches of the portal vein (which drains blood from the GI tract, spleen and pancreas and is responsible for around 75% of blood inflow to the normal liver), branches of the hepatic artery (responsible for 25% of blood flow to the normal liver) and terminal branches of the biliary tree. Incoming blood is then filtered from the portal vein and hepatic artery via hepatic sinusoids to the central vein. Conversely, bile secreted by the hepatocytes drains in the opposite direction via bile canaliculi to bile ducts. As the blood inflow is to the portal triad there is an oxygen and nutrient gradient across the sheets of parenchymal hepatocytes from the periportal area to the central vein. This creates the functional zonation of hepatocytes in the normal liver: zone 1 representing the periportal areas, zone 2 is the midlobular portion whilst zone 3 is around the central vein. These different zones of hepatocytes have specialised functions for example gluconeogenesis occurring mainly in zone 1 whilst drug metabolism occurs predominantly in zone 3 (Colnot and Perret, 2011). Different zones are susceptible to different modes of injury and can result in differing histological disease patterns.

Figure 1.1 –Hepatic Sinusoidal Structure in Health and Liver Fibrosis

(**A**) Schematic representation of the structure of the hepatic sinusoid in healthy liver. The sinusoid is surrounded by linear sheets of hepatocytes and is lined by hepatic sinusoidal endothelial cells. The space of Disse lies between the sinusoidal endothelial cells and hepatocytes and contains hepatic stellate cells. Blood flows into the sinusoid from the portal vein and hepatic artery and leaves the liver via the central vein. Kupffer cells (hepatic resident macrophages) lie within the sinusoidal space. Hepatocytes produce bile which drains via bile canaliculi in the opposite direction to sinusoidal blood flow, to the bile ducts. Bile ducts are lined with biliary epithelial cells known as cholangiocytes. Together the bile duct, portal vein and hepatic artery make up the portal triad. (**B**) In disease, chronic injury to the liver results in hepatocyte death. Hepatic stellate cells (HSCs) within the Space of Disse become activated and differentiate into extracellular matrix (ECM) producing hepatic myofibroblasts, which secrete scar tissue. Kupffer cells can become activated and there is recruitment of other inflammatory cells from the circulation including monocytes, lymphocytes, NK cells and neutrophils. Note the close proximity of activated myofibroblasts to the recruited immune cells. Also note that the activated myofibroblasts surround the hepatic sinusoid, meaning contraction can result in narrowing of the sinusoidal space and hence increased portal venous pressure.

Figure 1.1 - Hepatic Sinusoidal Structure in Health and Liver Fibrosis

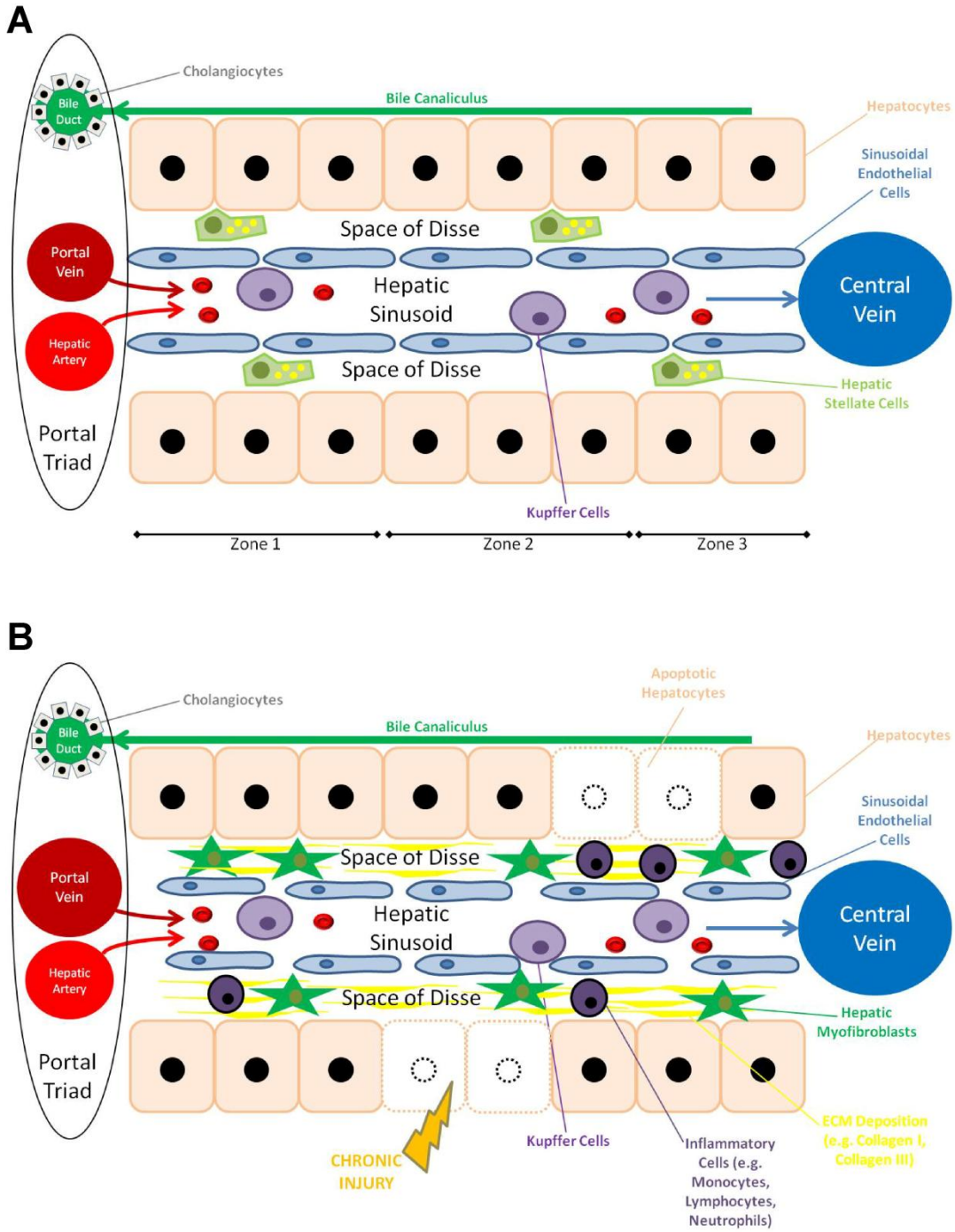

Liver Fibrogenesis

It has long been recognised that hepatic injury results in parenchymal cell damage/death and consequent inflammation mediated by a range of resident and recruited inflammatory cells (Iredale, 2008) (**Fig 1.1B**). In the acute setting this is rapidly followed by activation of regenerative pathways which can quickly restore the liver to normal architecture and function. Injury also results in the initiation of innate wound healing responses which, similar to most other tissues and organs, can result in scar deposition. In the acute setting, this ECM deposition is transient (Inuzuka et al., 1994) and far from being detrimental, this wound healing response is likely to be a key part of maintaining hepatic structure and functionality in the face of significant cell damage and death and is likely to facilitate the rapid regeneration we commonly observe. Similarly, there is a rapid hepatic fibrotic response in response to infection from liver parasites such as schistosomiasis, which serves to wall off the parasite and restrict growth (Anthony et al., 2010), and is hence protective to the host.

However, in the face of chronic and iterative injury, as observed with all causes of chronic liver disease, hepatic wound healing responses are recurrently and persistently activated. Over a period of years in human disease, this ultimately results in liver fibrosis and eventually dense scar deposition, encircling nodules of hepatocytes and causing significant architectural disturbance – changes characteristic of cirrhosis (Anthony et al., 1977). Generally the scar tissue is made up of the main fibrillar collagens I and III (Rojkind and Martinez-Palomo, 1976, Yamamoto et al., 1984), but as fibrosis progresses the composition of scars can also evolve, incorporating a range of other extracellular matrix (ECM) proteins including fibronectin, laminin, hyaluronan, proteoglycans and elastin (Bataller and Brenner, 2005). Indeed, the presence of increased amounts of elastin is associated with more advanced liver fibrosis (Shikata and Skai, 1974).

What is becoming increasingly clear is that even within the category that is pathologically described as cirrhosis, this is not a static process and there are differing degrees of cirrhosis which correlate with differing clinical consequences for the patients (Garcia-Tsao et al., 2010). Hence, closer correlation between specific pathological findings and clinical outcomes will be required moving forward. Furthermore, whilst often classified together as cirrhosis, differing modes of injury result in differing patterns of liver damage and fibrosis. For example, biliary injury (e.g. PBC or PSC) tends to follow a portal to portal pattern leading to porto-portal fibrotic septa surrounding nodules with preserved architecture between central vein and portal triads until a late stage. Conversely, chronic viral hepatitis is thought to cause both portal to central vein necrosis and interface hepatitis resulting in

portal-central fibrotic septa in addition to portal-portal scars. This causes an earlier derangement in vascular connections in the portal system, resulting in earlier portal hypertension. Liver disease due to alcohol or NAFLD, on the other hand, results in significant peri-sinusoidal ECM deposition in the space of Disse and around hepatocytes leading to the characteristic "Chicken wire" pattern (Hernandez-Gea and Friedman, 2011, Pinzani and Rombouts, 2004). Thus, whilst the clinical presentation may be common, it is important to bear in mind that cirrhosis can be heterogeneous, with differing patterns of fibrosis to differing degrees; hence caution should be observed in extrapolating data from one study or model to cirrhosis as a whole.

However, despite this it is also apparent that a number of common mechanisms exist for wound healing responses in the liver irrespective of the nature of injury and indeed a commonality of mechanism probably exists with fibrosis in other organs (Wynn, 2008). Hence, a greater knowledge of these processes is likely to be informative for the development of badly needed anti-fibrotic therapeutic strategies.

The Role of the Hepatic Myofibroblast in Fibrogenesis

A major step forward in our understanding of the biology of liver fibrosis has stemmed from the development of techniques to isolate individual cell populations from the liver around 25 years ago (Otto and Veech, 1980). Specifically, the isolation of pure populations of hepatic stellate cells (HSCs) identified them as the principal collagen producing population in the liver (Maher et al., 1988, Maher and McGuire, 1990, Friedman et al., 1985). Further work determined that these cells, in response to inflammatory signals or plating on tissue culture plastic *in vitro*, rapidly transdifferentiate into a myofibroblast-like population, losing their vitamin A content and expressing the intermediate filament alpha smooth muscle actin (α-SMA) (Friedman and Arthur, 1989, Friedman et al., 1992, Iredale, 2007). These changes recapitulate those observed in experimental liver injury and in human pathological samples (Iredale, 2008). These critical findings have heralded a plethora of studies into the biology of HSCs. Whilst this field is ever evolving it is now clear that these activated HSCs adopt a number of potentially pro-fibrotic properties (Friedman, 2008). These include:

1. **Synthesis of ECM:** Primarily in response to autocrine and paracrine TGF-β signalling but other factors such as Connective tissue growth factor (CTGF) also play a role

2. **Proliferation:** Increase in HSC number is also seen in liver injury, principally in response to platelet-derived growth factor (PDGF) which also acts in an autocrine and paracrine fashion
3. **Contractility:** Activation of HSCs also confers them with a contractile phenotype, partially related to α-SMA but also in association with other factors such as nitric oxide and enodthelin-1. This phenotypic change could be clinically relevant, as it may contribute to the portal hypertension commonly seen in human liver disease which is a major source of morbidity and mortality (**Fig 1.1B**)
4. **Release of Pro-inflammatory mediators:** HSCs can release mediators that modulate the inflammatory response (Marra, 1999, Friedman, 2000). For example, MCP-1 (CCL2), a potent chemokine for monocytes, has been shown to be expressed by activated HSCs in the *in vitro* and *in vivo* settings.
5. **Regulation of Matrix Degradation:** Activated HSCs are a major source of matrix metalloproteinases (MMPs) and the tissue inhibitors of metalloproteinases (TIMPs) which are involved in the dynamic balance regulating matrix deposition and degradation (see below) (Iredale, 2008).

Whilst HSC activation is now a well defined source of hepatic myofibroblasts, other potential cellular sources have also been identified. Portal myofibroblasts have been defined as a distinct population, located at each portal tract, which may have enhanced significance in chronic cholestatic disease or periportal fibrosis (Kinnman and Housset, 2002, Knittel et al., 1999, Tuchweber et al., 1996, Beaussier et al., 2007). Indeed, these cells have potentially been shown to have a different phenotype to activated hepatic stellate cells (Bosselut et al., 2010). Additionally, robust data from both human disease and animal models have defined a contribution from the bone marrow to the hepatic myofibroblast pool (Forbes et al., 2004, Russo et al., 2006). Furthermore, these bone marrow-derived cells have been shown to have a clear functional role in collagen expression *in vivo* (Russo et al., 2006, Kisseleva et al., 2006). Whether these cells represent a population derived from circulating haematopoietic fibrocytes or mesenchymal stem cells or both remains to be fully defined (Kisseleva and Brenner, 2012). A further source of myofibroblasts in liver fibrosis has been postulated to derive from epithelial-mesenchymal transition (EMT), where hepatic myofibroblasts arise from differentiation of hepatocytes or cholangiocytes under specific conditions (Ikegami et al., 2007, Kaimori et al., 2007, Rygiel et al., 2008). However, many of these studies rely on identification of cellular markers to define different populations. What has now become clear is that these markers, such as FSP-1, are not necessarily specific (Osterreicher et al., 2011) and no functional role for EMT in liver fibrosis has yet been demonstrated.

Overall, however, it seems likely that in liver fibrosis the hepatic myofibroblast pool will be heterogeneous. The relative contributions of different populations are likely to vary depending on the nature and response to injury, and this may well alter the biology of liver fibrosis.

Liver Fibrosis Progression – A balance of MMPs and TIMPs

Matrix metalloproteinases (MMPs) are a group of 25 zinc-dependent enzymes which together are capable of degrading a wide spectrum of ECM components including fibrillar collagens. MMPs are generally divided into 5 categories largely on the basis of their substrate specificity and location. Those which have been associated with liver fibrosis include collagenases (MMP-1, -8 and -13), stromelysins (MMP-3, -10 and -11), gelatinases (MMP-2, -9 and -7), metalloelastase (MMP-12) in addition to a number of membrane-type MMPs (Hernandez-Gea and Friedman, 2011). Regulation of MMP activity and hence ECM turnover *in vivo* is complex and variably dependent on transcriptional control, activation of inactive pro-MMPs and by inhibition of MMP activity by a family of 4 Tissue Inhibitor of Metalloproteinases (TIMPs), which can reversibly bind the active domain of all of the known MMPs, preventing matrix degradation.

Studies in fibrotic liver of both animal models and human cirrhosis have demonstrated an increase in expression of a range of MMPs (Arthur et al., 1999, Arthur et al., 1998, Benyon and Arthur, 2001, Iredale, 2008). Additionally, studies of isolated HSCs *in vitro* demonstrate that when activated they can express a plethora of these MMPs. Early during activation, there is transient upregulation of MMP-13 (collagenase-3) and MMP-3 (stromelysin), followed by increases in MMP-2 (gelatinase A), MMP-9 (gelatinase B) and MMP-14 (MT-MMP) (Iredale, 2007). Some of these enzymes may in fact serve to further enhance HSC activation via basement membrane degradation. However, it is clear that there is already significant matrix degrading potential within the fibrotic liver.

The key factor explaining the paradigm of progressive liver fibrosis in the face of increased amounts of ECM degrading MMPs are the aforementioned TIMPs. Even before upregulation of collagen 1 expression, HSCs express significantly increased amounts of TIMP-1 and TIMP-2, with an associated 20-fold gelatinase inhibition (Benyon et al., 1996, Iredale et al., 1996, Iredale et al., 1992). This increase has been confirmed in human and animal fibrotic liver tissue (Iredale, 2007, Hemmann et al., 2007). The robustness and reproducibility of these findings has even lead to the proposed use of TIMP-1 as a serum marker of fibrosis (Patel et al., 2004). Cogent evidence for a functional role for TIMP-1 in hepatic fibrogenesis

was shown by Yoshiji et al. They developed a transgenic mouse model with hepatic overexpression of TIMP-1. Whilst these mice did not show any differences compared to wild type mice in de novo liver fibrosis, following hepatic injury with CCl_4 the TIMP-overexpressing mice showed accelerated liver fibrogenesis (Yoshiji et al., 2000).

Thus, it is the balance between MMPs and TIMPs that determine the progression of hepatic fibrosis (**Fig 1.2**). This is emphasised by attempts to alter this balance with an anti-fibrotic aim. Hepatic overexpression of MMP-8 (neutrophil collagenase) using an adenoviral vector enhanced liver matrix degrading ability and resulted in reduced hepatic fibrosis following bile duct ligation in rats (Siller-Lopez et al., 2004). Attempts have also been made to inhibit TIMP activity *in vivo*. The use of a TIMP-1 neutralising antibody resulted in reduced progression of liver fibrosis in a rat CCl_4 model (Parsons et al., 2004). A particularly intriguing method for TIMP inhibition was developed by Roeb and colleagues. They developed a series of MMP-9 mutants which lacked gelatinolytic activity but had preserved TIMP binding properties. These mutant proteins were able to inhibit TIMP-1 activity *in vitro* and *in vivo* and resulted in reduced liver fibrosis in a murine model (Roderfeld et al., 2006, Roeb et al., 2000). This is potentially an attractive strategy as it is less likely to have any off target effects.

Is Human Liver Fibrosis Reversible?

As discussed above, our knowledge and understanding about the mechanisms involved in hepatic fibrogenesis have evolved greatly in the past 20 years. However, it was still widely viewed that the progression of liver fibrosis was an inexorable one way process. In recent years this dogma is being challenged (Ramachandran and Iredale, 2009, Ramachandran and Iredale, 2012a).

Anecdotal evidence has existed for many years to suggest that liver fibrosis is potentially reversible. However, it was only with the advent of effective anti-viral treatments for chronic hepatitis B and C and the resultant large scale clinical trials with pre- and post-treatment biopsies, that liver fibrosis reversibility was definitively demonstrated in large cohorts of patients (Dienstag et al., 2003, Iredale, 2001, Poynard et al., 2002, Marcellin et al., 2013). Now, evidence of liver fibrosis reversibility has been demonstrated in virtually every cause of chronic liver disease including alcohol (Pares et al., 1986), autoimmune hepatitis (Dufour et al., 1997, Serpaggi et al., 2006), chronic biliary obstruction (Hammel et al., 2001), hereditary haemochromatosis (Falize et al., 2006) and NAFLD (Dixon et al., 2006). Given the wide spectrum of hepatic diseases in which fibrosis regression can be observed, it seems

likely that generic rather than disease-specific mechanisms are at play. Furthermore, reversibility has been demonstrated in human tissue fibrosis in other organs including heart (Brilla et al., 2000, Diez et al., 2002), kidney (Fioretto et al., 1998), lung (Wallace et al., 2007) and bone marrow (Beham-Schmid et al., 2002). Thus, it seems clear that tissue fibrosis is at least partially reversible, highlighting the dynamic nature of this process. Given the array of data and the reproducible experimental models of fibrosis, the liver provides an excellent paradigm to study the process of fibrosis regression (Ramachandran and Iredale, 2012a).

Loss of Hepatic Myofibroblasts in Fibrosis Resolution

Rodent studies of bile duct ligation (BDL) followed by bilio-jejunal anastamosis or chronic carbon tetrachloride (CCl_4) administration followed by cessation of dosing are both excellent models to study the dynamics of hepatic fibrogenesis and spontaneous resolution. In both of these models, established hepatic fibrosis resolves to near normal liver architecture within 4-6 weeks (Iredale et al., 1998, Issa et al., 2001). During this resolution phase there is a striking and dramatic loss of the scar producing activated HSC/myofibroblast population. Closer analysis indicates that the activated HSCs are mainly lost by the process of programmed cell death, or apoptosis (Iredale et al., 1998, Issa et al., 2001).

This important finding has led to numerous studies assessing signals which regulate HSC apoptosis (Elsharkawy et al., 2005). Activation of NF-κB signalling regulates a range of inflammatory, immune, wound healing and cell survival responses. In HSCs NF-κB signalling results in expression of pro-inflammatory and pro-fibrotic genes and promotes resistance to apoptosis (Hernandez-Gea and Friedman, 2011, Watson et al., 2008). Conversely, a variety of molecules and pathways have been shown to promote HSC apoptosis. These include farsenoid X receptor (FXR or bile acid receptor), CEBP/β signalling, cannabinoid receptor 2 (CB2), adiponectin, or TRAIL (Hernandez-Gea and Friedman, 2011). Nerve growth factor (NGF) can be released from infiltrating inflammatory cells or regenerating hepatocytes and is pro-apoptotic for activated HSCs (Oakley et al., 2003, Trim et al., 2000, Kendall et al., 2009). Furthermore, direct cellular contact between macrophages and activated HSCs has been demonstrated to promote HSC death (Fischer et al., 2002). The exact contribution of these various mediators in determining HSC apoptosis *in vivo* remains to be elucidated, but it is likely that a complex cellular cross-talk exists which is impossible to recapitulate *in vitro*.

In addition to soluble mediators, interactions between the ECM itself and HSCs can modulate apoptosis. Binding between collagen-1 and HSCs promotes activation whereas loss of integrin-mediated contact can lead to the HSCs entering the apoptotic pathway (Zhou et al., 2004). Similar findings have been demonstrated *in vivo*, where a transgenic mouse expressing a non-degradable form of collagen-1 showed a failure of spontaneous fibrosis resolution and a persistence of activated HSCs in the scar following chronic CCl_4 (Issa et al., 2003). Hence, the myofibroblast-matrix interaction is critical in fibrosis resolution.

More recently, other potential fates for activated HSCs have been defined. Senescence, a stable form of cell cycle arrest, of activated HSCs has been implicated in reducing scar production and upregulating ECM-degrading enzyme expression following the cessation of injury (Krizhanovsky et al., 2008). Additionally, 2 recent studies have identified that a proportion of activated HSCs can revert back to a quiescent phenotype after removal of the injurious stimulus (Kisseleva et al., 2012, Troeger et al., 2012). Interestingly, in both studies the quiescent HSCs derived from previously activated HSCs were not identical to quiescent HSCs from uninjured livers, but rather appeared to be primed and responded to repeat hepatic injury with a more profound pro-fibrotic phenotype. These findings may have clinical relevance in explaining fibrosis progression in humans following iterative injury over many years.

Matrix Degradation in Fibrosis Resolution

Whilst the loss of the scar producing cells is an important factor in fibrosis resolution, clearly there also has to be significant remodelling of already deposited ECM in order to restore normal tissue architecture. As discussed above, fibrotic livers show a significant increase in MMP expression and hence scar degrading capability, which is held in check by high levels of TIMP expression. However, by studying a series of timepoints during fibrosis resolution authors identified a rapid reduction in the levels of TIMP-1 and TIMP-2 (Iredale et al., 1998, Issa et al., 2004) with an associated increase in overall collagenase activity due to a switch in the MMP-TIMP balance, resulting in net ECM degradation (Issa et al., 2004). Furthermore, hepatic overexpression of TIMP-1 inhibited scar resolution following the cessation of injury (Yoshiji et al., 2002). In addition, TIMP-1 in itself is an anti-apoptotic signal for HSCs (Murphy et al., 2004). Thus, a reduction in hepatic TIMP levels is a critical step during fibrosis resolution, releasing the ECM degrading ability of hepatic MMPs and potentially also contributing to the loss of scar producing myofibroblasts by apoptosis (**Fig 1.2**).

What Renders Liver Fibrosis Irreversible?

Whilst it is clear that there is a significant potential for hepatic fibrosis to regress, it is still uncertain whether advanced cirrhosis can return to normal architecture or whether a "point of no return" is eventually reached. Experimental hepatic fibrosis models have given us insight into this point. Issa and colleagues induced advanced micronodular cirrhosis in rats by 12 weeks of CCl_4 administration , and then allowed them to recovery for protracted periods of up to 1 year (Issa et al., 2004). 12 weeks of injury resulted in dense fibrotic septa. As anticipated during recovery, significant fibrosis remodelling was observed, particularly in the fresh scar adjacent to the nodules. However, strikingly the more mature scars failed to completely regress even after 1 year of recovery. This enabled more detailed study of the persistent scars, to identify features which could confer irreversibility. The authors identified 3 key features of irreversible scars:

1. Matrix crosslinking by tissue transglutaminase, which can render the ECM tissue more resistant to proteolytic degradation. However, the functional role of this mechanism has subsequently been challenged in murine liver fibrosis models (Popov et al., 2011)
2. Change in ECM composition containing more elastin, which may be more resistant to degradation
3. Hypocellularity in vicinity of irreversible scars, with a lack of scar associated activated myofibroblasts and macrophages compared to reversible scars. This could result in reduced local delivery of ECM degrading enzymes contributing to persistent scar tissue.

These histological findings were strikingly similar to those observed in regressing human liver cirrhosis (Wanless et al., 2000), suggesting a commonality of mechanism.

These data would suggest certain features of mature hepatic scars render them irreversible. However, a significant amount of remodelling did still occur in these livers, transforming micronodular cirrhosis into macronodular cirrhosis at least. Whilst this could suggest that normal liver architecture may never be fully restored, this degree of recovery may well be sufficient to abrogate a number of the clinical consequences observed and thus could still be relevant to patient outcomes.

The Role of the Immune System in Liver Fibrogenesis and Fibrosis Resolution

Hepatic inflammation is a key feature following injury and there is now good evidence that the immune system can regulate the fibrotic response. The roles of individual cellular components of the immune system have therefore been studied in models of liver fibrosis.

The majority of data exists for the role of cells of the monocyte/macrophage lineage in fibrogenesis and fibrosis resolution (see below). Other components of the innate immune response are also likely to have a role. Neutrophils, the early responders to tissue injury, are quickly recruited to sites of inflammation, have a high phagocytic capacity and possess a number of preformed antimicrobial molecules which can be rapidly released. Indeed hepatic neutrophil infiltration has been associated with worsening of a number of liver diseases including sepsis, ischaemia-reperfusion, alcoholic hepatitis, viral hepatitis and autoimmune hepatitis (Kubes and Mehal, 2012). However, evidence for the role of neutrophils in driving fibrogenesis is still limited. Specifically, in studies using either neutrophil anti-serum in BDL treated rats (Saito et al., 2003) or the administration of α-naphthylisothiocyanate (ANIT), a hepatotoxin causing periportal inflammation, to mice deficient in the key neutrophil chemokine receptor CXCR2 (Xu et al., 2004), a reduction in hepatic neutrophils was observed but no effect on liver fibrosis was seen. Conversely, by depleting neutrophils during recovery from biliary obstruction some authors have suggested that neutrophil MMP expression may have a role in collagen degradation during fibrosis resolution (Harty et al., 2008, Harty et al., 2010). Whether neutrophils are present in the liver in sufficient number during the resolution phase for this to be a meaningful finding remains to be defined.

Mast cells, another component of the innate immune response, have been shown to be increased in the liver in both animal models (Jeong et al., 2002) and human liver disease (Franceschini et al., 2007). These cells are a potential source of pro-fibrotic mediators such as TGF-β and PDGF (Li and Baek, 2002). However, studies in mast cell deficient rats and mice did not demonstrate any role in hepatic fibrogenesis using different experimental models (Sugihara et al., 1999, Okazaki et al., 1998).

Natural Killer (NK) Cells are large granular lymphocytes, which are another key component of the innate immune response. NK cells have a key role in immune defence and surveillance responding rapidly to pathogens, in particular quickly being activated in response to virally infected cells. NK cells can then produce a range of cytokines and kill target cells if exposed to the correct combination of receptors. NK cells represent the most numerous lymphocyte population in the liver and are altered in various liver diseases (Gao and Radaeva, 2012).

Initial studies in murine models demonstrated that NK cells can induce killing of activated hepatic stellate cells and hence act in an anti-fibrotic manner (Melhem et al., 2006, Radaeva et al., 2006). These findings have been replicated in several further studies (Gao and Radaeva, 2012). In addition to direct cell killing, NK cells also produce cytokines such as IFN-γ, which induces HSC apoptosis and cell cycle arrest, further contributing to the anti-fibrotic effect (Gao and Radaeva, 2012).

Researchers have also focussed on the role of the adaptive immune system in hepatic fibrosis. T cells play a central role in the adaptive immune response, with a variety of subtypes having differing immunomodulatory roles. T helper cells ($CD4^+$ T cells; T_H cells) become activated by interactions with antigen presenting cells (APCs) and secrete cytokines that influence other immune cells. The cytokine profile expressed by the T_H cells is dependent on the nature of the signalling from the APC. In liver fibrosis, the T_H2 subtype, expressing IL-4, IL-5, IL-13 and IL-21, has been shown to be strongly pro-fibrogenic, particularly in experimental models involving parasitic infection with schistosome eggs (Wynn, 2008). Conversely, a T_H1 immune response is associated with IFN-γ and IL-12 expression, which have been shown to be anti-fibrotic (Wynn, 2008). Thus, the relative balance of T_H1 and T_H2 cells may influence the degree of fibrosis progression (Shi et al., 1997). Cytotoxic T cells ($CD8^+$ T cells) destroy virally infected cells and adoptive transfer experiments have suggested they may have a pro-fibrogenic role in the liver (Safadi et al., 2004). However, in other studies mice deficient in CD4 or CD8 T cells showed no difference in liver fibrosis in response to CCl_4 when compared to control animals (Novobrantseva et al., 2005). Thus, the exact role of different T cell populations in hepatic fibrosis remains to be fully defined, and is likely to be dependent on the nature of the injury driving the fibrotic process.

B cells have also recently been examined as having a potential role in hepatic fibrogenesis. B cell deficient mice, whilst having a similar acute inflammatory response, were protected from the development of liver fibrosis in response to CCl_4 or the toxin ANIT. This effect was independent of B cell immunoglobulin production or interactions with T cells (Novobrantseva et al., 2005). Whilst the exact mechanisms responsible for this effect remain undefined, it may reflect local cytokine production or direct cell-cell interactions.

Overall, there is a clear and close relationship between the immune response and hepatic fibrogenesis. Whilst this is somewhat unsurprising given that fibrosis follows tissue injury and resultant inflammation, what is now becoming clear is that the multiple facets of the immune system are capable of fine tuning the fibrotic response and in fact promoting fibrosis

resolution. This may have important implications for the development of anti-fibrotic therapies.

Macrophages as Part of the Mononuclear Phagocyte System

Perhaps the most widely studied immune population in hepatic fibrosis is the macrophage. In order to understand the complex role of macrophages in liver injury and scarring it is important to understand basic macrophage biology.

Macrophages were first identified by Elie Metchnikoff in 1884. His pioneering work, for which he was awarded the Nobel prize along with Paul Ehrlich in 1908, was the first to define the process of phagocytosis and he went on to classify phagocytic cells as macrophages ("large eaters") and microphages ("small eaters"; now known as granulocytes). This discovery led to a plethora of work, identifying these highly phagocytic mononuclear cells and their precursors in numerous organs, in their entirety referred to as the mononuclear phagocyte system (MPS). Whilst this is obviously useful conceptual definition, it is now becoming clear that within the MPS there is vast heterogeneity in cell type, function and origin. This heterogeneity is critical to understanding the diverse range of biological functions served by this population.

Macrophages are now recognised as haematopoietic cells that are present in every tissue in the body. Most tissue macrophages are now felt to have several common functions including the clearance of foreign and damaged cells, the induction of innate immune responses and the killing of micro-organisms during tissue infection, antigen presentation to effector T cells and remodelling and repair of tissues after inflammation (Gordon and Taylor, 2005). Despite these common properties, these tissue macrophage populations have diverse names, often dependent on their expression of specific cell surface markers, the name of the scientist who discovered them or their location within the tissue in question (Hashimoto et al., 2011). Specific examples include red pulp, marginal zone and tingible body macrophages in the spleen, subcapsular sinus and medullary macrophages in lymph nodes, alveolar and interstitial macrophages in the lung, microglia in the brain and Kupffer cells in the liver. However, these distinctions provide limited information on the cells' origin and function.

In order to start to dissect the heterogeneity of these tissue macrophage populations *in vivo*, the identification of macrophage cell surface markers has been invaluable. The use of F4/80 in mice and CD68 in mice and humans, as "pan macrophage" markers has enabled more detailed study of the functionally distinct macrophage populations in different tissues. For example, in the lung, in addition to F4/80 and CD68, alveolar macrophages express high

levels of CD11c and CD169 and low levels of CD11b with high expression of pattern recognition receptors (such as mannose receptor and toll-like receptors which are responsible for rapidly recognising and binding conserved molecular structures on pathogens) and scavenger receptors (responsible for rapid internalisation of selected ligands). These findings likely represent the specialised role of alveolar macrophages in being the first line of defence in clearing inhaled microorganisms, viruses and particles from the lungs (Gordon and Taylor, 2005, Hashimoto et al., 2011). Conversely, the other main population of lung macrophages, the interstitial macrophage, which is likely to have a more immunomodulatory role (Bedoret et al., 2009), is said to be $F4/80^{+}$ $CD68^{+}$ $CD11c^{-}$ and MHC II^{+} (Hashimoto et al., 2011). Similarly, in the spleen distinct patterns of expression of various scavenger receptors and lectins can be used to define different macrophage populations (Taylor et al., 2005). Liver resident macrophages ("Kupffer cells") have been defined as $F4/80^{hi}$ $CD11b^{lo}$ $CD68^{+}$ $CD169^{+}$ $Galectin\text{-}3^{+}$ cells (Hashimoto et al., 2011). Given the expanding and seemingly endless range of macrophage markers, and the additional heterogeneity which will be introduced by tissue injury, there are an almost infinite number of phenotypic possibilities, which will be critically dependent on the tissue microenvironment. Whilst this is likely to be inherently useful given the diverse range of pathogens and injurious stimuli to which the body exposed, it provides an ongoing challenge for macrophage biologists in determining which populations are responsible for which functional effects.

Development of Tissue Macrophages

Another important factor to consider in the heterogeneity of tissue macrophages is their origin. During early development, macrophage-like cells are seen to develop from the yolk sac and then migrate to the head mesenchyme and its circulation. This so called primitive haematopoiesis, leads to brain tissue macrophages or microglia, which can persist into adult life via local self-renewal (Ginhoux et al., 2010). Later on in the development process, the foetal liver becomes a principal site of haematopoiesis and generates large populations of macrophages which then become present in most organs. In the adult, haematopoiesis occurs principally in the bone marrow. The currently favoured model is that haematopoietic stem cells give rise to the CMP (common myeloid precursor) which then differentiates into the bipotent GMP (granulocyte macrophage progenitor) cells which can give rise to a neutrophil differentiation pathway or MDP (macrophage dendritic cell progenitor). This myeloid differentiation program is critically dependent on the transcription factor PU.1 (Auffray et al., 2009). Within the bone marrow these MDPs differentiate into monocytes or the CDP (common dendritic cell precursor). The CDPs are potentially capable of generating lymphoid

conventional dendritic cells (cDCs) without a monocyte precursor (Auffray et al., 2009). The monocytes generated from the MDP are released into the circulation. The generation of monocytes and macrophages is dependent on the growth factor receptor Csf1r (CD-115, c-fms, M-CSFR), which is expressed on monocytes, macrophages and their precursors, and for which the natural ligands are Csf1 and IL-34. Op/op mice, which are constitutively deficient in Csf1, and Csf1r knockout mice both show profound deficiencies in both circulating monocytes and tissue macrophages in keeping with a key role for this system in MPS development (Dai et al., 2002).

The longstanding dogma is that these circulating monocytes populate and replenish tissue macrophages, in addition to dendritic cells and osteoclasts (Gordon and Taylor, 2005). Whilst this undoubtedly plays a role in certain organs and under certain conditions, studies have also demonstrated the capacity of tissue macrophages to proliferate locally and hence replenish their population without recruitment. There is now cogent evidence that local macrophage proliferation at least partially contributes to renewal of tissue macrophage populations in the spleen, skin, lung and brain, particularly during steady state conditions without injury (Gordon and Taylor, 2005). Indeed a recent study has also highlighted a role for local macrophage proliferation in generating the tissue inflammatory response in response to specific types of injury (Jenkins et al., 2011). Under steady state conditions in the liver, a low basal level of Kupffer cell proliferation can be detected (Crofton et al., 1978) and indeed rat Kupffer cells have been shown to be potentially long-lived (Bouwens et al., 1986). However, whole body irradiation, and presumably associated injury to existing Kupffer cells, results in repopulation of liver resident macrophages from the bone marrow (Crofton et al., 1978). Thus, Kupffer cells, like many other tissue macrophages, have the capacity to develop from either local proliferation or recruitment of circulating monocytes, depending on the circumstances to which they are exposed.

More definitive evidence for the origin and dynamics of monocytes and tissue macrophages under steady state came from a series of fate mapping experiments (Yona et al., 2013). This study was based on the widespread expression of the chemokine receptor CX_3CR1 in the mononuclear phagocyte system. The authors utilised transgenic mice constitutively expressing GFP ($Cx3cr1^{gfp}$) or Cre recombinase ($Cx3cr1^{cre}$) or conditionally Cre recombinase ($Cx3cr1^{creER}$) under the control of the CX_3CR1 promoter. This study demonstrated that in steady state, Kupffer cells, in addition to lung, peritoneal and splenic macrophages, are established before birth and remain independent of the monocyte pool in adulthood and are maintained by longevity and local self renewal (Yona et al., 2013).

Monocytes as Precursors of Tissue Macrophages

Recruitment of circulating monocytes and consequent differentiation into macrophages (or dendritic cells) is a key feature of the inflammatory response to tissue injury. Monocytes are effector cells in themselves, expressing a number of scavenger receptors capable of recognising microorganisms and are able to produce a range of inflammatory mediators and are hence vital for defence from pathogens (Auffray et al., 2009). Monocytes also show significant heterogeneity. In mice, 2 distinct populations of mature monocytes found in the bone marrow, blood and spleen have been defined, which can be distinguished on the basis of cell surface marker expression. Murine monocytes are generally identified by flow cytometry on the basis of their size (forward scatter; FSC), complexity (side scatter; SSC) and expression of antigens CD115, CD11b and F4/80. Differential expression of the cell surface glycoprotein Ly-6C (Gr-1) defines the 2 murine monocyte subsets: Ly-$6C^{hi}$ and Ly-$6C^{lo}$. Ly-$6C^{hi}$ monocytes show high levels of expression of the chemokine receptor CCR2, the adhesion molecule CD62L (L-selectin) and low levels of expression of the chemokine receptor CX_3CR1 (Auffray et al., 2009, Gordon and Taylor, 2005). This population has been termed the "inflammatory monocyte" as they are rapidly and selectively recruited to sites of tissue inflammation, primarily in response to the chemokine CCL2 (monocyte chemotactic protein-1; MCP-1), and are capable of producing inflammatory cytokines such as TNF-α and IL-1 (Auffray et al., 2009). This Ly-$6C^{hi}$ murine monocyte population has been shown to be analogous to the human $CD14^{++}$ $CD16^{-}$, albeit not identical (Ingersoll et al., 2009). Following recruitment, they are capable of forming tissue macrophages and potentially inflammatory DCs (Auffray et al., 2009, Gordon and Taylor, 2005, Ingersoll et al., 2011). An example, has been shown in elegant work by Arnold and colleagues, where following muscle injury in mice, Ly-$6C^{hi}$ (and not Ly-$6C^{lo}$) monocytes are recruited from the circulation, initially forming Ly-$6C^{hi}$ muscle macrophages with a pro-inflammatory phenotype which then change phenotype to anti-inflammatory Ly-$6C^{lo}$ muscle macrophages which promote muscle regeneration (Arnold et al., 2007). Similarly, following spinal cord injury Ly-$6C^{hi}$ monocytes are recruited and form an anti-inflammatory macrophage population which is important for recovery (Shechter et al., 2009). A further study on mammary tumours in mice, demonstrated that Ly-$6C^{hi}$ monocyte recruitment contributes to the heterogeneous population of tumour associated macrophages, which can have important roles in tumour suppression and progression (Movahedi et al., 2010). Thus, Ly-$6C^{hi}$ monocyte recruitment can lead to the formation of macrophages and dendritic cells with a range of functional phenotypes dependent on the micro-environmental cues to which they are exposed.

The second murine monocyte population is defined as Ly-6C^{lo} CCR2^{lo} CD62L^{lo} CX_3CR1^{hi} and have been termed "resident" or "patrolling" monocytes. This population is felt to be analogous to human CD14^{+} CD16^{+} monocytes (Ingersoll et al., 2009). Originally thought to be responsible for the replenishment of resident tissue macrophages, the exact function of this population remains poorly defined. Ly-6C^{lo} monocytes have been shown to crawl on the endothelial surface of blood vessels but rarely extravasate in the absence of inflammation, suggesting a role in scavenging lipids and dead cells from the endothelium during steady state conditions (Auffray et al., 2009). This population is also potentially capable of a very early response to inflammation. For example, irritants, aseptic wounding and peritoneal infection with Listeria monocytogenes result in CX_3CR1-dependent rapid extravasation of Ly-6C^{lo} monocytes within 1-2 hours. In this context these cells can express inflammatory cytokines, pattern-recognition receptors, scavenger receptors, tissue remodelling genes and importantly genes involved in a macrophage differentiation programme (Auffray et al., 2007). However, this extravasation is very short lived and is rapidly overtaken by a more conventional recruitment of neutrophils and Ly-6C^{hi} monocytes. The ability of Ly-6C^{lo} monocytes to form tissue macrophages following injury has also been demonstrated in other studies. In response to experimental myocardial injury in mice, there is an early recruitment of Ly-6C^{hi} monocytes resulting in inflammation, proteolysis and clearance of debris by phagocytosis, with a second late phase recruitment of Ly-6C^{lo} monocytes results in myofibroblast accumulation, collagen deposition and angiogenesis resulting in wound healing (Nahrendorf et al., 2007). Additionally, Ly-6C^{lo} monocytes can give rise to lung macrophages following adoptive transfer (Landsman et al., 2007). In atherosclerotic plaques, both Ly-6C^{hi} and Ly-6C^{lo} monocytes are recruited, forming plaque macrophages with seemingly different phenotypes (Tacke et al., 2007). Thus, dependent on the tissue and the nature of injury, both monocyte subsets have the capacity to form macrophages.

An additional level of complexity to the relative roles of monocyte subsets in inflammation is the inter-relationship between the Ly-6C^{hi} and Ly-6C^{lo} monocyte populations. Previous data has suggested that Ly-6C^{lo} monocytes are derived from differentiation of Ly-6C^{hi} monocytes (Sunderkotter et al., 2004). This has recently been confirmed in transgenic fate mapping experiments, which demonstrated that in a steady state, Ly-6C^{hi} monocytes are obligatory precursors of Ly-6C^{lo} monocytes (Yona et al., 2013). In order to form Ly-6C^{lo} monocytes, Ly-6C^{hi} monocytes must be released from the bone marrow into the circulation in a CCR2 dependent manner. Intriguingly, Ly-6C^{hi} monocytes also restrict the lifespan of their Ly-6C^{lo} progeny, potentially by acting as a sump for CSF-1 (Yona et al., 2013). The

exact role of these mechanisms during inflammatory responses remains unclear, but shown be borne in mind when considering lineage tracing data.

Dendritic Cells – a Distinct Entity?

The discovery, by Steinman and Cohn in the early 1970s, of a population of haematopoietic cells in the mouse spleen which excelled at antigen presentation and T cell activation, termed dendritic cells (DCs) has added further complexity to the study of the mononuclear phagocyte system. DCs, similar to macrophages, were subsequently found to populate virtually all lymphoid and non-lymphoid tissues. DCs were initially felt to be poorly phagocytic but accumulating evidence now shows that they also have potent phagocytic capacity, leading to a paradigm where DCs sample tissue antigens, migrate to draining lymph nodes, present extracellular antigens and initiate tissue specific T-cell immunity (Hashimoto et al., 2011). Given the difficulties of studying antigen presentation *in vivo*, progress in the field of DC biology has been dependent on the identification of cell surface markers such as CD11c (Integrin α_x) and the development of culture systems to produce pure populations of DCs *in vitro* (Hume, 2008).

The heterogeneity of DCs is now being widely studied and numerous subtypes have now been defined. Classical DCs (cDCs) are initially equipped with a high phagocytic capacity followed by the capacity to produce a large array of cytokines to elicit and regulate T cell responses. They are short lived and highly migratory, rapidly transiting from tissues to lymphatic organs, being replaced by blood borne precursors (Geissmann et al., 2010). Plasmacytoid DCs (pDCs) are found in all organs, are longer lived than cDCs and have adapted to respond to viral infections in addition to antigen presentation and control of T cell responses (Geissmann et al., 2010). Both cDCs and pDCs are thought to derive from the bone marrow from common DC precursors (CDPs), independent of monocytes. This process is thought to be driven by signalling via the cytokine receptor fms-related tyrosine kinase 3 (FLT3) (Geissmann et al., 2010, Hashimoto et al., 2011).

Once again this DC development paradigm applies during steady state conditions, but will be significantly different in response to inflammation. Specifically, there is now evidence that in response to inflammation, Ly-6C^{hi} monocytes can differentiate into DCs which can express TNF-α, iNOS and reactive oxygen species, known as TipDCs (Serbina et al., 2003, Cheong et al., 2010, Ingersoll et al., 2011). However, this raises an important point – how to differentiate between these DCs and macrophage populations within tissue? This has thus far been done on the basis the expression of cell surface markers such as CD11c, and functions

such as antigen presentation. However, it is now apparent that macrophage subpopulations can also express similar cell surface markers and perform similar functions to DCs. This is particularly apparent in response to inflammation, where the features attributed to TipDCs are also characteristic of macrophages. Furthermore, depletion of the monocyte/macrophage differentiation factor CSF1R also results in reduced numbers of DCs (Hume, 2008). Thus, whilst in steady state separate differentiation pathways may well exist, in response to inflammation the distinction between macrophages and DCs becomes blurred and it would be better to view both as part of a heterogeneous spectrum of mononuclear phagocytes rather than separate populations.

The Spectrum of Macrophage Activation

As described, significant heterogeneity exists in macrophages on the basis of their localisation and origin. Macrophages are also well known to be multifunctional and plastic cells which can adopt distinct activation states depending on the signals to which they are exposed. These macrophage activation states have broadly been classified as M1 (classically activated) and M2 (alternatively activated) in a manner analogous to T_H1 and T_H2 responses for T cells. The classically activated M1 phenotype is said to be the adopted by macrophages in response to IFN-γ alone or in combination with bacterial products such as lipopolysaccharide (LPS) or cytokines such as TNF-α. Indeed, ligation of TLR ligands on monocytes/macrophages can lead to self production of TNF-α which can act in an autocrine manner (Mosser and Edwards, 2008). This results in a macrophage phenotype which produces large quantities of pro-inflammatory cytokines, chemokines and free radicals. This phenotype is critical for host defences from micro-organisms (Mosser and Edwards, 2008). Characteristically this M1 phenotype results in an IL-1^{hi} IL-6^{hi} IL-12^{hi} IL-23^{hi} IL-10^{lo} population, which also expresses high levels of chemokines such as CXCL9 and CXCL10 attracting T_H1 cells (Mantovani et al., 2004, Mantovani et al., 2013). Importantly, the mediators produced by M1 macrophages are also capable of producing host tissue damage and therefore this population must be tightly regulated (Mosser and Edwards, 2008).

M2 alternatively activated macrophage phenotype was originally described in response to cytokines IL-4 and IL-13 (Gordon, 2003). This resulted in a IL-10^{hi} IL-12^{lo} IL-23^{lo} phenotype, with low expression of other inflammatory cytokines and high expression of chemokines such as CCL17 and CCL22 which are important in T_H2 immune responses. These M2 cells also upregulate genes such as arginase-1, YM-1 and multiple other scavenger receptors and they are generally felt to take part in parasite clearance, immunomodulation, angiogenesis and wound healing (Mantovani et al., 2013). What is now becoming clear is

that numerous other signals can induce an "M2 like" macrophage phenotype, with some but not all of the features of the traditional IL-4/IL-13 polarized macrophage. Examples of such signals include immune complexes in combination with LPS or IL-1, glucocorticoids, TGF-β or IL-10 (Mantovani et al., 2013). Each of these results in a slightly different macrophage phenotype, highlighting the vast complexity and the range of potential macrophage activation states. When considering that these phenotypes are largely defined *in vitro*, in the presence of 1 or 2 signals, the range of signals to which macrophages are exposed *in vivo* will result in an almost infinite number of potential macrophage phenotypes. Thus the traditional paradigm of M1 and M2 polarization is generally inadequate to define populations *in vivo* and macrophages should be considered on a spectrum of activation states. This consideration has resulted in experts aiming to classify macrophage phenotypes more on the basis of function such as classically activated, regulatory and wound healing macrophages (Mosser and Edwards, 2008). A good example of this in practice is the identification and characterisation of a macrophage population responsible for the resolution of peritoneal inflammation in mice, which shows features of both classical and alternatively activated macrophages (Bystrom et al., 2008).

Macrophages are also plastic cells capable of ongoing changes in phenotype according to their microenvironment (Stout et al., 2005). This principle of macrophage plasticity has also been demonstrated *in vivo* in diverse pathologies such as cancer and tumour associated macrophages, obesity and adipose tissue macrophages, macrophages in skin wounding, macrophages in chronic venous ulceration, renal macrophages following kidney injury and monocyte-derived macrophages following muscle injury (Lucas et al., 2010, Mantovani et al., 2013, Mosser and Edwards, 2008, Arnold et al., 2007, Alikhan and Ricardo, 2013). This plasticity and constantly evolving phenotype provides challenges in defining distinct functional macrophage populations *in vivo*.

Phagocytosis as a Modulator of Macrophage Function

One of the key functions of macrophages is the rapid and efficient removal of a variety of particulate matter. This includes microorganisms, environmental material and of course dead cells. The clearance of dead or dying cells occurs in both health and disease, with an estimated 1 million apoptotic deaths per second occurring in health. Clearly, in diseased/damaged tissue this will increase, with epithelial and immune cell death both key features of acute and chronic inflammation. Importantly, in addition to the removal of potentially harmful cell debris, phagocytosis itself modulates the phenotype of the

phagocyte, which can have important implications for the inflammatory response (Henson, 2005).

The process of phagocytosis is itself complex, potentially involving numerous receptors and soluble mediators with a large amount of redundancy to ensure adequate clearance even in the face of inhibition of one pathway. These multiple mediators of phagocytic clearance may act together, forming the so called "phagocytic synapse". In the first stage in the process *in vivo*, phagocytes must find the apoptotic cells. Data now exists that apoptotic cells release "find me" signals which leads to phagocyte recruitment. Examples of such signals include CX3CL1 (Fractalkine) which acts on CX3CR1 on mononuclear phagocytes, lysophosphatidylcholine (LPC) acting on the G2A receptor, sphingosine-1-phosphate (S1P), and the nucleotides ATP and UTP which are sensed by the P2Y2 receptor on monocytes (Hochreiter-Hufford and Ravichandran, 2013). Intriguingly, apoptotic cells secrete lactoferrin, which can act as a "stay away" signal to neutrophils but not mononuclear phagocytes and may thus determine the type of phagocyte engulfing them and hence the post-phagocytic response (Bournazou et al., 2009). Having come into proximity with the apoptotic cells, the phagocyte then encounters "eat me" signals on the surface of the dying cell. These include phosphatidylserine (PS), ICAM3, oxidised low density lipoprotein (LDL)-like moiety or bound opsonins such as thrombospondin or complement C1q. These "eat me" signals are recognised by a wide range of engulfment receptors on the surface of the phagocyte (Hochreiter-Hufford and Ravichandran, 2013). Examples of these receptors include:

- Lectins which bind altered sugars on apoptotic cells
- Integrins $\alpha_v\beta_3$ and $\alpha_v\beta_5$ in conjunction with CD36 which binds thrombospondin
- LRP1/CD91 which binds C1q
- CD14 which binds ICAM3
- Scavenger receptors which bind oxidised LDL
- Integrins $\alpha_v\beta_3$ and $\alpha_v\beta_5$ which bind the secreted molecule MFG-E8, which can bind PS
- TAM receptor family (Tyro-3-Axl-Mer) which bind bridging molecules Growth-arrest-specific 6 (Gas6) and Protein S, which are in turn bound to PS
- Direct PS receptors including Brain-specific angiogenesis inhibitor 1 (BAI1), T-cell immunoglobulin and mucin-domain-containing molecule 4 (TIM-4), Stabilin-2 and the Receptor for advanced glycation end products (RAGE)

Following engagement of the apoptotic cell with the phagocyte synapse, a number of signalling pathways are activated leading to cytoskeletal rearrangement and engulfment. Following internalisation the phagosomes become progressively more acidic, eventually fusing with lysosomes, which contain the digestive enzymes for degradation. The phagocyte must process the degradation products efficiently in order to maintain homeostasis and molecules such as mitochondrial UCP2 for energy balance, DNase II to prevent accumulation of DNA fragments within phagocytes and ABCA1 to increase cholesterol efflux (Hochreiter-Hufford and Ravichandran, 2013).

At all stages in the phagocytic process including post-ingestion, complex signalling cascades are activated within the phagocyte, ultimately leading to a change in phenotype. The method of death, the location and the means by which the cells are cleared will ultimately determine the response of the phagocyte. Generally organs such as the spleen and liver are thought to be tolerogenic and apoptotic cells cleared by resident macrophages in these organs are likely to be immunologically silent. Conversely, apoptotic cells cleared by incoming monocyte-derived macrophages in an inflamed environment are likely to induce an immunomodulatory phenotype (Geissmann et al., 2010, Hochreiter-Hufford and Ravichandran, 2013). Specifically, in this context phagocytes can secrete increased amounts of anti-inflammatory cytokines such as IL-10 and TGF-β and pro-resolution lipid mediators whilst the production of pro-inflammatory cytokines is inhibited (Erwig and Henson, 2007). Indeed, the administration of apoptotic cells to inflamed peritoneum or lung shows an anti-inflammatory effect *in vivo* (Huynh et al., 2002). This is in contrast to the clearance of pathogens and necrotic cells, which despite being recognised by similar receptors to apoptotic cells, result in a pro-inflammatory macrophage phenotype, potentially due to activation of pattern recognition molecules such as TLRs (Erwig and Henson, 2007). Overall, it is clear that macrophage phagocytosis has significant effects on the cellular phenotype. The precise phenotypic effects are likely to be dependent on the exact micro-environmental cues which are impossible to recreate *in vitro*.

Macrophages can Promote Hepatic Fibrosis

Having discussed the complexity of macrophage heterogeneity, it is important to consider the current evidence suggesting a potential role in hepatic fibrosis. There is now an evolving tranche of evidence that macrophages play a key role in this process. On the morphological level it is clear that in the fibrotic liver, hepatic macrophages localise in close proximity to activated myofibroblasts and the scar tissue, leading to the term scar-associated macrophage (SAM) and suggesting a potential role in the fibrotic process (Duffield et al., 2005,

Fallowfield et al., 2007). The major functional evidence has come from *in vivo* macrophage depletion and blockade strategies. One group utilised gadolinium chloride ($GdCl_3$) to deplete hepatic macrophages in rats and demonstrated reduced myofibroblast activation and fibrosis in response to thioacetamide injury (Ide et al., 2005). Furthermore, inhibition of principal monocyte chemokine CCL2 in rats or knockout of its receptor CCR2 in mice reduced hepatic macrophage infiltration in response to injury and significantly inhibited liver fibrosis (Imamura et al., 2005, Mitchell et al., 2009). However, both these approaches can potentially have "off target" effects on hepatic stellate cells. The seminal work in this field came from the use of a conditional macrophage depletion strategy using CD11b-DTR transgenic mice, which express the human diphtheria toxin receptor under the control of the CD11b promoter, enabling selective depletion of monocytes/macrophages by administration of diphtheria toxin (DT). Using this strategy the authors clearly demonstrated that macrophage depletion during ongoing hepatic injury with CCl_4 resulted in inhibited liver fibrogenesis, hence confirming the pro-fibrogenic role of macrophages in this setting (Duffield et al., 2005). A similar pro-fibrotic role for liver macrophages during injury has been demonstrated using a liposomal clodronate depletion strategy in both a transgenic model of hepatic injury and in response to CCl_4 or BDL (Sunami et al., 2012, Pradere et al., 2013).

Given the aforementioned heterogeneity in tissue macrophages, work has subsequently focussed on which liver macrophage population might mediate this pro-fibrotic effect. In response to hepatic injury, resident Kupffer cells and recruited monocyte-derived macrophages can be differentiated by flow cytometry (Holt et al., 2008). In an excellent study by Karlmark et al., the authors defined that a Ly-$6C^{hi}$ hepatic macrophage population derived from CCR2-dependent recruitment of Ly-$6C^{hi}$ inflammatory monocytes were the main pro-fibrogenic population in a murine CCl_4 fibrosis model (Karlmark et al., 2009).

Similarly, macrophages have now been identified as potentially pro-fibrotic cells in tissue fibrosis in other organs including the kidney (Conway and Hughes, 2012, Vernon et al., 2010, Ricardo et al., 2008, Lin et al., 2009), heart (Hayashidani et al., 2003, Rickard et al., 2009), lung (Osterholzer et al., 2013, Gibbons et al., 2011) and skin (Mahdavian Delavary et al., 2011, Lucas et al., 2010). Indeed, in several circumstances, similar to the liver, Ly-$6C^{hi}$ monocyte-derived macrophages are the main pro-fibrogenic macrophage population (Lin et al., 2009, Gibbons et al., 2011, Osterholzer et al., 2013).

Focus has then turned to the mechanism of the pro-fibrogenic activity of macrophages in liver fibrosis. Macrophages can be potent producers of a wide variety cytokines, chemokines and other soluble mediators which could potentially have direct effects on hepatic stellate

cells and myofibroblast populations. Specifically, macrophages have been shown to express TGF-β, the archetypal pro-fibrotic cytokine which can promote myofibroblast activation and matrix synthesis (Karlmark et al., 2009, Wynn and Barron, 2010). Furthermore, macrophages have been shown to express PDGF, a potent myofibroblast mitogen, and T_H2 cytokines IL-4 and IL-13 which can directly stimulate collagen synthesis in fibroblasts. Macrophages have also been associated with the production of a range of chemokines which can recruit myofibroblasts and further inflammatory cells to the site of inflammation thereby perpetuating the response (Wynn and Barron, 2010). Galectin-3 is a lectin that has been shown to promote myofibroblast activation in both liver and kidney fibrosis models and is secreted by macrophages (Henderson et al., 2008, Henderson et al., 2006). More recently, hepatic macrophage derived pro-inflammatory cytokines TNF-α and IL-1β have been shown to act on activated hepatic stellate cells to induce NF-κB activity, promote stellate cell survival and increase liver fibrosis (Pradere et al., 2013). Indeed, macrophage subsets isolated from cirrhotic human liver also express high levels of pro-inflammatory mediators (Zimmermann et al., 2010). These pro-fibrogenic activities of hepatic macrophages are summarised in **Fig 1.2** (adapted from (Ramachandran and Iredale, 2012b)).

Thus, there is clear evidence of a pro-fibrotic role of macrophages in liver and other organs. The traditional view was that this "wound healing" fibrotic response was dependent on M2 alternatively activated macrophages. However, as discussed previously, this binary classification is limited in an *in vivo* context, and in fact features of both M1 and M2 macrophages can potentially be pro-fibrogenic. Thus, a functional characterisation of macrophages is likely to be more useful.

Macrophages are Critical for Fibrosis Resolution

Whilst the role of macrophages in promoting fibrosis is well established, there is emerging data which also indicates that macrophages are critical for liver fibrosis regression (Ramachandran and Iredale, 2012b). Principally, using the CD11b-DTR transgenic system, macrophage depletion by DT administration during the recovery phase following CCl_4 injury resulted in a striking failure of scar resolution (Duffield et al., 2005). Additionally, in mice deficient in CCR2, a failure to recruit monocytes to the liver in response to CCl_4 injury results not only in reduced fibrogenesis but also impaired fibrosis regression (Mitchell et al., 2009). Similar findings have also been demonstrated in the lung, where macrophage depletion using liposomal clodronate during the recovery phase following bleomycin injury prevents the resolution from fibrosis (Gibbons et al., 2011).

So how do macrophages mediate this pro-resolution effect? Scar associated macrophages lie in close proximity to the fibrotic tissue and are hence ideally placed to mediate fibrosis degradation. Our group has previously demonstrated that hepatic macrophages are a key source of matrix degrading MMP enzymes, including MMP-13 (Fallowfield et al., 2007) and MMP-12 (Pellicoro et al., 2011), both of which are important for ECM degradation. Macrophages are also capable of expressing genes such as MMP-9 or TRAIL which have been shown to promote myofibroblast apoptosis. As described, another key feature of macrophages during inflammation is the clearance of cellular debris. Whilst, it had been felt that the process of phagocytosis may be pro-fibrogenic via the induction of TGF-β expression in macrophages, the phagocytic clearance of cellular debris will remove signals that can potentiate the inflammatory response. Indeed, macrophage phagocytosis has been associated with an upregulation of MMP expression (Popov et al., 2010).

In addition to pro-resolution properties, the loss of some of the described pro-inflammatory and/or pro-fibrotic macrophage properties may result in a change in the local milieu to favour fibrosis regression. Specific signals such as CX3CL1 acting on CX3CR1 on macrophages (Karlmark et al., 2010) or the opsonin serum amyloid P (SAP) protein acting via Fcγ receptors (Castano et al., 2009) have been shown to promote an anti-inflammatory macrophage phenotype and consequent protection from tissue fibrosis. Current understanding of the pro-resolution macrophage and its mechanism of formation and action is summarised in **Fig 1.2** (adapted from (Ramachandran and Iredale, 2012b))

Another proposed indirect mechanism for the role of macrophages in fibrosis resolution is via recruitment of other effector cell types. One group, for example, has proposed that in the repairing liver, hepatic macrophages cause the recruitment of neutrophils which express matrix degrading enzymes and result in scar resolution (Harty et al., 2008). Whilst, as discussed previously, the exact role of neutrophils in this process remains unclear, macrophages have the capacity to alter other cellular components of the immune response. Indeed, adoptive transfer of exogenous macrophages to mice during CCl_4 liver injury has been shown to recruit host effector cells to mediate an anti-fibrotic effect (Thomas et al., 2011).

Dendritic cells have also been explored in the context of liver fibrosis resolution. Using CD11cC-DTR transgenic mice to deplete hepatic dendritic cells during the recovery phase following CCl_4 injury, supplemented by adoptive transfer data and *in vivo* DC expansion using FLT3 Ligand, the authors demonstrated that DCs may also have a role in matrix degradation, potentially via MMP-9 expression (Jiao et al., 2012). Similarly, CD11c positive

DCs have been shown to have a role in the recovery from hepatic ischaemia/reperfusion injury (Bamboat et al., 2010). Whilst this needs to be proven in other studies, given the overlap between monocyte, macrophage and dendritic cell identity and function, particularly in the context of inflammation, caution needs to be adopted in ascribing specific functions to DCs.

Overall, these data highlight an emerging understanding of the potential role of macrophages in the resolution of tissue fibrosis and the restoration of normal tissue architecture. However, a number of questions remained unanswered (Friedman, 2005, Wynn and Barron, 2010). Are the pro-resolution effects mediated by a specific restorative macrophage subset? Does this population derive from recruited or resident macrophages? Is there a contribution of local macrophage proliferation? Are they formed as a distinct population or do they form from pro-fibrotic macrophages via a change in phenotype *in situ*? What signals cause the formation of the pro-resolution phenotype? What genes do restorative macrophages express? It is only by trying to identify the pro-resolution macrophage and characterising it that we can hope to address some of these important questions. Ultimately, a greater understanding of the macrophage biology of fibrosis regression could lead to the development of badly needed novel therapies to manipulate macrophage phenotype *in vivo* and promote fibrosis resolution.

Figure 1.2 – Macrophages can Promote Liver Fibrogenesis and Fibrosis Resolution

Schematic representation of the role of macrophages in hepatic fibrogenesis and fibrosis regression (adapted from (Ramachandran and Iredale, 2012b)). During fibrogenesis Ly-6C^{hi} monocytes are recruited to the inflamed live via the CCL2/CCR2 axis forming pro-fibrotic Ly-6C^{hi} (Gr-1^{hi}) macrophages. These cells potentially have a range of potential pro-fibrogenic features. Specifically they can express pro-inflammatory cytokines such as TNF-α and IL-1β which can perpetuate the inflammatory response and hepatocellular damage and also promote survival of hepatic myofibroblasts. They can also express chemokines which promote recruitment of monocytes, other inflammatory cells and hepatic stellate cells. Direct effects of pro-fibrogenic macrophages on hepatic myofibroblasts may be mediated by TGF-β or galectin-3 expression to promote activation or PDGF production to stimulate proliferation. Myofibroblasts themselves express TIMP-1 which inhibit MMPs and promote scar deposition. In contrast less is known about the pro-resolution macrophage population. They may derive from separate recruitment of monocytes or a change in macrophage phenotype, potentially via hepatic expression of anti-inflammatory signals such as CX3CL1. Pro-resolution macrophages are likely to remove cellular debris and consequent pro-fibrogenic signals by phagocytosis. They may also express signals such as TRAIL or MMP-9 which promote myofibroblast apoptosis. This apoptosis removes the source of scar production and TIMP-1 expression, enabling endogenous MMPs to degrade ECM. Finally, pro-resolution macrophages are likely to be a source of MMPs such as MMP-13 and MMP-12 which directly breakdown scar tissue. Hepatic dendritic cells may also express MMP-9 and promote fibrosis resolution.

Figure 1.2 - Macrophages can Promote Liver Fibrogenesis and Fibrosis Resolution

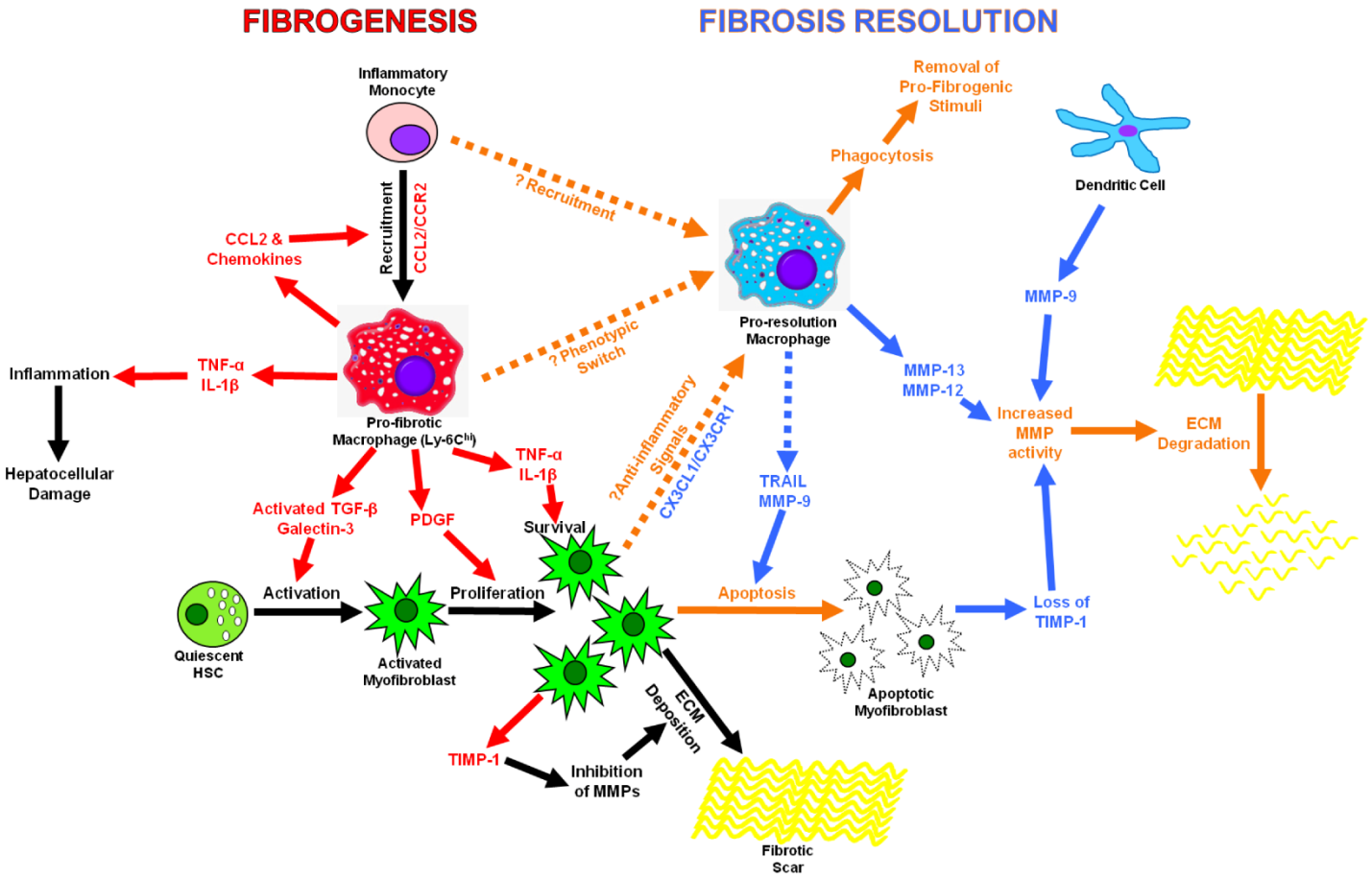

Hypothesis

A distinct hepatic macrophage population, derived from circulating cells, mediates matrix remodelling in the reversal of liver fibrosis

Aims and Objectives

The overall aim of this thesis is that is to identify and characterise the hepatic macrophage population responsible for the resolution of liver fibrosis, the so called restorative macrophage.

I will address this aim in several ways:

- Establishing and characterising a robust and reproducible model of reversible murine liver fibrosis
- In depth study of changes in hepatic macrophage populations during fibrosis resolution
- Use of macrophage depletion during fibrosis resolution to identify the functionally relevant populations
- Defining the origin and dynamics of the liver macrophage populations involved in fibrosis regression
- Detailed characterisation of the phenotype of the pro-resolution hepatic macrophage and the signals involved in generating it
- To use the above data to develop strategies to alter macrophage phenotype *in vivo* with a view to accelerating fibrosis regression

CHAPTER 2 – MATERIALS AND METHODS

Animals

C57BL/6 mice ($CD45.2^+$) were purchased from Harlan, UK and were utilised for the majority of experiments presented in this thesis unless otherwise stated. CD11b-DTR mice were used for macrophage depletion studies and have been previously described by our group (Duffield et al., 2005). This mouse strain was originally obtained from R. Lang (Children's Hospital Research Foundation, Cincinnati) and was maintained as heterozygotes on a C57BL/6 background. $CD45.1^+$ C57BL/6 mice were provided by Professor S.M. Anderton (University of Edinburgh) and have been described (O'Connor et al., 2010). These mice were used for adoptive transfer experiments as CD45.1 positive cells can be identified by flow cytometry, but as they are derived from the same background mouse strain should not induce an immune response in the recipient animal. CD11c-DOG mice were provided by Dr A.S. MacDonald (University of Edinburgh). These mice have been described (Phythian-Adams et al., 2010) and enable depletion of CD11c positive dendritic cells in response to diphtheria toxin administration. Mice were bred under specific pathogen-free conditions at the University of Edinburgh and all experiments had local ethical approval and were conducted under UK home office legislation.

CCl_4 Murine Models

For the CCl_4 model, adult male C57BL/6 mice aged at least 6 weeks were used. Hepatic fibrosis was induced by twice-weekly intraperitoneal carbon tetrachloride (CCl_4; 0.4µl/g; Sigma*)* diluted 1:3 in olive oil (Sigma). Injury was continued for 4 weeks (9 injections). Animals were culled at stated timepoints following the final CCl_4 injection.

For depletion studies in male CD11b-DTR mice, diphtheria toxin (DT; 10ng/g in PBS; List Biological Laboratories Inc.) or PBS control was administered intravenously via the tail vein to mice following CCl_4 injury for 4 weeks (9 injections) at the stated timepoints. As an additional control, DT (10ng/g) or PBS was administered intravenously to wild-type C57BL/6 mice at identical timepoints following 4 weeks of CCl_4 injury.

For dendritic cell depletion, adult male CD11c-DOG mice were injured with 4 weeks of CCl_4 followed by administration of DT (12ng/g) or PBS control intraperitoneally at the stated timepoints following the final CCl_4 injection.

For macrophage depletion studies using liposomal clodronate, adult male C57BL/6 wild type mice were injured with 4 weeks (9 injections) of CCl_4. Liposomal clodronate was obtained from Nico van Rooijen (Van Rooijen and Sanders, 1994). 250µl of liposomal clodronate (or

PBS control) was administered to mice intravenously via the tail vein 48, 72 and 96 hrs following the final CCl_4 injection, followed by harvest at 120 hrs.

For lineage tracing of monocytes, wild-type adult male CD57BL/6 mice ($CD45.2^+$) were injured with 4 weeks of CCl_4. 4 hours following the final CCl_4 injection, $9x10^5$ $CD45.1^+$ Ly-$6C^{hi}$ monocytes suspended in 200µl of RPMI 1640 medium (or RPMI vehicle control) were injected via the tail vein. Livers were harvested at 24, 72 and 168 hrs after the final CCl_4 injection.

For *in situ* fluorescent labelling of monocytes, wild-type C57BL/6 mice were injured with 4 weeks of CCl_4 as before. 4 hours following the final CCl_4 injection, 250µl of fluorescent latex beads (0.5µm Fluoresbrite polychromatic red microspheres; 2.5% solids [wt/vol] diluted 1:25 in PBS for injection; Polysciences Inc.) or PBS vehicle control was injected intravenously via the tail vein, followed by harvest 24, 72 and 168 hrs after the final CCl_4 injection.

To modify PPAR-γ signalling *in vivo*, wild-type adult male C57BL/6 mice were injured with 4 weeks of CCl_4 as before. At 24, 48 and 72 hrs following the final CCl_4 injection, mice were given intraperitoneal injections of either the PPAR-γ activator rosiglitazone (10mg/kg dissolved in DMSO) or DMSO control. Animals were harvested at 96 hours.

To inhibit the phosphatidylserine binding molecule MFG-E8 *in vivo*, wild-type adult male C57BL/6 mice were injured with 4 weeks of CCl_4 as before, followed by intraperitoneal administration of the monoclonal anti-MFG-E8 blocking antibody (Clone 18A2-G10; Caltag Medsystems) or hamster IgG isotype control (Santa-Cruz Biotechnology) at a dose of 2mg/kg. Antibodies were given 24, 48 and 72 hrs following the final CCl_4 injection with harvest at 96 hours.

To attempt to block the phagocytic receptor Integrin α_v (ITGAV) *in vivo*, wild-type adult male C57BL/6 mice were injured with 4 weeks of CCl_4. At 24, 48 and 72 hrs after the final CCl_4 dose, mice were administered intraperitoneal injections of 200 µg of anti-ITGAV antibody (Clone RMV-7; Cambridge Biosciences) or Rat IgG1 κ isotype control (Clone RTK2071; Cambridge Biosciences). Animals were harvested at 96 hrs.

To induce phagocytosis in hepatic macrophages during fibrosis resolution *in vivo*, wild-type adult male C57BL/6 mice were injured with 4 weeks of CCl_4. At 48, 72 and 96 hrs after the final CCl_4 injection, mice were administered 250µl of liposomal PBS (multilamellar liposomes made with 8mg of cholesterol and 86mg phosphatidylcholine with 10mls PBS as

described (Van Rooijen and Sanders, 1994) and provided by Nico Van Rooijen), or PBS control intravenously via the tail vein. Animals were harvested at 120 hrs. In order to trace the *in vivo* fate of administered liposomes, this experiment was repeated using CM-DiI – labelled liposomes (CM-DiI from Invitrogen and used to label liposomes as per manufacturers' instructions) or PBS control.

TAA Murine Models

For the TAA model of liver fibrosis, adult male C57BL/6 mice with a weight of at least 25g were treated continuously with thioacetamide (Sigma) in the drinking water at a dose of 300mg/l or 600mg/l. Control animals remained on normal water. Free access to normal chow diet continued throughout. For the progressive fibrosis TAA model, mice were treated with TAA for up to 52 weeks, with harvests at 8, 12, 16, 20, 36 and 52 weeks of treatment. Animals were weighed weekly throughout to assess the effect of TAA treatment on expected weight gain.

For the reversible TAA model, only the 600mg/l dose of TAA was used and comparison made to normal drinking water. Mice were treated with TAA for either 8 weeks or 52 weeks. Following reaching the treatment duration, they were changed onto normal drinking water. In addition to harvests at the end of TAA treatment (8 weeks and 52 weeks), mice were harvested at 72 hrs, 1 week, 2 weeks and 8 weeks after conversion to normal water for the 8 week model, and 1 week, 2 weeks and 8 weeks after conversion to normal water for the 52 week model.

Hepatic Non-parenchymal cell isolation

Isolation of hepatic non-parenchymal cell (NPC) fraction was performed using a modified MACS protocol (http://www.miltenyibiotec.com/download/protocols_gentlemacs_en/1105/gentleMACS-Liver-04.pdf), from Miltenyi Biotech. In summary, mouse livers *in situ* were perfused with 10ml of 0.9% NaCl solution via the Inferior Vena Cava (IVC) followed by cutting the portal vein, to remove circulating cells. Livers were then harvested, weighed and either the whole liver or the right lobe homogenised using a scalpel and digested in RPMI 1640 medium containing Collagenase B (1.6mg/ml; Roche) and DNase I (100µg/ml; Roche) for 45 minutes at 37^{o}C. Digested livers were passed through 40µm cell strainers and enzymes inactivated by addition of RPMI 1640 with 10% FCS. Contaminating hepatocytes were removed by 2x centrifugation at 50G for 5 minutes, with the supernatant preserved. Erythrocytes were lysed

by adding lysis buffer (NH_4Cl 0.15M, $KHCO_3$ 10mM, EDTA 0.1mM in H_2O) for 5 minutes on ice. The remaining non-parenchymal cell fraction, containing hepatic macrophages, was then harvested by centrifugation at 300G for 10 minutes. Total cell number was counted using an aliquot of cell suspension and analysis using nucleocassettes (941-0002, Chemometec, Denmark) and a nucleocounter (SCC-100, Chemometec, Denmark). The non-parenchymal cell fraction was then used for flow cytometry and FACS sorting.

Flow cytometry and FACS sorting

Flow cytometry (using BD LSR Fortessa II) and FACS sorting (using BD FACSAria II) were performed on hepatic non-parenchymal cells containing the total hepatic leukocyte population.

Initially, non-specific antibody binding was blocked by incubating cells with 10% mouse serum for 20 minutes at 4^{o}C, followed by incubation with combinations of primary antibodies (each used at 1/100 dilution unless stated) for 30 minutes at 4^{o}C in the dark. The following pre-conjugated antibodies were used: CD11b (Clone M1/70, Rat IgG2b kappa), CD11c (Clone N418, Armenian Hamster IgG), Ly-6C (Clone HK1.4, Rat IgG2c kappa), CD45.2 (Clone 104, Mouse IgG2a kappa), CD45.1 (Clone A20, Mouse IgG2a kappa), CD115 (Clone AFS98, Rat IgG2a kappa), CD36 (Clone No.72-1, Rat IgG2a kappa) (All Ebioscience), F4/80 (Dilution 1:50; Clone BM8, Rat IgG2a kappa; Invitrogen), Ly-6G (Clone 1A8, Rat IgG2a kappa), CD3 (Clone 17A2, Rat IgG2b kappa), NK1.1 (Clone PK136, Mouse IgG2a kappa), B220 (Clone RA3-6B2, Rat IgG2a kappa), CD14 (Clone Sa14-2, Rat IgG2a kappa), CD16/32 (Dilution 1:200; Clone 93, Rat IgG2a lambda), CD80 (Clone 16-10A1, Armenian Hamster IgG), CD86 (Clone GL-1, Rat IgG2a kappa), CD81 (Clone Eat-2, , Armenian Hamster IgG) (All Biolegend). Fluorophores used were varied depending on the staining combination. However, commonly used combinations included Ly-6G-Pacific Blue, CD11b-AF488, CD11c-PE, Ly-6C-PerCp.Cy5.5, F4/80-APC, CD45.2-AF700, CD3-PE.Cy7, NK1.1-PE.Cy7, B220-PE.Cy7. Flow cytometry compensations were set up using single stained samples and stained CompBeads (BD biosciences). In samples, staining was confirmed by comparison to appropriate isotype antibodies where available. Cell viability was assessed with Propidium Iodide (Sigma, UK) or Fixable Viability Dye eFluor780® (Ebioscience) according to manufacturers protocols. Ki-67 staining for flow cytometric analysis was performed using Ki-67 staining kit (Clone B56, Mouse IgG1 kappa, BD biosciences) and Fix and perm kit (Ebioscience) as described (Jenkins et al., 2011). Following antibody staining, samples were either analysed immediately or fixed with 10% buffered-formalin. For FACS sorting, stained cells were resuspended in GIBCO Hank's

balanced salt solution supplemented with 1% FCS. Cells were collected into RPMI 1640 medium supplemented with 10% FCS. Data was analysed using FlowJo7.5 software (Treestar).

Hepatic macrophages were defined as viable $CD45^+$ $Ly\text{-}6G^-$ $CD3^-$ $NK1.1^-$ $B220^-$ $CD11b^+$ $F4/80^+$ cells from NPC fraction of digested livers and used to identify macrophage subsets. Subsets were expressed as proportions of total hepatic macrophages or total hepatic $CD45^+$ cells. Quantification of absolute numbers of cells per liver was performed by expressing each subset as a proportion of NPCs, counting total number of NPCs in the digested portion of liver, calculating the total number of NPCs in the whole liver by weight differential and thus the total number of each subset. Where stated these values were expressed relative to the mean of the control liver, which was assigned a value of 1.

For identification of circulating monocytes, whole blood was obtained from tail vein nicks prior to cull and diluted 1:1 in 4.8% Sodium Citrate buffer. This was stained with antibodies to CD11b (Clone M1/70, Rat IgG2b kappa), Ly-6C (Clone HK1.4, Rat IgG2c kappa), CD115 (Clone AFS98, Rat IgG2a kappa), CD45 (Clone 104, Mouse IgG2a kappa) (All Ebioscience) and Ly-6G (Clone 1A8, Rat IgG2a kappa; Biolegend), all at a dilution of 1:200 for 30 mins at 4^oC in the dark. Comparison was made to appropriate isotype control staining. Following staining, cells were washed x3 followed by red cell lysis and fixation using BD FACSlyse (BD bioscience) prior to analysis. Monocytes were identified as $CD45^+$ $CD115^+$ $CD11b^+$ $Ly\text{-}6G^-$ $Ly\text{-}6C^{hi}$ and $Ly\text{-}6C^{lo}$ cells from whole blood and expressed as a percentage of total peripheral mononuclear cells. Alternatively, the number of each cell type per ml of blood was quantified using counting beads. Specifically, 20µl of the blood:citrate mix (equivalent to 10µl of whole blood) was stained with antibodies as described. Prior to flow cytometric analysis, 10µl of Flow Count fluorospheres (Beckman Coulter; A91346) with a known concentration were added. Hence the number of beads per ml of whole blood could be quantified. Flow cytometry was then performed, with cell counts expressed relative to the number of beads in the sample and hence the number of cells per ml of blood could be calculated.

For isolation of bone-marrow derived $Ly\text{-}6C^{hi}$ monocytes, whole bone marrow was obtained from adult male $CD45.1^+$ C57BL/6 mice by harvesting of femurs and tibias and flushing using 10ml RPMI 1640 culture medium supplemented with 10% FCS under aseptic conditions. Cells were incubated with Fc block (rat anti-mouse CD16/CD32, BD Europe) for 15 minutes at 4^oC. Cell suspensions were spun at 300g for 5 minutes and re-suspended in GIBCO Hank's balanced salt solution (14170120, Invitrogen, UK). Antibodies to CD11b

(Clone M1/70), Ly-6C (Clone HK1.4), CD115 (Clone AFS98), CD45 (Clone 104) (All Ebioscience) and Ly-6G (Clone 1A8; Biolegend), were added all at a dilution of 1:200 for 30 mins at 4^{o}C in the dark. Cells were then spun at 300g for 5 minutes, washed x 2, and re-suspended in GIBCO Hank's balanced salt solution supplemented with 1% FCS for FACS sorting. Cells were sorted using a BD FACSAria II and collected into RPMI 1640 supplemented with 10% FCS. Ly-6C^{hi} monocytes were defined as viable CD45.1^{+} Ly-6G^{-} CD115^{+} CD11b^{+} Ly-6C^{hi} cells and used for adoptive transfer experiments. FACS sorting routinely yielded cell purity levels of over 95%. Cells were then spun at 300g for 5 minutes, washed x 2 with RPMI 1640 and resuspended in RPMI 1640 at a concentration of 4.5x10^{6}/ml, with 200µl (9x10^{5} cells) or 200µl of RPMI 1640 alone injected to mice via the tail vein.

Detection of *in vivo* MMP activity

To detect *in vivo* MMP activity, 2 nmol of the MMPsense 680 (Perkin Elmer) (or vehicle control) was administered to animals via the tail vein, 24 hrs prior to harvest, according to the manufacturers protocol. Hepatic macrophages were identified using flow cytometry of hepatic non-parenchymal cells as before, followed by identification of MMPsense positive macrophages with excitation laser at 635nm (Cortez-Retamozo et al., 2008).

Microarray analysis

50ng of RNA from FACS-sorted cells was processed using Ovation® Pico WTA system (NuGen) according to manufacturers protocol (n=3 per group). Processed RNAs were hybridized to Affymetrix GeneChip Mouse Gene 1.0 ST Arrays. RNA/microarray processing was carried out by ARK Genomics (Roslin Institute, Edinburgh, UK).

Data extraction and analysis were performed by Donald Dunbar and Johnathan Manning. Data were extracted through the GCOS software, and CEL files used for further data processing. CEL files were imported into Bioconductor (Gentleman et al., 2004), normalised by RMA in the Oligo (http://www.bioconductor.org/packages/2.0/bioc/html/oligo.html) module, and statistically analysed with the Limma (Smyth, 2004). A fold change of >2 with adjusted *P*-value <0.05 was considered significant for individual gene changes. Gene ontology and KEGG pathway enrichment analysis was done with the DAVID tool (Dennis et al., 2003, Huang da et al., 2009b), on genes which were significantly differentially expressed. Microarray data are available in the ArrayExpress database (www.ebi.ac.uk/arrayexpress) under accession number E-MEXP-3177.

In vitro phagocytosis assay

Bone marrow derived macrophages (BMDMs) were prepared from adult male C57BL/6 mice as previously described (Henderson et al., 2008). Whole bone marrow was isolated under aseptic conditions by flushing femurs with 10ml of DMEM/F12 Glutamax (Gibco, UK) medium with 10% Fetal Calf Serum (FCS). Whole bone marrow was then cultured for 7 days at 37^{o}C 5% CO_2 in DMEM/F12 Glutamax (Gibco, UK) medium with 10% Fetal Calf Serum (FCS) and 20% L929 conditioned medium (as a source of M-CSF), under non-adherent conditions using Ultra Low Adherence Flasks (Corning, UK). 25% of the medium was replaced at days 2, 4 and 6 of the culture process. After 7 days, cells were analysed by flow cytometry. Briefly, cells were harvested by centrifugation at 300g for 5 mins, washed x2 with PBS, incubated with 10% mouse serum in PBS to block non-specific staining, and then stained with antibodies to F4/80 (Clone BM8; Invitrogen; Dilution 1:50), CD11b (Clone M1/70; Ebioscience; Dilution 1:100) and CD11c (Clone N418; Ebioscience; Dilution 1:100) for 30 mins at 4^{o}C in the dark. Cells were then washed x 2 with PBS, resuspended in PBS and either analysed immediately or fixed with 10% formalin solution. Analysis was performed on BD LSR Fortessa II. This routinely yielded a macrophage population of >90% purity as assessed by flow cytometry for CD11b and F4/80. Alternatively, to assess cell morphology, cells were counted using nucleocassettes (941-0002, Chemometec, Denmark) and a nucleocounter (SCC-100, Chemometec, Denmark) and cytospins created (20-40,000 cells per slide) using a Shandon Cytospin 4 cytocentrifuge (Thermo Scientific). Cells were then fixed and stained using Quik-Diff kit (Reagena, UK).

Primary murine hepatocytes were prepared using a modified two-stage perfusion technique (http://tools.invitrogen.com/content/sfs/manuals/3736.pdf). Briefly, adult male C57BL/6 mice were anaesthetised with intraperitoneal Ketamine and Medetomidine. Following cannulation of the portal vein with a 24G intravenous cannula (BD biosciences), livers were perfused with 50ml Liver Perfusion Medium (Gibco, UK) followed by 50ml Liver Digestion Medium (Gibco, UK), the perfusion fluid exiting via a cut in the IVC. Livers were then removed aseptically into a 50ml BD falcon tube containing 15ml of Williams E culture medium (Gibco, UK) on ice. Hepatocytes were then released gently by pipetting with a 5ml pipette. Cells were filtered through a 100µm cell strainer (BD biosciences) and harvested by low speed centrifugation at 50G for 5 mins. Hepatocytes were washed x3 in cold hepatocyte wash medium (Gibco, UK), then plated into tissue culture flasks (T162) which had been precoated with collagen (10µg/cm^2 Rat Tail Collagen; Sigma) for 4 hours. Hepatocytes were cultured overnight at 37^{o}C 5%CO_2 Williams E medium (Gibco, UK) supplemented with

10% FCS and 1% Pen/Strep solution. For preparation of hepatocyte debris, adherent viable hepatocytes were washed with PBS then detached using trypsin and washed x 2 with PBS. Hepatocytes in suspension were counted then cultured in suspension in serum-free Williams E medium containing Anti-Mouse CD95 (1/500 dilution; Clone Jo-2; BD Pharmingen) at 37^{o}C for 8 hours. This yielded a population >95% trypan blue positive hepatocytes.

Apoptotic thymocytes were prepared as previously described (Ferenbach et al., 2010). Briefly, thymi were removed aseptically from C57BL/6 mice, aged 3-5 weeks. Thymi were aseptically homogenised between microscope slides in RPMI 1640 medium, enabling extraction of thymocytes. Thymocytes were cultured in RPMI 1640 medium supplemented with Dexamethasone (1 µM; Mayne Pharma, UK) and 1% FCS at 37^{o}C 5%CO_2 for 16 hours. Cells were then harvested by centrifugation at 300g for 10 mins and washed x 3 with PBS before use in further experiments. An aliquot of cells was taken for cell counting and was also stained with trypan blue. Routinely, this methodology yielded a population of dead thymocytes, with over 90% trypan blue positive.

For the phagocytosis assay, 2x10^{5} BMDMs were seeded per well in 12-well plates followed by addition of 5x10^{5} washed dead hepatocytes (or control medium), 1 x 10^{6} washed dead thymocytes or Liposomes (liposomal PBS, provided by Nico Van Rooijen (Van Rooijen and Sanders, 1994) 1:10 dilution by volume (or PBS control)) and cultured for 16 hrs (or 12 hrs for thymocytes) at 37^{o}C 5%CO_2 in DMEM/F12 Glutamax (Gibco, UK) medium with 10% FCS. Where stated, inhibitors PD98059 (50µM; Cayman Chemical), UO126 (20µM; New England Biolabs), SB203580 (10 µM; Cayman Chemical) or DMSO control were added to the plated BMDMs, for 1 hr prior to and maintained throughout the 16 hr incubation with hepatocyte debris. Supernatants were then harvested, cellular debris removed by centrifugation at 400g for 15 mins and residual supernatant removed and stored at -80^{o}C. For cellular data, non-ingested hepatocytes or liposomes were removed by vigorous washing x3 with PBS and residual adherent macrophages used for further analysis. Prior to harvest, these adherent macrophages were viewed by phase contrast microscopy using a Nikon Eclipse E600 microscope and photographed. In control wells containing hepatocyte debris alone, no adherent cells were detected.

In some studies, after harvest of the cultured murine hepatocytes and prior to the incubation in suspension with anti-CD95, hepatocyte debris was fluorescently labelled using the red membrane dye PKH26 (Sigma-Aldrich) according to the manufacturers' protocol. Induction of hepatocyte death then proceeded as described, apart from cells being incubated in the dark. In the same experiment, BMDMs, after 7 days of differentiation and prior to plating in

12 well plates for phagocytosis assay, were fluorescently labelled using Celltracker™ Green (Invitrogen) as per the manufacturers protocol. Co-culture with PKH26 labelled hepatocyte debris (or medium control) was then performed for 16 hours. Following vigorous washing, cells were examined by fluorescence microscopy using a Nikon Eclipse E600 microscope and NIS-Elements D3.1 Software.

RNA extraction and quantitative RT-PCR

For whole liver, the caudate lobe was snap frozen in liquid nitrogen and stored at -80^{o}C. RNA was extracted using Trizol reagent (Invitrogen) and RNeasy mini columns (Qiagen) according the manufacturers protocol, followed by quantification using Nanodrop Spectrophotometer (Thermo Scientific). 1µg of RNA was reverse transcribed using Superscript III (Invitrogen) according to the manufacturers protocol. Gene expression was calculated using the $\Delta\Delta C_T$ method relative to housekeeping gene 18S.

For FACS sorted cells, RNA was extracted using RNeasy micro plus kit (Qiagen) according to the manufacturers protocol. RNA was quantified using Nanodrop Spectrophotometer (Thermo Scientific) and 10ng of RNA was reverse transcribed and amplified using Whole Transcriptome kit (Qiagen) as per the manufacturers' protocol. Gene expression was calculated using the $\Delta\Delta C_T$ method relative to housekeeping gene β2M.

For the *in vitro* phagocytosis assay, RNA was extracted using RNeasy micro plus kit (Qiagen) and 100ng RNA reverse transcribed using Superscript III (Invitrogen) as per the manufacturers protocol. Gene expression was calculated using the $\Delta\Delta C_T$ method relative to housekeeping gene β2M.

Where stated relative gene expression was calculated by normalising to the mean expression of one group which was assigned a value of 1.

The following primer or primer/probe sets were purchased - 18S eukaryotic primer/probe set (Ambion AM1718), β2M (ABI, Mm00437762_m1), Chi3l3 (ABI, Mm00657889_mH), Ccr2 (ABI, Mm00438270_m1), Cx3cr1 (ABI, Mm02620111_s1), Igf1 (Qiagen QT 00154469), Thbs1 (Qiagen QT01748187), Il-1β (Qiagen QT01048355) and Cxcl10 (Qiagen, QT00093436). The remaining primer sequences were designed using primer express software and the sequences are as follows:

TIMP-1 (Forward CAT GGA AAG CCT CTG TGG ATA TG; Reverse AAG CTG CAG GCA CTG ATG TG; Probe CTC ATC ACG GGC CGC CTA AGG AAC)

MMP9 (Forward CGA ACT TCG ACA CTG ACA AGA AGT; Reverse GCA CGC TGG AAT GAT CTA AGC; Probe TCT GTC CAG ACC AAG GGT ACA GCC TGT TC)

MMP12 (Forward GAA ACC CCC ATC CTT GAC AA; Reverse TTC CAC CAG AAG AAC CAG TCT TTA A; Probe AGT CCA CCA TCA ACT TTC TGT CAC CAA AGC)

CCL2 (Forward CTT CTG GGC CTG CTG TTC A; Reverse CCA GCC TAC TCA TTG GGA TCA)

Genes were then analysed using either TaqMan Express qPCR supermix (Invitrogen) or Quantifast SYBR green PCR kit (Qiagen), on an ABI 7500Fast Realtime system, according to the manufacturers' instructions.

Immunohistochemistry and Immunofluorescence

Following harvest, liver tissue was fixed overnight in 10% neutral buffered formalin (Sigma) or Methacarn (60% Methanol: 30% Chloroform: 10% Glacial Acetic acid) solution, followed by paraffin embedding. Human cirrhotic liver was fixed in formalin. 4μm tissue sections were dewaxed and rehydrated in decreasing concentrations of ethanol. Where stated, antigen retrieval was performed by boiling for 15 mins in 10mM Sodium Citrate buffer, pH6. Endogenous peroxidise activity was inhibited with 3% hydrogen peroxide followed by Avidin/biotin block (Vector Labs) and then non-specific binding minimised using protein block solution (Dako). Primary antibody was then applied. All primary antibodies were incubated overnight at 4^{o}C. Species appropriate anti-IgG biotinylated secondary antibodies (Dako) were used at 1/300 dilution, at room temperature for 1hr. Immunostaining was developed using 3,3'-diaminobenzidine (DAB; Dako, UK). The following primary antibodies and conditions were used: Collagen 1 (Southern Biotech 1310-08; 1/100 dilution; Formalin-fixed; Antigen Retrieval), Collagen 3 (Southern Biotech 1330-01; 1/100 dilution; Formalin-fixed; Antigen Retrieval), α-SMA (Sigma-Aldrich Clone 1A4; 1/4000 dilution; Formalin-fixed; Antigen Retrieval), F4/80 (Abcam ab6640; 1/200 dilution; Formalin-fixed; No Antigen Retrieval), Chi3l3 (Stemcell Technologies 01404; 1/100 dilution; Formalin-fixed; Antigen Retrieval), MMP-12 (Santa Cruz sc-8839; 1/240 dilution; Formalin-fixed; 20mins Antigen Retrieval), Murine and Human Gpnmb (Santa Cruz sc-47006; 1/200 dilution; Formalin-fixed; 15mins antigen retrieval), Human MMP-12 (Abcam AB52897; 1/400 dilution; 20 mins antigen retrieval by boiling in Tris-EDTA pH9). Picrosirius red staining was performed according to standard protocols. Where stated, morphometric pixel analysis to quantify histological staining was performed. Briefly, sections were blinded and a minimum of 20 non-overlapping fields per section were photographed at x100 magnification

using a Nikon Eclipse E600 microscope and camera (DXM1200F) and acquired using NIS-Elements D3.1 Software. All images had a matched exposure time and light intensity. Pixel counts of positive staining were performed in Adobe Photoshop CS2 and expressed as a % of the total pixel count and hence % area. Where stated relative % area was calculated by normalising to the mean % area of one group which was assigned a value of 1. Where stated, cell counts were performed at x200 magnification on blinded slides, with a minimum of 20 non-overlapping fields counted per mouse.

Dual immunofluorescence for F4/80 and phospho-ERK was performed on formalin fixed paraffin embedded sections. Tissue was prepared and blocked with protein block solution (Dako) then sequentially incubated first with F4/80 (Abcam ab6640) or isotype control at 1:100 for 2 hours, rinsed, then rabbit anti-rat HRP (1/300 Dako P0450) was added followed by the TSAT Plus Cyanine 3 System (PerkinElmer NEL744B001KT). Sections were then antigen retrieved for 10 mins with 10mM sodium citrate buffer and blocked again with protein block solution (Dako). The second primary antibody pERK (Cell signalling 4370) or isotype control was incubated at 1:100 overnight followed by donkey anti-rabbit Alexa 488 (Invitrogen A21206). Sections were mounted in dapi hard set mounting medium (Vector Labs H1500). All photographs were taken using a Nikon Eclipse e600 microscope and camera (DXM1200F) and acquired using NIS–Elements D software (Nikon)

For dual immunofluorescence on human tissue for CD68 and MMP-12, antigen retrieval (20mins; Tris EDTA pH9) was followed by protein block (Dako X0909), then sequential incubation with anti-MMP-12 (Abcam ab52897; 1/100 dilution; overnight) or isotype control then donkey anti-rabbit Alexa 488 (Invitrogen A21206), followed by protein block, followed by anti-CD68 (Dako M0867; 1/50 dilution; 2 hrs) or isotype control followed by donkey anti-mouse Alexa 555 (Invitrogen A31570). For CD68 and GPNMB, antigen retrieval (15mins; Tris EDTA pH9), followed by protein block (Dako X0909), then sequential incubation of GPNMB (Santa Cruz sc47006; 1/100 dilution; overnight) or isotype control followed by donkey anti goat Alexa 488 (Invitrogen A11055) followed by protein block, followed by anti-CD68 (Dako M0867; 1/50 dilution; 2 hrs) or isotype control followed by donkey anti mouse Alexa 555 (Invitrogen A31570). For both, sections were then blocked with 0.1% Sudan Black B (Sigma) and mounted with Dapi hard set mounting medium (Vector Labs H1500). All photographs were taken using a Nikon Eclipse e600 microscope and camera (DXM1200F) and acquired using NIS–Elements D software (Nikon).

Immunocytochemistry

TUNEL-staining of FACS-sorted Ly-6C^{hi} and Ly-6C^{int} macrophage subsets was performed using TACS® TdT-Fluor *In Situ* Apoptosis Detection Kit – Fluorescein (R&D systems) according to the manufacturers' protocol. Briefly, cells were obtained by FACS sorting of liver digests as before. Cells were resuspended in 3.7% buffered formaldehyde for 10 mins, then in 80% ethanol and spotted onto microscope slides. They were then dried for 2 hours at 45^{o}C, then immersed in 70% ethanol for 10 mins and then dried at room temperature overnight. Slides were then stored at -20^{o}C. For labelling, cells were rehydrated by immersing for 5 minutes each in 100%, 95%, and 70% ethanol, then immersed PBS and stained according to the manufacturers' protocol. The association between apoptotic debris and macrophages was assessed using a Leica SP5 Confocal microscope with z-stacks on each field. Images were blinded and analysed using ImageJ software for the presence of cell-surface or intracellular apoptotic debris. A minimum of 25 macrophages were counted per slide. The percentage of macrophages associated with TUNEL-positive nuclei was quantified followed by quantification of the localisation of the apoptotic debris.

Western blotting and Zymography

For TIMP-1 western blotting, whole tissue protein extracts were made by homogenisation of samples in lysis buffer (50mM HEPES, 1mM DTT, 0.1mM EDTA, 0.1% CHAPS, pH 7.4). Protein concentration was determined by Bradford Assay and equal amounts (20µg of protein/well) were subjected to SDS-PAGE on 12% gels. Following electrophoresis, samples were transferred onto nitrocellulose membranes and blocked for 2 hrs at room temperature in 5% non-fat dry milk in tris-buffered saline + 0.1% Tween (TBST). Membranes were incubated overnight at 4^{o}C with primary antibody in TBST containing 5% BSA (TIMP-1 at 1:500 dilution, Calbiochem, UK, 7-6C1). Membranes were then washed (x3, 15 minutes each) in TBST before the addition of an HRP-conjugated secondary antibody (1:2000 dilution; Abcam) in TBST containing 5% non-fat dry milk for 1 hour at room temperature. Following incubation, membranes were washed again (x3) in TBST for 15 minutes each, followed by development using enhanced chemiluminescence (ECLplus, Amersham, UK) and visualization on a VersaDoc.

For western blotting and zymography on *in vitro* phagocytosis assays, culture supernatants were harvested. Protein levels were quantified using Bradford reagent (Sigma-Aldrich) and equalised with PBS to ensure equal protein loading. Gelatin zymography was performed as previously described (Souza-Tarla et al., 2005). Briefly, samples were subjected to electrophoresis on a 10% SDS-PAGE gel co-polymerised with 1% gelatin substrate. Following electrophoresis, gels were renatured in 2.5% Triton X-100 for 30 minutes before

incubation in activity buffer (50mM Tris, 200mM NaCl, 5mM CaCl2 (anhydrous), 0.02% Brij-35, pH 7.5) at 37^0C for 16-24 hrs. Gels were then stained with 0.5% Coomassie Brilliant Blue before destaining in 40% methanol, 10% acetic acid. MMP-9 gelatinolytic activity was detected as destained bands against a background of coomassie stained gelatin. The active form of MMP-9 was detected at 92kDa. Casein zymography was performed as previously described (Poppelmann et al., 2002, Pellicoro et al., 2011). Equalised culture supernatants were subjected to electrophoresis on a 12% SDS-PAGE gel containing 0.25% skimmed milk powder. Following electrophoresis, gels were rinsed in deionised water and renatured in 2.5% Triton X-100 for 1 hour before incubation in activity buffer (50mM Tris, 200mM NaCl, 5mM $CaCl_2$, 0.02% Brij-35, pH 7.5) at 37°C for 72 hours. Subsequently, the gel was stained with SimplyBlue Safe Stain (Life Technologies, UK) before destaining in water. Proteolytic activity was detected as destained bands against a background of SimplyBlue stained casein. For MMP-12 western blotting, media from the phagocytosis assay were freeze-dried and equalised resuspended samples were subjected to SDS-PAGE on a 10% gels. Following electrophoresis, samples were transferred onto nitrocellulose membranes and blocked for 2hrs at room temperature in 3% BSA (Sigma-Aldrich) in tris-buffered saline + 0.05% Tween (TBST). Membranes were incubated overnight at 4^oC with primary antibody in TBST containing 3% BSA (MMP-12 at 1:1000 dilution, Biomol International, SA453-0100). Membranes were then washed (x3, 10 minutes each) in TBST before the addition of an HRP-conjugated secondary antibody (1:2000 dilution; Abcam) in TBST containing 5% non-fat dry milk for 1 hour at room temperature. Following incubation, membranes were washed again (x3) in TBST for 10 minutes each, followed by development using Immobilon western Chemiluminescent HRP Substrate (Millipore, UK) and visualization on a VersaDoc™ Imaging system (BioRad).

ELISA

For tissue cytokine ELISA, whole tissue protein extracts were made in T-PER (Thermo Scientific) (containing protease inhibitors aprotinin 10µg/ml, leupeptin 10µg/ml and PMSF 1mM). A Bradford assay was performed and samples equalised to a total protein concentration 50µg/µl. These were then assayed using Bio-plex mouse cytokine assay (Bio-Rad, UK) according to the manufacturers' protocol.

Serum analysis

At the time of harvest, whole blood was collected from the Inferior Vena Cava (IVC) and serum isolated by centrifugation at 7000g for 5 mins. Serum samples were stored at -80^oC

and analysed for Alanine aminotransferase (ALT) and Aspartate aminotransferase (AST) levels using a standard bioanalyser.

Statistical Analysis

All data are expressed as Mean±S.E.M. Statistical analysis was performed using GraphPad Prism 5 software. For analysis, data was first tested for normality. If data was normally distributed, statistical evaluation of multiple groups was performed using a one-way ANOVA with post-hoc Tukey test. Statistical evaluation of 2 groups was performed using a Student's t-test. If not normally distributed, comparison between multiple groups was performed using a Kruskal-Wallis test with Dunn's multiple comparison and comparison between 2 groups was performed using a Mann-Whitney test. A value of $P < 0.05$ was considered statistically significant.

CHAPTER 3 – CHARACTERISATION OF HEPATIC MACROPHAGE HETEROGENEITY IN MURINE MODELS OF LIVER FIBROSIS

INTRODUCTION

The overall aim of this work was to study macrophage heterogeneity in the resolution of hepatic fibrosis. As discussed previously, the majority of the work identifying and characterising distinct monocyte and macrophage subsets has been done in murine models, requiring identification of a number of cell surface markers to distinguish distinct populations. Currently there is much more limited data on differentiating macrophage subsets with more limited reagents available in rats. I therefore aimed to establish a robust, reproducible and predictable murine model of reversible hepatic fibrosis to enable in depth study of monocyte and macrophage dynamics.

Carbon tetrachloride (CCl_4), a solvent previously used as a refrigerant, is the most widely used hepatotoxin in experimental hepatic fibrosis models. CCl_4, when administered *in vivo*, is metabolised by the hepatic Cyp2E1 enzyme system, forming trichloromethyl peroxy free radicals, which result in lipid peroxidation followed by cell membrane damage and loss of integrity, activation of intracellular calcium-dependent proteases, ultimately leading to hepatocyte death, via apoptosis and necrosis (Manibusan et al., 2007, Shi et al., 1998). Given that Cyp2E1 is predominantly expressed in centrilobular (zone 3) hepatocytes, the majority of cell death occurs in this region of the liver (Shi et al., 1998). This is analogous to alcohol related liver damage and NASH which are also related to hepatic Cyp2E1 activity, resulting in free radical production, lipid peroxidation and zone 3 hepatocyte damage (Lieber, 2004). Chronic iterative administration of CCl_4 results in recurrent hepatocellular death, leading to a wound-healing response and ultimately to liver fibrosis and cirrhosis, showing histological similarities to human chronic liver disease (Perez Tamayo, 1983). Furthermore, in rodent models, cessation of chronic CCl_4 dosing results in matrix remodelling and fibrosis resolution in a manner very similar to that seen in human disease (Issa et al., 2004, Wanless et al., 2000). Bile duct ligation followed by biliary re-anastamosis, the other widely-used model of reversible hepatic fibrosis (Issa et al., 2001), is generally only used in rats and would be very technically challenging to perform reliably in mice. Thus, a CCl_4 model of reversible hepatic fibrosis would be a reproducible, tractable and clinically relevant model with which to study hepatic macrophage biology.

Thioacetamide (TAA) is another hepatotoxin, widely-used in experimental fibrosis models. TAA is hepatotoxic via effects on DNA, RNA and protein synthesis and induction of changes in intrahepatic metabolism (Noda et al., 1996). Continuous administration of TAA to rats in drinking water causes a distinct pattern of fibrosis/cirrhosis to that seen with CCl_4 administration. Specifically, marked biliary proliferation is seen, with an associated fibrotic

response and the progressive development of micronodular cirrhosis (Jeong et al., 2001, Noda et al., 1996). Furthermore, whilst some reversibility still exists, overall the liver fibrosis in this model seems less reversible than CCl_4, with persistent cirrhosis seen after protracted recovery times (Gu et al., 2011, Noda et al., 1996). The use of oral TAA in mice, however, is only rarely described in the literature (Hung et al., 2005, Salguero Palacios et al., 2008), with very limited data on the degree of fibrosis regression observed following cessation of injury.

Given the role of macrophages in liver fibrosis resolution (Duffield et al., 2005), I sought to study macrophage heterogeneity in these fibrosis models, with the aim of identifying a specific macrophage subtype associated with the regression of liver fibrosis. As previously described, macrophages are multifunctional and plastic cells and the identification of macrophage subsets in the liver largely relies on flow cytometric analysis to simultaneously assess the expression of a number of cell surface markers (Holt et al., 2008, Karlmark et al., 2009). Therefore, having developed and characterised murine liver fibrosis models, I sought to identify distinct hepatic macrophage populations, with the overall aim of identifying specific populations which were most associated with fibrosis resolution.

In terms of the cell surface markers to be used, Holt and colleagues defined that the hepatic macrophage pool is principally made up of 2 populations: resident tissue macrophages (Kupffer cells) and a population of "induced macrophages" (IMs) which are derived from recruited monocytes (Holt et al., 2008). These could be defined on the basis of expression of macrophage markers F4/80 and CD11b. Specifically, resident Kupffer cells were defined as $F4/80^{hi}$ $CD11b^{intermediate}$ hepatic macrophages whilst the IMs or monocyte-derived macrophages were $CD11b^{hi}$ $F4/80^{intermdediate}$. An additional marker of increasing interest is Ly-6C. This is a cell surface glycoprotein whose function remains uncertain, but is widely used to identify functionally distinct murine monocyte subsets (Gordon and Taylor, 2005, Ingersoll et al., 2009). More recently differential Ly-6C expression has been employed to identify functionally distinct murine macrophage subsets in a range of tissues including injured muscle, fibrotic kidney, mouse mammary tumours and ischaemic myocardium (Arnold et al., 2007, Lin et al., 2009, Movahedi et al., 2010, Nahrendorf et al., 2007). Indeed, a recent study has identified a $Ly\text{-}6C^{hi}$ ($Gr\text{-}1^{hi}$) hepatic macrophage population, derived from the recruitment of $Ly\text{-}6C^{hi}$ circulating monocytes via the CCL2-CCR2 chemokine axis, as being the principal pro-fibrogenic macrophage subset in the liver (Karlmark et al., 2009). Therefore, differential Ly-6C expression in combination with CD11b and F4/80 may potentially be useful in identifying distinct macrophage populations in the fibrotic liver.

The markers described, whilst useful in defining distinct macrophage populations, do not have known functional effects in liver fibrosis. One of the key features of the macrophage population responsible for the resolution of hepatic fibrosis is MMP expression to mediate, at least in part, the matrix degradation (Sakaida et al., 2003, Popov et al., 2010, Fallowfield et al., 2007, Pellicoro et al., 2011). Hence, when trying to define the pro-resolution hepatic macrophage subset, a functional readout of MMP activity will be vital. Furthermore, if this can be combined with flow cytometric analysis, the principal MMP expressing macrophage subsets could be defined. In order to achieve this, a pan-MMP substrate, MMPsense™ 680 could be used. This MMP substrate is optically silent in its unactivated state and becomes highly fluorescent when cleaved by active MMPs. It is not specific to individual MMPs, but rather is activated by a number of key MMPs including MMP-2, -3, -9 and -13, thus giving an indication of overall MMP activity. In a recent study, *in vivo* administration of MMPsense™ to mice, enabled flow cytometric identification and quantification of MMP activity in lung eosinophils in a model of allergic airway inflammation (Cortez-Retamozo et al., 2008). The authors also demonstrated a critical role for MMP-12 in the *in vivo* activation of MMPsense™, an enzyme we have previously shown to be expressed in macrophages in the fibrotic liver, and which is critical to elastin turnover (Pellicoro et al., 2011). Hence, the use of MMPsense™ 680 in liver fibrosis models might identify the main MMP expressing and hence likely restorative macrophage population.

AIMS

- To establish and characterise a reversible murine model of CCl_4 induced hepatic fibrosis
- To determine the utility of oral TAA as a murine model of reversible hepatic fibrosis
- To study macrophage heterogeneity in murine models of hepatic fibrosis
- To identify a macrophage subset associated with the resolution of hepatic fibrosis

RESULTS

Distinct Phases of Fibrogenesis and Fibrosis Resolution Following Chronic CCl_4 Administration

I established and characterised a model of reversible murine hepatic fibrosis by administration of twice weekly CCl_4 to adult male C57BL/6 mice for 4 weeks (9 injections in total), followed by harvests at serial timepoints (24, 48, 72, 96, 168 and 256 hrs) following

the final CCl_4 injection (as shown in Experimental Schematic **Fig. 3.1A**). Comparison was made to age-matched uninjured control mice. Previous data from within our group has demonstrated that olive oil (vehicle) controls are identical to uninjured mice in terms of fibrosis, and in any case the experimental aim was to compare time-related changes following CCl_4 dosing, rendering olive oil controls redundant in this context.

As shown in **Figures 3.1B** and **3.1C** and described in the associated legend, total hepatic fibrosis was quantified by Picrosirius Red staining (PSR) and morphometric pixel analysis at each timepoint (24, 48, 72, 96, 168 and 256 hrs; n=4 per timepoint) following the final CCl_4 injection. These data demonstrate that scar accumulation is occurring at 24 hrs after the final CCl_4 injection in this 4 week model, whilst liver fibrosis peaks 48-72 hours, followed by fibrosis resolution. The most rapid resolution occurs between 72 and 96 hours with a more progressive protracted regression thereafter.

As shown in **Figures 3.2** and **Fig 3.3** and described in detail in the legends, I went on to assess hepatic levels of the main fibrillar collagens, Collagen 3 and Collagen 1 respectively, by immunohistochemical staining and morphometric pixel analysis. Analysis was again performed on tissue harvested 24, 48, 72, 96, 168 and 256 hrs (n=4 per timepoint) following the final CCl_4 injection after 4 weeks of iterative injury, with comparison to age-matched uninjured control mice. These data again demonstrate that net collagen deposition is occurring at 24 hrs after the final CCl_4 with hepatic collagen levels peaking at 48-72 hrs, followed by fibrosis resolution with the most rapid resolution occurring between 72 and 96 hrs.

I then proceeded to quantify myofibroblast activation, the main scar producing cells in hepatic fibrosis, by immunohistochemistry and morphometric pixel analysis of α-SMA (as shown in **Fig 3.4** and described in the legend), using the same experimental timepoints as before (n=4 per timepoint). In keeping with the observed timing of scar accumulation and peak fibrosis, myofibroblast activation is high between 24 and 72 hrs following the final CCl_4 injection, followed by a rapid loss of α-SMA expression between 72 and 96 hrs with a more protracted loss of the residual myofibroblasts thereafter.

In order to confirm the consistency and reproducibility of these findings, this experimental time course has been repeated in our group in 2 independent experiments, with 4-6 mice per timepoint (in collaboration with Dr Steven Hartland). These studies showed an identical pattern to that presented in **Fig 3.1 to 3.4**. Furthermore, as shown and described in the

respective figure legends, the changes observed in this model show statistically robust changes, suggesting this is a useful model to study mechanisms of fibrosis resolution.

Figure 3.1 – Murine Model of Reversible of Hepatic Fibrosis

(**A**) Schematic representation of model of reversible hepatic fibrosis in C57BL/6 mice by 4 weeks of twice-weekly intraperitoneal carbon tetrachloride (CCl_4) followed by harvest at serial timepoints following the final injection. Comparisons were made to control (uninjured) animals. (**B**) Representative images of hepatic picrosirius red staining (PSR) are shown for control animals and each timepoint (Scale bar=100μm). (**C**) Quantification of histological changes of PSR by morphometric pixel analysis (Expressed relative to mean % area of control animals; n=4 per timepoint). Data shown as Mean±S.E.M; **P*<0.05, ***P*<0.01, ****P*<0.001.

Figure 3.1 - Murine Model of Reversible Hepatic Fibrosis

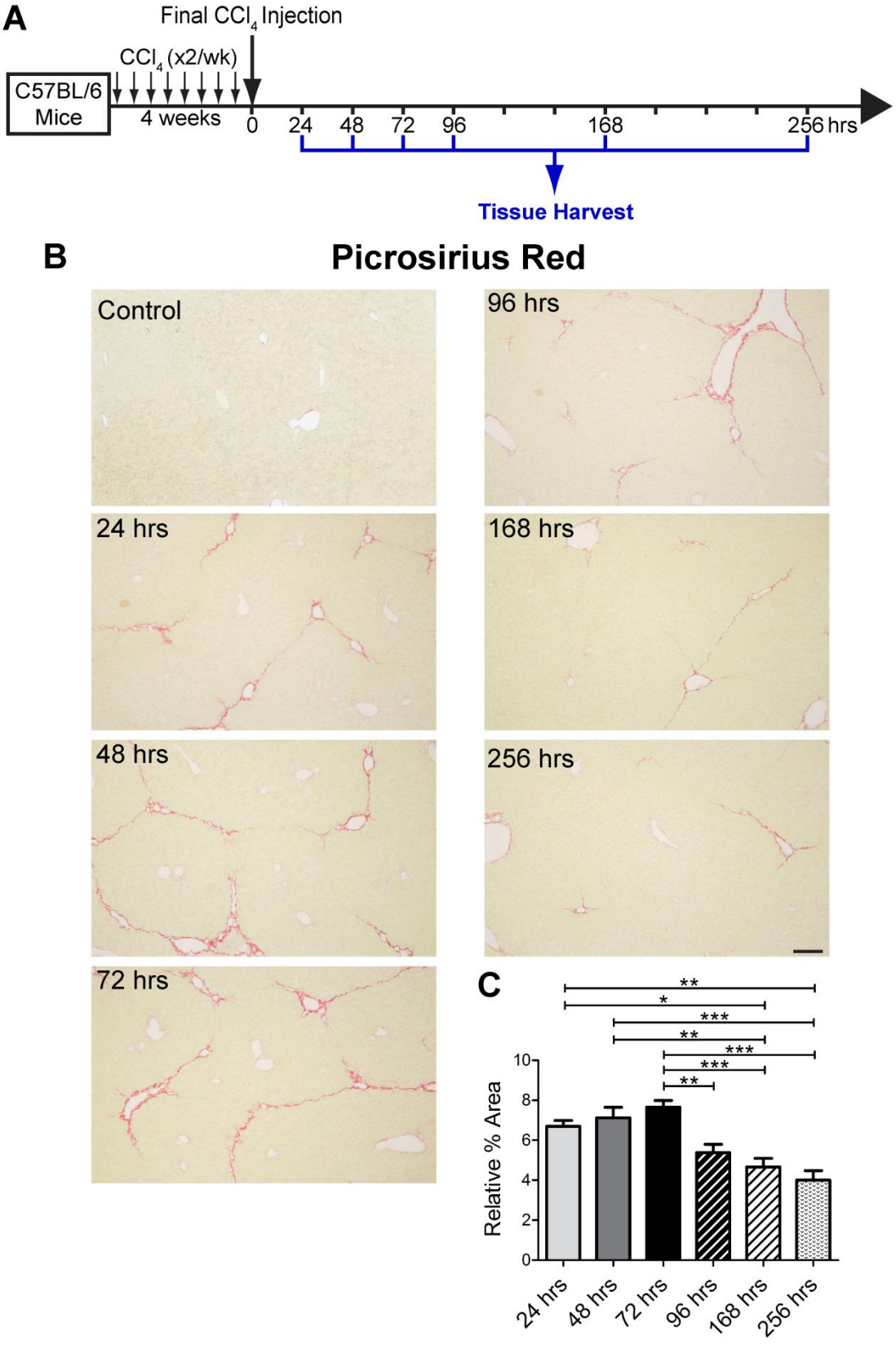

Figure 3.2 – Quantification of Hepatic Collagen 3 following Cessation of CCl_4 Injury

(**A**) Representative images of hepatic collagen 3 immunohistochemistry are shown for control (uninjured) animals and each timepoint following cessation of CCl_4 (Scale bar=100μm). (**B**) Quantification of histological changes of Collagen 3 by morphometric pixel analysis (Expressed relative to mean % area of control animals; n=4 per timepoint). Data shown as Mean±S.E.M; **P*<0.05, ***P*<0.01.

Figure 3.2 - Quantification of Hepatic Collagen 3 following Cessation of CCl_4 Injury

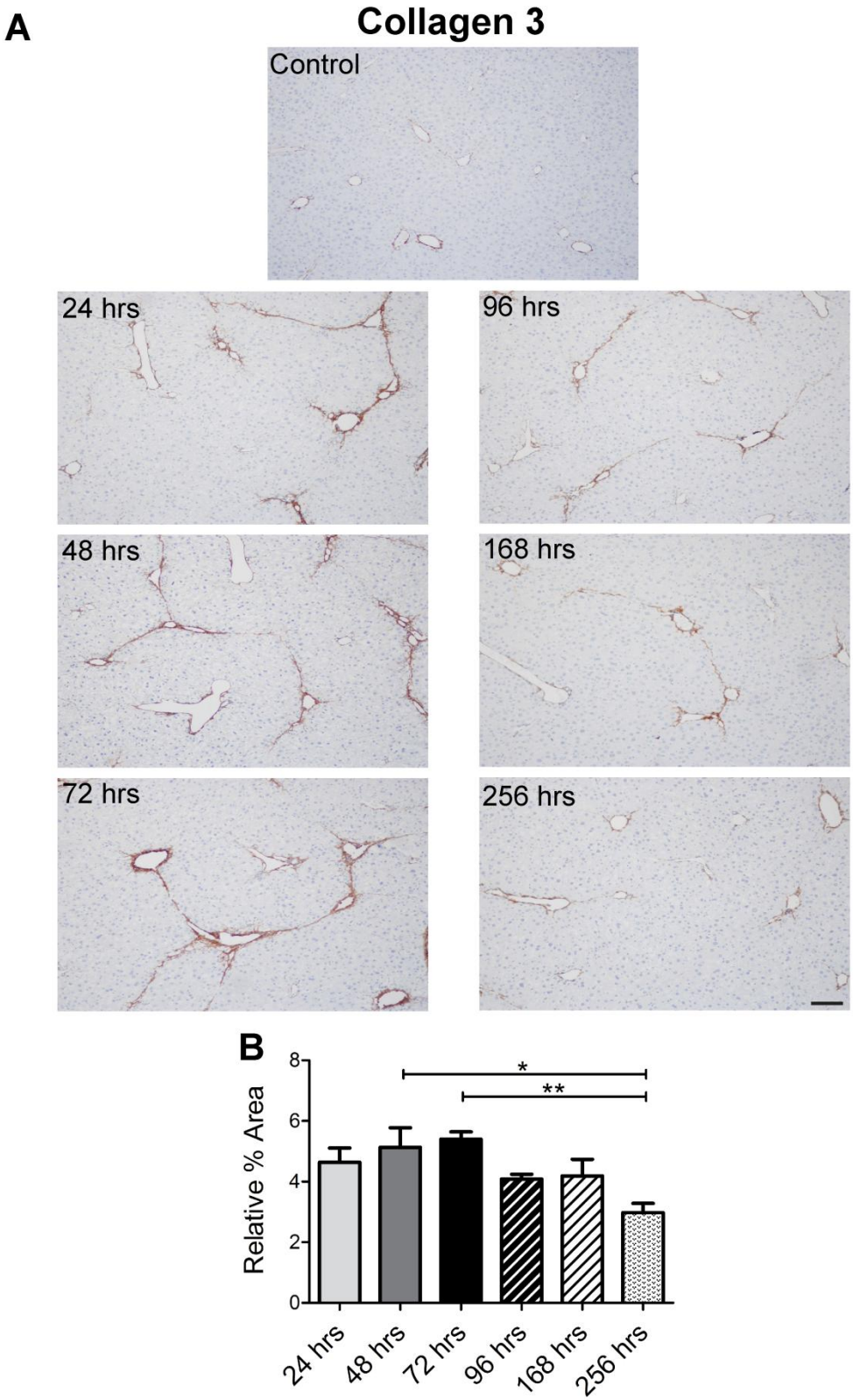

Figure 3.3 - Quantification of Hepatic Collagen 1 following Cessation of CCl_4 Injury

(**A**) Representative images of hepatic collagen 1 immunohistochemistry are shown for control (uninjured) animals and each timepoint following cessation of CCl_4 (Scale bar=100μm). (**B**) Quantification of histological changes of Collagen 1 by morphometric pixel analysis (Expressed relative to mean % area of control animals; n=4 per timepoint). Data shown as Mean±S.E.M; **P*<0.05.

Figure 3.3 - Quantification of Hepatic Collagen 1 following Cessation of CCl_4 Injury

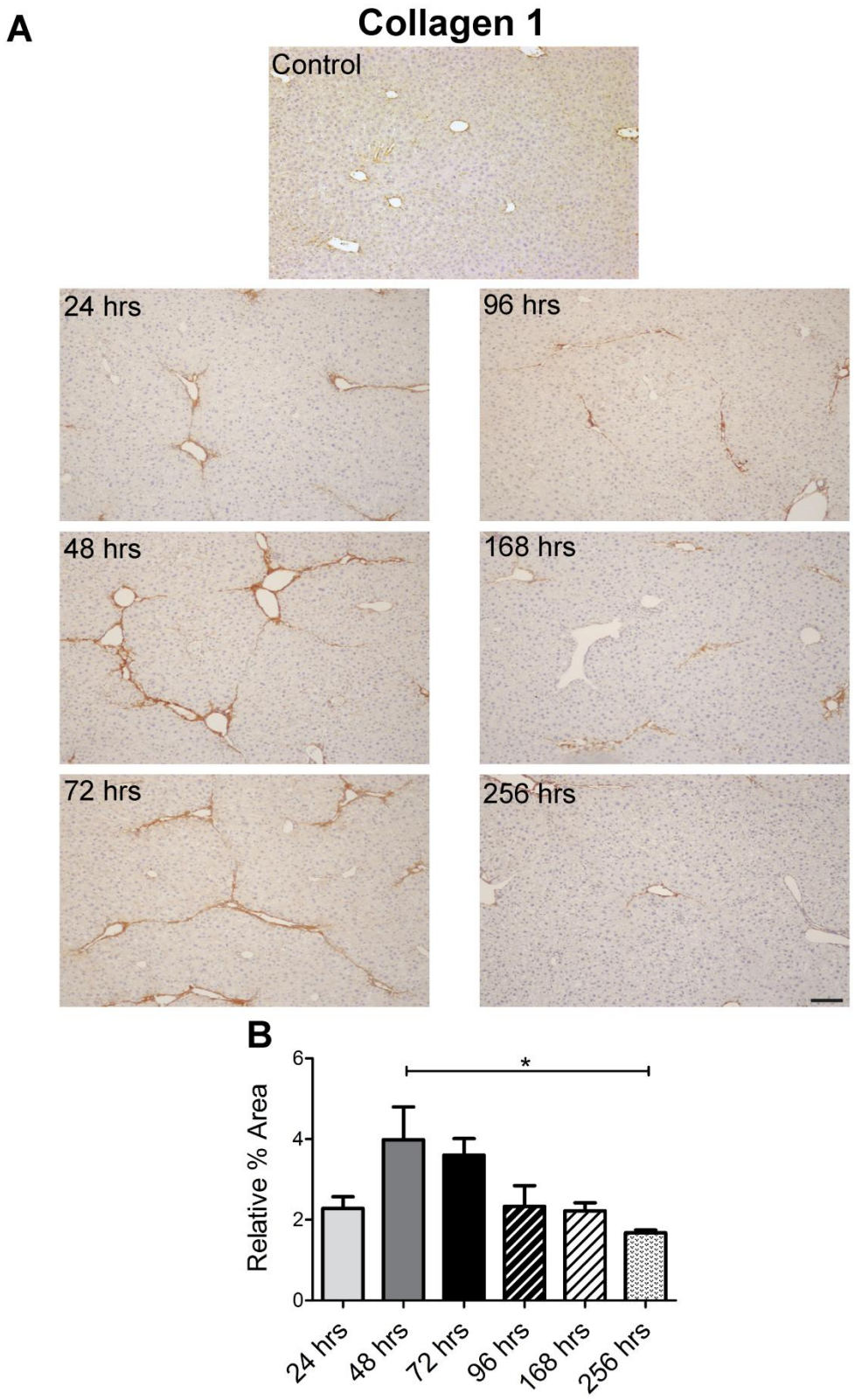

Figure 3.4 - Quantification of Hepatic Myofibroblast Activation following Cessation of CCl_4 Injury

(**A**) Representative images of hepatic α-smooth muscle actin (α-SMA) immunohistochemistry are shown for control (uninjured) animals and each timepoint following cessation of CCl_4 (Scale bar=100μm). (**B**) Quantification of histological changes of α-SMA by morphometric pixel analysis (Expressed relative to mean % area of control animals; n=4 per timepoint). Data shown as Mean±S.E.M; **P*<0.05, ***P*<0.01, ****P*<0.001.

Figure 3.4 - Quantification of Hepatic Myofibroblast Activation following Cessation of CCl_4 Injury

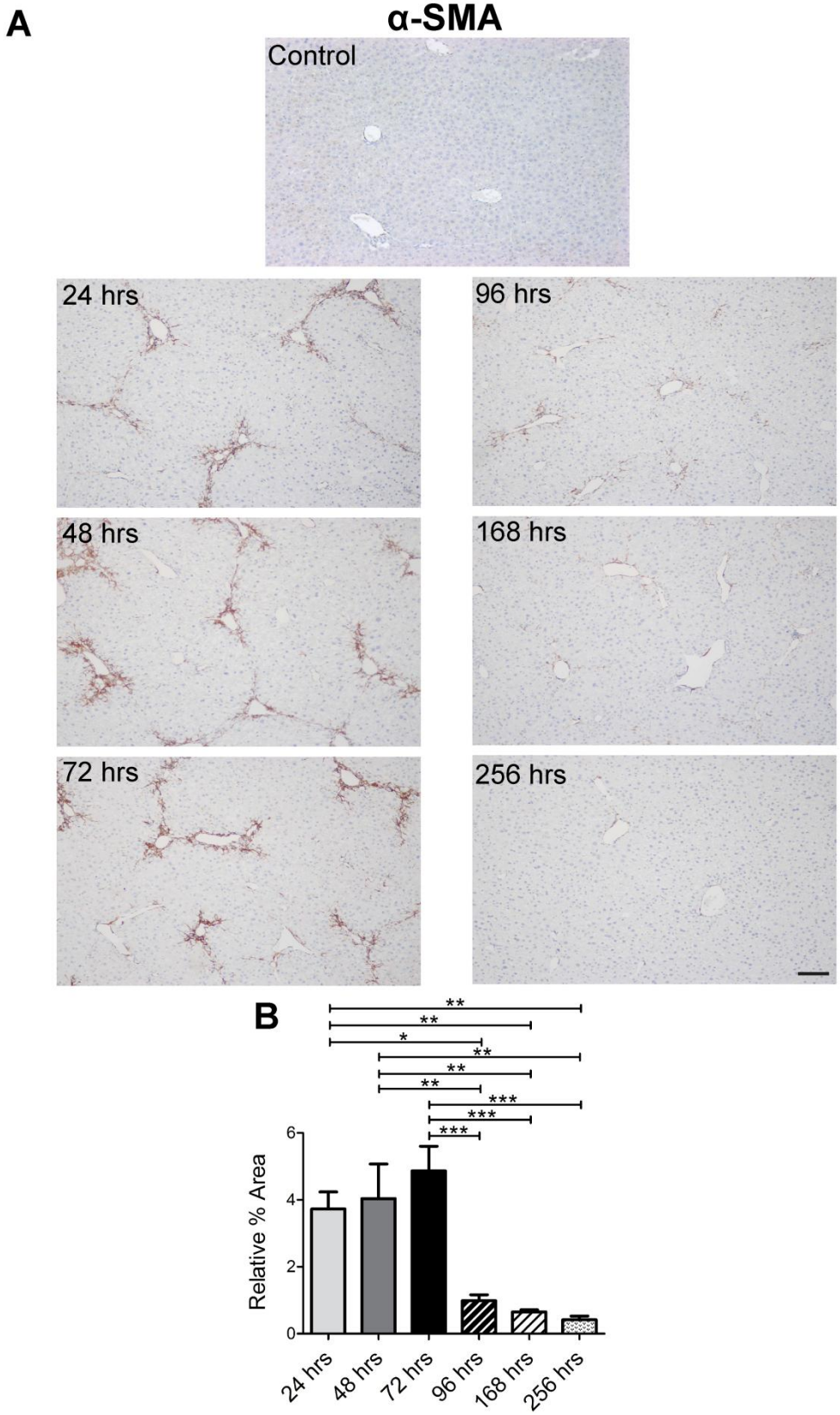

Fibrosis Resolution following Chronic CCl_4 Occurs Following a Reduction in Hepatic Inflammation and TIMP-1 levels

Given the close relationship between inflammation and fibrosis, I sought to determine the temporal relationship between the changes in hepatic fibrosis and hepatic inflammation in the 4 week CCl_4 model which I have described (**Fig 3.1A**). Alanine transaminase (ALT) and Aspartate transaminase (AST) are enzymes normally present within hepatocytes and are released into the circulation following hepatocyte death. Thus, serum levels of ALT and AST are surrogates for the degree of liver damage in both human disease and animal models. Measurement of serum ALT and AST at 24, 48, 72, 96 and 168 hrs following the final CCl_4 injection after 4 weeks of injury (n=5-6 per timepoint from 2 independent experiments), demonstrated that both serum AST and ALT peaked at 24 hrs, the time of active scar accumulation above, and had returned to baseline levels by 72 hrs (**Fig. 3.5A**).

To more directly study the degree of hepatic inflammation in the 4 week CCl_4 model, I proceeded to quantify hepatic protein levels of a number of inflammatory cytokines and chemokines at 24, 48, 72, 96 and 168 hrs following the cessation of CCl_4 injections (**Fig 3.5B;** n=7-9 per timepoint from 2 independent experiments). In order to do this I established a method utilising a multiplex cytokine ELISA on whole liver homogenates. As shown, hepatic levels of important pro-inflammatory cytokines and chemokines IL-1β, CCL2, CCL3 and CXCL2 peak at the 24 hr timepoint and have rapidly declined by 72 hrs (**Fig 3.5B**). Using the same multiplex ELISA, no significant differences were detected in hepatic levels of TNF-α, IFN-γ, IL-4, IL-13, IL-10, IL-6, RANTES, CCL4 or CXCL1 at the studied timepoints. However, technical issues such as the sensitivity of the assay or the stability of individual proteins during sample preparation must be considered in the interpretation of these negative results

Our group and others have previously shown that a reduction in hepatic TIMP-1 levels causes an increase in matrix degrading activity and is a pre-requisite for fibrosis resolution (Iredale, 2007, Iredale et al., 1998, Ramachandran and Iredale, 2009). In my 4 week CCl_4 model, I proceeded to quantify whole liver TIMP-1 at a gene (**Fig 3.5C;** n=4-8 from 2 independent experiments) and protein level (**Fig. 3.5D**). These data demonstrate that in this model, TIMP-1 levels peak at 24 hrs and have declined by 72 hrs.

Figure 3.5 – Quantification of Hepatic Inflammation and TIMP-1 levels following Cessation of CCl_4 Injury

(**A**) Serum Alanine aminotransferase (ALT) and Aspartate aminotransferase (AST) levels in control (uninjured) mice and at stated timepoint following the final CCl_4 injection (n=5-6 per timepoint from 2 independent experiments). (**B**) Whole liver protein levels of IL-1β, CCL2, CCL3 and CXCL2 measured by multiplex cytokine assay at stated timepoint following final CCl_4 injection (Expressed relative to mean protein concentration at 24 hr timepoint for each; n=7-9 per timepoint from 2 independent experiments). (**C**) Whole liver Timp-1 gene expression measured by qPCR at stated timepoints following the final CCl_4 injection (Expressed relative to mean expression at 24 hr timepoint; n=4-8 from 2 independent experiments). (**D**) Whole liver TIMP-1 protein expression assessed by western blot (representative blot shown; Blot performed in collaboration with Dr Timothy Gordon-Walker). All data shown as Mean±S.E.M; **P*<0.05, ***P*<0.01, ****P*<0.001.

Figure 3.5 - Assessment of Hepatic Inflammation and TIMP-1 Following Cessation of CCl_4 dosing

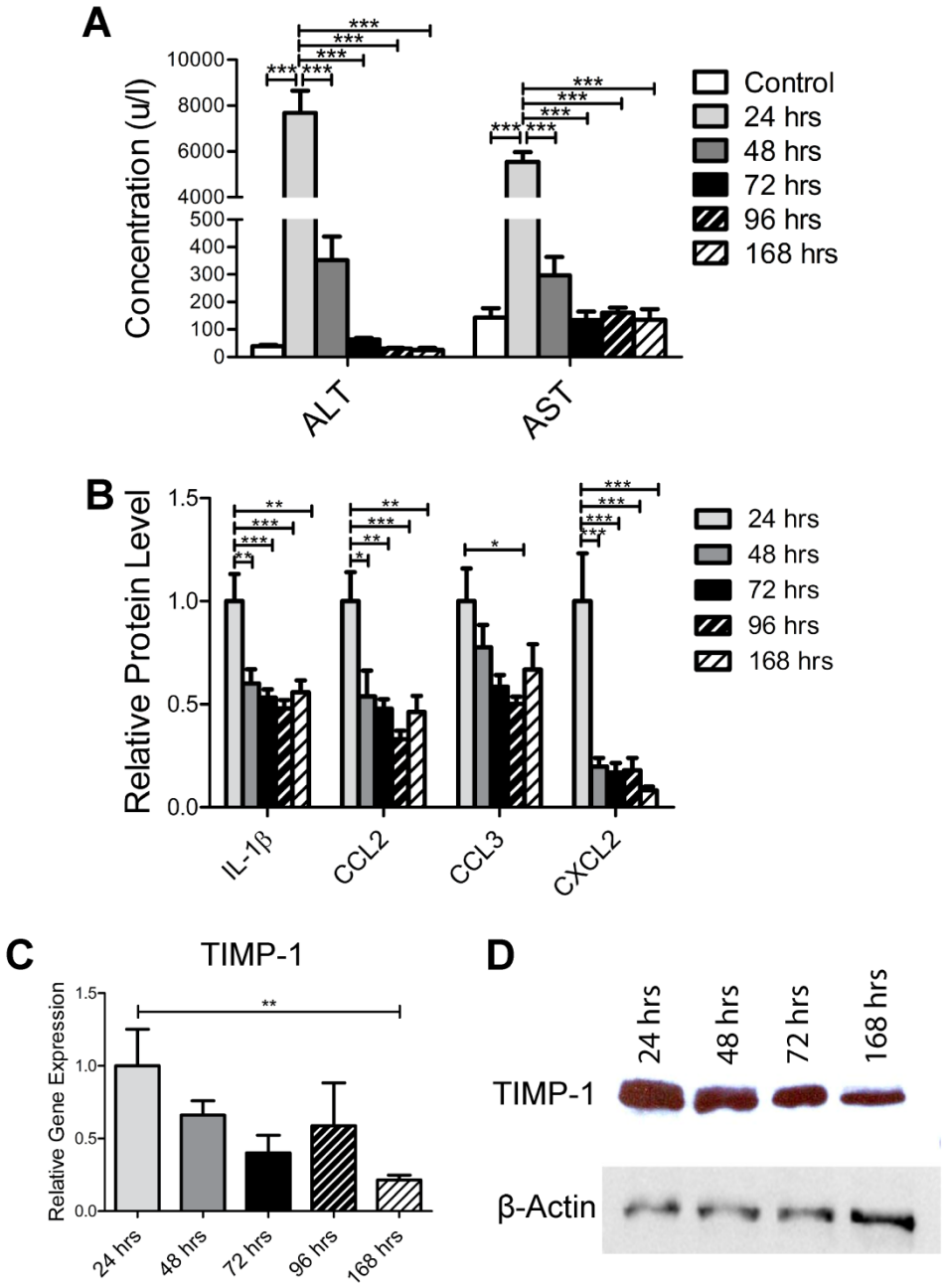

High Dose Oral TAA Administration to Mice Causes a Progressive Fibrotic Response

I sought to determine the utility of oral thioacetamide (TAA) as a second murine model of hepatic fibrosis. I established cohorts of C57BL/6 mice on either low dose (300mg/l) or high dose (600mg/l) thioacetamide in their drinking water, with tissue harvests following 8, 12, 16, 20, 36 and 52 weeks of treatment (as shown in **Fig 3.6A** and described in the legend). These animals were compared to uninjured control animals, maintained on normal water.

Animals were weighed weekly throughout the experimental protocol. As shown, both doses of TAA caused a significant reduction in the animals' weight, and inhibited weight gain throughout the treatment period (**Fig 3.6B**). Livers were analysed for total hepatic fibrosis by picrosirius red (PSR) staining and morphometric pixel analysis following treatment with each dose of TAA for 8, 12, 16, 20, 36 and 52 weeks (**Fig 3.6C and 3.6D;** n=2-7 per timepoint). As shown, treatment with low dose TAA, even for 52 weeks, did not induce a significant degree of hepatic fibrosis (**Fig 3.6C and 3.6D**). However, high dose TAA caused a progressively worsening degree of hepatic fibrosis over the treatment duration, with statistically significant increases in PSR staining detectable as early as 8 weeks of treatment (**Fig 3.6C and 3.6D**). Indeed, morphological analysis of livers from animals after 52 weeks of high dose TAA demonstrates established cirrhosis (**Fig 3.6C**). Importantly administration of normal water for 52 weeks did not in itself cause a significant increase in hepatic fibrosis (**Fig 3.6D**).

Figure 3.6 – High Dose Oral Thioacetamide induces a Progressive Hepatic Fibrosis

(**A**) Schematic representation of model of thioacetamide (TAA) induced hepatic fibrosis in male C57BL/6 mice. TAA was administered continuously in the drinking water at either low dose (300mg/L; blue) or high dose (600mg/L; red) to adult mice. Animals were harvested following stated durations on TAA treatment. Comparisons were made to control animals, maintained on normal drinking water. (**B**) Average mouse weight was measured on a weekly basis during treatment with low dose and high dose TAA and compared to weight on normal drinking water (n=3-39). (**C**) Representative images of hepatic picrosirius red staining (PSR) are shown for treatment with low and high dose TAA for the stated duration (Scale bar=100μm). (**D**) Quantification of histological changes of PSR by morphometric pixel analysis compared to control (8 weeks of water) animals (Expressed relative to mean % area of control animals; n=2-7 per timepoint). Data shown as Mean±S.E.M; **P*<0.05, ***P*<0.01, ****P*<0.001.

Figure 3.6 - High Dose Oral Thioacetamide Induces a Progresive Hepatic Fibrosis

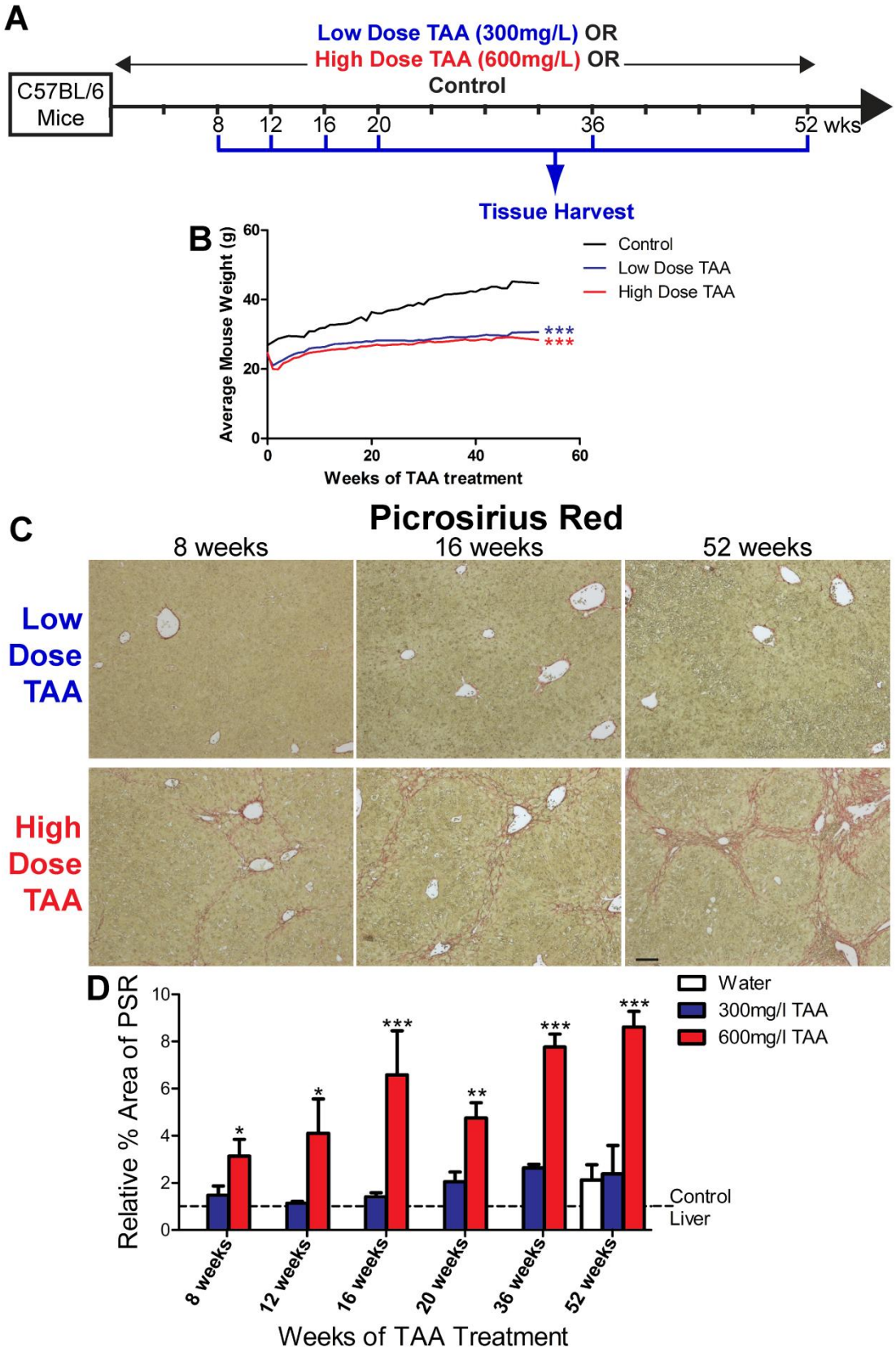

Liver Fibrosis following High Dose Oral TAA is Irreversible in the Short-Term

Having established that high dose oral TAA induces detectable hepatic fibrosis by 8 weeks of treatment and cirrhosis by 52 weeks (**Fig 3.6C and 3.6D**), I then aimed to determine whether fibrosis induced by oral TAA was reversible and could be used as a fibrosis regression model. C57BL/6 mice were administered high dose oral TAA (600mg/l) continuously in the drinking water for either 8 weeks or 52 weeks. Cohorts of animals were then changed back onto normal drinking water and organs harvested at 72 hrs (for 8 week treatment group only) and 1, 2 and 8 weeks following the cessation of TAA treatment (as shown in **Fig 3.7** and described in the legend). Comparison was made to an age-matched control group, kept on normal water throughout. To assess hepatic fibrosis, livers were harvested and stained for PSR followed by morphometric pixel analysis. As shown, following 8 weeks of 600mg/l TAA treatment, no significant regression of liver fibrosis was observed for recovery times of up to 8 weeks (**Fig 3.7A;** n=4-5 per timepoint). Similarly, after high dose TAA treatment for 52 weeks, no significant fibrosis reversibility was evident following cessation of injury for up to 8 weeks (**Fig 3.7B;** n=3-5 per timepoint)

Figure 3.7 – Liver Fibrosis following High Dose Oral TAA is Irreversible in the Short Term

(**A**) Quantification of histological changes of PSR by morphometric pixel analysis in C57BL/6 mice treated with high dose TAA for 8 weeks, followed by conversion onto normal drinking water (recovery) for the stated amount of time (Expressed relative to mean % area of control (uninjured) animals; n=4-5). (**B**) Quantification of histological changes of PSR by morphometric pixel analysis in C57BL/6 mice treated with high dose TAA for 52 weeks, followed by conversion onto normal drinking water (recovery) for the stated amount of time (Expressed relative to mean % area of control (uninjured) animals; n=3-5). Data shown as Mean±S.E.M.

Figure 3.7 - Liver Fibrosis following High Dose Oral TAA is Irreversible in the Short Term

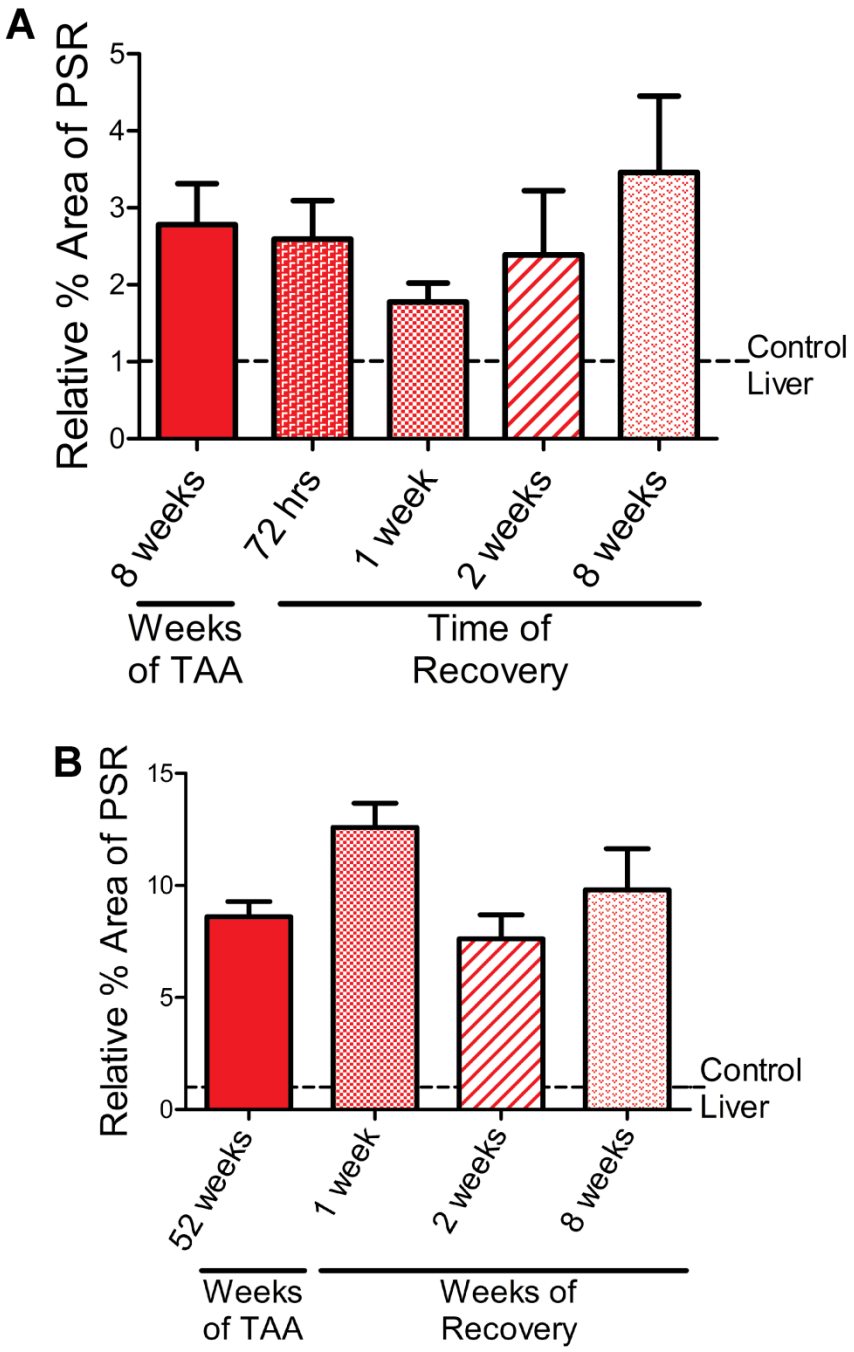

Macrophages Localise around Hepatic Scars at Maximal Fibrosis Resolution

Having characterised the CCl_4 and TAA models in terms of fibrosis, I then wished to study the macrophage populations. I initially wanted to assess whether there were any gross differences in macrophage localisation during the distinct phases of inflammation/fibrogenesis, maximal fibrosis resolution and late resolution in the 4 week CCl_4 model. I focussed on key timepoints of 24 hrs, 72 hrs and 168 hrs following the final CCl_4 injection. As shown previously (**Fig 3.1 to 3.4**), these points represent a time of active scar deposition (24 hrs), the initiation of maximal scar resolution (72 hrs) and a time of more protracted fibrosis regression (168 hrs).

F4/80 is a cell surface glycoprotein, which is used a murine pan-macrophage maker. Immunohistochemistry for F4/80 in livers in the CCl_4 model demonstrated a clear topographic change during the distinct phases (**Fig 3.8A**). At 24 hrs, the time of hepatic inflammation and fibrogenesis, F4/80 positive macrophages are diffusely infiltrating the liver parenchyma, with numerous cells in Zones 1 and 2, surrounding the areas of maximal hepatocyte death (centrilobular, Zone 3). At 72 hrs, the time of maximal fibrosis resolution, there is a clear association between liver macrophages and the hepatic scars. Indeed, the areas of scar can be easily identified by the localisation of F4/80 staining, without the need for collagen staining. By 168 hrs, when the majority of scar has resolved, F4/80 hepatic macrophages were fairly homogenously distributed through the liver parenchyma.

Hepatic Macrophage Number Peaks at Maximal Fibrosis Resolution

I proceeded to study the hepatic macrophage populations in the 4 week CCl_4 model, using multicolour flow cytometry at the key timepoints of 24 hrs, 72 hrs and 168 hrs, compared to livers from age-matched uninjured mice. Hepatic Non-Parenchymal Cells (NPCs), containing the hepatic leukocyte pool, were isolated from livers at the stated timepoints using a digestion technique as described in detail in **Chapter 2**. Of note, livers were perfused with saline prior to harvest to remove contamination from circulating cells. Hepatic macrophages were then identified using flow cytometry of NPCs. In order to specifically identify hepatic macrophages a stringent gating strategy was used (**Fig. 3.8B**). In summary, non-viable cells were excluded initially using a live-dead marker. I then proceeded to define all hepatic leukocytes using the pan-leukocyte marker CD45. On this viable $CD45^+$ population, neutrophils were first defined as $CD11b^+$ $Ly\text{-}6G^+$ cells and T cells, B cells and NK cells identified by positivity for CD3, B220 and NK1.1. Both the neutrophils and these other immune populations were excluded from further analysis when defining the

macrophages. Macrophages were then identified from the remaining cells as $CD11b^+$ $F4/80^+$. Thus, hepatic macrophages were classified as $CD45^+$ $Ly\text{-}6G^-$ $CD3^-$ $NK1.1^-$ $B220^-$ $CD11b^+$ $F4/80^+$ cells. The genuine nature of all staining was confirmed by comparison to appropriate isotype control antibodies. This strategy robustly and reproducibly identified macrophages on the basis of expression of 2 specific markers, whilst minimising contamination from other immune cells such as neutrophils, NK cells, B cells and T cells. This therefore represents the most specific method for studying macrophage heterogeneity.

Having identified hepatic macrophages by flow cytometry, I proceeded to quantify the total number of macrophages in the CCl_4 model during inflammation/fibrogenesis (24 hrs), maximal resolution (72 hrs) and late resolution (168 hrs), in comparison to age matched uninjured mice (**Fig 3.8C;** n=8-12 per timepoint). Macrophage number was initially quantified as a proportion of total NPCs by flow cytometry, which enabled quantification of absolute number per liver on the basis of total NPC counts. As shown in **Fig 3.8C** and described in the legend, hepatic macrophage number, whilst increased compared to uninjured controls at the 24 hr timepoint, actually peaked at the 72 hr timepoint and returned towards baseline by 168 hrs. This indicates that the maximum numbers of macrophages are present at the initiation of scar resolution (72 hrs) in this model.

I was also able to quantify the number of hepatic neutrophils, which have also been associated with fibrosis resolution by some authors (Harty et al., 2008, Harty et al., 2010). As shown, hepatic neutrophil number peaked at 24 hrs, having returned to near control levels by the 72 hr timepoint (**Fig. 3.8D;** n=10-17 per timepoint).

Figure 3.8 – Identification and Quantification of Hepatic Macrophages in Reversible Fibrosis Model

Analysis of hepatic macrophages after the final CCl_4 injection following 4 weeks of injury. (**A**) F4/80 immunohistochemistry of livers at stated timepoint following the final CCl_4 injection indicates that macrophages localise around areas of scar at time of maximal fibrosis resolution (72 hrs) (representative images shown; scale bar=100μm). (**B**) Gating strategy for identification of hepatic macrophages. The hepatic non-parenchymal cell fraction was isolated. Viable cells were selected by propidium iodide (PI) exclusion. CD45 positive viable cells were gated. Cells positive for CD3, B220 or NK1.1 were excluded from subsequent macrophage gating. Neutrophils were identified as Viable CD45+ CD11b+ and Ly-6G+ cells, and were excluded from subsequent macrophage gating. Macrophages were selected as viable CD45+ Ly-6G- NK1.1- B220- CD3- and dual-positive CD11b+ F4/80+ cells. Representative flow cytometry plots are shown. (**C**) Total hepatic macrophage number was quantified by flow cytometry at stated timepoint following the final CCl_4 injection or in control (uninjured) mice (Expressed relative to mean number of macrophages in control liver; n=8-12 per timepoint from 2 independent experiments). (**D**) Total hepatic neutrophil number was quantified by flow cytometry at stated timepoint following the final CCl_4 injection or in control (uninjured) mice (Expressed relative to mean number of neutrophils in control liver; n=10-17 per timepoint from 3 independent experiments). Data shown as Mean±S.E.M; **P*<0.05, ***P*<0.01, ****P*<0.001.

Figure 3.8 - Identification and Quantification of Hepatic Macrophages in Reversible Fibrosis Model

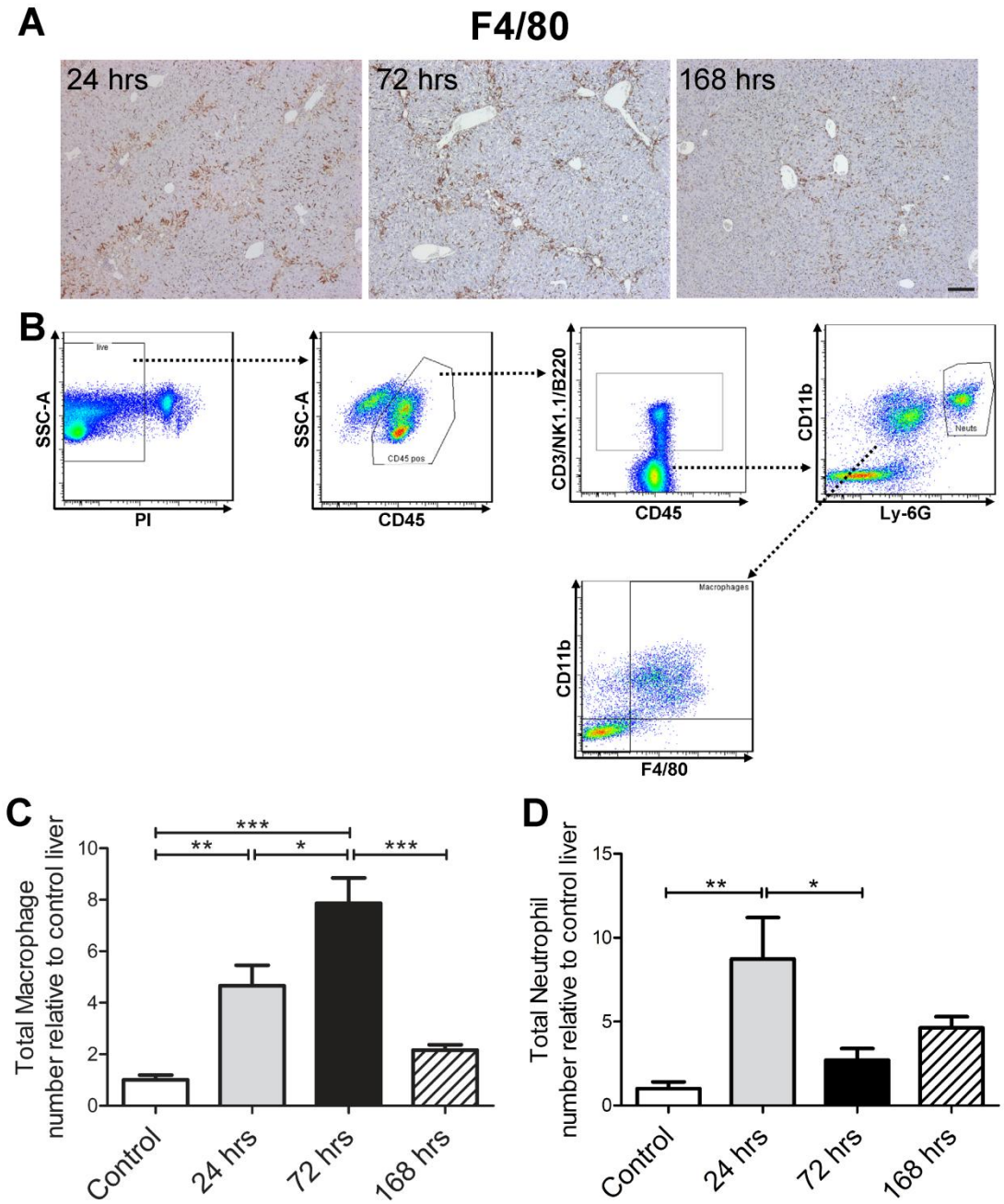

Resident Kupffer Cells are reduced during Fibrogenesis and Reaccumulate during Fibrosis Resolution

Having identified hepatic macrophages on flow cytometry, I then sought to study the heterogeneity of these cells by examining differential expression of additional cell surface markers. I initially focussed on identifying the previously defined resident tissue macrophages (Kupffer cells) and monocyte-derived macrophages on the basis of CD11b and F4/80 expression (Holt et al., 2008). I performed a similar analysis on hepatic macrophages isolated from the CCl_4 model (**Fig. 3.9A**). I could clearly identify 2 distinct macrophage populations, analogous to those seen in the previously published work: $CD11b^{hi}$ $F4/80^{intermediate}$ monocyte-derived macrophages and $F4/80^{hi}$ $CD11b^{intermediate}$ "resident" macrophages.

Focussing on the $F4/80^{hi}$ $CD11b^{int}$ resident macrophages, as expected these cells represented the predominant macrophage subset in uninjured control livers, making up 67.5±6.6% of the total macrophage pool (**Fig. 3.9A and 3.9C;** n=10-17 per timepoint). Using the 4 week CCl_4 fibrosis model, the relative contribution of resident macrophages to the hepatic macrophage pool had declined significantly at the 24 hr timepoint (12.2±3% at 24 hrs). There was then a progressive reaccumulation of the resident macrophage subset during fibrosis resolution, making up 24.9±2.5% at maximal resolution (72 hrs) and 48.7±26% during late resolution (168 hrs) (**Fig. 3.9A and 3.9C**). A similar trend was seen when absolute numbers of resident macrophages were quantified, and expressed relative to the total macrophage number in control livers (**Fig. 3.9D;** n=12-17 per timepoint). This confirms a reduction in resident macrophage number at 24 hrs and a progressive increase during fibrosis resolution.

Differential Ly-6C Expression Identifies a Novel Hepatic Monocyte-Derived Macrophage Population which Accumulates at Maximal Fibrosis Resolution

As described above, differential Ly-6C expression is potentially useful for defining distinct macrophage subsets in tissue. I therefore assessed Ly-6C expression on the hepatic $CD11b^{hi}$ $F4/80^{int}$ monocyte-derived macrophage subset, isolated from livers at 24, 72 and 168 hrs after the final CCl_4 injection in the 4 week CCl_4 model (**Fig. 3.9B**). Using this strategy, I could clearly identify 2 distinct subpopulations of hepatic monocyte-derived macrophages: $Ly\text{-}6C^{hi}$ and $Ly\text{-}6C^{lo}$. Critically, these changed dynamically during these key timepoints. As shown in **Fig 3.9B,** quantified in **Fig 3.9C** (n=10-17 per timepoint) and described in detail in the accompanying legend, $Ly\text{-}6C^{hi}$ macrophages represented the principal subset at 24 hrs (43.44±2.1% of the total macrophage pool). However at 72 hrs, the time of maximal fibrosis

resolution, there is loss of the Ly-6C^{hi} population and a significant increase in Ly-6C^{lo} monocyte-derived macrophages, making up 63.6±2.8% of the macrophage population at this timepoint (**Fig. 3.9B and 3.9C)**. This dramatic change is even more pronounced when macrophage number is quantified, demonstrating that Ly-6C^{lo} macrophages at 72 hours are the most numerous macrophage subset at any studied timepoint during the fibrogenesis-resolution model, 4.14±0.5 times more than the total macrophage number in control liver (**Fig. 3.9D;** n=12-17 per timepoint).

During late resolution (168 hrs), both the proportion and number of Ly-6C^{hi} macrophages had returned to control levels. There remained an increase in the number and proportion of Ly-6C^{lo} macrophages, but these had declined compared to the 72 hr timepoint, when matrix degradation was maximal (**Fig. 3.9B, 3.9C and 3.9D**).

Figure 3.9 – Dynamic Changes in Hepatic Macrophage Subsets in Reversible Fibrosis Model

Analysis of hepatic macrophages at stated timepoints after the final CCl_4 injection following 4 weeks of injury. Comparison was made to control (uninjured) mice. (**A**) $F4/80^{hi}$ $CD11b^{int}$ "resident" Kupffer cells during injury and resolution (Representative percentages indicate $F4/80^{hi}$ $CD11b^{int}$ cells as proportion of total macrophages). (**B**) Subset analysis of $CD11b^{hi}$ $F4/80^{int}$ monocyte-derived macrophages on the basis of differential Ly-6C expression identifies 2 distinct populations: Ly-$6C^{hi}$ and Ly-$6C^{lo}$ with dynamic changes during injury and resolution (Representative percentages indicate each subset as a proportion of total hepatic macrophages). (**C**) Quantification of Ly-$6C^{hi}$, Ly-$6C^{lo}$ and Resident macrophage subsets, as a proportion of total hepatic macrophage number (n=10-17 per timepoint from 4 independent experiments). (**D**) Relative number per liver of each macrophage subset at stated timepoint (Expressed relative to mean total macrophage number in control liver; n=12-17 per timepoint from 4 independent experiments). All data shown as Mean±S.E.M; *P<0.05, **P<0.01, ***P<0.001. Representative flow cytometry plots shown.

Figure 3.9 - Dynamic Changes in Hepatic Macrophage Subsets in Reversible Fibrosis Model

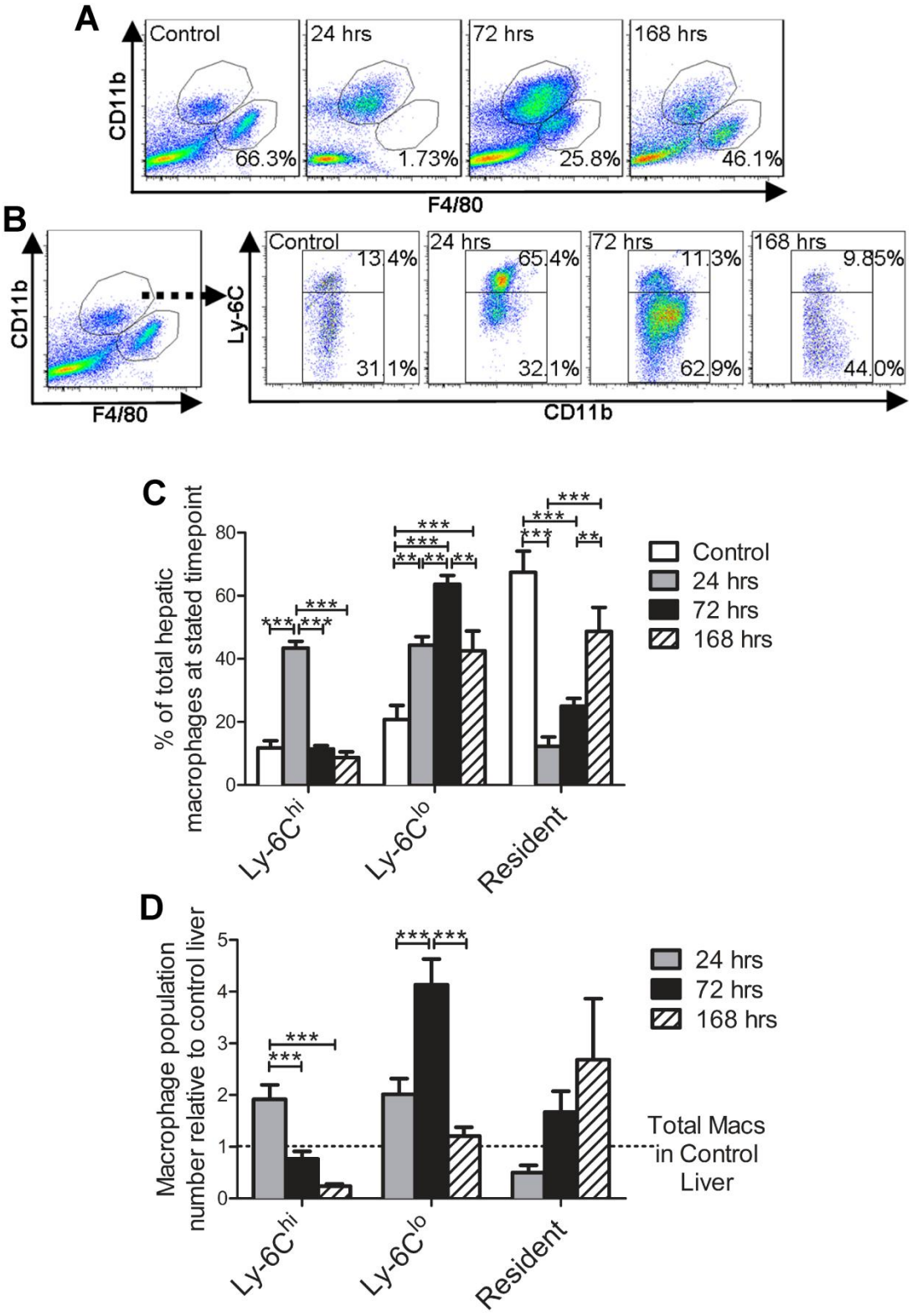

Increased Circulating Monocyte Subsets During Fibrogenesis and Fibrosis Regression

The dramatic changes in the hepatic $CD11b^{hi}$ $F4/80^{int}$ monocyte-derived macrophages during fibrogenesis and resolution, suggests changes in monocyte recruitment during these phases. I therefore sought to identify analogous changes in circulating monocyte number in the 4 week CCl_4 fibrogenesis-resolution model.

As discussed previously, 2 functionally distinct murine monocyte populations have been identified. Ly-$6C^{hi}$ monocytes (analogous to human $CD14^{hi}$ $CD16^{lo}$ human monocytes) are recruited early to inflammatory environments and thought to be pro-inflammatory whilst Ly-$6C^{lo}$ monocytes (analogous to $CD14^{lo}$ $CD16^{hi}$ human monocytes) are a more "patrolling" cell-type and can replenish resident tissue macrophages (Gordon and Taylor, 2005, Ingersoll et al., 2009). Using flow cytometry on blood, we identified circulating murine monocytes as $CD11b^{+}$ $CD115^{+}$ peripheral mononuclear cells (Geissmann et al., 2008), subsequently defining the Ly-$6C^{hi}$ and Ly-$6C^{lo}$ subsets (**Fig 3.10A**).

I proceeded to quantify each monocyte subset in our 4 week CCl_4 model. As shown, compared to normal (uninjured) animals, circulating Ly-$6C^{hi}$ "inflammatory" monocytes, as a proportion of total peripheral mononuclear cells, were increased during at the 24 hr timepoint (**Fig 3.10B;** n=5 per timepoint). As shown previously, this corresponds with maximal hepatic levels of CCL2, the principal chemokine for this monocyte subset (**Fig 3.5B**). The increase in Ly-$6C^{hi}$ monocytes persisted at 72 hrs, whilst the relative number of these cells returned towards control levels by 168 hrs (**Fig 3.10B**). Ly-$6C^{lo}$ "patrolling" monocytes were also increased at the 24 hr timepoint, although this increase was much more short- lived, returning to basal levels by 72 hrs (**Fig 3.10C**).

Figure 3.10 - Quantification of Circulating Monocyte Subsets in Reversible Fibrosis Model

(**A**) Ly-6C^{hi} and Ly-6C^{lo} circulating monocytes were identified in blood, gating on CD11b+ Ly-6G- CD115+ Ly-6C^{hi} and Ly-6C^{lo} cells. (**B**) Ly-6C^{hi} monocytes were quantified as a proportion of total circulating mononuclear cells at stated timepoints during injury and resolution following chronic CCl_4 administration and uninjured control mice (normal) (n=5) (**C**) Ly-6C^{lo} monocytes were quantified as a proportion of total circulating mononuclear cells during injury and resolution following chronic CCl_4 administration and uninjured control mice (normal) (n=5). All data expressed as Mean±S.E.M; *P<0.05, **P<0.01. Representative flow cytometry plots shown.

Figure 3.10 - Quantification of Circulating Monocyte Subsets in Reversible Fibrosis Model

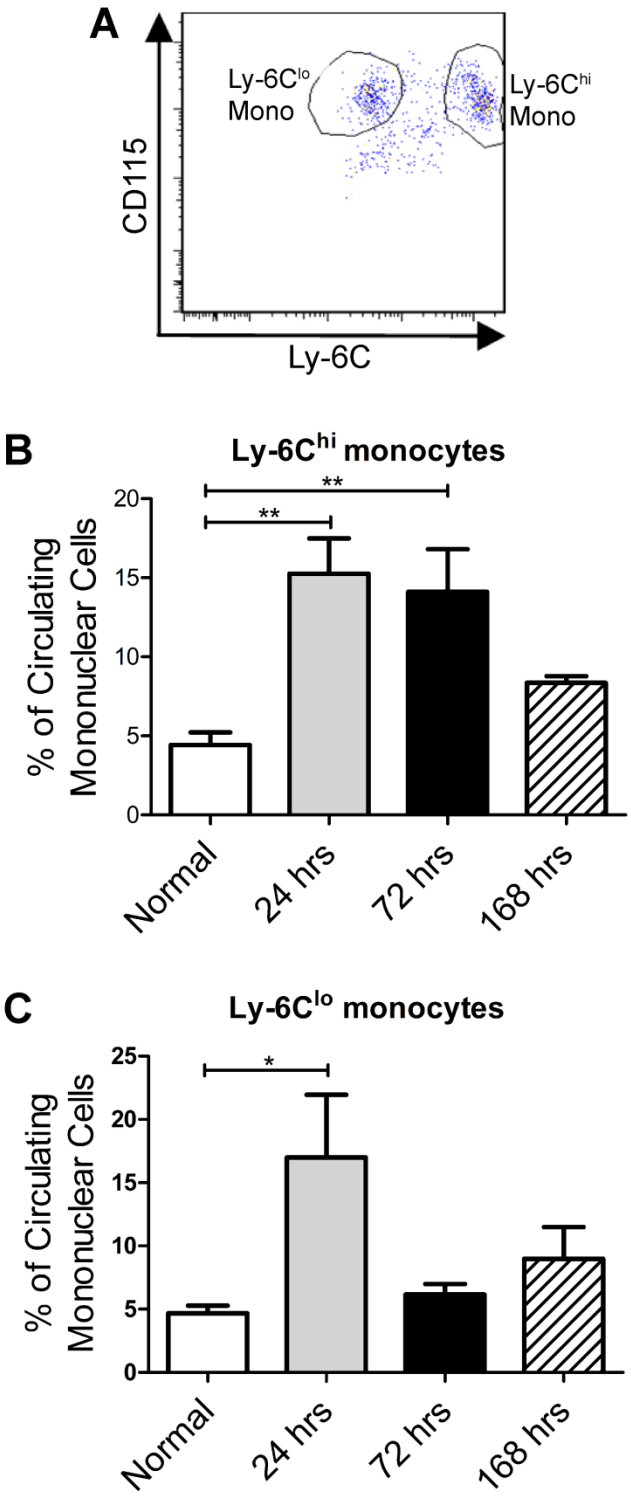

Ly-6C^{lo} Macrophages Represent the Principal MMP-Expressing Subset during Maximal Fibrosis Resolution

Our group and others have identified MMP expression as a key feature of the macrophage population responsible for the resolution of hepatic fibrosis (Sakaida et al., 2003, Popov et al., 2010, Fallowfield et al., 2007, Pellicoro et al., 2011). I therefore sought to determine the principal MMP-expressing macrophage subset in our 4 week CCl_4 model, both during inflammation/fibrogenesis (24 hrs) and at the time of maximal fibrosis resolution (72 hrs), as this would indicate a functional role for these cells in scar degradation. To do this, I utilized the pan-MMP substrate, MMPsense™ 680, described above. I administered MMPsense™ 680 or vehicle control to mice, 0 or 48 hrs following the final CCl_4 dose in my 4 week model, followed by tissue harvest and flow cytometry analysis at 24 or 72 hrs respectively (**Fig. 3.11A**). Hepatic macrophages were identified by flow cytometry, as described before (**Fig. 3.8B**), and assessed for MMPsense™ fluorescence. A population of MMPsense™ positive macrophages could be clearly distinguished on flow cytometry, indicative of active MMP expression by these cells (**Fig. 3.11B**). I then performed macrophage subset analysis on the MMPsense™ positive hepatic macrophages, using the previously discussed markers CD11b, F4/80 and Ly-6C. As shown, this methodology identified the Ly-6C^{lo} monocyte-derived macrophages as the predominant MMPsense™ positive subset at both 24 and 72 hrs, representing 70.4±4% of the detected MMP-expressing macrophages during maximal fibrosis regression (**Fig. 3.11C**).

Figure 3.11 - Identification of MMP-expressing Macrophage Subsets during Inflammation and Fibrosis Resolution

(**A**) Following 4 weeks of CCl_4, mice were given fluorescent MMP substrate (MMPsense™) or vehicle control at 0 or 48 hrs with harvest at 24 or 72 hrs respectively. (**B**) Identification of MMPsense™ positive macrophages at 24 and 72 hrs by flow cytometry. (**C**) Macrophage subset analysis of the MMPsense™ positive hepatic macrophage population at 24 and 72 hrs (n=3-4). All data shown as Mean±S.E.M; **P*<0.05, ***P*<0.01, ****P*<0.001. Representative histograms shown.

Figure 3.11 - Identification of MMP-expressing Macrophage Subsets during Inflammation and Fibrosis Resolution

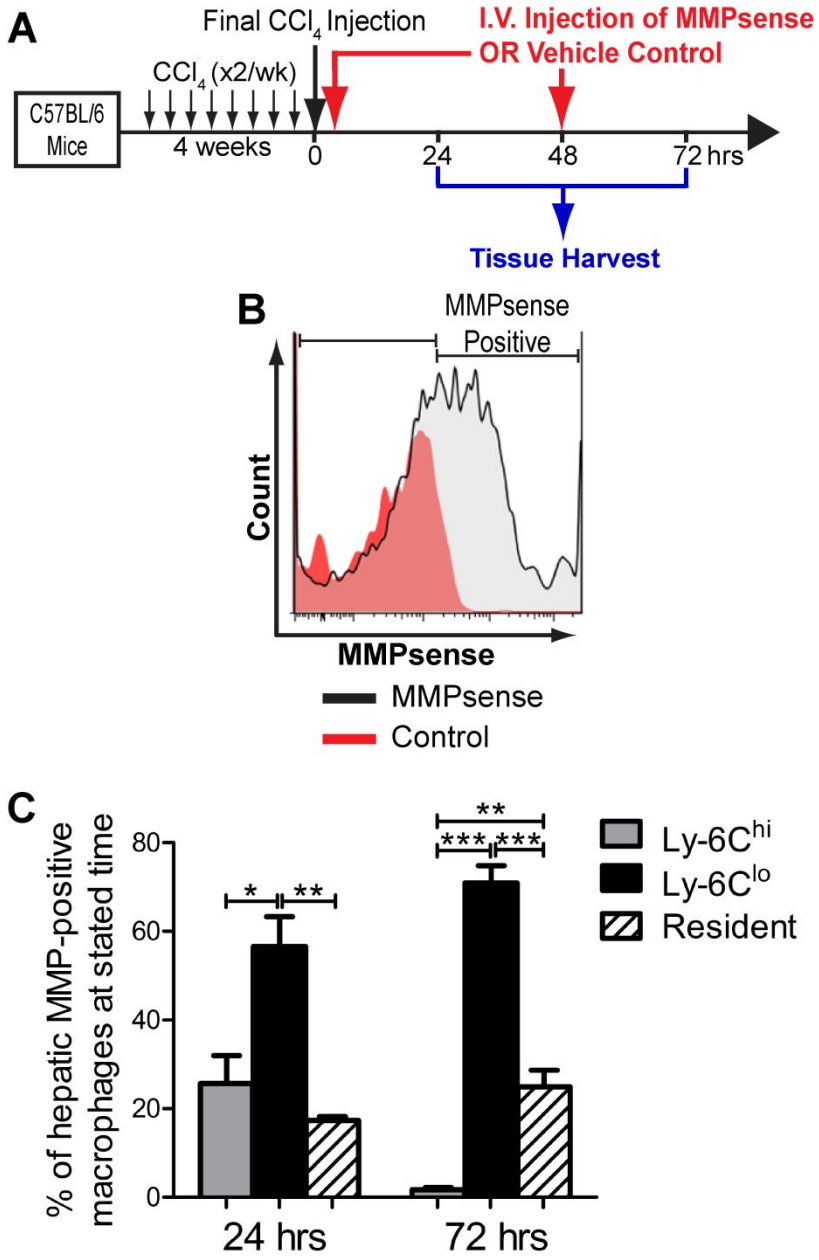

A Lack of a Dynamic Macrophage Population Response in the Irreversible Oral Thioacetamide Model

Having identified dynamic changes in hepatic macrophage subsets in the reversible 4 week CCl_4 model, I then sought to study macrophage dynamics in the irreversible TAA model. Adult male C57BL/6 mice were administered high dose oral TAA (600mg/l) in their drinking water for 8 weeks. They were then converted onto normal drinking water, with livers harvested at serial timepoints following the conversion. Comparison was made to uninjured mice. As described previously, this model induces liver fibrosis with no reduction in PSR staining seen at 8 weeks of recovery (**Fig 3.7A**).

Hepatic macrophages were identified using flow cytometry on hepatic non-parenchymal cells, exactly as described with the CCl_4 model (**Fig 3.8B**). Once again I was able to identify $F4/80^{hi}$ $CD11b^{int}$ "resident" macrophages and a $CD11b^{hi}$ $F4/80^{int}$ monocyte-derived macrophage subset (**Fig 3.12A**), which could be subdivided into Ly-$6C^{hi}$ and Ly-$6C^{lo}$ populations (**Fig 3.12B**).

I proceeded to quantify macrophage subsets at timepoints following the cessation of TAA, in comparison to control (uninjured liver). Interestingly, and in contrast to the CCl_4 model, the contribution of macrophages to the hepatic leukocyte population actually declines with TAA injury, and is gradually replenished to control levels during the first 2 weeks of recovery (**Fig 3.12C**). Subset analysis demonstrated that this reduction in macrophages is due to a loss of "resident" macrophages (**Fig 3.12D**), which again reaccumulate during the first 2 weeks following the cessation of TAA. This loss of "resident" macrophages and gradual repopulation after stopping the injury mirrors what I observed in the CCl_4 model (**Fig 3.9 A and C**). However, in the TAA model, no significant changes were seen in the contribution of Ly-$6C^{hi}$ or Ly-$6C^{lo}$ macrophage subsets to liver leucocytes (**Fig 3.12 E and F**).

Figure 3.12 – A lack of Dynamic Macrophage Population Response in the Irreversible Oral TAA Model

Adult male C57BL/6 mice were administered high dose oral TAA (600mg/l) in their drinking water for 8 weeks. They were then converted onto normal drinking water, with livers harvested at the stated timepoints following the conversion. Comparison was made to uninjured mice. (**A**) Hepatic macrophages were identified by flow cytometry as viable CD45+ Ly-6G- NK1.1- B220- CD3- CD11b+ F4/80+ cells with subclassification of $F4/80^{hi}$ $CD11b^{int}$ "resident" Kupffer cells and $CD11b^{hi}$ $F4/80^{int}$ monocyte-derived macrophages. (**B**) Subset analysis of monocyte-derived macrophages on the basis of differential Ly-6C expression identifies Ly-$6C^{hi}$ and Ly-$6C^{lo}$ subsets. (**C**) Quantification of total hepatic macrophages as a percentage of hepatic CD45-positive leucocytes in uninjured (control) mice and at stated timepoint following cessation of TAA (n=4). (**D to F**) Quantification of stated macrophage subset as a percentage of total hepatic CD45-positive leucocytes in uninjured (control) mice and at indicated timepoint following cessation of TAA (n=4). All data shown as Mean±S.E.M; $**P<0.01$, $***P<0.001$. Representative flow cytometry plots shown.

Figure 3.12 - A lack of Dynamic Macrophage Population Response in the Irreversible Oral TAA Model

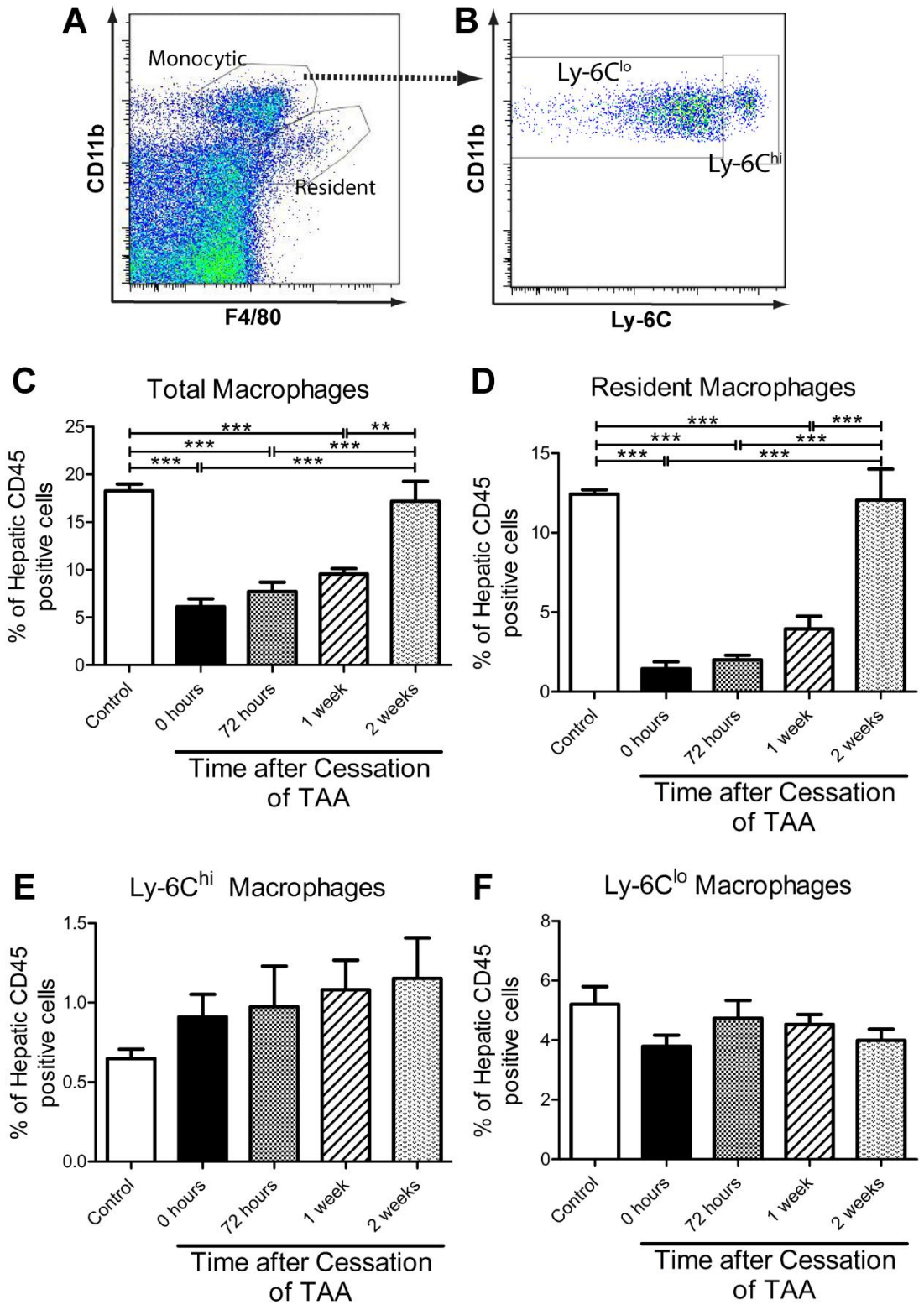

DISCUSSION

In this chapter, I have established and analysed 2 distinct models of murine liver fibrosis and gone on to extensively characterise the dynamics of the hepatic macrophage populations following withdrawal of hepatic injury. As previously described, the CCl_4 model of murine liver fibrosis is the most widely used and characterised model and shows robust reversibility following the withdrawal of injury (Issa et al., 2004, Wanless et al., 2000). In this work I have utilised a short 4 week CCl_4 model in C57BL/6 mice. As shown in **Figures 3.1 to 3.4**, this model induces a robust hepatic fibrosis and myofibroblast activation. This shows a characteristic portal-portal bridging pattern, albeit without the animals being cirrhotic. However, more importantly, serial analysis following the final CCl_4 injection in this model shows a reproducible pattern of fibrosis resolution in a tractable timeframe, enabling detailed analysis of cellular dynamics. Specifically, hepatic fibrosis and myofibroblast activation peak 48-72 hours after the final CCl_4 injection. Hence, 24 hours after the final CCl_4 injection is a time of active scar deposition. Correspondingly, this pro-fibrogenic 24 hour timepoint also shows the highest hepatocellular death as assessed by serum AST and ALT levels (**Fig 3.5A**), the highest hepatic levels of a number of pro-inflammatory cytokines and chemokines (**Fig 3.5B**) and the highest hepatic levels of the critical MMP-inhibitor TIMP-1 (**Fig 3.5C**). Thus, 24 hours after the final CCl_4 injection in this 4 week model can reliably be used as a pro-inflammatory pro-fibrogenic timepoint.

On the other hand, maximal scar regression and myofibroblast loss commences at 72 hours after the final CCl_4 injection and occurs by 96 hrs, followed by a more protracted resolution of the residual scar thereafter. This initiation of the rapid phase of fibrosis regression in the 4 week CCl_4 model at the 72 hour timepoint occurs after a reduction in AST and ALT levels to baseline, after a significant decline in inflammatory cytokines and chemokines (IL-1β, CCL2, CCL3 and CXCL2) and a reduction in hepatic TIMP-1. Hence, this 72 hour timepoint represents a pro-resolution environment and an ideal time to identify the presence of pro-resolution cell types. During the later timepoints following the final CCl_4 dose, scar resolution is much slower and hence the chance of detecting the pro-resolution macrophage population in sufficient number is likely to be lower.

The second murine fibrosis model I have described in this chapter is the much less well characterised oral TAA model. As shown in **Fig 3.6C and D**, administration of chronic high-dose (600mg/l) but not low dose (300mg/l) TAA in the drinking water of C57BL/6 mice induces a statistically significant liver fibrosis by 8 weeks of treatment, which progresses

over time and results in cirrhosis by 52 weeks of treatment. However, after either 8 or 52 weeks of TAA, no reversibility in this fibrotic response could be seen following conversion on to normal drinking water for up to 8 weeks (**Fig 3.7**). Hence, this TAA model is likely to have limited utility in identifying the pro-resolution macrophage population. However, the contrast to the more reversible CCl_4 model could provide novel insights.

Having identified the robust timepoints of fibrogenesis and resolution in the 4 week CCl_4 model, I proceeded to characterise macrophage dynamics. Previous studies by our group have identified scar-associated macrophages (SAMs) as the major source of collagenases to degrade scar during liver fibrosis regression (Fallowfield et al., 2007). Perhaps unsurprisingly, morphological analysis of macrophage distribution in the CCl_4 model using F4/80 immunostaining, demonstrated that at the time of initiation of fibrosis resolution (72 hrs), macrophages localised around the scars topographically in a prime position to orchestrate matrix degradation (**Fig 3.8A**).

Currently there are no known entirely specific markers for functionally distinct subpopulations of hepatic macrophages, and the subsets can only be identified by the simultaneous assessment of variable degrees of expression of multiple cell surface markers. Hence, the distinct populations cannot currently be identified by immunohistochemistry and I proceeded to use multicolour flow cytometry to study macrophage heterogeneity in more depth. Firstly, I developed a method to specifically identify hepatic macrophages with minimal contamination from other cell types. This stringent flow cytometric gating strategy is the most robust and reproducible way of doing this (**Fig 3.8B**). Interestingly, when total hepatic macrophage number was quantified by this flow cytometric method, it was seen to peak at 72 hours following the final CCl_4 injection, the time of initiation of fibrosis regression and after the most pro-inflammatory phase of this model (**Fig 3.8C**). This is particularly relevant, as increasing macrophage number has been associated with worsening hepatic inflammatory scores (McElroy and Peterson, 2011), whilst in this model, it is clear that macrophage number actually peaks following a reduction in hepatic inflammation. This should be borne in mind when using macrophage number to quantify disease activity. Total hepatic neutrophil number, on the other hand, peaks during the more inflammatory pro-fibrogenic phase of the model, 24 hours after the final CCl_4 dose (**Fig 3.8D**). Thus, an increase in hepatic macrophage and not neutrophil number coincides with hepatic fibrosis regression. This makes it less likely that hepatic neutrophils are the key effector cells in fibrosis regression, a theory proposed by some authors (Harty et al., 2010, Harty et al., 2008).

Proceeding to analyse the macrophage subsets in the 4 week CCl_4 model, it is clear that the resident hepatic macrophages (Kupffer cells), defined as F4/80^{hi} CD11b^{int} cells, actually decline in number during active inflammation/fibrogenesis (24 hrs after the last CCl_4 injection) (**Fig 3.9**). Whilst there is a subsequent increase during fibrosis resolution, they still represent the minority of hepatic macrophages at the time of initiation of scar degradation (72 hrs) in this model and do not account for the large increase in total macrophage number seen at this timepoint. These findings suggest that resident macrophages are unlikely to represent the principal macrophage subset responsible for fibrosis regression.

Focussing on the CD11b^{hi} F4/80^{int} monocyte-derived macrophage population in the liver, more dynamic changes could be seen in the different phases of the 4 week CCl_4 model. The importance of the monocyte-derived macrophage population in this model is emphasised by the increase in circulating monocytes I observed at the 24 and 72 hour timepoints after the final CCl_4 injection (**Fig 3.10**). This was most prominent for the inflammatory Ly-6C^{hi} circulating monocytes, which peaked at the 24 hour timepoint, when the key chemokine CCL2 is at its highest levels in the inflamed liver (**Fig 3.5B**).

I proceeded to analyse the hepatic CD11b^{hi} F4/80^{int} monocyte-derived macrophage population in more detail. Key to defining the dynamics of this population was the identification of differential Ly-6C expression in these cells. Specifically, they could be clearly divided into a Ly-6C^{hi} and Ly-6C^{lo} expression populations (**Fig 3.9B**). The Ly-6C^{hi} population accumulated principally at the time of maximal hepatic inflammation and fibrogenesis, 24 hours after the last CCl_4 injection (**Fig 3.9**). This is in keeping with previous work which has identified this subset as the main pro-fibrogenic macrophage population in the liver, potentially having direct fibrosis promoting actions on HSCs via TGF-β (Karlmark et al., 2009). When analysing the key 72 hour timepoint, when fibrosis regression commences in my model, there was a reduction in the pro-fibrogenic Ly-6C^{hi} subset and a clear and striking increase in the hepatic Ly-6C^{lo} monocyte-derived macrophage population. Indeed, this Ly-6C^{lo} macrophage subset was by far the most numerous macrophage subset at this timepoint, accounting for the increase in total hepatic macrophage number seen (**Fig 3.9C and D**). Hence, given the numerical and temporal association between these Ly-6C^{lo} macrophages and fibrosis resolution in this model, they were identified as representing the prime candidate subset responsible for mediating hepatic matrix degradation.

To study the functionality of these macrophage subsets in more detail, I utilised the MMPsense™680 probe, which when administered *in vivo* can detect cells expressing active MMPs by flow cytometry (Cortez-Retamozo et al., 2008). Critically, when this probe was

administered to mice following CCl_4 injury, I could identify hepatic macrophages showing MMPsense fluorescence (**Fig 3.11B**). Analysing which of the macrophage subsets predominantly expressed MMPs, demonstrated that the Ly-6C^{lo} monocyte-derived macrophages were the main MMP expressing subset at both the 24 and 72 hour timepoint (**Fig 3.11C**). Hence, these Ly-6C^{lo} macrophages accumulate maximally at the initiation of fibrosis regression and represent the main MMP expressing subset, highlighting their likely functional role in liver fibrosis resolution in this CCl_4 model.

The non-reversible 8 week TAA model in contrast, shows quite different macrophage population dynamics to those observed in the CCl_4 model. Following 8 weeks of high dose TAA treatment, the contribution of hepatic macrophages to the liver leukocyte pool had actually declined compared to control animals. This decline was mainly due to a reduction in the resident macrophage population. During 2 weeks of recovery from TAA injury on normal drinking water, the resident macrophage population progressively recovered to control levels (**Fig 3.12**). However, no change was seen in the contribution of either Ly-6C^{hi} or Ly-6C^{lo} monocyte-derived macrophages to the hepatic leucocyte pool in response to TAA or during the recovery phase (**Fig 3.12**). This clearly contrasts to the dynamic changes in these populations in the CCl_4 model. This lack of hepatic accumulation of potentially matrix degrading Ly-6C^{lo} macrophages in the TAA model may potentially explain the lack of fibrosis reversibility seen.

SUMMARY

- Administration of 4 weeks of intraperitoneal CCl_4 to mice induces a robust and reproducible hepatic fibrosis which rapidly resolves
- Fibrosis resolution occurs after a reduction in hepatocyte death, a decline in hepatic inflammatory cytokines and chemokines and following a loss of hepatic TIMP-1
- In this model distinct phases can be identified following cessation of CCl_4 injury: active inflammation and scar deposition (24 hrs), peak fibrosis (48-72 hrs), maximal fibrosis regression and myofibroblast loss (72-96 hrs) followed by a more protracted loss of residual scar.
- Continuous treatment of mice with high dose oral TAA (600mg/l) in drinking water induces significant hepatic fibrosis by 8 weeks and cirrhosis by 52 weeks.
- Liver fibrosis induced by high dose TAA in C57BL/6 mice does not show any resolution with recovery times of up to 8 weeks
- In the reversible CCl_4 fibrosis model, hepatic macrophages localise around scars at time of maximal fibrosis regression.
- Hepatic macrophage number peaks at the time of maximal fibrosis resolution
- Circulating Ly-6C^{hi} inflammatory monocytes are increased at times of hepatic inflammation/fibrogenesis and maximal fibrosis regression
- Distinct hepatic macrophage subsets can be identified by flow cytometry
    - F4/80^{hi} CD11b^{int} resident Kupffer cells
    - CD11b^{hi} F4/80^{int} Ly-6C^{hi} monocyte-derived macrophages
    - CD11b^{hi} F4/80^{int} Ly-6C^{lo} monocyte-derived macrophages
- Dynamic changes in macrophage subsets characterise the reversible CCl_4 fibrosis model
- The Ly-6C^{lo} hepatic macrophage subset accumulates predominantly at the time of maximal fibrosis resolution
- Ly-6C^{lo} hepatic macrophages represent the main MMP-expressing subset during fibrogenesis and fibrosis regression
- A lack of dynamic changes in hepatic monocyte-derived macrophages is seen in the irreversible TAA model of liver fibrosis

CHAPTER 4 – MODELS OF MACROPHAGE DEPLETION

INTRODUCTION

As described previously, cells of the MPS, in particular macrophages but also DCs have been implicated in fibrosis resolution. In order to define the function of specific cell populations *in vivo*, a number of methods have previously been described to deplete cells of the mononuclear phagocyte system (MPS), including monocytes, macrophages and dendritic cells. These can broadly be classified as non-genetic or genetic methods of depletion (Chow et al., 2011). The most widely used non-genetic method utilizes the administration of clodronate-encapsulated liposomes, which are engulfed by cells of the MPS, causing intracellular release of the clodronate and subsequent cell death via apoptosis. Whilst a degree of tissue specificity of depletion can be gained by varying the route of administration, this system is based on the ability of the cells to phagocytose, a fairly ubiquitous feature of many monocytes, macrophages and dendritic cells, and thus the depletion is often widespread. This can make it difficult to draw conclusions about the specific role of subpopulations of MPS cells. Another non-genetic strategy involves the use of blocking antibodies to the M-CSF receptor (CSF1R/CD115/c-fms) (Lim et al., 2009, Ma et al., 2009, MacDonald et al., 2010). This can also cause broad-spectrum protracted depletion, sometimes making interpretation of results challenging.

The alternative is to use genetic depletion strategies. A number of models have been developed for this purpose, using a variety of cell-specific promoters, enabling conditional depletion at a designated time. The most widely used transgenic systems for this purpose utilize the human diphtheria toxin receptor (DTR) gene also known as the membrane anchored form of heparin-binding epidermal growth factor-like growth factor (hbEGF). This receptor binds diphtheria toxin (DT), which is then internalized, inhibits protein synthesis and rapidly results in apoptosis in both dividing and terminally differentiated cells. The human DTR is 10^3 to 10^5 times more sensitive to diphtheria toxin (DT) then the murine DTR. Thus, murine cells which express the human DTR will die in the presence of DT. CD11b-DTR mice express the human DTR under the control of the CD11b promoter. The administration of DT to these animals therefore causes depletion of CD11b-expressing cells, specifically cells of the MPS. This system has been widely used to deplete myeloid populations in bone marrow, circulation, spleen, peritoneum, kidney, pancreas and liver amongst other organs (Chow et al., 2011). Whilst this method of depletion cannot be entirely specific for macrophage subsets, it does offer some advantages over non-genetic strategies, in that relative selectivity can be obtained for $CD11b^{hi}$ monocytes and monocyte-derived macrophages compared to $CD11b^{lo}$ tissue "resident" macrophages. The relative sparing of

resident macrophages following DT administration in these mice has been demonstrated for lung alveolar macrophages (Altmann et al., 2012) and in the liver (Cailhier et al., 2005, Devey et al., 2009). Concerns exist with the potential depletion of other CD11b-expressing populations such as neutrophils, NK cells and a subset of CD3 positive cells. However, existing data suggests that these populations are preserved in CD11b-DTR mice despite DT administration (Duffield et al., 2005, Stoneman et al., 2007, Cailhier et al., 2005). The explanation for this finding remains unclear, although it may be dependent on the degree of active CD11b gene rather than protein expression.

Dendritic cells (DCs) have also been targeted using a conditional depletion strategy. As discussed in **Chapter 1**, CD11c expression is relatively specific to DCs. CD11c-DTR mice have been generated, which express the human DTR under the control of the CD11c promoter. Such mice have been utilised in various studies to deplete hepatic DCs (Bamboat et al., 2010, Jiao et al., 2012, Phythian-Adams et al., 2010). One of the key problems in studying the relative role of macrophages and DCs in disease pathogenesis is the lack of entirely specific markers for each cell type. It was long thought that MHCII and CD11c positivity was a marker of DCs (Hashimoto et al., 2011). However, it is now apparent that subsets of monocytes and macrophages can also express these markers under certain conditions (Hashimoto et al., 2011, Hume, 2008). Similarly, subsets of DCs can arise from circulating monocytes and can express more traditional macrophage markers such as CD11b or F4/80 (Hashimoto et al., 2011). Thus caution must be exerted when attributing functions specifically to macrophages or DCs using these markers.

Overall, cellular depletion provides an excellent experimental method to determine the functional role of a particular population *in vivo*. Therefore, in order to define the function of specific macrophage subsets during the resolution of hepatic fibrosis, I sought to deplete macrophages during this critical phase. As discussed, a number of depletion strategies exist, each with pros and cons. Given that the most pronounced changes in macrophage subsets that we observed in the 4 week CCl_4 fibrosis resolution model were dependent on the $CD11b^{hi}$ monocyte-derived macrophages (**Fig 3.9B to 3.9D**), I focused on the CD11b-DTR transgenic system, which could potentially offer some selectivity to this hepatic macrophage population. Comparison was made to alternative MPS depletion strategies using liposomal clodronate and CD11c-DTR mice.

AIMS

- To characterise hepatic macrophage subset depletion in CD11b-DTR mice during fibrosis regression following CCl_4 injury
- To study the effect of macrophage depletion in CD11b-DTR mice on fibrosis resolution
- To characterize hepatic macrophage depletion using liposomal clodronate during fibrosis resolution following CCl_4 injury
- To compare the phenotypic effects of macrophage depletion using CD11b-DTR mice and liposomal clodronate
- To determine the contribution of dendritic cells to subsets during fibrosis regression using CD11c-DTR mice

RESULTS

DT Administration to CD11b-DTR Mice causes Depletion of Circulating Monocytes

Adult male CD11b-DTR mice maintained on a C57BL/6 background, were injured with 4 weeks of CCl_4, using the same schedule and dosing previously described for wild type animals. In order to ensure maximal macrophage depletion during the time of maximal fibrosis regression, intravenous diphtheria toxin (DT; 10ng/g) or PBS control was administered 48, 72 and 96 hrs following the final CCl_4 dose, with harvest at 120 hrs, according to the schedule shown (**Fig 4.1A**).

As before, circulating monocytes were identified as $CD11b^+$ $CD115^+$ mononuclear cells by flow cytometry. Ly-$6C^{hi}$ and Ly-$6C^{lo}$ monocyte subsets were identified at 120 hrs in the peripheral blood of CD11b-DTR mice that received DT or PBS control and quantified (**Fig 4.1B**). As shown in **Fig. 4.1B and 4.1C**, described in detail in the associated legend and in keeping with previous data using CD11b-DTR mice (Lin et al., 2009), administration of DT to these mice during liver fibrosis regression induced a significant reduction in the number of both circulating monocyte subsets (n=11-13). Ly-$6C^{hi}$ "inflammatory" monocytes were depleted by 75.4±3.1% following DT administration, whilst Ly-$6C^{lo}$ "patrolling" monocytes were reduced by 97.8±0.5% (**Fig 4.1C**).

Figure 4.1– DT Administration to CD11b-DTR Mice causes Depletion of Circulating Monocytes

(**A**) Schematic representation of model of macrophage depletion during fibrosis resolution in CD11b-DTR mice after 4 weeks of injury, by administration of diphtheria toxin (DT) (or PBS control) 48, 72 and 96 hrs following the final CCl_4 injection with harvest at 120 hrs. (**B**) Analysis of circulating monocytes by flow cytometry. Ly-6C^{hi} and Ly-6C^{lo} circulating monocytes were identified in blood, gating on CD11b+ Ly-6G- CD115+ Ly-6C^{hi} and Ly-6C^{lo} cells. (**C**) Ly-6C^{hi} and Ly-6C^{lo} circulating monocyte number per ml of blood in CD11b-DTR mice given DT or PBS control (n=11-13 from 2 independent experiments). All data shown as Mean±S.E.M; ***P<0.001. Representative flow cytometry plots shown.

Figure 4.1 - DT Administration to CD11b-DTR Mice causes Depletion of Circulating Monocytes

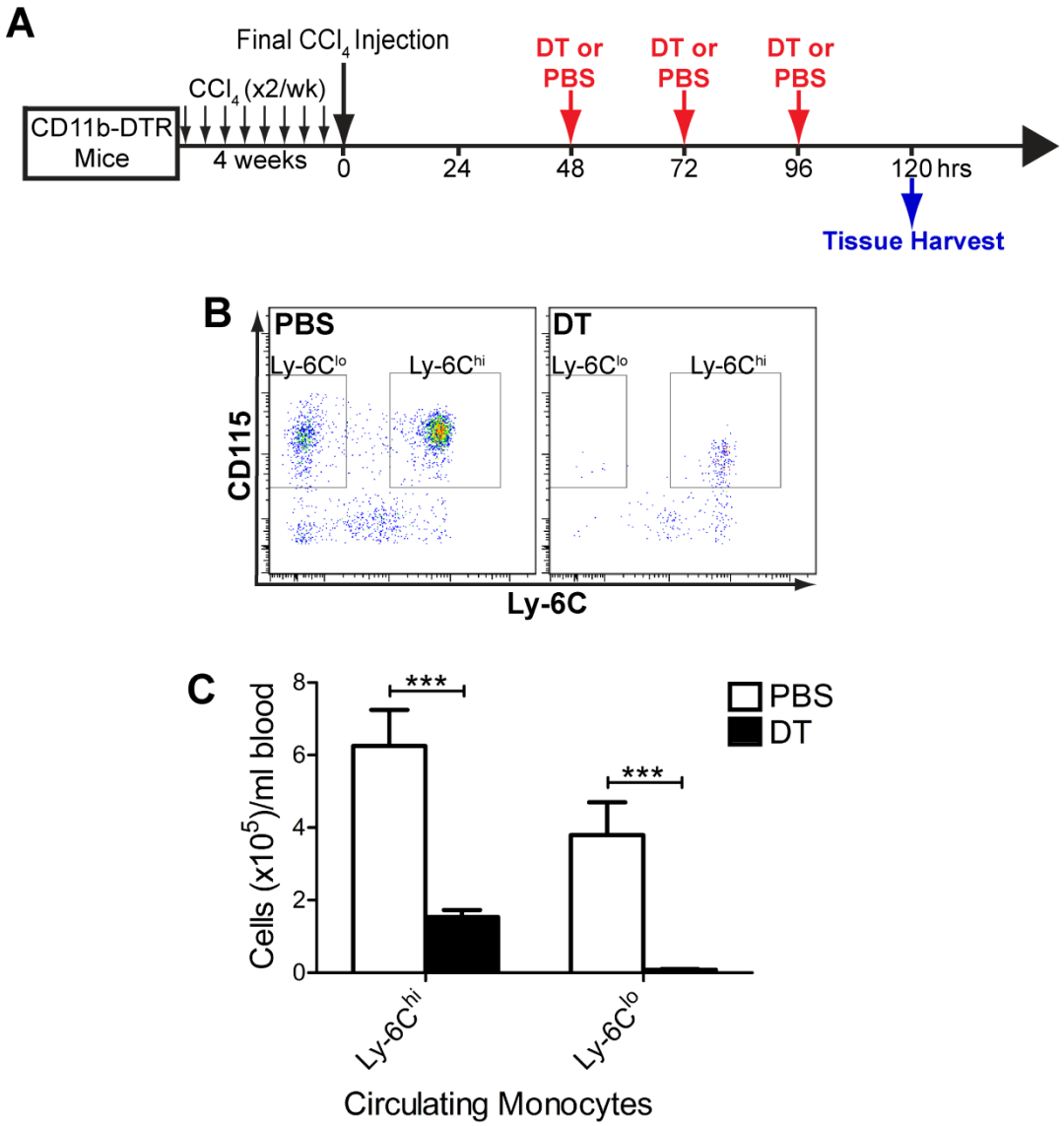

Selective Depletion of Ly-6C^{lo} Hepatic Macrophages during Fibrosis Resolution in CD11b-DTR Mice

Having confirmed monocyte depletion during fibrosis resolution following DT administration to CD11b-DTR mice, I proceeded to characterize the effects of depletion on hepatic macrophage subsets. CCl_4 and DT (or PBS control) were again administered according to the schedule shown (**Fig 4.1A**). Hepatic macrophages and macrophage subsets were identified from digested livers by flow cytometry of hepatic non-parenchymal cells, as described previously (**Fig 3.8B, 3.9A and B**).

As shown in **Fig 4.2A** and **Fig 4.2B** and described in detail in the associated legend, administration of DT to CD11b-DTR mice resulted in a clear depletion of hepatic Ly-6C^{lo} macrophages at the 120 hr timepoint (n=11-13). Indeed, I observed a 76.7 ± 3.16% reduction in the relative number of Ly-6C^{lo} macrophages at 120 hrs (**Fig 4.2B**). Furthermore, no significant depletion was detected for hepatic Ly-6C^{hi} macrophages, whilst the "resident" macrophage population actually showed a small increase in number following DT administration (**Fig 4.2B**). Additionally, flow cytometric analysis of hepatic neutrophil (**Fig 4.2C**; n=11-13) and CD3 positive cell number (**Fig 4.2D**; n=11-13) at the same timepoint showed no significant depletion of either population in CD11b-DTR mice in response to DT.

Thus, in the CCl_4 model, macrophage depletion in CD11b-DTR mice during maximal fibrosis regression causes specific depletion of hepatic Ly-6C^{lo} monocyte-derived macrophages. This provides an opportunity to study the function of this population in liver fibrosis regression.

Figure 4.2 - Selective Depletion of Ly-6C^{lo} Hepatic Macrophages during Fibrosis Resolution in CD11b-DTR Mice

(**A**) Flow cytometry data from livers of PBS and DT-treated mice, gated on viable CD45+ Ly-6G- CD11b^{hi} F4/80^{int} hepatic macrophages (Percentages shown indicate mean±SEM of each subset as a proportion of total hepatic macrophages; n=11-13). (**B**) Quantification of relative number of each hepatic macrophage subset (Expressed relative to mean total macrophage number in PBS-treated livers; n=11-13 pooled from 2 independent experiments). (**C**) Quantification of relative number of hepatic neutrophils in DT and PBS-treated mice (Expressed relative to total neutrophil number in PBS-treated livers; n=11-13 pooled from 2 independent experiments). (**D**) Quantification of relative number of hepatic CD3 positive cells in DT and PBS-treated mice (Expressed relative to total CD3 cell number in PBS-treated livers; n=11-13 pooled from 2 independent experiments). All data shown as Mean±S.E.M; *P<0.05, ***P<0.001, NS-non-significant. Representative flow cytometry plots shown.

Figure 4.2 - Selective Depletion of Ly-6C^{lo} Hepatic Macrophages during Fibrosis Resolution in CD11b-DTR Mice

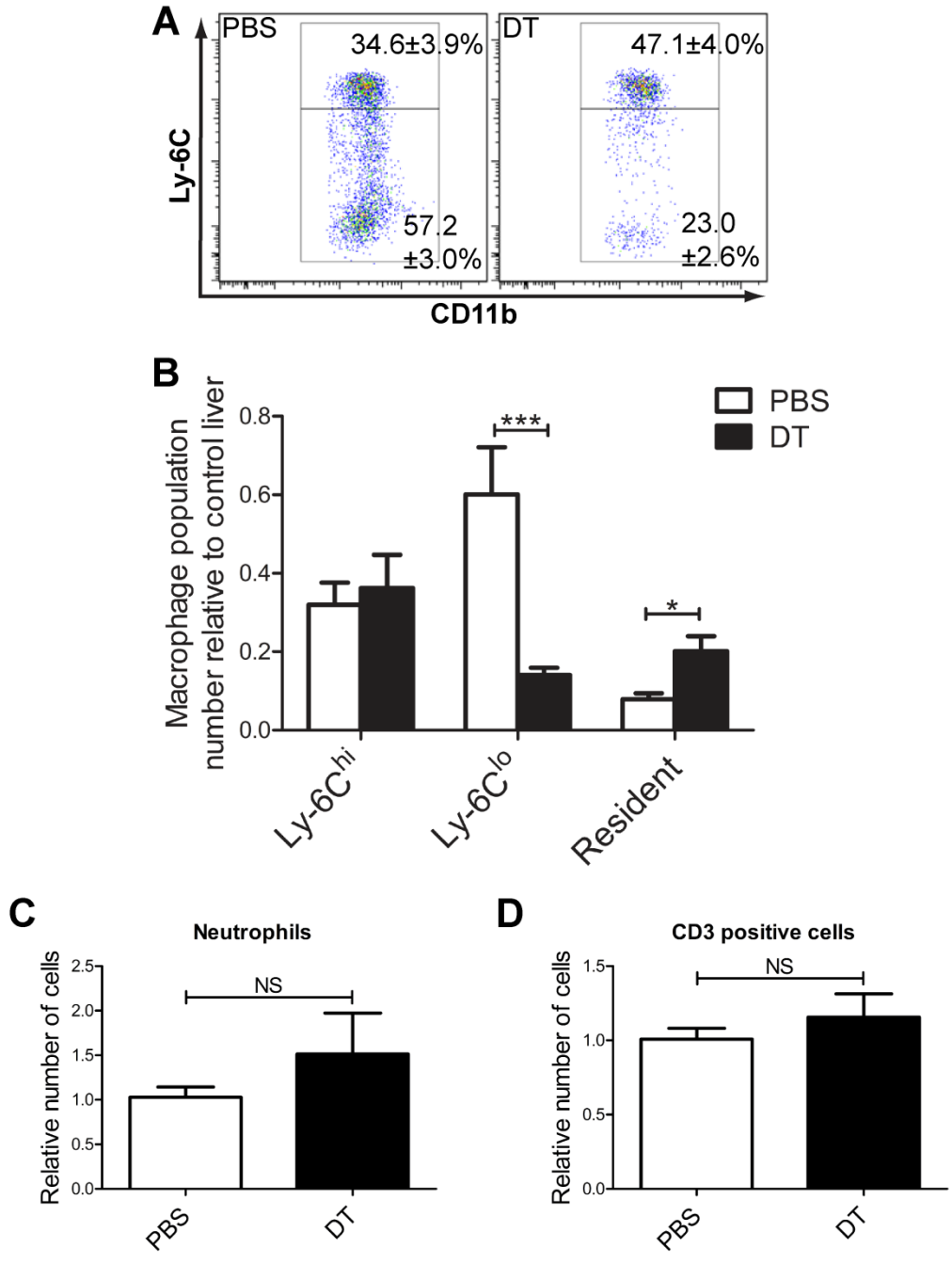

Macrophage Depletion during Fibrosis Resolution in CD11b-DTR Mice Induces a Failure of Scar Remodelling

I then proceeded to ascertain the effect of macrophage depletion in the CD11b-DTR mice, on the resolution of hepatic fibrosis. Injury and depletion were performed as shown (**Fig 4.1A**).

As described previously (**Fig 3.1 to 3.3**), the degree of fibrosis was analysed by immunohistochemistry with morphometric pixel analysis of Picrosirius Red (PSR), Collagen 3 and Collagen 1. As shown in **Fig 4.3A to 4.3C** and described in detail in the legend, DT administration to CD11b-DTR mice resulted in higher levels of hepatic fibrosis as assessed by all 3 measures, when compared to vehicle (PBS) control-treated animals (n=10-12). Additionally, as shown in **Fig 4.3D**, immunohistochemical analysis of α-SMA expression following macrophage depletion with DT, showed no significant difference compared to PBS control indicating a similar degree of myofibroblast activation with either treatment (n=10-12).

Thus, macrophage depletion during the fibrosis resolution phase results in a failure of scar regression. As described above, depletion in this model predominantly affected Ly-6C^{lo} hepatic macrophages, suggesting this is the pro-resolution macrophage subset.

Figure 4.3 - Macrophage Depletion during Fibrosis Resolution in CD11b-DTR Mice Induces a Failure of Scar Remodelling

(**A**) Representative Picrosirius red (PSR) staining and quantification of histological changes by pixel analysis following DT or PBS administration to CD11b-DTR mice during fibrosis resolution (Expressed relative to mean % area in PBS-treated liver; n=10-12 pooled from 2 independent experiments). (**B**) Representative liver immunohistochemistry of Collagen 3 and quantification of histological changes by pixel analysis following DT or PBS administration to CD11b-DTR mice during fibrosis resolution (Expressed relative to mean % area in PBS-treated liver; n=10-12 pooled from 2 independent experiments). (**C**) Representative liver immunohistochemistry of Collagen 1 and quantification of histological changes by pixel analysis following DT or PBS administration to CD11b-DTR mice during fibrosis resolution (Expressed relative to mean % area in PBS-treated liver; n=10-12 from 2 independent experiments). (**D**) Representative liver immunohistochemistry of α-SMA and quantification of histological changes by pixel analysis following DT or PBS administration to CD11b-DTR mice during fibrosis resolution (Expressed relative to mean % area in PBS-treated liver; n=10-12 pooled from 2 independent experiments). All data shown as Mean±S.E.M; *P<0.05, ***P<0.001, NS-non-significant. Representative images shown with scale bar=100μm.

Figure 4.3 - Macrophage Depletion during Fibrosis Resolution in CD11b-DTR Mice Induces a Failure of Scar Remodelling

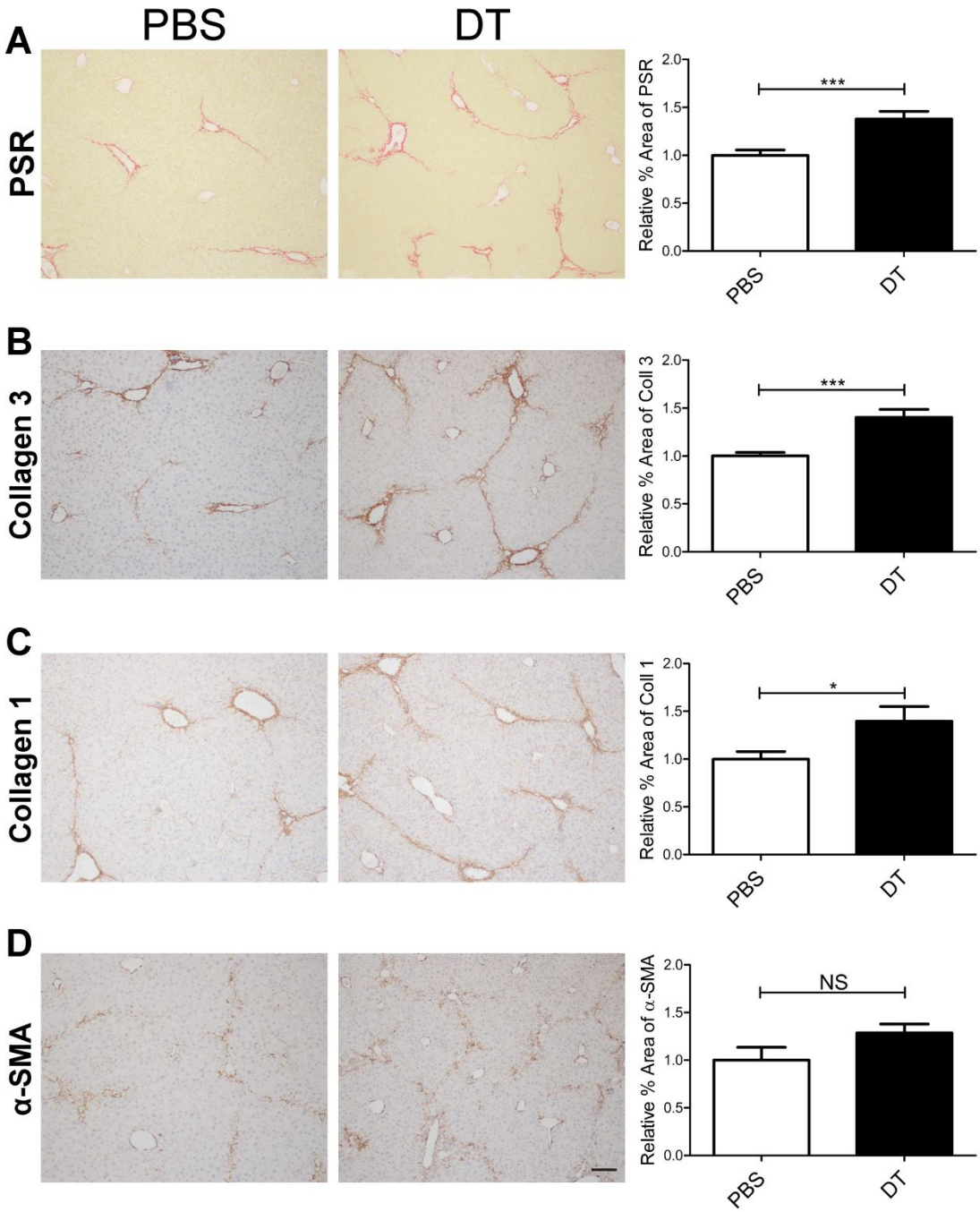

Ly-6C^{lo} Macrophage Number Correlates with the Degree of Fibrosis Resolution

Having demonstrated that in CD11b-DTR mice, DT administration during fibrosis regression results in selective depletion of hepatic Ly-6C^{lo} macrophages, and that this induces a failure of scar remodelling, I sought to strengthen the association been these findings by assessing for the presence of correlations between macrophage subset number and the degree of fibrosis which could indicate a more causal link.

In order to do this, CD11b-DTR mice, were injured with 4 weeks of CCl_4 and given DT or PBS control at 48, 72 and 96 hrs with harvest at 120 hrs, according to the previous schedule (**Fig 4.1A**). For each mouse, a proportion of the liver was harvested for hepatic macrophage subset counts by flow cytometry and the remainder of the liver was fixed and assessed histologically for the degree of liver fibrosis using PSR staining and immunohistochemistry for collagen 3 and collagen 1 as before. Thus, I could make a simultaneous assessment of hepatic macrophage populations and the degree of fibrosis in individual mice and hence determine if there is a correlation between the number of each hepatic macrophage subset and fibrosis levels between different mice. As shown in **Fig 4.4A**, and described in detail in the associated legend, the number of hepatic Ly-6C^{lo} macrophages showed a statistically significant inverse correlation with the degree of fibrosis, as assessed by PSR, Collagen 3 or Collagen 1 staining (n=22). No correlations were detected between Ly-6C^{hi} macrophage (**Fig 4.4B**, n=22) or resident macrophage (**Fig 4.4C**, n=22) number and the degree of fibrosis. This indicates a "dose-response" effect, in that the degree of depletion of Ly-6C^{lo} hepatic macrophages directly relates to the degree of residual scar.

DT has No Effect on Hepatic Macrophages in Wild Type Mice

In order to exclude a non-specific effect of DT contributing to our findings, DT or PBS control was administered to fibrotic wild-type C57BL/6 mice using an identical treatment schedule to that used for CD11b-DTR mice (**Fig 4.1A**). DT had no effect on hepatic macrophage subsets in wild-type mice (**Fig 4.4D**, n=2). Furthermore, administration of DT to these animals did not affect fibrosis resolution, as assessed by PSR quantification (**Fig 4.4E**, n=2).

Figure 4.4 – Ly-6C^{lo} Macrophage Number Correlates with the Degree of Fibrosis Resolution

(**A**) Correlation of degree of fibrosis assessed by PSR, Collagen 1 and Collagen 3 % area, with the relative number of Ly-6C^{lo} macrophages (n=22 pooled from 2 independent experiments). (**B**) Correlation of degree of fibrosis assessed by PSR, Collagen 1 and Collagen 3 % area, with the relative number of hepatic Ly-6C^{hi} macrophages in CD11b-DTR mice (n=22 from 2 independent experiments). (**C**) Correlation of degree of fibrosis assessed by PSR, Collagen 1 and Collagen 3 % area, with the relative number of resident hepatic macrophages in CD11b-DTR mice (n=22 from 2 independent experiments). (**D** & **E**) Administration of DT or PBS to wild-type mice after 4 weeks of injury at 48, 72 and 96 hrs following the final CCl_4 injection with harvest at 120 hrs (experiments in collaboration with Dr A Pellicoro). (**D**) Analysis of hepatic macrophage subsets in wild-type mice receiving DT or PBS (Percentages shown indicate mean±SEM of each subset as a proportion of total hepatic macrophages; n=2). (**E**) Quantification of fibrosis in wild-type mice receiving DT or PBS by picrosirius red staining and morphometric pixel analysis (Expressed relative to mean % area for PBS-treated liver; n=2). All data shown as Mean±S.E.M; NS-non-significant. Representative flow cytometry plots shown.

Figure 4.4 - Ly-6C^{lo} Macrophage Number Correlates with the Degree of Fibrosis Resolution

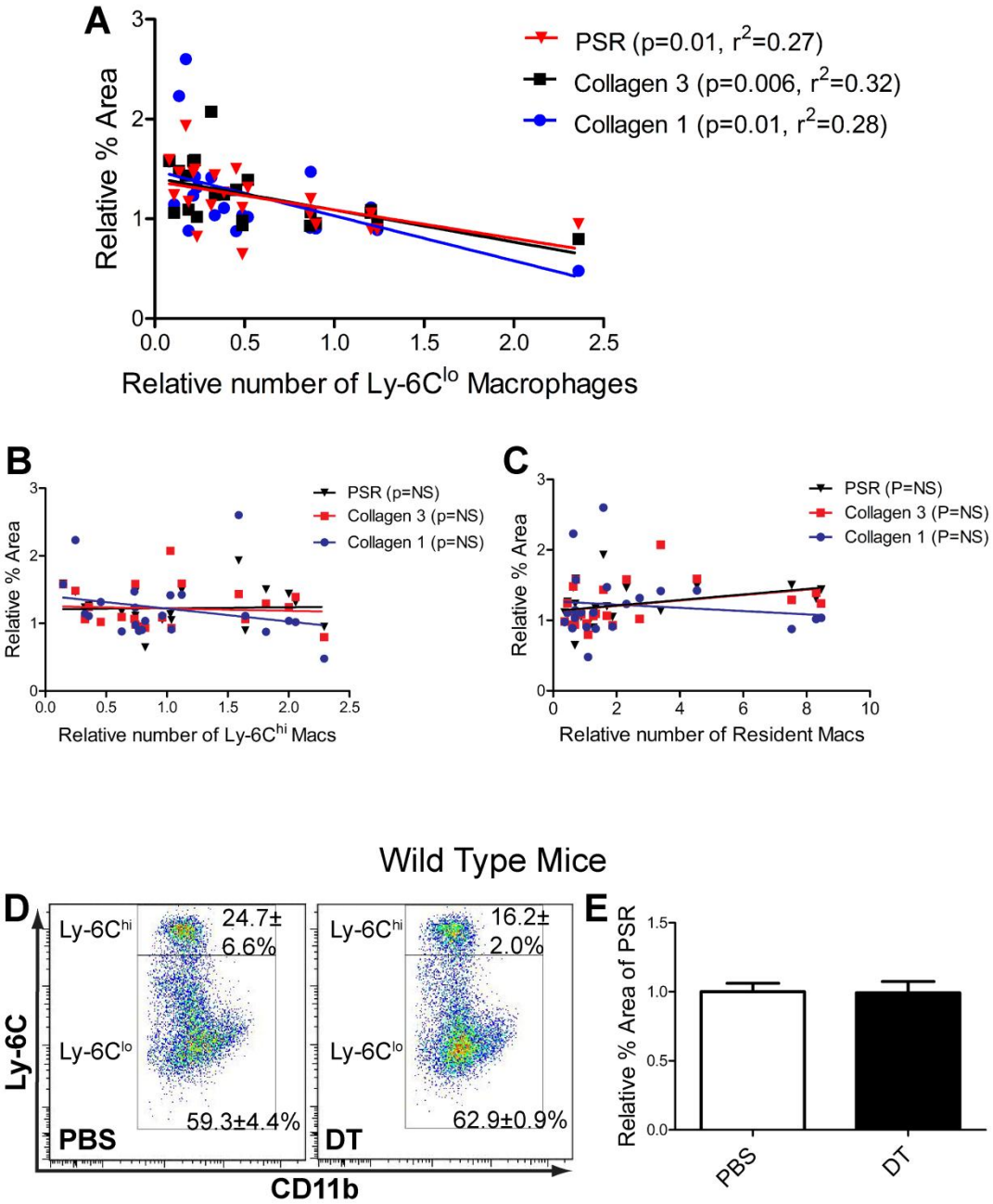

Liposomal Clodronate Administration to Mice Causes Depletion of Ly-6C^{lo} Monocytes

For comparison, I also used liposomal clodronate as an alternative macrophage depletion strategy during fibrosis regression. Wild type C57BL/6 mice were injured with 4 weeks of CCl_4 as before, followed by intravenous administration of 200µl of liposomal clodronate (or PBS control) 48, 72 and 96 hrs after the final CCl_4 injection, with harvest at 120 hrs, according to the schedule shown (**Fig 4.5A**).

As before, circulating monocytes were identified as CD11b$^+$ CD115$^+$ mononuclear cells by flow cytometry. Ly-6C^{hi} and Ly-6C^{lo} monocyte subsets were identified at 120 hrs in the peripheral blood of mice that received liposomal clodronate or PBS control and quantified (**Fig 4.5B**). As shown in **Fig. 4.5B and 4.5C** and described in detail in the associated legend, liposomal clodronate administration caused a significant reduction in circulating Ly-6C^{lo} monocytes, amounting to 55.3±4.9% depletion (n=12-14). However, Ly-6C^{hi} monocyte number actually increased by 72.6±12.6% following clodronate administration (**Fig 4.5 B and C**, n=12-14). Interestingly, both monocyte subsets show reduced CD115 expression following liposomal clodronate administration, suggesting that a change in monocyte phenotype may also occur using this strategy (**Fig 4.5B**).

Figure 4.5 – Liposomal Clodronate Administration to Mice causes Depletion of Ly-6C^{lo} Monocytes

(**A**) Schematic representation of model of macrophage depletion during fibrosis resolution in C57BL/6 mice after 4 weeks of injury, by administration of liposomal clodronate (or PBS control) 48, 72 and 96 hrs following the final CCl_4 injection with harvest at 120 hrs. (**B**) Analysis of circulating monocytes by flow cytometry. Ly-6C^{hi} and Ly-6C^{lo} circulating monocytes were identified in blood, gating on CD11b+ Ly-6G- CD115+ Ly-6C^{hi} and Ly-6C^{lo} cells. (**C**) Ly-6C^{hi} and Ly-6C^{lo} circulating monocyte number per ml of blood in C57BL/6 mice given liposomal clodronate or PBS control (n=12-14 pooled from 2 independent experiments). All data shown as Mean±S.E.M; ***P<0.001. Representative flow cytometry plots shown.

Figure 4.5 - Liposomal Clodronate Administration to Mice causes Depletion of Ly-6C^{lo} Monocytes

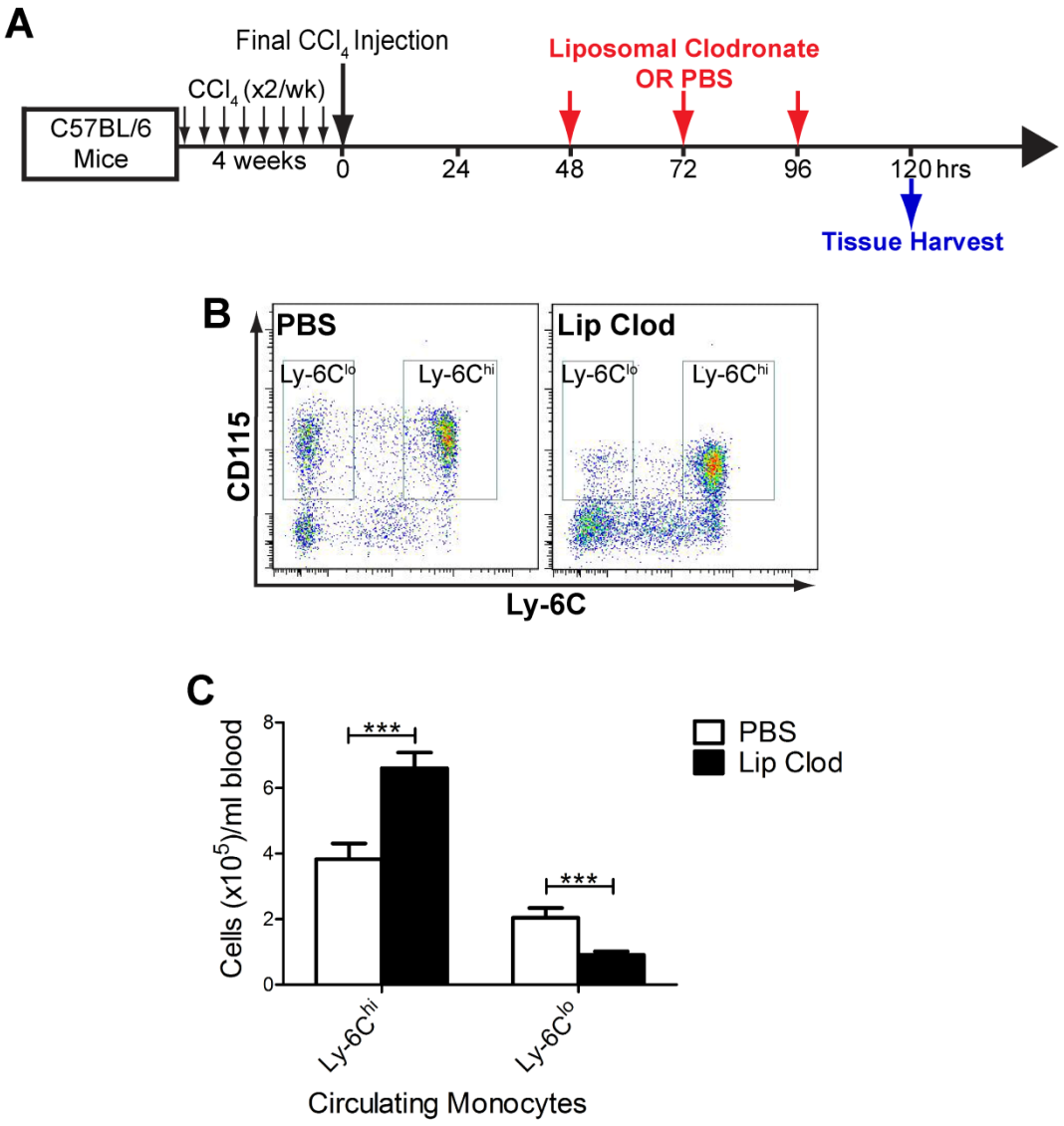

Liposomal Clodronate Administration Causes Generalized Hepatic Macrophage Depletion

I proceeded to determine the effects of liposomal clodronate on hepatic macrophage subsets and other immune cell populations. Wild type C57BL/6 mice were injured with 4 weeks of CCl_4 as before, followed by intravenous administration of 200µl of liposomal clodronate (or PBS control) 48, 72 and 96 hrs after the final CCl_4 injection, with harvest at 120 hrs, according to the schedule shown (**Fig 4.5A**). Hepatic macrophages and other cell types were identified by flow cytometry on hepatic non-parenchymal cells isolated from digested livers as before (**Fig 3.8B, 3.9A and B**).

As demonstrated in **Fig 4.6A**, liposomal clodronate induced depletion of all 3 macrophage subsets in the liver when compared to PBS control. The degree of depletion for the critical Ly-$6C^{lo}$ subset was 60.9±7.8% following clodronate administration (**Fig 4.6A**, n=13-14). Furthermore, liposomal clodronate administration caused a 25.8 ± 5.5% reduction in hepatic Ly-$6C^{hi}$ monocyte-derived macrophages and an 80.9 ± 3.0% depletion of resident hepatic macrophages (**Fig 4.6A**, n=13-14).

Additionally, as shown in **4.6B and 4.6C**, the effect of liposomal clodronate administration on hepatic neutrophil and CD3 positive cell number was assessed by flow cytometry. Liposomal clodronate caused a statistically significant increase in hepatic neutrophil number (**Fig 4.6B**, n=13-14) and a significant reduction in hepatic CD3 positive cells suggesting reduced hepatic T cell number (**Fig 4.6C**, n=13-14).

Liposomal Clodronate Administration does not Alter Hepatic Fibrosis Resolution

I proceeded to assess the effect of liposomal clodronate administration on the regression of hepatic fibrosis in the model described and shown in **Fig 4.5A**. Liver fibrosis was assessed by picrosirius red staining and morphometric pixel analysis as before. As shown in **Fig 4.6D**, no difference in total hepatic fibrosis was detected following liposomal clodronate administration, when compared to PBS-treated control animals (n=13-14). This indicates that liposomal clodronate does not affect the resolution of hepatic fibrosis in this 4 week CCl_4 model.

Figure 4.6 – Liposomal Clodronate causes Generalized Hepatic Macrophage Depletion and No Effect on Fibrosis

(**A**) Hepatic macrophage subsets were identified by flow cytometry from livers of PBS and liposomal clodronate treated mice. Quantification of relative number of each hepatic macrophage subset (Expressed relative to mean total macrophage number in PBS-treated livers; n=13-14 pooled from 2 independent experiments). (**B**) Quantification of relative number of hepatic neutrophils by flow cytometry in liposomal clodronate and PBS treated mice (Expressed relative to total neutrophil number in PBS-treated livers; n=13-14 from 2 independent experiments). (**C**) Quantification of relative number of hepatic CD3 positive cells by flow cytometry in liposomal clodronate and PBS treated mice (Expressed relative to total CD3 cell number in PBS-treated livers; n=13-14 from 2 independent experiments). (**D**) Quantification of histological changes by picrosirius red staining and pixel analysis following liposomal clodronate or PBS administration to C57BL/6 mice during fibrosis resolution (Expressed relative to mean % area in PBS-treated liver; n=13-14 from 2 independent experiments). All data shown as Mean±S.E.M; *P<0.05, ***P<0.001, NS-non-significant.

Figure 4.6 - Liposomal Clodronate Administration causes Generalized Hepatic Macrophage Depletion and No Effect on Fibrosis

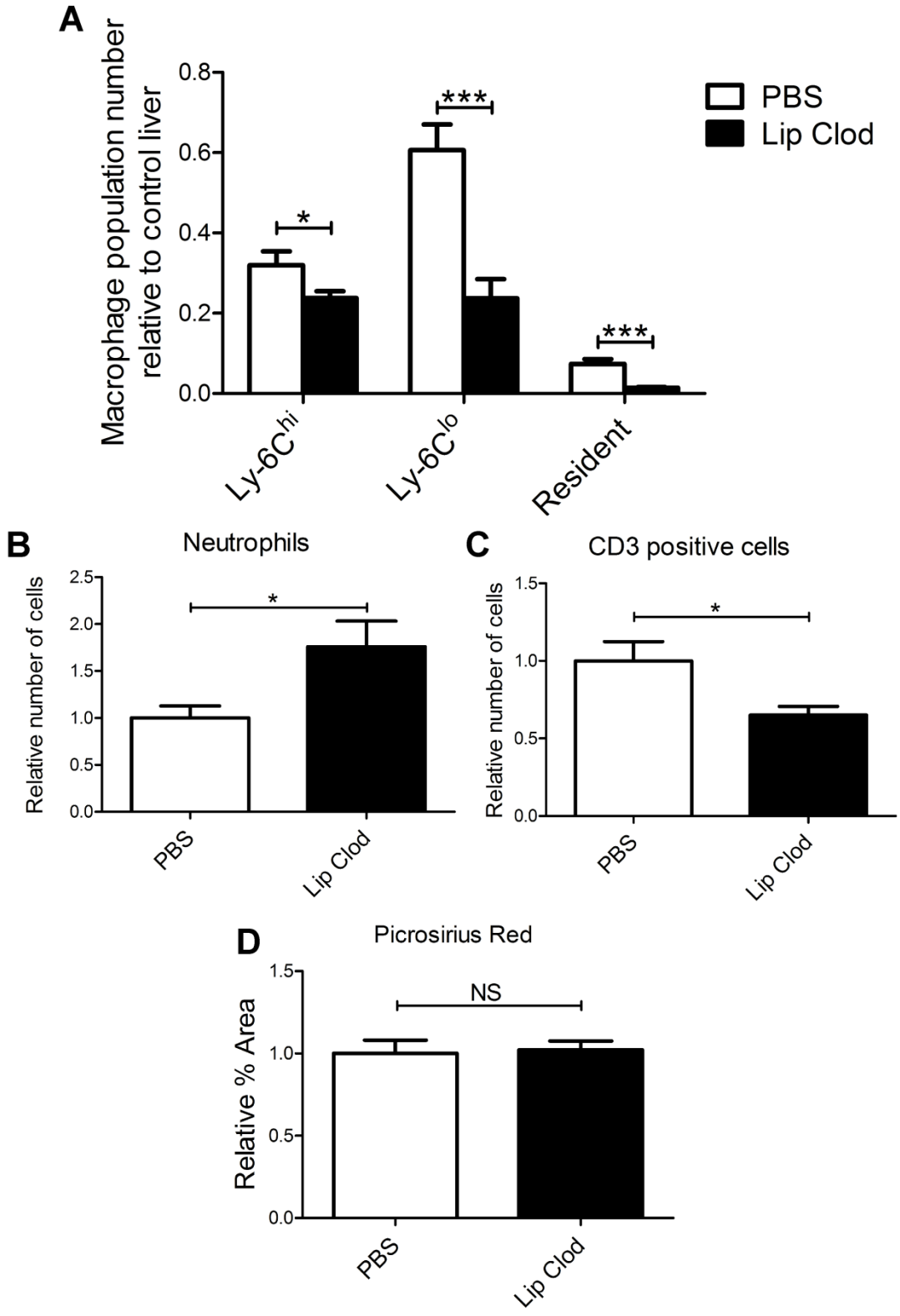

DT Administration to CD11c-DTR Mice has No Effect on Hepatic Macrophage Subsets

As previously discussed, there can be significant overlap between function and cell surface marker expression between macrophages and DCs. I therefore wished to assess if there is a contribution of hepatic DCs to the defined macrophage subsets during resolution of liver fibrosis.

I initially determined the degree of expression of the putative DC marker CD11c, on the previously defined hepatic macrophage subsets by flow cytometry. I focussed on the time of maximal fibrosis resolution (72 hrs) following 4 weeks of CCl_4 injury. As shown in **Fig 4.7A,** some CD11c expression was detected in each of the macrophage populations at the 72 hr timepoint. Whilst expression was lowest in the Ly-6C^{hi} macrophage subset and highest in the resident macrophage population, the likely pro-resolution Ly-6C^{lo} macrophages, expressed showed only intermediate levels (n=5).

I went on to utilize CD11c-DTR mice, in which hepatic DC depletion has been demonstrated in response to DT (Phythian-Adams et al., 2010). Adult male CD11c-DTR mice were injured with 4 weeks of CCl_4 as before, followed by intraperitoneal administration of DT (12ng/g) or PBS control, 48 and 72 hrs following the final CCl_4 injection, with harvest at 96 hrs. This dose of DT in this mouse strain is higher than the dose that has previously been shown to deplete hepatic DCs (Phythian-Adams et al., 2010), and thus we can be confident of achieving DC depletion in our model. As shown in **Fig 4.7B**, administration of DT to these mice did not cause a significant change in the total hepatic macrophage number when compared to PBS-treated controls, as assessed by flow cytometry (n=7). I proceeded to study the 3 defined liver macrophage subsets in these mice. There was no significant change in any of the macrophage subsets following DT administration to CD11c-DTR mice (**Fig 4.7C,** n=7).

Figure 4.7 – No depletion of Hepatic Macrophage Subsets in CD11c-DTR Mice

(**A**) CD11c expression of each macrophage subset 72 hrs following the final CCl_4 injection after 4 weeks of injury (Expressed as Mean Fluorescence Intensity (MFI) of CD11c assessed by flow cytometry, n=5). (**B** & **C**) Adult male CD11c.DOG mice were administered twice-weekly intraperitoneal CCl_4 for 4 weeks, followed by 12ng/g diphtheria toxin (or PBS control) 48 and 72 hrs following the final CCl_4 injection. Mice were harvested at 96 hrs. (**B**) Quantification of total hepatic macrophage number as a proportion of CD45 positive hepatic non-parenchymal cells following DT or PBS control (n=7). (**C**) Quantification of number of each macrophage subset as a proportion of total hepatic macrophages following DT or PBS control (n=7). All data shown as Mean±S.E.M; ***P<0.001, NS-non-significant.

Figure 4.7 - DT Administration to CD11c-DTR Mice has No Effect on Hepatic Macrophage Subsets

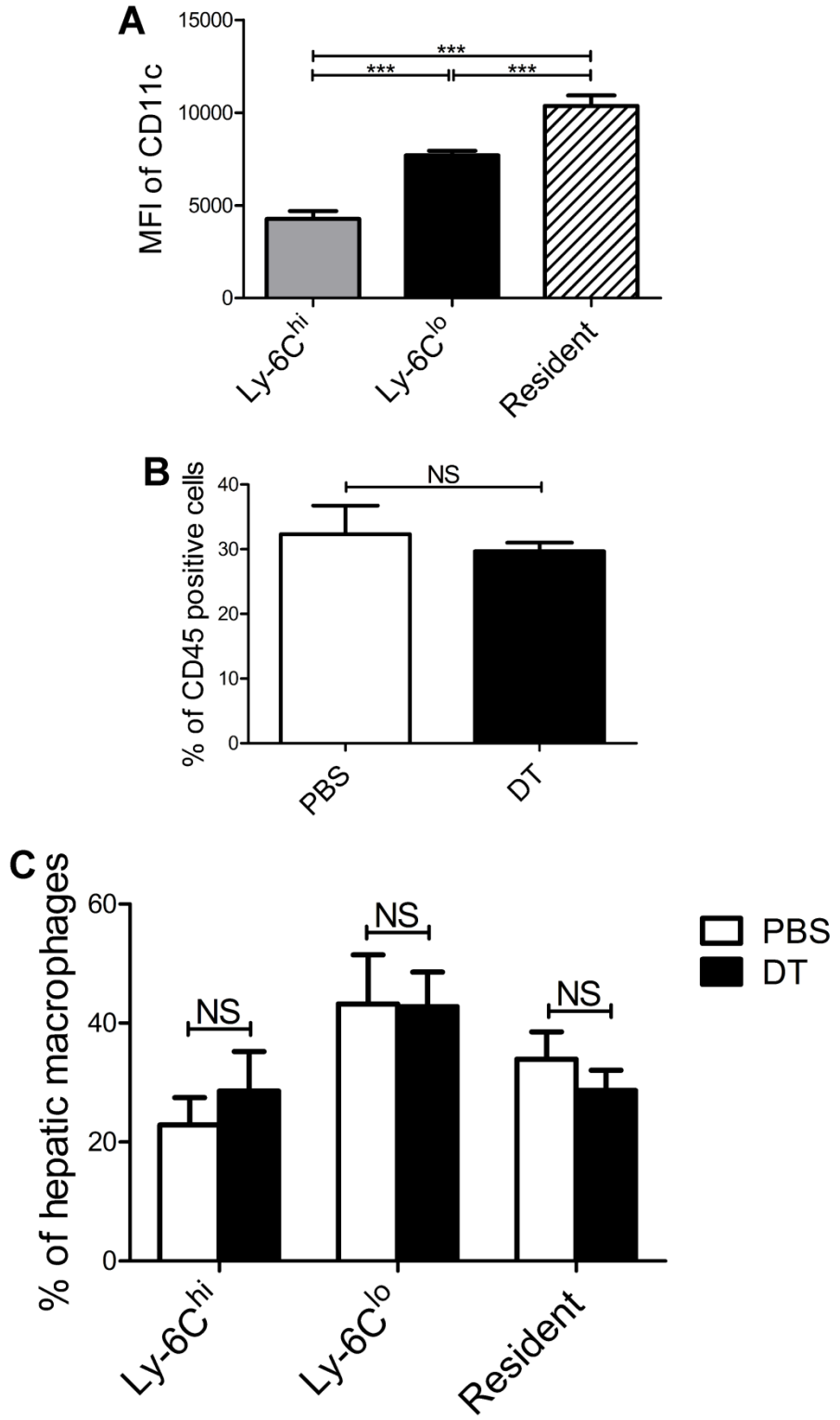

DISCUSSION

In this chapter I have characterised distinct macrophage depletion strategies in our 4 week CCl_4 model and utilised these data to confirm that the Ly-6C^{lo} hepatic macrophage subset is functionally responsible for liver fibrosis regression.

For both CD11b-DTR and liposomal clodronate based depletion during the resolution phase following CCl_4 injury, I initially characterised the effects on circulating monocytes. DT administration to CD11b-DTR mice resulted in depletion of both Ly-6C^{hi} and Ly-6C^{lo} circulating monocytes, with a more profound depletion of the Ly-6C^{lo} population. This is in keeping with Ly-6C^{lo} monocytes being a more mature cell type, formed from differentiation of Ly-6C^{hi} monocytes, and thus taking longer to replenish following depletion (Gordon and Taylor, 2005, Yona et al., 2013). Similarly, liposomal clodronate administration resulted in a significant reduction in Ly-6C^{lo} circulating monocytes. However, in this model I observed an increase in Ly-6C^{hi} circulating monocytes. This was in contrast to previous data, where liposomal clodronate caused depletion of Ly-6C^{hi} monocytes for up to 24 hrs (Sunderkotter et al., 2004). The reason for this difference is not clear. Of note previous analysis of monocyte dynamics following liposomal clodronate have been based on a single injection. In contrast, I have administered 3 doses of liposomal clodronate. It is therefore likely that repeated dosing may alter the sensitivity of the cells to depletion and hence the overall response of the animals. What is apparent when comparing these 2 depletion methods, is that CD11b-DTR based depletion induced a more profound loss of Ly-6C^{lo} monocytes whilst having the opposite effect on Ly-6C^{hi} monocyte number compared to liposomal clodronate. It is therefore feasible that this difference may contribute to differing functional effects.

I proceeded to characterise the effects of depletion during the resolution phase following CCl_4, on hepatic macrophage subsets. With the CD11b-DTR system, I observed a significant depletion of hepatic Ly-6C^{lo} monocyte-derived macrophages, with Ly-6C^{hi} monocyte-derived macrophage number unchanged, whilst resident macrophage numbers actually increased slightly (**Fig 4.2B**). The selectivity of depletion for the hepatic monocyte-derived macrophages compared to the "resident" macrophage population is likely related to the higher CD11b expression in this subset (**Fig 3.9A**). This is in keeping with the previously described resistance of resident Kupffer cells to depletion using the CD11b-DTR system (Cailhier et al., 2005, Devey et al., 2009). The fact we have observed a small increase in resident macrophage number, may represent a selection pressure favouring this population following depletion of the Ly-6C^{lo} monocyte-derived macrophages. The reasons behind the selectivity of depletion for hepatic Ly-6C^{lo} macrophages compared to pro-fibrogenic Ly-6C^{hi}

macrophages is likely to be multi-factorial. Firstly, we have shown that the Ly-6C^{lo} macrophage subset expresses higher levels of CD11b than the Ly-6C^{hi} population (Ramachandran et al., 2012) and **Appendix 2**). Additionally, the timing of depletion is likely to be critical. I have deliberately administered DT at 48, 72 and 96 hrs to maximize depletion during the rapid phase of fibrosis resolution. At these times, pro-fibrotic Ly-6C^{hi} macrophages have already declined significantly in number, whilst Ly-6C^{lo} macrophages make up the vast majority of the CD11b^{hi} monocyte-derived macrophages (**Fig 3.9B to D**). Therefore, administration of DT is likely to preferentially deplete the more numerous population. Published data do demonstrate that in this model, DT administration at an earlier timepoint during the inflammatory/fibrogenic phase when Ly-6C^{hi} cells are more numerous, results in loss of both Ly-6C^{hi} and Ly-6C^{lo} hepatic macrophages (Ramachandran et al., 2012) and **Appendix 2**). Furthermore, as discussed for circulating monocytes, depletion is more profound and protracted for the more mature population as it takes longer to replenish. It is likely that the Ly-6C^{lo} hepatic macrophage population also represents a more mature subset than Ly-6C^{hi} monocyte-derived macrophages, and therefore depletion with DT is more effective for these cells.

I was also able to define potential off target effects of the macrophage depletion methods on other cell types. In keeping with previous work (Cailhier et al., 2005, Duffield et al., 2005, Stoneman et al., 2007), there was no depletion of hepatic neutrophils (identified as shown in **Fig 3.8B**) following DT administration (**Fig 4.2C**). Furthermore, DT did not cause a change in hepatic CD3 positive cells, a marker of T cells (**Fig 4.2D**). This emphasises the specificity of depletion in the CD11b-DTR model.

Using this CD11b-DTR model, macrophage depletion during the resolution phase following CCl_4 resulted in higher levels of hepatic fibrosis as measured by picrosirius red, collagen 1 and collagen 3 staining. This indicates a failure of scar remodelling with macrophage depletion in this model, analogous to previous data (Duffield et al., 2005). Interestingly, I did not observe a significant difference in α-SMA staining following DT administration in these animals, suggesting that the observed phenotype is a result of failed matrix degradation rather than increased myofibroblast activation. To exclude a non-specific effect of DT administration on hepatic macrophages and fibrosis, I also administered DT (or PBS control) to wild-type mice during fibrosis resolution, using the same schedule. Importantly, this had no effect on macrophage subsets or hepatic fibrosis (**Fig 4.4**). These data, together with the previously described timing-dependent effects of DT in CD11b-DTR mice (Duffield et al., 2005), argue strongly against a non-specific effect.

I proceeded to use this CD11b-DTR model to determine associations between macrophage subset number and the degree of fibrosis resolution for individual animals. Strikingly, the number of Ly-6C^{lo} macrophages in the liver showed a statistically significant inverse correlation with the degree of liver fibrosis, emphasising that in mice with higher numbers of this Ly-6C^{lo} subset, fibrosis seems to regress more rapidly. No such correlation existed for either Ly-6C^{hi} or resident hepatic macrophages. These data, taken along with the previous evidence that hepatic Ly-6C^{lo} monocyte-derived macrophages accumulate in the liver maximally during the rapid phase of scar resolution (**Fig. 3.9**) and are the principal MMP-expressing subset (**Fig. 3.11**), identify them as the restorative hepatic macrophage, responsible for fibrosis regression and the restoration of normal tissue architecture following chronic injury.

The hepatic effects of liposomal clodronate administration to wild type mice during resolution from CCl_4 induced liver fibrosis were also studied. In contrast to the specific depletion seen in the CD11b-DTR system, liposomal clodronate resulted in significant depletion in all 3 hepatic macrophage subsets (Ly-6C^{hi}, Ly-6C^{lo} and Resident). Additionally, the degree of depletion for the critical Ly-6C^{lo} population was less when using liposomal clodronate (60.9±7.8%) when compared to CD11b-DTR (76.7 ± 3.16%). Furthermore, no effect on hepatic fibrosis was observed with liposomal clodronate administration during fibrosis resolution (**Fig. 4.6D**). The reason for this lack of effect, when compared to the striking changes in fibrosis resolution with depletion in the CD11b-DTR model despite identical depletion times, is probably multi-factorial. Ly-6C^{hi} hepatic macrophages have previously been shown to be the main pro-fibrogenic population (Karlmark et al., 2009), whilst my data suggests that Ly-6C^{lo} macrophages are the main restorative population. It is therefore likely that the balance of these populations of macrophages will determine whether active fibrogenesis or fibrosis regression occurs and hence the overall tissue phenotype. The fact that liposomal clodronate administration results in depletion of both these populations, whilst DT administration has selectivity for Ly-6C^{lo} cells and depletes this to a greater degree may well explain the differences in end effect. The other principal difference in hepatic macrophages when comparing CD11b-DTR depletion with liposomal clodronate is the effect on resident macrophages. These are increased slightly in CD11b-DTR whilst depleted significantly with liposomal clodronate. It is feasible that a potential pro-fibrogenic action of resident macrophages could explain the observed differences between the 2 depletion strategies.

Analysis of the effect of liposomal clodronate administration on other immune cells in the liver, demonstrated a significant increase in hepatic neutrophil number with a reduction in CD3 positive cells (**Fig 4.6B and C**). This increase in tissue neutrophils with liposomal clodronate treatment has also been observed in other studies (Wang et al., 2006, Mircescu et al., 2009). Thus, systemic liposomal clodronate administration during fibrosis resolution, has effects on cell types in the liver other than macrophages, potentially contributing to the differences observed with CD11b-DTR based depletion, and making it more difficult to draw specific conclusions about the functional role of individual macrophage populations.

Finally, the administration of liposomes alone has been shown to alter macrophage phenotype *in vivo* (Harel-Adar et al., 2011, Ma et al., 2011). This could potentially counteract the effects of depletion and thus must also be compared to administration of liposomes alone (See **CHAPTER 8**).

Finally, in this chapter, I sought to define the potential contribution of DCs to the macrophage populations I defined in the liver during fibrosis resolution. Using a CD11c-DTR system, which has previously been shown to deplete hepatic DCs (Phythian-Adams et al., 2010), no effect on macrophage subsets was observed following DT administration to these animals (**Fig. 4.7**). Thus, in our model it seems that DCs do not make any significant contribution to the dynamic changes we have seen during maximal fibrosis regression. Specifically, the Ly-6C^{lo} macrophage subset, the main MMP-expressing population which is critical for fibrosis resolution, is distinct from the phenotype attributed to hepatic DCs.

SUMMARY

- DT administration to CD11b-DTR mice during liver fibrosis resolution results in selective depletion of the Ly-6C^{lo} macrophage subset
- DT administration to CD11b-DTR mice during liver fibrosis resolution results in a failure in scar remodelling and hence persistent fibrosis
- Hepatic Ly-6C^{lo} macrophage number shows a statistically significant inverse correlation with the degree of persistent fibrosis, whilst other macrophage subsets do not. This confirms Ly-6C^{lo} hepatic macrophages as the likely restorative subset
- Liposomal clodronate administration to C57BL/6 mice during liver fibrosis resolution causes generalised hepatic macrophage depletion and alterations in liver neutrophil and T cell numbers
- Liposomal clodronate administration has no effect on liver fibrosis resolution
- Dendritic Cell depletion in CD11c-DTR mice has no effect on hepatic macrophage subsets

CHAPTER 5 – IDENTIFICATION OF THE CELLULAR SOURCE OF RESTORATIVE LY-6C^{lo} MACROPHAGES

INTRODUCTION

I have identified a novel Ly-6C^{lo} hepatic macrophage subset which accumulates maximally immediately prior to the rapid phase of fibrosis resolution following CCl_4 injury, represents the principal MMP-expressing macrophage population in the liver and whose selective depletion in CD11b-DTR mice causes a failure of matrix degradation. This population is therefore highly likely to be the hitherto elusive "restorative" hepatic macrophage. One of the key questions from previous data exploring the dual role of macrophages in hepatic fibrogenesis and fibrosis resolution was if these distinct functions were performed by resident or recruited cells and whether one population might change phenotype *in situ*, to cause differing effects (Friedman, 2005, Wynn, 2011). As described previously (**Fig 3.9B**), the Ly-6C^{lo} macrophage subset is CD11b^{hi} F4/80^{int}, in keeping with being a recruited monocyte-derived population (Holt et al., 2008). This would therefore indicate that this critical subset derives from one of the 2 main murine monocyte subsets: Ly-6C^{hi} or Ly-6C^{lo}. Previous work has identified hepatic Ly-6C^{hi} macrophages, derived from CCR2-dependent recruitment of Ly-6C^{hi} monocytes, as being the key pro-fibrogenic subset (Karlmark et al., 2009). Therefore, if restorative Ly-6C^{lo} macrophages also derive from Ly-6C^{hi} monocytes, this would indicate a change in macrophage phenotype *in vivo*. Conversely, if restorative Ly-6C^{lo} hepatic macrophages derive from Ly-6C^{lo} monocytes, it would suggest distinct phases of recruitment. Both of these mechanisms have been shown to be relevant in other forms of tissue injury and repair (Arnold et al., 2007, Nahrendorf et al., 2007). Additionally, recent data has suggested that local macrophage proliferation is important in chronic inflammation (Jenkins et al., 2011). The contribution of macrophage proliferation in liver fibrosis has not previously been defined.

AIMS

- To use adoptive transfer and lineage tracing of Ly-6C^{hi} monocytes to identify a phenotypic switch forming Ly-6C^{lo} macrophages
- To use *in situ* labelling to determine the contribution of circulating Ly-6C^{lo} monocytes to the restorative hepatic macrophage population
- To determine the contribution of local macrophage proliferation to the formation of restorative Ly-6C^{lo} hepatic macrophages

RESULTS

Adoptive Transfer of CD45.1^{+} Ly-6C^{hi} Monocytes

As previously shown, circulating Ly-6C^{hi} "inflammatory" monocytes were increased during fibrogenesis (24 hrs) and maximal fibrosis resolution (72 hrs) following 4 weeks of CCl_4 injury (**Fig 3.10B**). In contrast Ly-6C^{lo} "patrolling" monocytes were only increased in number during fibrogenesis (24 hrs) and had returned to basal levels by the resolution phase (72 hrs) (**Fig 3.10C**), the time when restorative Ly-6C^{lo} hepatic macrophages peak in number. These changes in monocyte populations could suggest Ly-6C^{hi} monocytes as a possible source for restorative Ly-6C^{lo} hepatic macrophages. In order to demonstrate this, I performed adoptive transfer experiments.

I initially developed a method for isolating Ly-6C^{hi} monocytes from bone marrow in sufficient numbers for adoptive transfer. Ly-6C^{hi} monocytes were identified using flow cytometry as viable CD115^{+} CD11b^{+} Ly-6G^{-} Ly-6C^{hi} cells from whole bone marrow in keeping with previous studies (Getts et al., 2008) (**Fig 5.1A**).

I then proceeded to injure wild type (CD45.2^{+} CD45.1^{-}) C57BL/6 mice with 4 weeks of CCl_4 in an identical manner to that described previously. Ly-6C^{hi} monocytes were then identified in bone marrow from CD45.1^{+} C57BL/6 mice by flow cytometry and isolated by FACS sorting (**Fig 5.1A**). These CD45.1^{+} mice are maintained on a C57BL/6 background, enabling adoptive transfer of immune cells to wild type C57BL/6 mice without generating an immune response but allowing detection of donor cells in recipient animals by identifying CD45.1 expression (O'Connor et al., 2010). $9x10^5$ CD45.1^{+} Ly-6C^{hi} monocytes (or vehicle control) were injected via the tail vein into the injured wild type mice, 4 hrs following the final CCl_4 injection. Livers were harvested at 24, 72 and 168 hrs after the final CCl_4 injection, and assessed for the presence of CD45.1^{+} cells by flow cytometry (**Fig 5.1B**).

Figure 5.1 - Adoptive Transfer of CD45.1^{+} Ly-6C^{hi} Monocytes

(**A**) Ly-6C^{hi} monocytes for adoptive transfer were isolated by FACS sorting of whole bone marrow from male CD45.1+ C57BL/6 mice, gating on the cells, excluding the neutrophils (CD11b+ Ly-6G+) and selecting CD115+ CD11b+ Ly-6C^{hi} cells. Representative flow cytometry plots shown. (**B**) Schematic representation of model of adoptive transfer of CD45.1+ Ly-6C^{hi} monocytes (or vehicle control) into C57BL/6 mice (CD45.2+), 4 hrs following the final CCl_4 injection, with livers harvested at 24, 72 and 168 hrs.

Figure 5.1 - Adoptive Tranfer of CD45.1^{+} Ly-6C^{hi} Monocytes

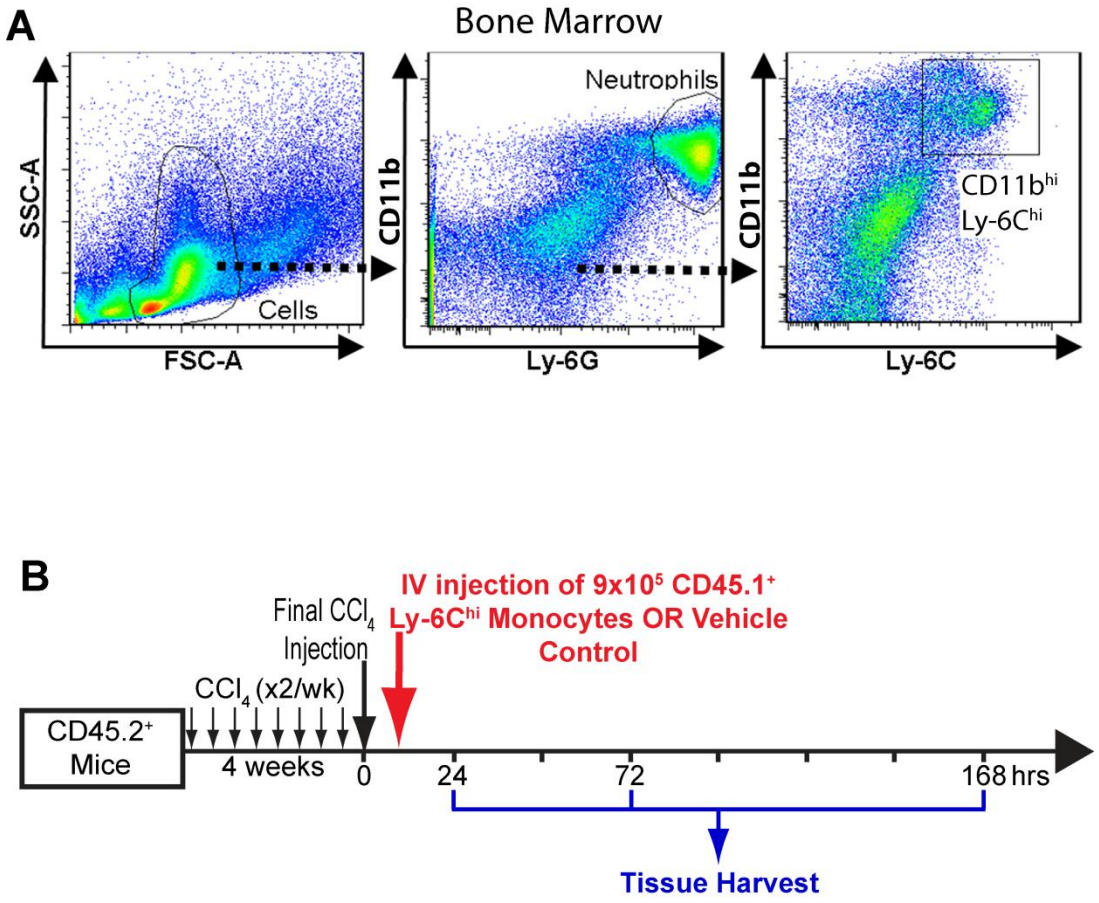

Ly-6C^{hi} Monocytes Differentiate into Hepatic Ly-6C^{lo} Macrophages

Having adoptively transferred Ly-6C^{hi} monocytes, I sought to identify the donor cells in the livers of recipient animals. As shown in **Fig 5.1B**, livers were harvests at 24, 72 and 168 hrs following the final CCl_4 injection. Flow cytometry was performed on hepatic non-parenchymal cells; staining for CD45.1 in addition to the leukocyte and macrophage markers I have used previously (**Fig 3.8B, 3.9A and B**).

As shown in **Fig 5.2A** and described in detail in the legend, a population of CD45.1^{+} cells could be identified in livers at the 24 and 72 hr timepoints, whilst they were no longer detectable by 168 hrs (n=3 per timepoint). By definition, these hepatic cells must be derived from the adoptively transferred injected Ly-6C^{hi} monocytes. To exclude non-specific CD45.1 staining, livers from CCl_4 treated animals injected with a vehicle control rather than cells were also harvested and stained in an identical manner. As shown, no significant CD45.1 staining was seen in these animals (**Fig 5.2A**). Additionally, no CD45.1^{+} cells were detected in the circulation by flow cytometry.

I went on to further characterize the hepatic CD45.1^{+} positive cells on the basis of the previously defined macrophage subsets. At both 24 and 72 hrs the vast majority of CD45.1^{+} cells were CD11^{hi} F4/80^{int}, indicative of a hepatic monocyte-derived macrophage population (**Fig 5.2B**, n=3). Analysis of Ly-6C expression on the CD45.1^{+} monocyte-derived macrophages identified the majority of the donor cells as being Ly-6C^{lo} hepatic macrophages (**Fig 5.2C**, n=3). Overall, as shown in **Fig 5.2D**, at least 90% of the CD45.1^{+} hepatic macrophages, derived from donor Ly-6C^{hi} monocytes, had formed Ly-6C^{lo} macrophages at both 24 and 72 hrs (n=3).

Figure 5.2 - Ly-6C^{hi} Monocytes Differentiate into Hepatic Ly-6C^{lo} Macrophages

(**A**) Identification of injected CD45.1+ cells in digested livers at 24 and 72 hr timepoints (Gating on viable CD45.2- cells). (**B**) Hepatic CD45.1+ cells have predominantly differentiated into CD11b^{hi} F4/80^{int} monocyte-derived macrophages. (**C**) CD45.1+ monocytes have largely formed the restorative Ly-6C^{lo} macrophage subset. (**D**) Quantification of proportion of identified CD45.1+ hepatic macrophages forming each of the macrophage subsets (n=3 per timepoint). All data shown as Mean±S.E.M; ***P<0.001; Representative flow cytometry plots and proportions shown.

Figure 5.2 - Ly-6C^{hi} Monocytes Differentiate into Hepatic Ly-6C^{lo} Macrophages

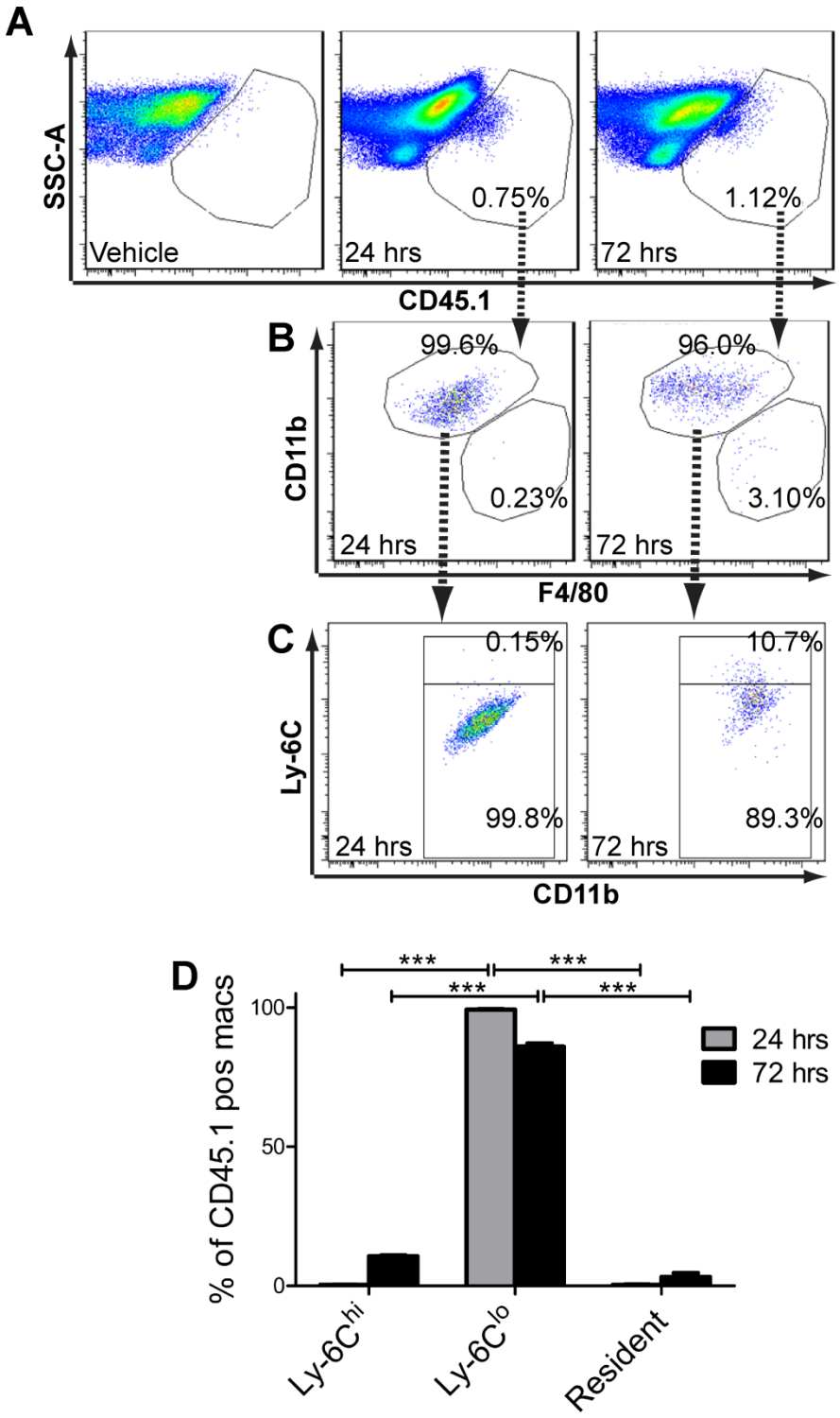

Selective *In Vivo* Labelling of Ly-6C^{lo} Monocytes to Enable Lineage Tracing

In order to determine the contribution of circulating Ly-6C^{lo} "patrolling" monocytes to hepatic macrophage subsets during fibrogenesis and fibrosis resolution, I employed a well-described *in vivo* labelling method. Intravenous administration of inert 0.5µm fluorescent latex microspheres selectively labels a proportion Ly-6C^{lo} monocytes, without activating the cells or altering their ability to traffic to sites of inflammation (Tacke et al., 2007, Tacke et al., 2006). The subsequent identification of latex positive cells in tissues identifies them as having a likely origin from Ly-6C^{lo} monocytes.

Wild type C57BL/6 mice were injured with 4 weeks of CCl_4, as before. According to the schedule shown in **Fig 5.3A**, mice then received an intravenous injection of 200µl fluorescent latex beads or vehicle control, 4 hours following the final CCl_4 dose. Blood and livers were then harvested at 24, 72 and 168 hours and assessed by flow cytometry.

Circulating Ly-6C^{hi} and Ly-6C^{lo} monocytes were identified by flow cytometry as previously described (**Fig 3.10A**). As shown in **Fig 5.3B**, I could then determine the proportion of each monocyte subset that was latex positive, indicating bead ingestion. Quantification of this at each timepoint, determined that using this method only a very small proportion of Ly-6C^{hi} monocytes contained latex beads, whilst up to 9% of Ly-6C^{lo} monocytes were labelled during early timepoints declining to around 4% at 168 hours (**Fig 5.3C**, n=4). This is broadly similar to previous studies using describing this technique (Tacke et al., 2007, Tacke et al., 2006).

Labelled Ly-6C^{lo} Monocytes Traffic to the Liver during Late Resolution and form Resident Macrophages

I then proceeded to assess hepatic macrophages for the presence of latex beads by flow cytometric analysis of livers at 24, 72 and 168 hr timepoints. As shown in **Fig 5.4A**, no hepatic latex positive macrophages were seen at 24 or 72 hrs, despite concurrent latex positive circulating Ly-6C^{lo} monocytes (**Fig 5.3C**). However, a latex positive hepatic macrophage population became apparent during late resolution, 168 hours following the final CCl_4 injection (**Fig 5.4A**). Further flow cytometric analysis of this latex positive population, using the previously described panel of cell surface markers, showed that the majority of these latex positive cells were F4/80^{hi} CD11b^{int}, in keeping with a "resident" macrophage phenotype (**Fig 5.4B**). As shown in **Fig 5.4C**, quantification of the phenotype of hepatic latex positive macrophages using this flow cytometry panel, demonstrated that over

90% of them were CD11b^{int} F4/80^{hi} “resident” macrophages, whilst virtually none were restorative CD11b^{hi} F4/80^{int} Ly-6C^{lo} monocyte-derived macrophages (n=4).

Figure 5.3 – Selective *In Vivo* Labelling of Ly-6C^{lo} Monocytes to Enable Lineage Tracing

(**A**) Schematic representation of model of *in situ* labelling of circulating Ly-6C^{lo} monocytes, by intravenous injection of fluorescent latex beads (or vehicle control) 4 hrs following the final CCl_4 injection, with harvests at 24, 72 and 168 hrs. (**B**) Circulating monocytes were identified in blood, gating on CD11b+ Ly-6G- CD115+ Ly-6C^{hi} and Ly-6C^{lo} cells. Flow cytometric analysis of circulating Ly-6C^{hi} and Ly-6C^{lo} monocyte subsets for latex positivity, indicating ingestion of fluorescent latex beads. (**C**) Quantification of the proportion of circulating Ly-6C^{hi} and Ly-6C^{lo} monocytes containing latex beads, as assessed by flow cytometry, at the stated timepoints following the final CCl_4 injection (n=4). All data shown as Mean±S.E.M; Representative flow cytometry plots shown.

Figure 5.3 - Selective *In Vivo* Labelling of Ly-6C^{lo} Monocytes to Enable Lineage Tracing

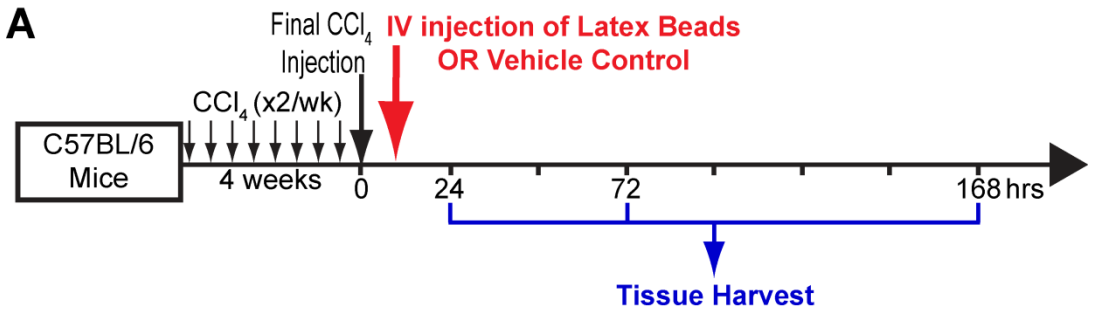

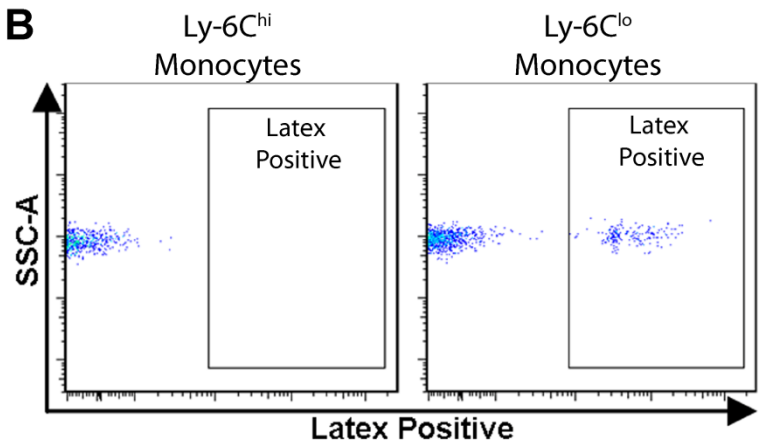

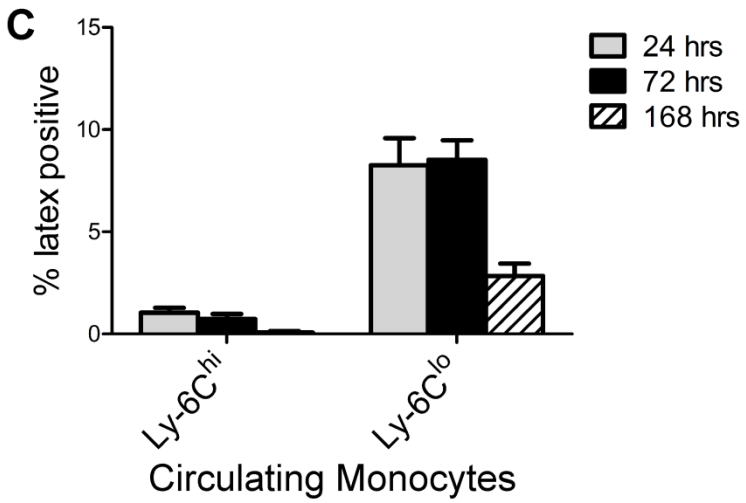

Figure 5.4 – Labelled Ly-6C^{lo} Monocytes Traffic to the Liver during Late Resolution and form Resident Macrophages

(**A**) Hepatic macrophages were identified by flow cytometry as CD45^{+} Ly-6G^{-} CD3^{-} NK1.1^{-} B220^{-} CD11b^{+} F4/80^{+} cells and assessed for latex positivity. Latex positive macrophages were identified in the liver only at 168 hrs (Representative proportion of latex positive macrophages as % of total hepatic macrophages shown). (**B**) The phenotype of hepatic latex positive macrophages was assessed by CD11b and F4/80 expression and divided into monocyte-derived macrophages (CD11b^{hi} F4/80^{int}) and resident macrophages (CD11b^{int} F4/80^{hi}). Representative proportion of each subset as a % of total latex positive macrophages shown. (**C**) Quantification of the proportion of latex positive macrophages forming each of the hepatic macrophage subsets (Ly-6C^{hi} CD11b^{hi} F4/80^{int}, Ly-6C^{lo} CD11b^{hi} F4/80^{lo} and resident CD11b^{int} F4/80^{hi}) at 168 hrs (Expressed as a % of latex positive macrophages; n=4). All data shown as Mean±S.E.M; ***P<0.001; Representative flow cytometry plots shown.

Figure 5.4 - Labelled Ly-6C^{lo} Monocytes only Traffic to the Liver during Late Resolution

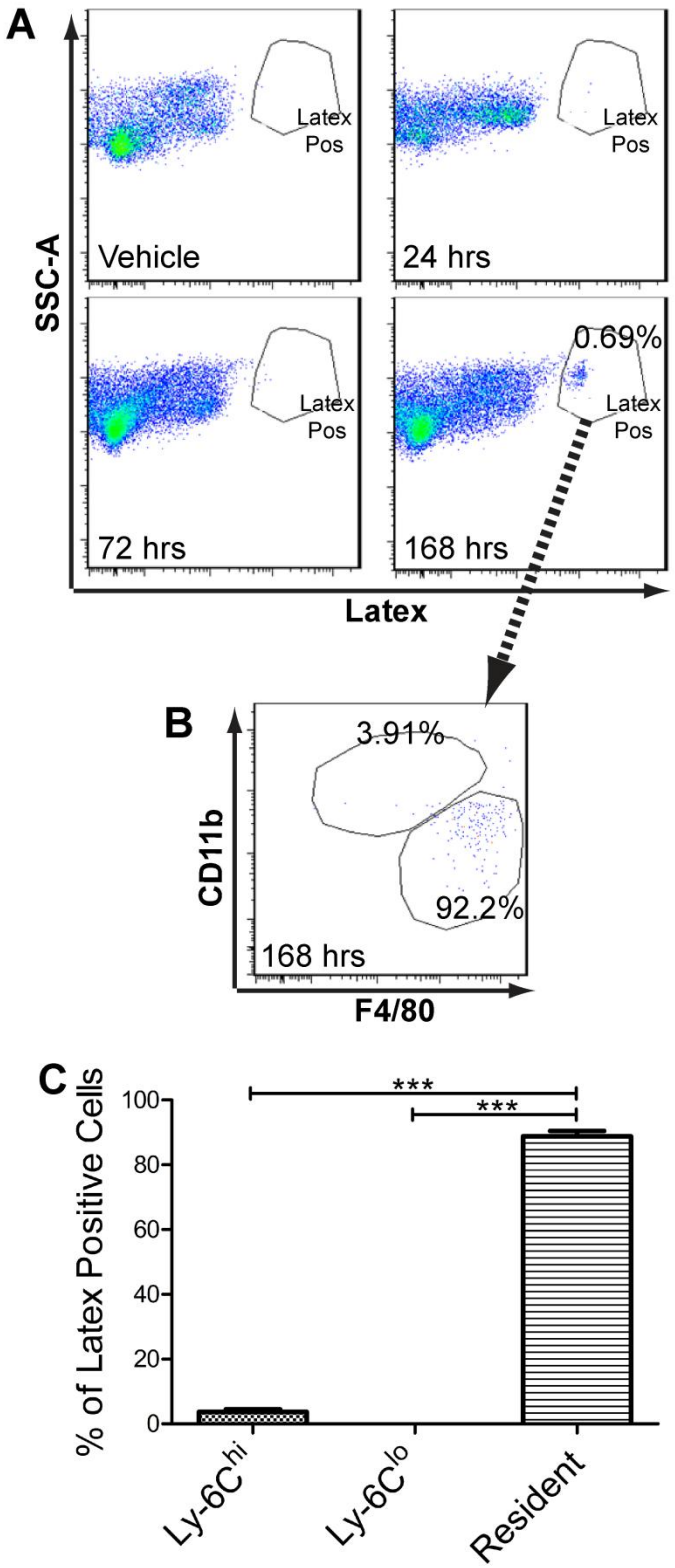

Local Proliferation of Hepatic Ly-6C^{hi} Macrophages Contributes to Changes in Subsets during Fibrogenesis and Fibrosis Resolution

Recent work has identified a role for local proliferation of macrophages in the expansion of the population during chronic inflammation (Jenkins et al., 2011). The role of this during hepatic fibrosis and fibrosis resolution has not previously been defined. In order to assess this, I injured wild type C57BL/6 mice with 4 weeks of CCl_4 as before, followed by liver harvests 24, 72 and 120 hrs after the final CCl_4 injection. Hepatic non parenchymal cells were isolated as before and stained with the previously described panel of markers (**Fig 3.8B**). On this occasion, cells were also co-stained for the proliferation marker Ki-67 (or isotype control) in a manner similar to that published (Jenkins et al., 2011). As shown in **Fig 5.5A**, using this method I was able to identify Ki-67 positive hepatic macrophages, when compared to an isotype control. This is indicative of active proliferation of these cells.

Using flow cytometry at each timepoint, I proceeded to subdivide the macrophages into the previously defined subsets Ly-6C^{hi} CD11b^{hi} F4/80^{int}, Ly-6C^{lo} CD11b^{hi} F4/80^{int} and resident CD11b^{int} F4/80^{hi}. Each of these was then assessed for the degree Ki-67 positivity, to determine which of the hepatic macrophage subsets was proliferating at which timepoint. As shown in **Fig 5.5B**, the pro-inflammatory Ly-6C^{hi} hepatic monocyte-derived macrophage population was the predominant Ki-67 positive macrophage subset at all 3 timepoints studied (n=3-6). Indeed, during the inflammatory/fibrogenic phase (24 hrs), 38.2±8.3% of these cells were Ki-67 positive indicative of a high level of proliferative activity (**Fig 5.5B**). Proliferative activity, whilst present, was at a significantly lower level in both Ly-6C^{lo} and resident macrophages (**Fig 5.5B**).

Figure 5.5 - Local Proliferation of Hepatic Ly-6C^{hi} Macrophages Contributes to Changes in Subsets during Fibrogenesis and Fibrosis Resolution

Wild type C57BL/6 mice were injured with 4 weeks of CCl_4, followed by liver harvests 24, 72 and 120 hrs after the final CCl_4 injection. Hepatic non-parenchymal cells were isolated at each timepoint and macrophages defined as $CD45^+$ Ly-$6G^-$ $CD3^-$ $NK1.1^-$ $B220^-$ $CD11b^+$ $F4/80^+$ cells by flow cytometry. (**A**) Ki-67 (or isotype control antibody) co-staining of hepatic non-parenchymal cells to enable identification of Ki-67 positive macrophages by flow cytometry. (**B**) Percentage of stated macrophage subset at indicated timepoint identified as Ki-67 positive (n=3-6). All data shown as Mean±S.E.M; **P*<0.05; Representative flow cytometry plots and proportions shown.

Figure 5.5 - Local Proliferation of Hepatic Ly-6C^{hi} Macrophages Contributes to Changes in Subsets during Fibrogenesis and Fibrosis Resolution

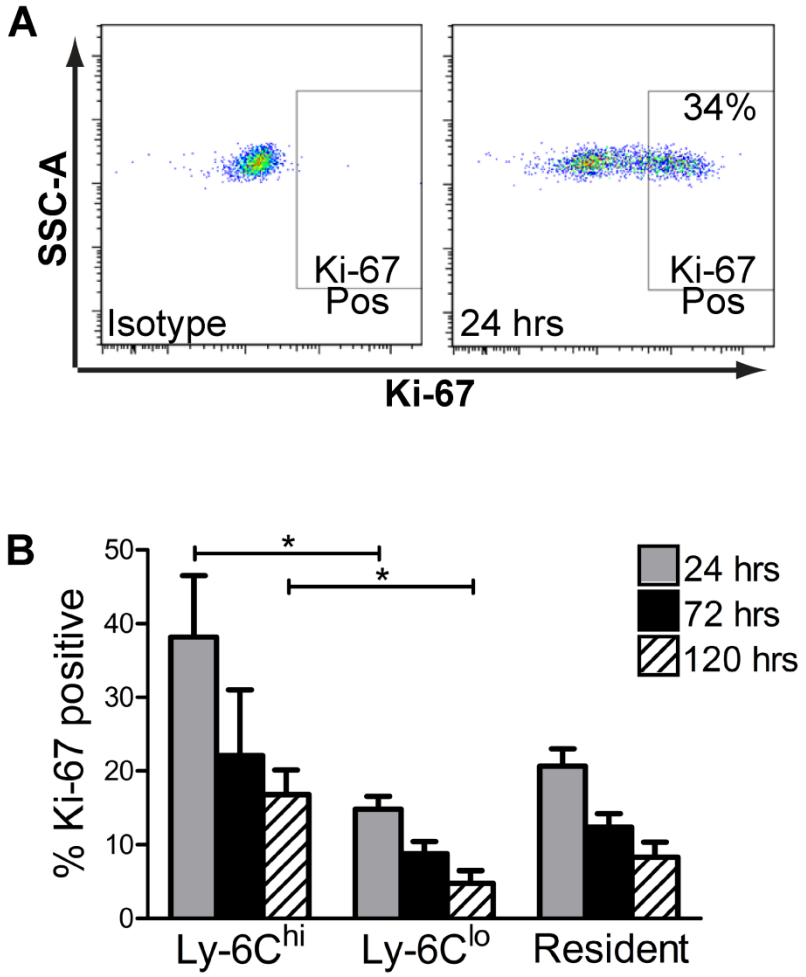

DISCUSSION

In this chapter, using an adoptive transfer of Ly-6C^{hi} bone-marrow derived monocytes, I have demonstrated that the restorative Ly-6C^{lo} hepatic macrophage subset is derived from Ly-6C^{hi} "inflammatory" monocytes. Given that previous work has shown pro-fibrotic Ly-6C^{hi} hepatic monocyte-derived macrophages also derive from recruited Ly-6C^{hi} monocytes (Karlmark et al., 2009), these data suggest that the restorative Ly-6C^{lo} hepatic macrophages form following a switch in macrophage phenotype *in situ*. This is strengthened by the close temporal relationship between the loss of hepatic Ly-6C^{hi} and increase in Ly-6C^{lo} macrophages (**Fig 3.9 B to D**) and the fact that the maximal increase in hepatic Ly-6C^{lo} macrophages (72 hrs) occurs after a decline in hepatic CCL2 levels (**Fig 3.5B**), the principal chemokine implicated in mediating recruitment of inflammatory monocytes.

I proceeded to study the contribution of Ly-6C^{lo} circulating monocytes to hepatic macrophage subsets during resolution from CCl_4 induced liver fibrosis. Using a well described *in situ* labelling technique with fluorescent latex beads (Tacke et al., 2007, Tacke et al., 2006), Ly-6C^{lo} circulating monocytes do not seem to contribute to any of the hepatic macrophage populations during inflammation/fibrogenesis (24 hrs) or maximal fibrosis resolution (72 hrs) phase following the final CCl_4 injection. Specifically, I have found no evidence that Ly-6C^{lo} monocytes form restorative Ly-6C^{lo} hepatic macrophages. Interestingly, during the late resolution phase (168 hrs) a proportion of the resident CD11b^{int} F4/80^{hi} hepatic macrophage subset was latex positive. This could suggest that Ly-6C^{lo} circulating monocytes may be relevant in repopulating the "resident" hepatic macrophages during late resolution. This has been a suggested function of this monocyte population by other authors (Gordon and Taylor, 2005). However, caution should be made in making this interpretation without further evidence, as hepatic macrophages are well known scavengers and may simply accumulate latex beads at this late juncture from dead or dying monocytes.

Overall, these data demonstrate that in the resolution from CCl_4-induced liver fibrosis, the key functional Ly-6C^{lo} macrophage subset derives from Ly-6C^{hi} and not Ly-6C^{lo} monocytes, indicating that an *in situ* change in macrophage phenotype rather than a separate phase of recruitment is critical. This is analogous to findings by *Arnold et al.* in skeletal muscle, where inflammatory Ly-6C^{hi} monocytes are recruited in response to injury and change phenotype to gain anti-inflammatory properties and promote muscle growth and regeneration (Arnold et al., 2007). In contrast, a murine model of myocardial infarction results in an initial recruitment of inflammatory Ly-6C^{hi} monocytes followed by a later second phase of

recruitment of Ly-6C^{lo} monocytes, which promote wound healing (Nahrendorf et al., 2007). Thus, the cellular dynamics of the macrophage response to tissue injury can vary significantly depending on the tissue involved and the nature of the injury.

I have also defined the relative contribution of local macrophage proliferation to hepatic macrophage subsets following CCl_4 injury. Interestingly, Ly-6C^{hi} monocyte-derived macrophages were the most proliferative subset during both the inflammatory/fibrogenic phase and fibrosis resolution phase. The fact that the number of these hepatic Ly-6C^{hi} macrophages declines rapidly during the switch to fibrosis regression (**Fig 3.9B and C**), despite active proliferation of this population (**Fig 5.5B**), emphasizes the point that this subset undergoes a change in phenotype *in situ*, leading to the formation of restorative Ly-6C^{lo} hepatic macrophages. The finding of proliferation of the monocyte-derived macrophages in the liver is seemingly in contrast with a recent study by *Jenkins et al.*, whereby resident, rather than recruited macrophage populations were the principal proliferative population in the context of chronic parasitic infection in the lung (Jenkins et al., 2011). However, on closer analysis the authors also showed the capacity of recruited monocyte-derived macrophages to proliferate in response to Il-4 stimulation in the context of more "classical" inflammatory stimuli (Jenkins et al., 2011), mirroring our observations. Therefore, it seems likely that the relative contribution of local proliferation of distinct macrophage subsets following injury will be critically dependent on the nature of the injury and the organ involved.

SUMMARY

- Restorative Ly-6C^{lo} hepatic macrophages derive from circulating inflammatory Ly-6C^{hi} monocytes, a common origin to pro-fibrotic Ly-6C^{hi} hepatic macrophages, indicating that a switch in macrophage function *in vivo* confers pro-resolution properties.
- Circulating Ly-6C^{lo} monocytes do not contribute to the restorative Ly-6C^{lo} hepatic macrophage population but may replenish "resident" macrophages following the cessation of injury.
- Pro-inflammatory Ly-6C^{hi} hepatic macrophages show a high level of Ki-67 staining during both liver fibrogenesis and early resolution, demonstrating that local proliferation of this subset contributes to macrophage expansion and potentially the change in phenotype in the CCl_4 model

CHAPTER 6 – CHARACTERISATION OF HEPATIC RESTORATIVE MACROPHAGE PHENOTYPE

INTRODUCTION

Having identified hepatic Ly-6C^{lo} monocyte-derived macrophages as the principle "restorative" population, responsible for the regression of liver fibrosis following chronic injury with CCl_4, I sought to characterize the phenotype of this population more extensively. In particular, I aimed to identify the specific mediators produced by this population that confer its pro-resolution properties. In order to do this, I compared the pro-resolution 72 hr Ly-6C^{lo} macrophages with pro-fibrotic 24 hr Ly-6C^{hi} hepatic macrophages given their common origin from Ly-6C^{hi} monocytes, their distinct functional roles and their relative predominance at the critical timepoints in the 4 week CCl_4 fibrogenesis-resolution model. This comparison could also enable the identification of factors that might promote the switch in macrophage phenotype from one enhancing fibrogenesis to one inducing fibrosis regression.

Traditional views of macrophage phenotype and polarization has focused on the M1 (classically activated) and M2 (alternatively activated) paradigm. It has been thought that M1 macrophages were pro-inflammatory, whilst M2 macrophages were responsible for wound healing responses (Mantovani et al., 2004, Mosser and Edwards, 2008). This classification was largely based on *in vitro* work and thus numerous markers of each activation state have been suggested. By analyzing the changes in expression of such markers from the unbiased microarray dataset, I also aimed to determine how the inflammatory and restorative hepatic macrophage subsets fitted into the traditional M1/M2 macrophage classification.

AIMS

- To profile gene expression of restorative Ly-6C^{lo} hepatic macrophages compared to pro-fibrotic Ly-6C^{hi} hepatic macrophages using microarray to identify key mediators produced by each subset
- To use gene expression profiles to identify key pathways that are expressed in each macrophage population
- To use gene expression profiles to identify specific markers of each subset which will enable identification by immunohistochemistry in murine and human tissue
- To utilize pathway analysis to identify factors that might induce the switch from pro-fibrotic to pro-resolution macrophage phenotype

RESULTS

Cell Sorting of Hepatic Ly-6C^{hi} and Ly-6C^{lo} Macrophage Subsets to Study Distinct Phenotypes

To study the phenotypes and identify specific mediators produced by the functionally distinct Ly-6C^{hi} and Ly-6C^{lo} hepatic macrophage subsets, I developed a method for isolating and purifying these populations. Wild type C57BL/6 mice were injured as before with 4 weeks of CCl_4. Livers were then harvested at 24 or 72 hrs following the final CCl_4 injection, the times of inflammation/fibrogenesis and maximal fibrosis resolution respectively. Digested livers were analysed by flow cytometry as before and macrophage subsets defined (**Fig 3.9 A and B**). The predominant macrophage population (Ly-6C^{hi} for 24 hrs; Ly-6C^{lo} for 72 hrs) at each timepoint was isolated by cell sorting using FACS (**Fig 6.1A**). This enabled direct comparison between pro-fibrotic 24 hr Ly-6C^{hi} hepatic macrophages and pro-resolution 72 hr Ly-6C^{lo} macrophages, given their common origin and opposing functional roles in this model.

I confirmed the effectiveness of cell sorting by FACS by analyzing the sorted population compared to the original flow cytometric gates (**Fig 6.1B**). Overall, sorting by this method routinely yielded over 95% purity of the targeted cell population (**Fig 6.1B**). Thus, this method enables robust comparisons between these populations to be made, with minimal contamination from the other subsets of hepatic macrophage.

Figure 6.1 – Cell Sorting of Hepatic Ly-6C^{hi} and Ly-6C^{lo} Macrophage Subsets to Study Distinct Phenotypes

(**A**) Isolation of hepatic macrophage subsets by FACS. Adult male C57BL/6 mice were injured with 4 weeks of CCl_4 with liver harvest at 24 or 72 hrs following the final CCl_4 dose. Macrophages were defined as viable CD45+ Ly-6G- NK1.1- B220- CD3- and dual-positive CD11b+ F4/80+ cells. 24 hr CD11b^{hi} F4/80^{int} Ly-6C^{hi} and 72 hr CD11b^{hi} F4/80^{int} Ly-6C^{lo} macrophages were then isolated by FACS. (**B**) Confirmation of effectiveness of cell sorting. 24 hr Ly-6C^{hi} hepatic macrophage subset was identified by flow cytometry and purified by FACS. Proportion of sorted cells lying within the Ly-6C^{hi} macrophage gate was then defined. Representative flow cytometry plots and percentages are shown.

Figure 6.1 - Cell Sorting of Hepatic Ly-6C^{hi} and Ly-6C^{lo} Macrophage Subsets to Study Distinct Phenotypes

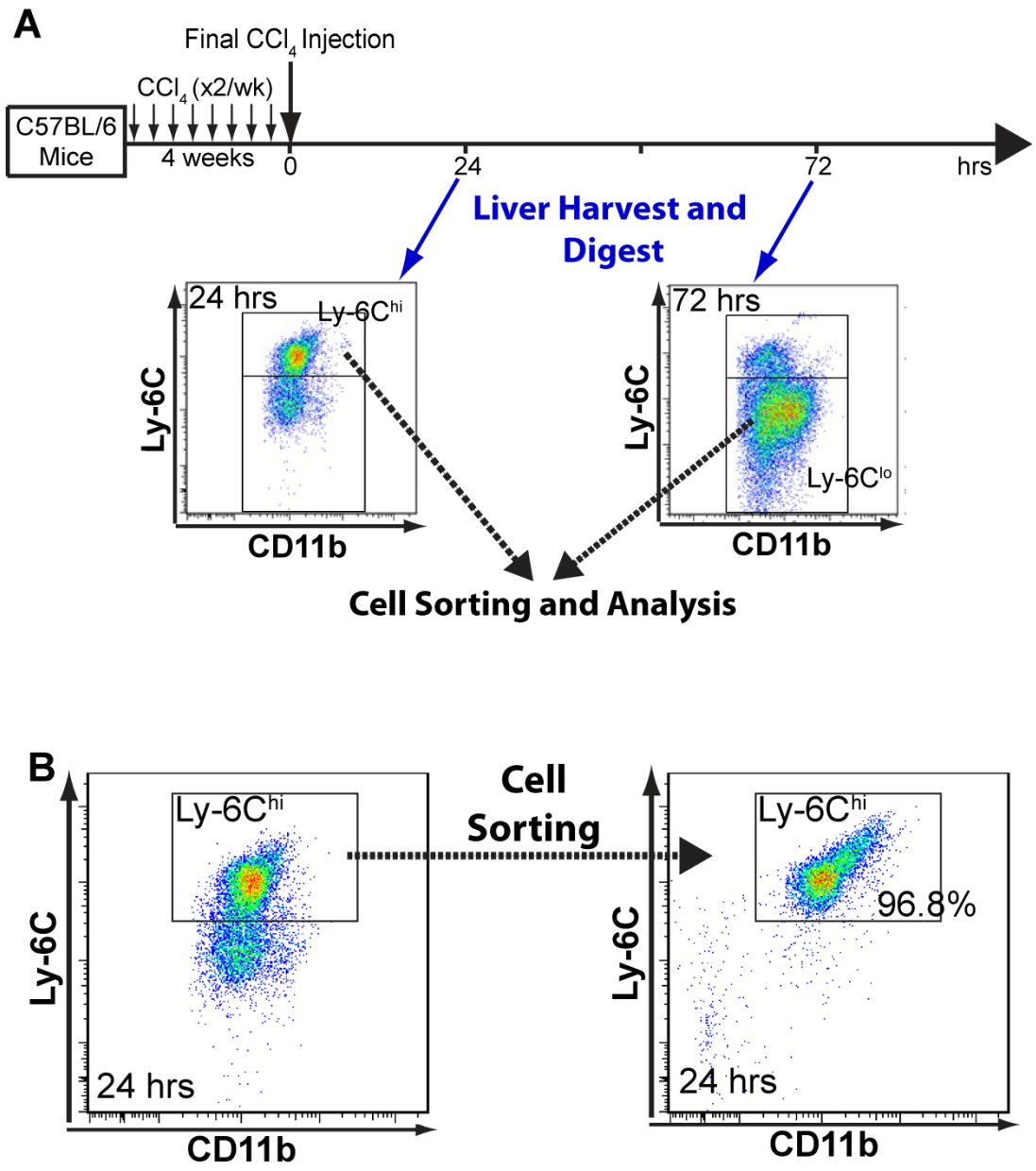

Gene Expression Profiling Demonstrates that Ly-6C^{lo} Hepatic Macrophages have a Number of Pro-Resolution Properties

Having established a robust method for isolating and purifying hepatic macrophage subsets using FACS, I proceeded to isolate RNA from inflammatory (24 hr Ly-6C^{hi}) and restorative (72 hr Ly-6C^{lo}) hepatic macrophages and performed whole transcriptome analysis using Affymetrix GeneChip microarrays. This provided an unbiased analysis of the expression of the whole mouse transcriptome (28,853 genes) in each of the critical macrophage populations. Given the low amounts of RNA obtained and the desire to avoid pooling animals, RNA had to be amplified using a commercially available kit, designed for purpose (**See Materials and Methods**). Data extraction and analysis was performed by Donald Dunbar and Jonathan Manning (QMRI Bioinformatics department). Overall, individual genes with a fold-change of >2 and P-value <0.05 between the 2 subsets were considered to be significantly different. Using these criteria, a full list of genes which are significantly more highly expressed in inflammatory macrophages and a list of genes more highly expressed in restorative macrophages are published (Ramachandran et al., 2012) and shown in **Appendix 2, Table S1 and S2**.

A number of relevant genes showed differential expression between the 2 subsets, highlighting some key features of each subset (**Fig 6.2A and 6.2B**, n=3). The full names of these genes are shown in **Appendix 1**. Our group and others have previously defined the key role of macrophage matrix metalloproteinase (MMP) expression in matrix degradation during fibrosis regression (Fallowfield et al., 2007, Pellicoro et al., 2011, Popov et al., 2010). In keeping with these findings, my data demonstrates an upregulation in macrophage MMP expression following the switch from inflammatory to restorative cells (**Fig 6.2A**). Conversely, a number of pro-inflammatory cytokines and chemokines are downregulated in the restorative macrophage subset (**Fig 6.2A**). TGF-β, the archetypal pro-fibrotic cytokine, showed mildly reduced expression in the restorative macrophages than the pro-fibrotic Ly-6C^{hi} macrophage subset (**Fig 6.2A**). However, more striking was the reduction in the expression of Thrombospondin-1, an important activator of latent TGF-β *in vivo* and a mediator that is increased in the fibrotic liver (Breitkopf et al., 2005, Crawford et al., 1998, Elpek et al., 2008, El-Youssef et al., 1999), in restorative macrophages when compared to pro-inflammatory macrophages (**Fig 6.2A**).

Restorative macrophages also showed increased expression of other genes which have been associated with an anti-fibrotic effect. For example, CX3CR1 expression has been associated with hepatic macrophage survival and the development of an anti-inflammatory macrophage

phenotype which restricts the degree of liver fibrosis following chronic injury (Karlmark et al., 2010). I have shown a trend towards increased CX3CR1 expression in the pro-resolution macrophages (**Fig 6.2A**). Similarly, macrophage migration inhibitory factor (MIF), acting via its receptor CD74, has been shown to have anti-fibrotic effects in the liver, potentially via an effect on hepatic stellate cells (Heinrichs et al., 2011). My data demonstrates an increase in CD74 expression in restorative macrophages (**Fig 6.2A**), potentially suggestive of an additional anti-fibrotic mechanism for this pathway. I have also identified increases in potentially relevant growth factors in restorative macrophages. For example, insulin like growth factor-1 (IGF-1) gene transfer to cirrhotic rats has been shown to induce matrix degradation and fibrosis resolution and to improve liver function (Sobrevals et al., 2010). Pro-resolution Ly-6C^{lo} hepatic macrophages show a striking increase in Igf-1 expression (**Fig 6.2A**).

Hepatic Macrophage Subsets do not Conform to the Traditional M1/M2 Paradigm

As shown in **Fig 6.2B** and described in detail in the legend, Ly-6C^{lo} restorative hepatic macrophages showed increased expression of some previously described M2 macrophage markers such as Mrc1 (Macrophage Mannose Receptor 1), Arg1 (Arginase-1) and Retnla (Fizz-1) (n=3). However, these cells also downregulated other traditional M2 markers such as Chi3l3 (YM-1), Il1rn (Il-1 receptor antagonist), Kdm6b (Jmjd3), Ccl24, Il-10 and TGF-β (**Fig 6.2A and 6.2B**) (Lawrence and Natoli, 2011, Mantovani et al., 2004). Simultaneously, Ly-6C^{lo} macrophages upregulated traditional M1 genes such as Ciita (MHC class II transactivator), CD16, CD32 and Serpine1 (PAI-1, plasminogen activator inhibitor type 1) (**Fig 6.2A and 6.2B**) (Shi et al., 1998, Lawrence and Natoli, 2011, Mantovani et al., 2004). Thus, both inflammatory Ly-6C^{hi} and restorative Ly-6C^{lo} hepatic macrophages demonstrate features of M1 and M2 polarization.

Figure 6.2 – Differential Expression of Key Genes Define Inflammatory and Restorative Hepatic Macrophages

Microarray analysis of inflammatory Ly-6C^{hi} and restorative Ly-6C^{lo} hepatic macrophage populations isolated by FACS sorting from livers 24 and 72 hrs following the final CCl_4 injection respectively. Full names of abbreviated genes are shown in **Appendix 1**. (**A**) Differential regulation of cytokines, chemokines, chemokine receptors, growth factors and matrix degrading enzymes between the inflammatory and restorative macrophage populations (Expressed as fold change between the 2 macrophage subsets) (**B**) Differential expression of opsonins, phagocytosis-related genes, PPAR-γ target genes and macrophage phenotype markers (M1-classical, M2-alternative) between the macrophage subsets on microarray (Expressed as fold change between the 2 macrophage populations). All microarray data based on n=3 per group taken from 2 independent experiments; *P<0.05, **P<0.01, ***P<0.001.

Figure 6.2 - Differential Expression of Key Genes Define Inflammatory and Restorative Hepatic Macrophages

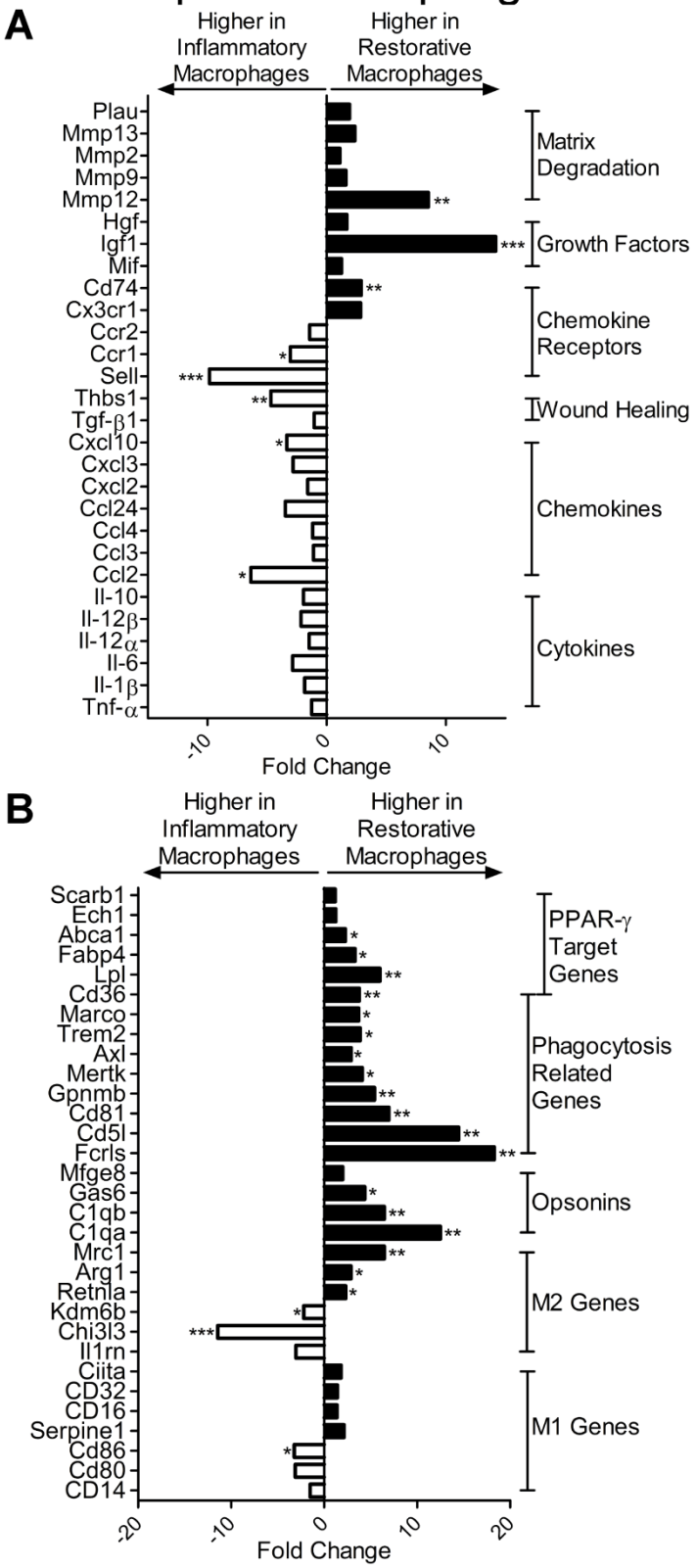

Pathway Analysis of Differentially Expressed Genes Identifies Phagocytosis as a Key Feature of Restorative Macrophages

Having identified numerous genes which were differentially regulated between inflammatory and restorative hepatic macrophages (**see Appendix 2, Table S1 and S2**), I proceeded to perform a further analysis on these genes to determine which pathways might be relevant in each subset. I utilized the DAVID tool, which enables the classification of large lists of genes into functional clusters, on the basis of known pathways including gene ontology and KEGG, to identify pathways which show enrichment in the list (Dennis et al., 2003, Huang da et al., 2009b, Huang da et al., 2009a). I inputted the list of genes from the microarray which were statistically more highly expressed in inflammatory (**see Appendix 2, Table S1**) or restorative macrophages (**see Appendix 2, Table S2**). Using these lists, the DAVID tool identified pathways which were statistically enriched in inflammatory (**Fig 6.3A**) and restorative (**Fig 6.3B**) macrophages, at a P-value of < 0.05.

Analysis of genes more highly expressed in inflammatory 24hr Ly-6C^{hi} hepatic macrophages demonstrated enrichment for pathways such as response to wounding, coagulation cascade and chemotaxis (**Fig 6.3A**). These pathways have all been associated with fibrogenesis (Anstee et al., 2009, Sahin et al., 2010), in keeping with the known pro-fibrotic role of this cell population.

Pathway analysis of genes upregulated in restorative 72hr Ly-6C^{lo} hepatic macrophages demonstrated enrichment in lysosomes, endocytosis, scavenger receptors and antigen processing and presentation, all of which are implicated in phagocytosis (**Fig 6.3B**). Additionally, I identified enhancement of fatty acid metabolism and PPAR signalling pathways (**Fig 6.3B**)

The enrichment of phagocytosis related pathways in restorative macrophages was particularly striking. I therefore went on to confirm the upregulation of phagocytosis-related genes in this macrophage subset on an individual basis (**Fig 6.2B**). Specifically, Ly-6C^{lo} macrophages upregulated a number of opsonins, receptors and genes involved in the clearance of cellular debris. Additionally, a number of specific PPAR-γ target genes were increased in the restorative macrophage population (**Fig 6.2B**).

Figure 6.3 – Pathway Analysis of Differentially Expressed Genes from Macrophage Subsets

Pathway analysis using the DAVID tool of genes upregulated in each macrophage subset as identified on microarray (Expressed as number of upregulated genes in the stated pathway). (**A**) Pathways enriched in pro-inflammatory macrophage subset. (**B**) Pathways enriched in the restorative macrophage subset. Microarray data based on n=3 per group taken from 2 independent experiments. *P<0.05, **P<0.01, ***P<0.001.

Figure 6.3 - Pathway Analysis of Differentially Expressed Genes from Macrophage Subsets

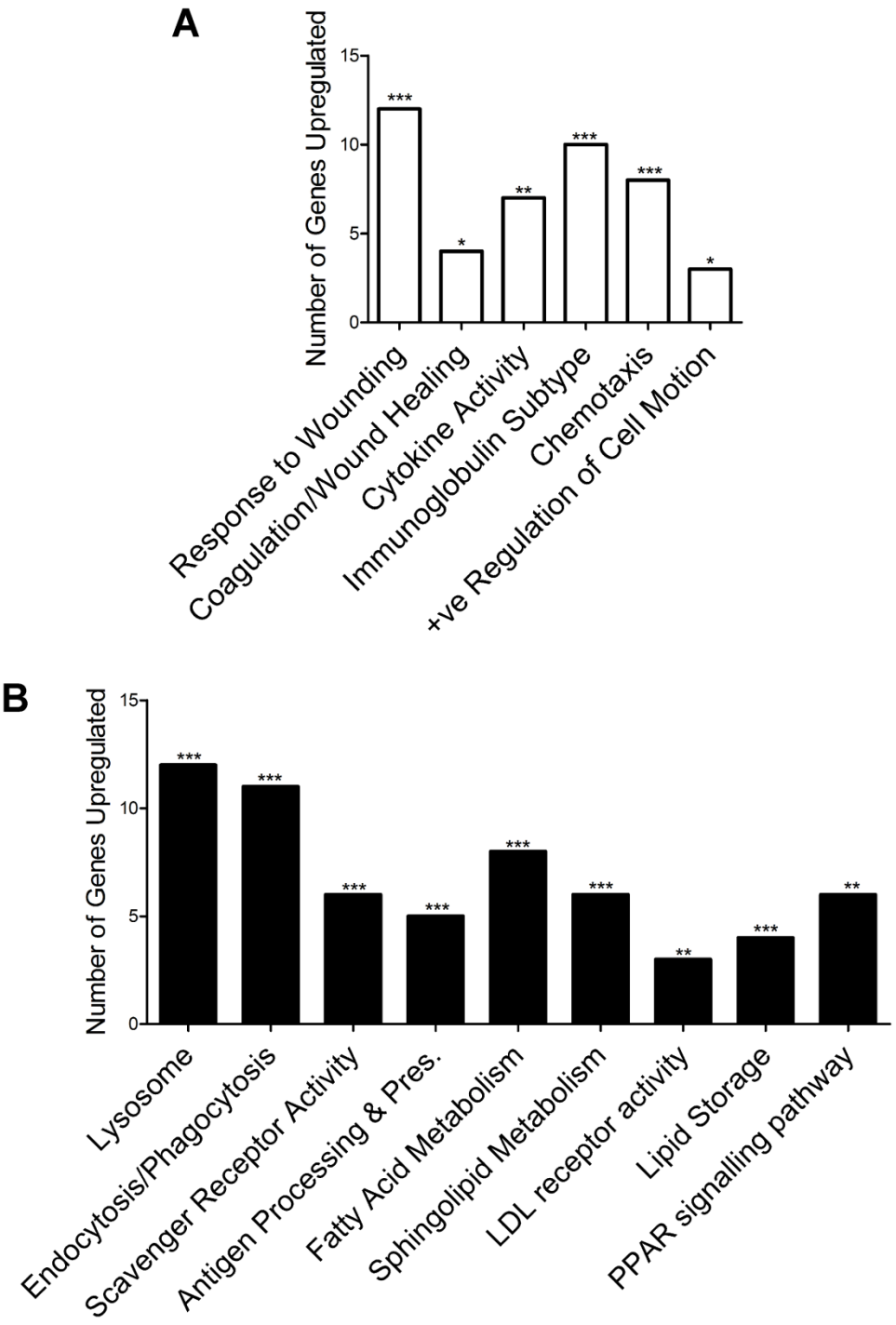

Confirmation of Microarray Findings at a Gene and Protein Level

In order to confirm the reliability of the microarray findings, I performed standard qPCR on amplified cDNA from each of the sorted macrophage subsets, for a number of the differentially expressed genes previously identified (**Fig 6.4A**, n=7-10). Importantly, the differences in gene expression were very similar with this method to those observed using the microarray (**Fig 6.2 A and B**), demonstrating the reliability and validity of the microarray data.

I went on to assess protein expression of a number of the identified differentially expressed genes on both inflammatory and restorative macrophages using flow cytometry (**Fig 6.4B**, n=3-6). These data confirmed that observed differences in gene expression on the microarray were also translated into differences in protein expression in each of the macrophage subsets.

I also determined and compared the overall MMP activity of inflammatory and restorative macrophage subsets. MMPsense was administered to mice according to the schedule previously shown (**Fig 3.11A**), followed by isolation of inflammatory (24 hr Ly-6C^{hi}) and restorative (72 hr Ly-6C^{lo}) macrophages and assessment of the degree of MMPsense fluorescence and hence MMP activity. Importantly, each subset was isolated 24 hrs after an MMPsense injection. Comparison of MMPsense fluorescence, identified that restorative macrophages have greater MMP activity than inflammatory macrophages, mirroring the increase in MMP gene expression (**Fig 6.4B**, n=3-6). Thus, the switch forming restorative macrophages results in increased MMP activity.

Figure 6.4 – Confirmation of Microarray Findings at a Gene and Protein Level

Comparison of inflammatory Ly-6C^{hi} and restorative Ly-6C^{lo} hepatic macrophage populations isolated by FACS sorting from livers 24 and 72 hrs following the final CCl_4 injection respectively. (**A**) Expression of stated gene in restorative hepatic macrophages relative to mean expression in inflammatory macrophages as assessed by qPCR (n=7-10). (**B**) Flow cytometric analysis assessing the expression of stated marker in restorative macrophages relative to the mean expression in inflammatory macrophages. MMPsense was administered 24 hrs prior to the time of harvest to compare MMP activity between macrophage subsets. (MFI=Mean fluorescence Intensity; Relative to average MFI for inflammatory macrophage subset; n=3-6). All data shown as Mean±S.E.M; *P<0.05, **P<0.01, ***P<0.001.

Figure 6.4 - Confirmation of Microarray Findings at a Gene and Protein Level

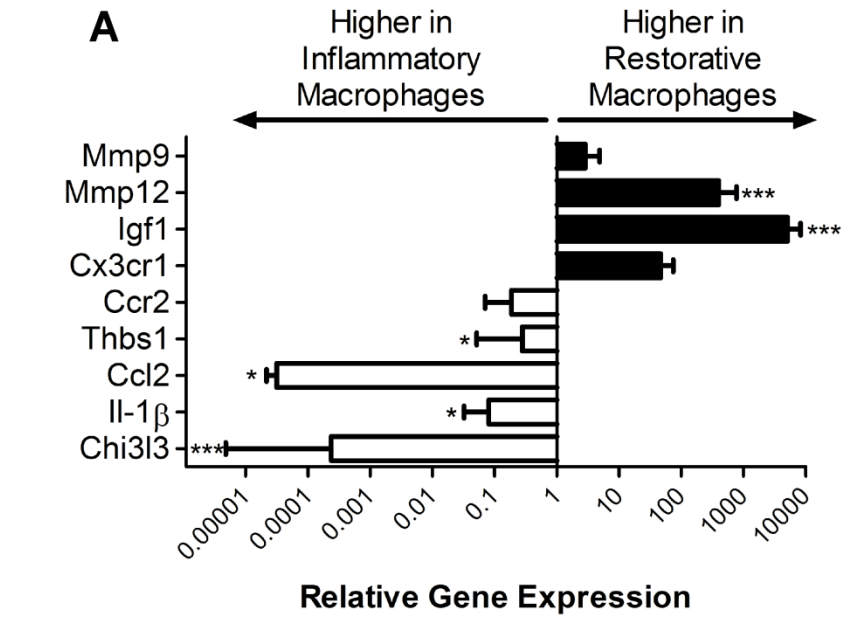

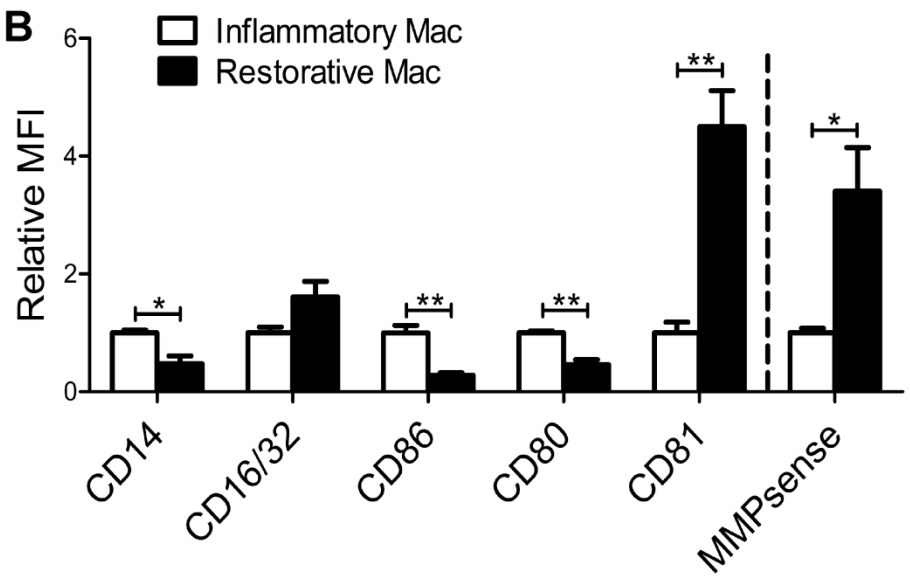

Identification of Macrophage Subsets by Immunohistochemistry in Murine and Human Liver

One of the key problems in studying macrophage heterogeneity is the lack of specific markers that identify functionally distinct populations *in situ*. This necessitates the use of multi-colour flow cytometry on freshly isolated tissue to identify distinct populations. This is obviously particularly problematic when attempting to study human disease. Having performed unbiased gene expression profiling on functionally distinct Ly-6C^{hi} and Ly-6C^{lo} hepatic macrophages, I sought to utilize these data to identify specific markers of each subset which could be used to identify these populations *in vivo*. Chi3l3 (YM-1) was very highly expressed in inflammatory Ly-6C^{hi} macrophages and rapidly downregulated following transition to the Ly-6C^{lo} phenotype (**Fig 6.2B**). Conversely MMP-12 and GPNMB showed a significant upregulation in the restorative macrophage population (**Fig 6.2A and 6.2B**).

I proceeded to perform immunohistochemistry for these markers in livers during the inflammatory (24 hrs) and maximal resolution (72 hrs) phases of our 4 week CCl_4 model. Numerous Chi3l3 positive cells were detected in livers at 24 hrs with a significant decline in number at 72 hrs (**Fig 6.5A**), mirroring the changes in Ly-6C^{hi} macrophage number seen on flow cytometry at these timepoints (**Fig 3.9 B to D**). Conversely, the number of hepatic MMP-12 and GPNMB positive cells increased from 24 to 72 hrs (**Fig 6.5A**), mirroring the flow cytometric changes in Ly-6C^{lo} macrophages (**Fig 3.9 B to D**). Furthermore, the spatial distribution of these MMP-12 and GPNMB positive cells are closely related to the hepatic scars at 72 hrs (**Fig 6.5A**), in keeping with a role in matrix degradation.

For further confirmation of the utility of these markers in identifying the distinct macrophage subsets, I determined the number of hepatic Chi3l3 and MMP-12 positive cells in my CD11b-DTR model (**Fig 4.1A**). Blinded cell counts showed that MMP-12 positive cells were reduced following DT administration (**Fig 6.5B**, n=5-6), whilst no difference in Chi3l3 positive cells was observed (**Fig 6.5C**, n=5-6). Once again these data mirror previous flow cytometric findings (**Fig 4.2B**), and highlight the potential utility of Chi3l3 and MMP-12 as specific markers of inflammatory (Ly-6C^{hi}) and restorative (Ly-6C^{lo}) hepatic macrophages respectively.

I went on to attempt to identify similar macrophage populations in human liver disease. Unfortunately, no human equivalent of Chi3l3 exists. I therefore focused on MMP-12 and GPNMB as potential markers of the human hepatic restorative macrophage. Immunohistochemistry of cirrhotic human liver identified both MMP-12 and GPNMB

positive cells, in association with hepatic scars (**Fig 6.5A**). In order to confirm that these populations represent macrophage subsets, I proceeded to perform dual immunofluorescence for MMP-12 and GPNMB with the macrophage marker CD68 in cirrhotic human liver. Both MMP-12 (**Fig 6.5D**) and GPNMB (**Fig 6.5E**) co-localized with CD68, indicating that they are expressed by a subpopulation of human hepatic macrophages, analogous to the murine data from the CCl_4 model.

Figure 6.5 - Identification of Macrophage Subsets by Immunohistochemistry in Murine and Human Liver

(**A**) Immunohistochemistry for genes differentially-regulated on microarray in murine liver at 24 and 72 hr timepoints and in cirrhotic human liver (Scale bars=100μm; Representative Images shown). (**B** & **C**) CD11b-DTR mice were injured for 4 weeks with CCl_4 followed by administration of DT or PBS 48, 72 and 96 hrs after the final CCl_4 injection with harvest at 120 hrs. Immunohistochemistry for MMP-12 and Chi3l3 was performed. (**B**) Average cell counts of MMP-12 positive cells per x200 field (Expressed relative to average count from PBS-treated mice; n=5-6). (**C**) Average cell counts of Chi3l3 positive cells per x200 field (Expressed relative to average count from PBS-treated mice; n=5-6). (**D**) Dual immunofluorescence for CD68 (red), MMP-12 (green) and DAPI (blue) in cirrhotic human liver (scale bar=10μm; arrows indicate cells with co-localization; staining in collaboration with R. Aucott). Comparison was made to tissue stained with isotype control antibodies. (**E**) Dual immunofluorescence for CD68 (red), GPNMB (green) and DAPI (blue) in cirrhotic human liver (scale bar=10μm; arrows indicate cells with co-localization; staining in collaboration with R. Aucott). Comparison was made to tissue stained with isotype control antibodies. Representative images shown. All data expressed as Mean±S.E.M; $^{**}P<0.01$, NS-Not significant.

Figure 6.5 - Identification of Macrophage Subsets by Immunohistochemistry in Mouse and Human Liver

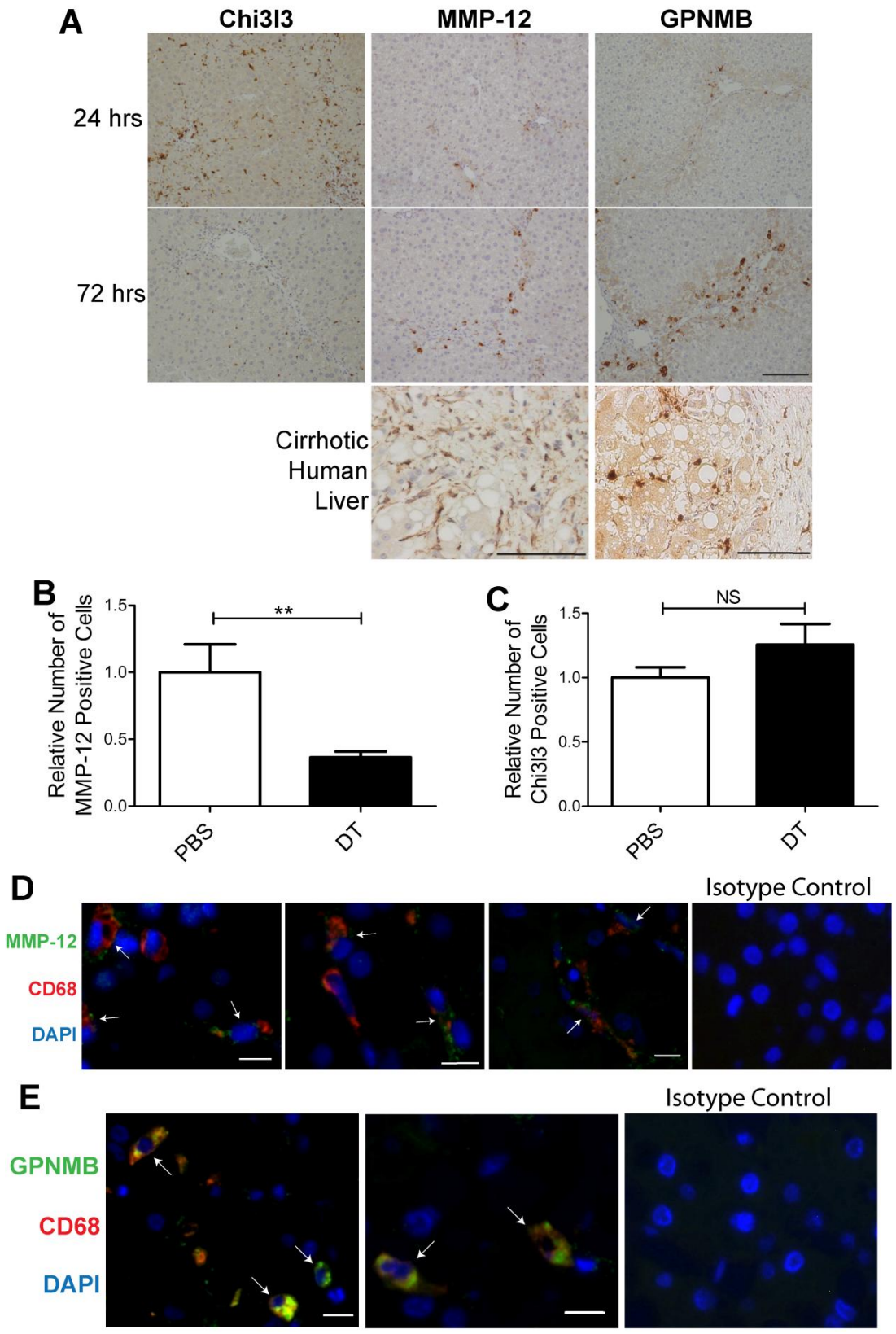

Restorative Macrophages are Post-Phagocytic

Phagocytosis and the removal of dead or dying cells is a critical function of tissue macrophages in inflammation, and has an important effect on the resultant macrophage phenotype (Devitt and Marshall, 2011, Erwig and Henson, 2007, Savill et al., 2002). As described, I defined an upregulation of pathways (**Fig 6.3B**) and individual genes (**Fig 6.2B**) which are important in phagocytosis, as a key feature of the restorative macrophage subset. Furthermore, the greatest increase in restorative macrophage number occurred after a significant reduction in hepatocyte death as assessed by serum AST and ALT levels (**Fig 3.5A**), suggesting that this macrophage subset emerges following the clearance of hepatocyte debris. I therefore sought to determine whether the restorative macrophage population showed evidence of prior phagocytosis. This could implicate the ingestion of debris as an important factor in the switch from inflammatory to pro-resolution macrophages.

I first investigated the morphological characteristics of hepatic inflammatory (24 hr Ly-6C^{hi}) and restorative (72hr Ly-6C^{lo}) macrophages. Using flow cytometry, restorative macrophages were larger (FSC-A) and showed increased granularity/complexity (SSC-A) (**Fig 6.6A**, n=13). Furthermore, hepatic scar associated macrophages were visually larger at 72 hrs than 24 hrs when examined using immunohistochemistry (**Fig 6.6B**). These changes could represent an effect of phagocytosis or simply differentiation of a more monocytic population into a more mature macrophage subset.

I therefore sought to identify the presence of intracellular debris in the macrophage subsets as categorical evidence of post-phagocytic phenotype. Inflammatory and restorative hepatic macrophages were FACS sorted as before (**Fig 6.1A**). Each subset was then fixed on slides, TUNEL stained and assessed using confocal microscopy to quantify the presence of intra- and extracellular apoptotic debris (**Fig 6.6C**). I then performed blinded cell counts on each subset. Importantly, no difference was seen between the percentage of inflammatory or restorative macrophages which were associated with TUNEL-positive apoptotic debris (**Fig 6.6D**, n=3-4). However, when the localization of apoptotic debris was compared between the 2 macrophage populations, a clear difference was observed (**Fig 6.6E**, n=3-4). Specifically, apoptotic debris was predominantly bound to the cell surface with inflammatory macrophages, whilst restorative macrophages had ingested the debris.

Figure 6.6 – Restorative Macrophages are Post-Phagocytic

Comparison of inflammatory (24 hr Ly-6C^{hi}) and restorative (72 hr Ly-6C^{lo}) macrophage subsets following 4 weeks of CCl_4. (**A**) Size (FSC-A) and complexity (SSC-A) of macrophage subsets assessed by flow cytometry (Expressed relative to average MFI for inflammatory macrophages; n=13 pooled from 3 independent experiments). (**B**) F4/80 immunohistochemstry demonstrates larger scar-associated macrophages at 72 hrs (Scale bar=50μm). (**C** to **E**) TUNEL-staining and confocal microscopy of FACS-sorted inflammatory and restorative hepatic macrophage subsets. (**C**) Stained DAPI, TUNEL, F4/80 and merged image for macrophage subsets (Scale Bars=10μm; Arrowheads=cell-surface debris; Arrows=ingested debris). (**D**) Percentage of each subset associated with TUNEL-positive nuclei by cell counting (n=3-4). (**E**) Percentage of TUNEL-associated macrophages with ingested or cell-surface debris (n=3-4). Data shown as Mean±S.E.M; **P*<0.05, ***P*<0.01, ****P*<0.001, NS=Non-significant. Representative images shown.

Figure 6.6 - Restorative Macrophages are Post-Phagocytic

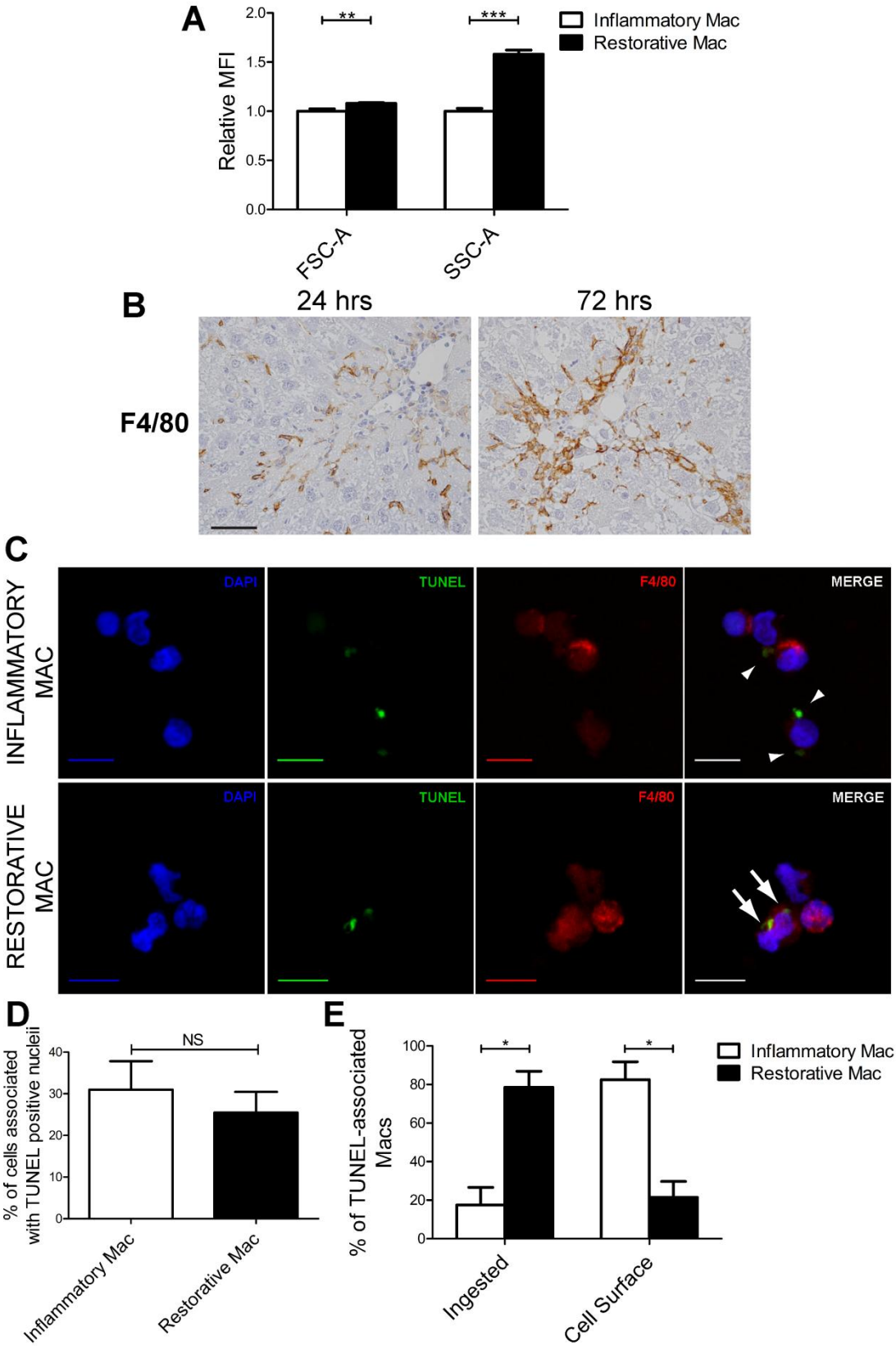

DISCUSSION

In this chapter I have isolated pure populations of "inflammatory" 24 hr Ly-6C^{hi} and "restorative" 72 hr Ly-6C^{lo} hepatic macrophages by FACS, enabling in depth analysis of the phenotype of these cells. Specifically, using an unbiased microarray approach, I have been able to exhaustively characterise these key hepatic macrophage subsets. This is the first such analysis of macrophage subsets isolated from fibrotic liver and is certainly the first to relate full gene expression profiles of macrophages to function in the liver.

Overall, these data show that the switch from pro-inflammatory pro-fibrotic Ly-6C^{hi} macrophages to restorative Ly-6C^{lo} macrophages confers a number of properties that could contribute to fibrosis regression. As anticipated, this change in macrophage phenotype results in an increase in MMP expression and overall MMP activity. Our group and others have previously demonstrated that macrophage MMP expression is critical for liver fibrosis regression (Fallowfield et al., 2007, Pellicoro et al., 2011, Popov et al., 2010). Interestingly, MMP-12 seems to be the most upregulated of the matrix degrading enzymes in the restorative macrophage subset. MMP-12 has matrix degrading properties important in liver fibrosis resolution (Pellicoro et al., 2011). However, the scope of activity of MMP-12 extends beyond simple matrix degradation and has also been shown to control the inflammatory response, particularly through modulation of chemokine activity (Chan et al., 2013, Dean et al., 2008). A number of other inflammatory cytokines and chemokines are reduced in the restorative macrophage population when compared to the pro-fibrogenic subset, in keeping with a less inflammatory macrophage phenotype when fibrosis resolution commences. TGF-β is the archetypal pro-fibrotic cytokine. Macrophages are a known source of TGF-β production, and logic would dictate that the switch from pro-fibrotic Ly-6C^{hi} to restorative Ly-6C^{lo} hepatic macrophages might result in reduced macrophage TGF-β expression. Whilst this was the case (**Fig 6.2A**), the difference was not statistically significant. Importantly, TGF-β activity is not regulated at the level of gene expression but rather it is secreted as a latent precursor complexed with a binding protein, which requires cleavage for activation (Leask and Abraham, 2004). Interestingly, thrombospondin-1, a molecule which is a key activator of latent TGF- β (Murphy-Ullrich and Poczatek, 2000) with a consequent pro-fibrogenic effect on hepatic stellate cells (Breitkopf et al., 2005), shows a striking downregulation in restorative macrophages (**Fig 6.2A**). This suggests a possible mechanism linking inflammatory Ly-6C^{hi} macrophages to activation of TGF-β signalling and hence a pro-fibrogenic role and thus may provide the link between macrophage phenotype and TGF-β activation.

I have also identified a number of other potentially pro-resolution genes which are up regulated in restorative Ly-6C^{lo} macrophages. In 2 murine knockout studies, CX3CR1 has been shown to have anti-fibrotic effects in the liver (Karlmark et al., 2010, Aoyama et al., 2010). In keeping with my data, CX3CR1 was predominantly expressed on Ly-6C$^{lo/negative}$ hepatic macrophages following injury (Aoyama et al., 2010). In both these studies, CX3CR1 deficiency resulted in increased levels of hepatic inflammation, injury and macrophage infiltration in response to CCl_4. Furthermore, the lack of CX3CR1 on hepatic macrophages resulted in a more pro-inflammatory pro-fibrogenic macrophage phenotype with higher expression levels of TNF-α and TGF-β and lower levels of IL-10 and arginase-1 (Aoyama et al., 2010). Interestingly, CX3CR1 promotes expression of the anti-apoptotic gene bcl2 in hepatic monocyte-derived macrophages and hence may be important for macrophage survival as well as differentiation (Karlmark et al., 2010). Thus, CX3CL1-CX3CR1 signalling may represent an important mechanism in the generation of restorative macrophages in my model.

CD74 has also been shown to have an anti-fibrotic effect in a murine liver fibrosis model (Heinrichs et al., 2011). CD74 is upregulated in restorative macrophages (**Fig 6.2**). However, in the published study the anti-fibrogenic effect of MIF-CD74 signalling was felt to be mediated by HSCs (Heinrichs et al., 2011), and so nothing is known of the role of this pathway in hepatic macrophages. Interestingly, CD74 is also upregulated in resolution phase macrophages in the peritoneum (Stables et al., 2011). Hence, the role of CD74 in macrophage phenotype would certainly merit further study.

Insulin-like growth factor-1 (IGF-1) expression was also strongly upregulated in restorative hepatic macrophages (**Fig 6.2A**). IGF-1 has previously been shown to have anti-fibrotic effects in the liver in rodents, with gene transfer to rats capable of inhibiting fibrosis progression during ongoing injury (Vera et al., 2007) and also enhancing fibrosis regression following the cessation of injury (Sobrevals et al., 2010). Indeed, the administration of recombinant IGF-1 has undergone a limited clinical study in cirrhotic patients with an improvement in serum albumin, albeit with no clinical benefit in a small number of patients (Conchillo et al., 2005). This beneficial effect may be mediated via effects on other fibrogenic mediators such as increasing levels of MMPs and reducing levels of TGF-β and TIMPs (Bonefeld and Moller, 2011). Intriguingly, IGF-1 also stimulates hepatocyte proliferation and survival, either directly via the IGF-1 receptor (Kundu et al., 2003, Desbois-Mouthon et al., 2006) or by stimulating the production of other growth factors such as hepatocyte growth factor (HGF) (Sanz et al., 2005). Hence, IGF-1 expression could link

the restorative macrophage population with liver regeneration, although the relative functional contribution of macrophage-derived IGF-1 versus that derived from other cell types such as hepatocytes or HSCs remains to be defined.

An additional advantage of the microarray dataset, is that it enabled me to characterise the distinct macrophage subsets according to the M1/M2 macrophage activation paradigm. Using a range of M1 and M2 macrophage markers, it was clear that both Ly-6C^{hi} and Ly-6C^{lo} hepatic macrophages share features of M1 and M2 cells and the change from inflammatory to restorative cells does not conform to this linear model of macrophage activation, but rather these cells represent novel phenotypes. In many ways this is unsurprising, as the traditional M1/M2 classification is largely based on *in vitro* studies and hence cannot hope to recapitulate the complex milieu seen *in vivo* (Lawrence and Natoli, 2011, Mantovani et al., 2004). This highlights the importance of defining macrophage populations on the basis of function. Having said that, the lack of specific markers of functionally distinct macrophage populations limits the study of macrophage dynamics *in vivo*, as multicolour flow cytometry on freshly isolated tissue is usually needed to define distinct populations. This is particularly relevant in human disease, where tissue samples are limited. Hence, identification of markers which specifically select either pro-fibrogenic or restorative macrophages and can be studied by immunohistochemistry will be a major advantage. Again, my unbiased microarray approach was useful to this end. Specifically, the aforementioned MMP-12 and the glycoprotein nonmetastaic melanoma B (GPNMB) were strikingly upregulated in restorative macrophages. Immunohistochemically, MMP-12 and GPNMB positive cells showed a macrophage morphology and accumulated around hepatic scars at the time of maximal scar resolution following CCl_4 injury, mirroring the increase in Ly-6C^{lo} macrophages seen by flow cytometry (**Fig 6.5A**). Both of these proteins were also detected immunohistochemically in a subset of hepatic macrophages in human cirrhotic liver (**Fig 6.5A, D and E**). Hence, this may represent a method of detecting human hepatic restorative macrophages. Conversely, chitinase-3-like 3 (Chi3l3 or YM-1), a characteristic M2 marker, is highly expressed in pro-fibrogenic Ly-6C^{hi} macrophages and hence can be utilised as an immunohistochemical marker of this macrophage subset (**Fig 6.5A**). Unfortunately, no exact human analogue of this gene exists. However, chitinase-3-like 1 (Chi3l1 or YKL-40), an enzyme from the same mammalian chitinase-like protein family, has been identified as a serum marker of human hepatic fibrosis (Johansen et al., 2000), found to be upregulated in fibrotic human liver (Sarma et al., 2012) and shown to be expressed by a subpopulation of hepatic macrophages in a rat model (Pizano-Martinez et al., 2011). Hence, this may serve as a potential marker of the pro-fibrotic macrophage subset in humans.

In addition to the range of individual gene changes identified, the microarray dataset also enabled pathway analysis, identifying which gene clusters are enriched in each subset and hence shedding light on specific functional characteristics. Whilst the pathways enriched in inflammatory Ly-6C^{hi} macrophages could be anticipated by their pro-fibrogenic effects (**Fig 6.3A**), restorative Ly-6C^{lo} macrophages showed a striking upregulation in phagocytosis-related genes (**Fig 6.3B**). It is well recognized that phagocytosis has significant effects on macrophage phenotype (Devitt and Marshall, 2011, Erwig and Henson, 2007, Savill et al., 2002). Therefore, phagocytosis may represent a key event in the change in phenotype from inflammatory to restorative macrophages. Should this be the case, one would anticipate that restorative macrophages would show features of being post-phagocytic. I therefore developed a technique to prove this, and categorically showed an increased in intracellular apoptotic debris in restorative macrophages whilst debris was predominantly bound to the cell surface in the inflammatory subset (**Fig 6.6C**). Hence, I have confirmed that the restorative macrophage subset represents a post-phagocytic population.

SUMMARY

- FACS can be utilised to isolate functionally distinct inflammatory and restorative hepatic macrophage subsets, enabling detailed analysis of the characteristics of each of these populations
- Microarray analysis of inflammatory and restorative hepatic macrophage subsets enables an unbiased assessment of genes expressed by each population, and which genes change expression in association with the changes in macrophage function
- Restorative macrophages show a number of pro-resolution features including reduced expression of pro-inflammatory cytokines, chemokines and TGF-β activating proteins such as thrombospondin-1, whilst upregulating anti-fibrotic genes including MMPs and IGF-1.
- Both inflammatory and restorative macrophages show features of M1 and M2 macrophage phenotypes and cannot be categorised according to this paradigm
- Microarray data demonstrated specific markers for each subset (Chi3l3 for inflammatory macrophages; MMP-12 and GPNMB for restorative macrophages) which enabled identification of these populations *in situ* using immunohistochemistry and hence may permit more detailed study of macrophage subsets in human liver disease.
- Pathway analysis of genes upregulated in restorative macrophages identified phagocytosis as a key feature of this subset.

- Restorative hepatic macrophages, when compared to inflammatory macrophages, show clear evidence of being post-phagocytic, suggesting that phagocytosis may be a key event in the generation of this pro-resolution phenotype

CHAPTER 7 – MODELLING THE GENERATION OF RESTORATIVE MACROPHAGES *IN VITRO*

INTRODUCTION

Having identified the key mediators expressed by the restorative Ly-6C^{lo} hepatic macrophage population *in vivo*, determined that this subset was formed from a phenotypic switch *in situ* and demonstrated that a key feature of this population was being post-phagocytic, I sought to model this macrophage phenotype *in vitro*. Specifically I aimed to ascertain whether macrophage phagocytosis *in vitro* would induce a similar macrophage phenotypic switch and enhance matrix degrading capability. This would enable me to study the macrophage signalling cascades that could contribute to this phenotype. Specifically MAPK signalling, in particular the ERK and p38 cascades, have previously been reported to be activated in macrophages in response to phagocytosis and to regulate a number of macrophage responses (Chung et al., 2007, Hu et al., 2002, Jehle et al., 2006, Kurosaka et al., 2003, Weigert et al., 2006).

Furthermore, the development of an *in vitro* model would enable the study of the effects of non-cellular material such as liposomes which could potentially be used to modify macrophage phenotype *in vivo*.

AIMS

- To determine whether macrophage phagocytosis of hepatocyte debris *in vitro* causes a similar macrophage phenotypic switch to that observed *in vivo*
- To determine whether this results in increased matrix degrading activity
- To ascertain whether this phenotypic switch occurs with alternative forms of cellular debris
- To determine the signalling pathways that are important for the matrix degrading phenotype
- To determine if a similar macrophage phenotype was induced by liposome ingestion which could be used *in vivo*

RESULTS

Differentiation of Primary Bone Marrow Derived Macrophages Results in a Pure Population

In order to develop assays to study the effect of phagocytosis on macrophage phenotype, I used primary bone marrow derived macrophages (BMDMs) from C57BL/6 mice. These are

the most consistently available and widely used primary murine macrophages in such studies (Marim et al., 2010). I utilized a well established 7 day differentiation protocol from whole bone marrow in non-adherent flasks (to minimize activation) in the presence of L929 conditioned medium as a source of M-CSF (Henderson et al., 2008). As shown by Diff Quik staining, morphologically this differentiation process yielded a pure population of macrophages (**Fig 7.1A**). I went on to perform flow cytometry to assess the purity of these cells. As demonstrated, consistently over 90% of the differentiated BMDMs were positive for the macrophage markers F4/80 (**Fig 7.1B**) and CD11b (**Fig 7.1C**), with minimal positivity for the more dendritic cell marker CD11c (**Fig 7.1D**). Thus, whilst clearly not identical to the isolated hepatic monocyte and macrophage subsets, BMDMs provide a pure and robust primary macrophage population to perform mechanistic studies *in vitro*.

Figure 7.1 – Differentiation of Bone Marrow Derived Macrophages Yields a Pure Population

Bone marrow derived macrophages (BMDMs) were cultured and differentiated for 7 days in L929 containing culture medium. (**A**) Diff Quik staining of cytospins of day 7 BMDMs demonstrated macrophage morphology (x200 magnification). (**B** to **D**) Flow cytometric analysis of BMDMs for macrophage markers F4/80 (**B**) and CD11b (**C**) and the dendritic cell marker CD11c (**D**). Antibody staining (red) was compared with relevant isotype control antibodies (green). Representative flow cytometry plots and percentages are shown.

Figure 7.1 - Differentiation of Bone Marrow Derived Macrophages Yields a Pure Population

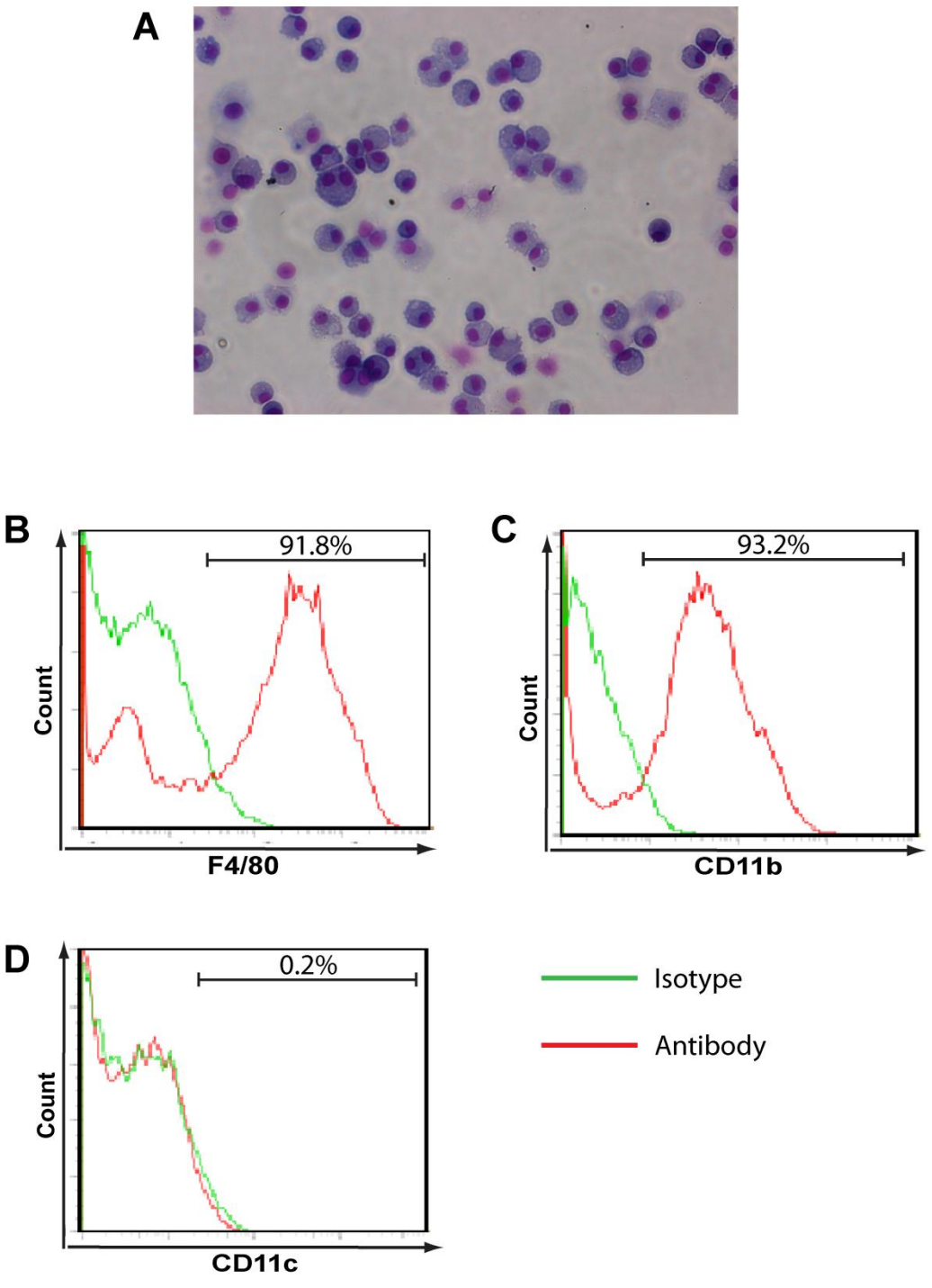

Co-Culture of BMDMs and Primary Hepatocyte Debris Results in an Restorative-like Macrophage Phenotype

Given that the majority of hepatic cell debris in the CCl_4 model is from hepatocytes, I initially sought to determine the effect of hepatocyte debris on BMDM phenotype. Primary murine hepatocytes were isolated from adult C57BL/6 mice using a standard protocol (see materials and methods). They were cultured overnight, followed by induction of cell death by incubating with anti-CD95 in serum free medium for 8 hours, resulting in >95% trypan blue positivity. This hepatocyte debris was then co-cultured with BMDMs for 16 hours. As shown in **Fig 7.2A**, addition of hepatocyte debris resulted in a significant change in macrophage morphology, evident on phase contrast microscopy. Importantly, tissue culture wells containing hepatocyte debris alone did not show significant cellular attachment following washing. To further confirm the interaction between BMDMs and hepatocyte debris, macrophages and hepatocytes were fluorescently labelled green (CFSE) and red (PKH-26) respectively, followed by co-culture. Fluorescence microscopy following vigorous washing, clearly demonstrated a direct interaction between the majority of BMDMs and hepatocyte debris, in keeping with macrophage ingestion (**Fig 7.2B**).

I then proceeded to identify gene expression changes in BMDMs following co-culture with hepatocyte debris by qPCR. In order to compare the macrophage phenotypic changes with those I identified *in vivo*, I focused on genes which were differentially regulated between inflammatory (Ly-6C^{hi}) and restorative (Ly-6C^{lo}) hepatic macrophages (**Fig 6.2A and B**). As an additional control, any genes which showed significant expression in hepatocyte debris alone were excluded from further analysis to prevent the potential for contamination of macrophage RNA. As shown in **Fig 7.2C,** a number of relevant genes showed differential expression following macrophage phagocytosis of hepatocyte debris (n=11-12). In particular, the important matrix metalloproteinase enzymes MMP-12 and MMP-9, both of which are upregulated following the switch from inflammatory to restorative hepatic macrophages *in vivo*, are more highly expressed in BMDMs following co-culture with hepatocyte debris. Furthermore, the upregulation of IGF-1 and downregulation of Thbs1 and Chi3l3 in response to macrophage phagocytosis (**Fig 7.2C**), also closely mirrors the changes observed *in vivo* (**Fig 6.2A and B**).

I wished to confirm the secretion of active MMPs and to determine if the observed changes were a general effect of phagocytosis on macrophages, irrespective of the nature of the cellular debris. I therefore utilized the well described *in vitro* model of the phagocytosis of apoptotic thymocytes (Ferenbach et al., 2010), routinely using a population of thymocytes

which were >90% trypan blue positive. Culture supernatants were harvested from tissue culture wells containing macrophages alone, macrophages and thymocyte debris and thymocyte debris alone and subjected to either gelatin zymography or western blotting. As shown, co-culture of BMDMs with thymocyte debris resulted in increased secretion of active MMP-9 (**Fig 7.2D**) and MMP-12 (**Fig 7.2E**), mimicking the changes in gene expression following culture with hepatocyte debris.

Figure 7.2 – Co-Culture of Hepatocyte Debris and BMDMs results in a Restorative-like Phenotype

Co-culture of Bone Marrow-derived Macrophages (BMDMs) with primary murine hepatocyte debris. (**A**) Changes in macrophage morphology on phase-contrast microscopy. Hepatocyte debris alone was non-adherent (Scale bar=100 µm). (**B**) CFSE (green) labelled BMDMs were cultured in the absence and presence of PKH-26 (red) labelled hepatocyte debris (Scale bar=50µm). (**C**) Changes in BMDM gene expression following co-culture with hepatocyte debris (Expressed relative to mean expression of macrophages alone; n=11-12 pooled from 2 independent experiments). (**D** & **E**) Co-culture of BMDMs with apoptotic thymocytes. (**D**) Gelatin zymography of culture supernatants equalized for protein content, showing active MMP-9 (representative zymogram from n=4 from 2 independent experiments; experiments performed in collaboration with Dr Steve Hartland). (**E**) Western blot for MMP-12 on culture supernatants, equalised for protein content (representative blot from n=4 from 2 independent experiments; experiments performed in collaboration with Dr Antonella Pellicoro). Data shown as Mean±S.E.M; **P*<0.05, ***P*<0.01, ****P*<0.001. Representative blots and images shown.

Figure 7.2 - Co-culture of Hepatocyte Debris and BMDMs Results in a Restorative-like Phenotype

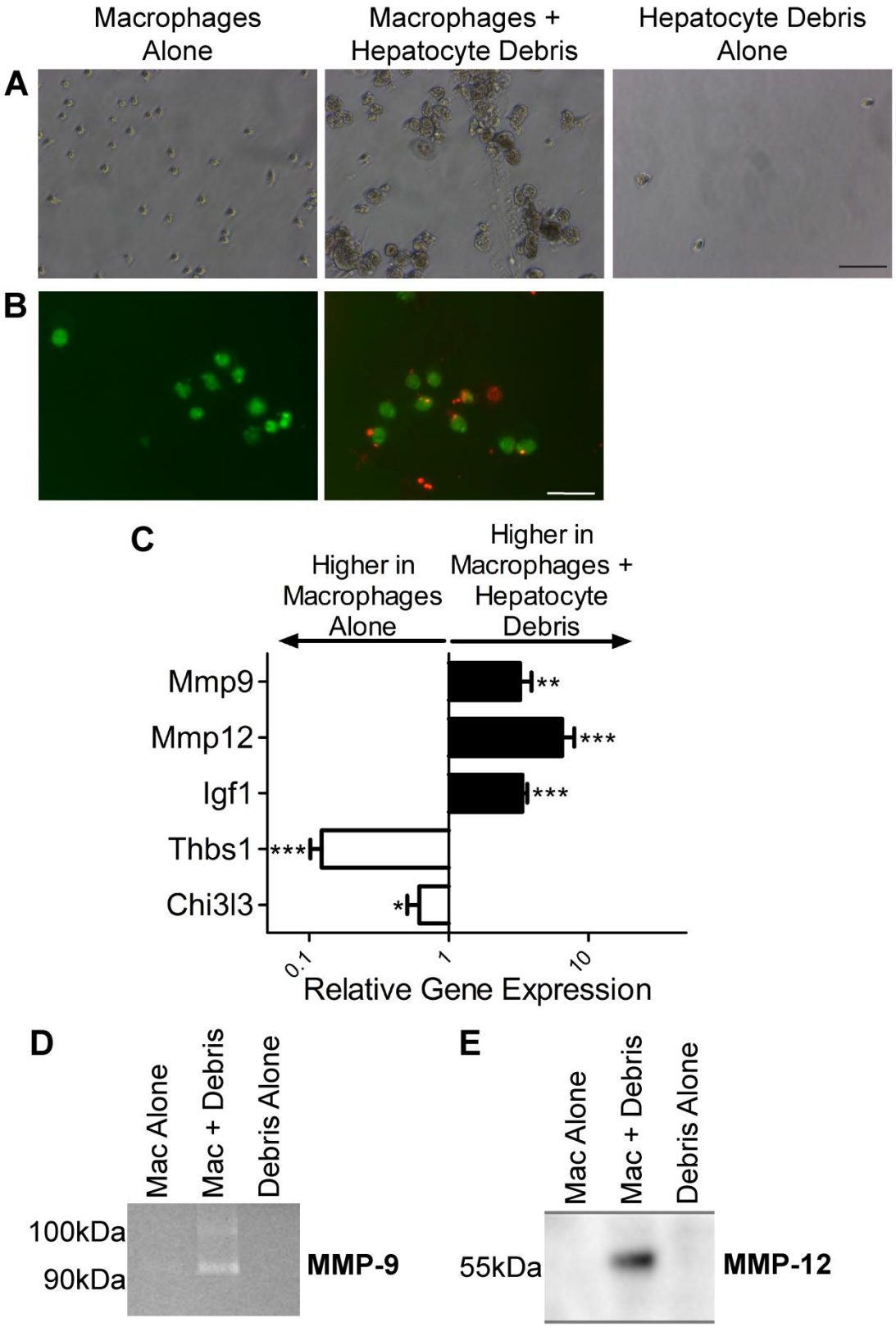

The Phagocytosis Induced Matrix Degrading Macrophage Phenotype is Induced by ERK Signalling

Having developed an *in vitro* model for studying the role of macrophage phagocytosis in the induction of matrix degrading properties, I sought to utilise this system to determine which signalling cascades might contribute to this change in phenotype. I therefore used specific chemical inhibitors of the ERK and p38 cascades (or vehicle controls), added to my co-culture system, to ascertain if either of these pathways was relevant to the matrix degrading phenotype I observed following the phagocytosis of cellular debris. Initially I used PD98059, a specific ERK kinase (MEK1/2) inhibitor, at a dose of 50µM according to published effective concentrations in macrophages (Raza et al., 2000, Valledor et al., 2000). As shown in **Fig 7.3A**, PD98059 administration significantly inhibited the upregulation of both MMP-12 and MMP-9 gene expression in macrophages in response to hepatocyte debris (n=6). Furthermore, the observed increase in IGF-1 expression was also prevented (**Fig 7.3A**). I proceeded to confirm these changes at a protein level. As demonstrated in **Fig 7.3B**, Casein zymography shows that PD98059 inhibited the secretion of active MMP-9 and MMP-12 by macrophages in response to hepatocyte debris (n=3).

Given this potential role of ERK signalling in the matrix degrading phenotype, I sought to determine if I could identify evidence of *in vivo* ERK activation in hepatic macrophages at the time of maximal scar resolution (72 hrs) in my 4 week CCl_4 model. Dual immunofluorescence demonstrated the presence of nuclear pERK staining in a proportion of F4/80 positive hepatic macrophages (**Fig 7.3C**), indicative of ERK activation in macrophages *in vivo*, and emphasising the relevance of my *in vitro* data.

I proceeded to confirm the specificity of the effects of MEK1/2 inhibition on MMP-12 expression in macrophages, using an alternative specific inhibitor UÖ126 (20µM), again at a published dose (Chi et al., 2006, Shin et al., 2008) (**Fig 7.4A**, n=3). I then wished to determine whether ERK inhibition affected the other relevant macrophage phenotypic changes I observed in response to co-culture with hepatocyte debris (**Fig 7.2C**). As shown in **Fig 7.4B**, administration of PD98059 had no effect on macrophage downregulation of Thbs1 and Chi3l3 in this system (n=6).

Finally, I wished to determine whether the p38 in addition to ERK signalling contributed to the upregulation of MMPs and matrix degrading phenotype following phagocytosis. As shown in **Fig 7.4C**, administration of the specific p38 inhibitor SB203580 (10µM) (Shin et

al., 2008, Chi et al., 2006), had no effect on the MMP-12, MMP-9 and Igf1bgg BMDM responses to hepatocyte debris (n=6).

Figure 7.3 – Phagocytosis induced ERK Signalling Causes Matrix Degrading Macrophage Phenotype

(**A** & **B**) Culture of BMDMs ± MEK1/2 inhibitor (PD98059; 50µM) ± hepatocyte debris. (**A**) Changes in macrophage gene expression following co-culture measured by qPCR (Expressed relative to mean expression of macrophages alone; n=6). (**B**) Casein zymography of culture supernatants equalised for protein content, showing active MMP-9 and MMP-12 (representative zymogram from n=3 shown). (**C**) Dual immunofluorescence for F4/80 (red) and phospho-ERK (green) in mouse liver, 72 hrs after final CCl_4 dose following 4 weeks of injury (Arrows=nuclear pERK and F4/80 dual positive cells; Scale bars=10µm). Comparison was made to staining with isotype control antibodies. Staining was performed in collaboration with R Aucott. Data shown as Mean±S.E.M; **P*<0.05, ***P*<0.01, ****P*<0.001. Representative images shown.

Figure 7.3 - Phagocytosis induced ERK Signalling Causes Matrix Degrading Macrophage Phenotype

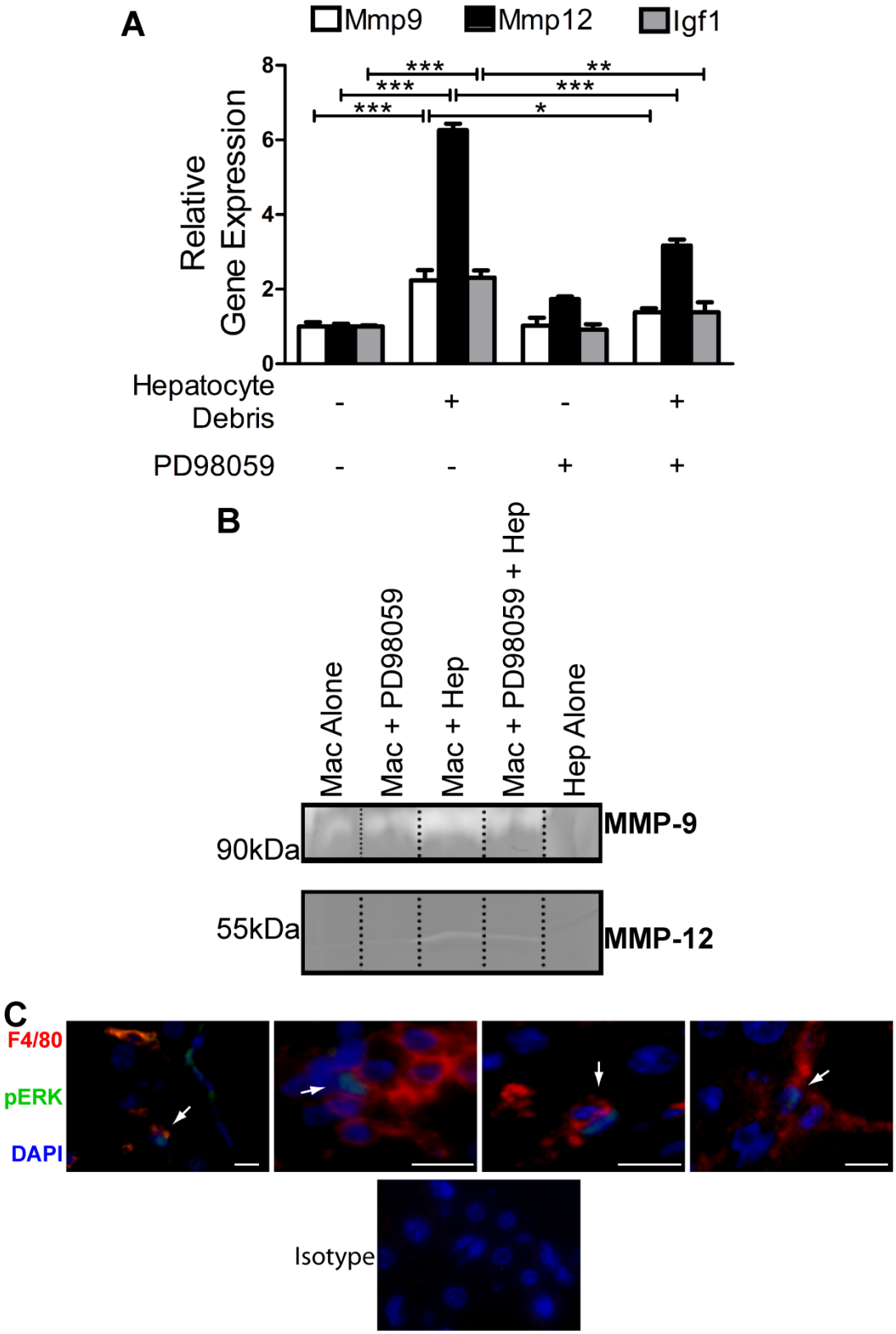

Figure 7.4 – p38 Inhibition has no Effect on Matrix Degrading Macrophage Phenotype

(**A**) Co-culture of BMDMs ± MEK1/2 inhibitor (UO126; 20µM) ± hepatocyte debris. Changes in macrophage Mmp12 gene expression following co-culture (Data shown relative to mean Mmp12 expression of macrophages alone; n=3). (**B**) Co-culture of Bone Marrow-derived Macrophages (BMDMs) ± MEK1/2 inhibitor (PD98059; 50µM) ± hepatocyte debris. Changes in macrophage gene expression following co-culture (Data shown relative to mean expression of macrophages alone; n=6). (**C**) Co-culture of BMDMs ± p38 MAPK inhibitor (SB203580; 10µM) ± hepatocyte debris. Changes in macrophage gene expression following co-culture (Data shown relative to mean expression of macrophages alone; n=6). All data expressed as Mean±S.E.M; **P*<0.05, ***P*<0.01, ****P*<0.001, NS-Non-significant.

Figure 7.4 - p38 Inhibition has no Effect on Matrix Degrading Macrophage Phenotype

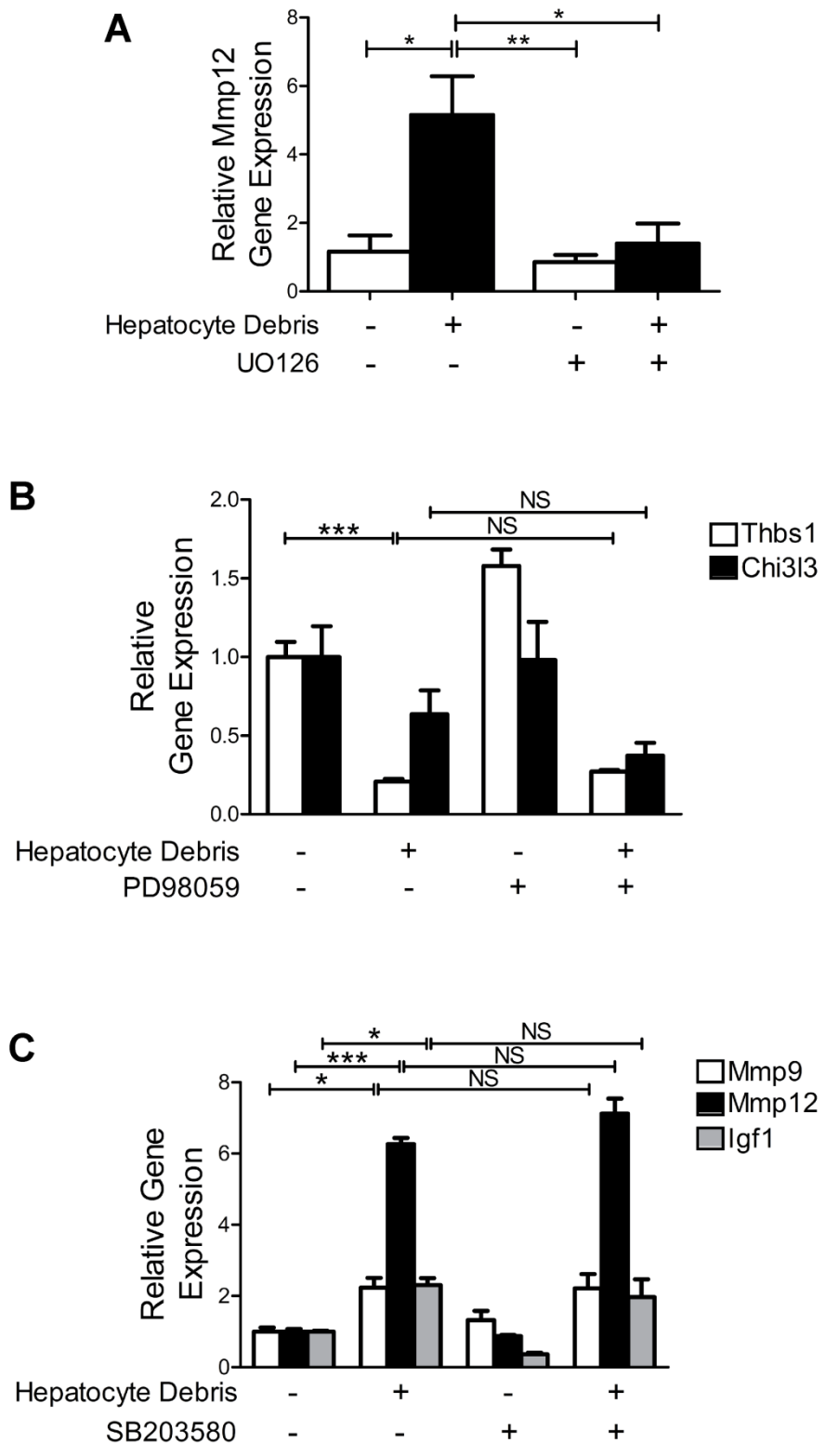

Macrophage Ingestion of Liposomes Induces a Restorative-Like Phenotype

The macrophage ingestion of liposomes has been demonstrated to be a genuine phagocytosis event (Perry and Martin, 1995, Van Rooijen and Sanders, 1994). Furthermore, recent studies have suggested that liposome ingestion by macrophages can induce a change in phenotype at least partially via ERK signalling (Lin et al., 2011, Ma et al., 2011). I therefore aimed to determine whether the administration of liposomes to BMDMs might mimic the changes observed following the phagocytosis of cellular debris, and result in a macrophage phenotype analogous to the *in vivo* restorative macrophage. BMDMs were cultured in the presence and absence of liposomes. Gene expression was then analysed by qPCR. As shown in **Fig 7.5**, liposome administration resulted in a significant increase in macrophage MMP-12 expression (n=6). There were also trends to increased expression of MMP-9 and Igf1. Furthermore, liposomes induced a significant downregulation in Thbs1, Cxcl10 and Ccl2 with a trend to reduction in Chi3l3 (**Fig 7.5**).

Figure 7.5 – Macrophage Ingestion of Liposomes Induces a Restorative-like Phenotype

Culture of BMDMs with and without liposomes. (**A**) Expression of stated gene in BMDMs following *in vitro* culture with liposomes relative to mean expression in BMDMs alone (n=6). All data expressed as Mean±S.E.M; **P*<0.05, ***P*<0.01, ****P*<0.001.

Figure 7.5 - Macrophage Ingestion of Liposomes Induces a Restorative-like Phenotype

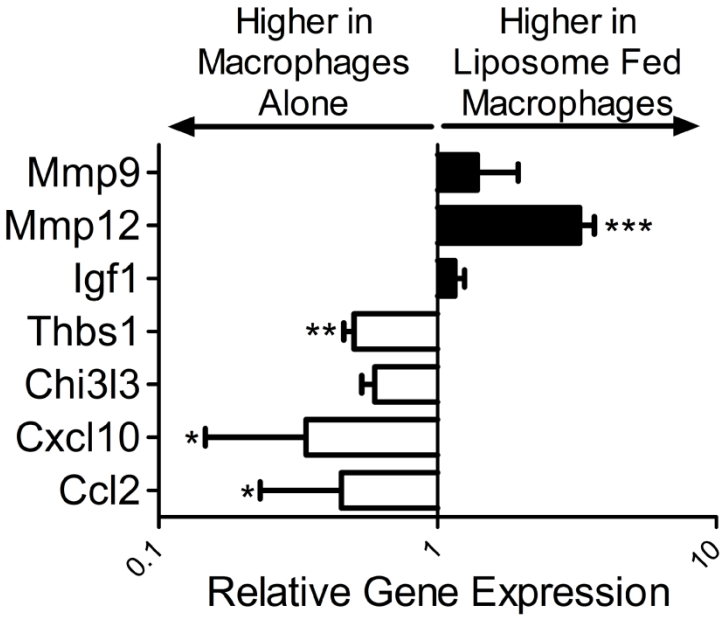

DISCUSSION

In this chapter, I have attempted to recapitulate some of the features of the *in vivo* restorative Ly-6C^{lo} hepatic macrophages using an *in vitro* model, and hence enable me to identify some of the key signalling mechanisms responsible for the generation of the matrix degrading phenotype. Whilst, in an *in vitro* setting it is clearly impossible to exactly recapitulate the complex range of signals to which *in vivo* macrophages are exposed, I have previously shown in Chapter 6 that evidence of phagocytosis seems to be a key feature of the restorative macrophage. I therefore focussed on macrophage phagocytosis as a potential inducer of the matrix degrading phenotype. Indeed, other authors have previously identified phagocytosis as an inducer of MMP expression in macrophages (Popov et al., 2010, Vos et al., 2003).

Utilising bone marrow derived macrophages (BMDMs) as a pure population of primary murine macrophages, co-culture with cell debris from primary murine hepatocytes resulted in macrophage phagocytosis and a change in phenotype mirroring that observed *in vivo*. Specifically, I observed a striking increase in BMDM expression of MMPs -9 and -12 and IGF-1 and a reduction in Chi3l3 and Thbs1 in response to hepatocyte debris (**Fig 7.2C**). Hence, a similar change in expression patterns of a number of key genes is seen in BMDMs exposed to hepatocyte debris *in vitro* as I observed during the switch from pro-fibrotic Ly-6C^{hi} hepatic macrophages to restorative Ly-6C^{lo} macrophages *in vivo* (**Fig 6.2**). Interestingly, the increased expression of MMP-9 and MMP-12 in BMDMs in response to phagocytosis is not specific to hepatocyte debris, but also occurred in separate co-culture experiments with apoptotic thymocytes (**Fig 7.2D and E**), suggesting this may be a more generic response and hence may also be relevant in organs other than the liver.

Using this model, I then wished to determine which signalling pathways might link macrophage phagocytosis and the generation of the matrix-degrading phenotype. Clearly, phagocytosis is a complex process with multiple receptors involved and hence potential activation of a number of signalling cascades at different stages. Whilst full exploration of these was beyond the scope of this thesis, MAPK signalling, specifically the ERK and p38 cascades, have been shown to regulate a range of macrophage responses and are known to be activated in response to phagocytosis (Chung et al., 2007, Hu et al., 2002, Jehle et al., 2006, Kurosaka et al., 2003, Weigert et al., 2006). I therefore focussed on these pathways and used highly specific chemical inhibitors of these in my *in vitro* phagocytosis model. Principally, using the MEK1/2 inhibitor PD98059, which inhibits ERK signalling, prevented macrophage upregulation of MMP-12 and -9 in response to phagocytosis (**Fig 7.3A and B**). Similar findings were replicated with a alternative MEK 1/2 inhibitor UÖ126. To confirm the

potential *in vivo* relevance of this, I was able to identify active ERK in hepatic macrophages at the time of initiation of scar resolution in my 4 week CCl_4 model (**Fig 7.3C**). Hence, ERK signalling in macrophages via MEK1/2 seems to have an important role in generating the matrix degrading properties observed. Conversely, ERK inhibition seemed to have no effect on other features of the restorative macrophage such as downregulation of Thbs1 or Chi3l3 (**Fig 7.4B**). These data would suggest, perhaps unsurprisingly, that cross-talk between different signalling pathways is required to generate the overall complex phenotype of the restorative macrophage. This clearly merits further study. My preliminary ERK data could be expanded to determine the timescale of ERK activation in response to phagocytosis. Furthermore, I have used published doses of signalling inhibitors, but further strength to my findings would be given by replicating these experiments to show a dose response effect, with expansion to include other signalling pathways. Most importantly, attempts to inhibit ERK signalling in hepatic macrophages *in vivo* might shed important new insights into the functional relevance of these observations. However, given the ubiquitous nature of this pathway in a range of cell types, this may be difficult to achieve without confounding off target effects.

Finally in this chapter, I sought to determine whether non-cellular debris might induce a similar macrophage phenotype *in vivo*. As mentioned above, liposome ingestion has been demonstrated to be a genuine phagocytosis event (Perry and Martin, 1995, Van Rooijen and Sanders, 1994) and interestingly induces ERK signalling in macrophages (Lin et al., 2011, Ma et al., 2011). Therefore, it is relevant that liposome administration to BMDMs *in vitro* induced a similar change in phenotype to that I observed with macrophage ingestion of hepatocyte debris *in vitro* (**Fig 7.5**) and also mirrors the changes I observed in the formation of the restorative Ly-$6C^{lo}$ hepatic macrophage subset *in vivo* (**Fig 6.2A and 6.2B**). Whilst the changes in BMDMs gene expression in response to liposomes seems less pronounced than the changes induced by cellular debris, liposome ingestion may provide a novel means of enhancing the restorative macrophage phenotype *in vivo*.

SUMMARY

- Primary BMDMs, differentiated for 7 days, provide a pure population of macrophages for the study of macrophage biology *in vitro*.
- Co-culture of BMDMs and primary murine hepatocyte debris induces a change in macrophage phenotype including an increase in MMP expression, which mirrors the change in hepatic macrophage phenotype seen *in vivo*.
- The increase in BMDM matrix degrading activity following co-culture with hepatocyte debris, also occurs following co-culture with apoptotic thymocytes suggesting this may be a generic phagocytosis effect.
- The increase in MMP-9, MMP-12 and Igf1 expression in BMDMs in response to hepatocyte debris is at least partially mediated by the ERK signalling cascade.
- BMDM phagocytosis of liposomes induces a number of restorative macrophage features and may have utility to alter macrophage phenotype *in vivo*.

CHAPTER 8 – MANIPULATION OF MACROPHAGE PHENOTYPE *IN VIVO*

INTRODUCTION

I have previously defined the macrophage subset responsible for the regression of hepatic fibrosis and extensively characterised it, specifically identifying that phagocytosis was likely to be a key determinant of the switch in macrophage phenotype *in vivo* from an inflammatory pro-fibrogenic Ly-6C^{hi} population to a pro-resolution Ly-6C^{lo} subset which has acquired increased matrix degrading activity. I then wished to utilise this dataset to identify methods to manipulate macrophage phenotype *in vivo*, with the ultimate aim of enhancing the formation of restorative macrophages and hence accelerating fibrosis resolution.

Initially, having identified PPAR signalling as being upregulated in the restorative macrophage subset (**Fig 6.2B and 6.3B**), I sought to explore this potential association further. PPAR-γ signalling in macrophages has been shown to regulate multiple processes including inflammatory gene expression, macrophage polarisation and to be important in promoting the resolution of inflammation (Bouhlel et al., 2007, Castrillo and Tontonoz, 2004, Gautier et al., 2012). Additionally, the administration of PPAR-γ agonists has been shown to alter macrophage phenotype *in vivo* (Li et al., 2011, Hasegawa-Moriyama et al., 2012, Stienstra et al., 2008). Furthermore, data has suggested an anti-fibrotic effect of PPAR-γ agonists *in vivo* in a number of organs including liver (Aoki et al., 2009, Chen et al., 2008, Higashi et al., Ihm et al., Kiss et al.). Most recently, a study showed an increased susceptibility to CCl_4 induced liver fibrosis in mice with macrophage-specific PPAR-γ knockout (Moran-Salvador et al., 2013). There is therefore a strong rationale to think that manipulation of the PPAR-γ pathway might alter hepatic macrophage phenotype. I therefore wished to determine whether the administration of the widely-used PPAR-γ agonist rosiglitazone might alter hepatic macrophage subsets and enhance fibrosis resolution.

Secondly, I wanted to determine whether inhibition of macrophage phagocytosis *in vivo* during the resolution phase following CCl_4 injury, might alter hepatic macrophage subsets and consequently affect recovery following cessation of CCl_4. Given the complexity of macrophage phagocytosis (described in detail in Chapter 1) potentially involving numerous molecules and receptors, I used commercially available blocking antibodies against the extracellular bridging molecule MFG-E8 or the phagocytic receptor integrin α_v. Milk fat globule-EGF factor 8 (MFG-E8, lactadherin) is a glycoprotein that is a key extracellular part of the phagocytic process, one domain binding to phosphatidylserine on apoptotic cells and another to $\alpha_v\beta_3$ and $\alpha_v\beta_5$ integrins on the surface of phagocytic cells, thus facilitating engulfment and ingestion (Aziz et al., 2011a, Toda et al., 2012). Additionally, recent studies

have suggested that MFG-E8 might have a direct anti-inflammatory effect on macrophages (Aziz et al., 2011a, Aziz et al., 2011b). Furthermore, in a separate study MFG-E8 has been shown to be anti-fibrotic in a pulmonary fibrosis model, by targeting collagen for uptake by macrophages (Atabai et al., 2009). Given the importance of phagocytosis in the formation of the restorative hepatic macrophage phenotype, MFG-E8 was an attractive candidate molecule which could contribute to the generation of this cell type and hence promote hepatic fibrosis regression.

Integrin α_v (ITGAV) on the surface of phagocytes in complexes with integrin β_3 or β_5 is a key phagocytic receptor (Savill et al., 1990, Toda et al., 2012, Wu et al., 2005, Ravichandran and Lorenz, 2007). Analysis of the microarray data demonstrated significant gene expression of ITGAV in both inflammatory and restorative macrophages. Hence, blockade of ITGAV could potentially inhibit macrophage phagocytosis and hence alter hepatic macrophage subsets and fibrosis resolution.

Finally, having determined that macrophage liposome ingestion *in vitro* results in a similar change in phenotype to that observed *in vivo* (**Fig 7.5**), I aimed to determine the effects of liposome administration to mice on hepatic macrophage phenotype and fibrosis resolution.

AIMS

- To determine the effect of rosiglitazone administration on hepatic macrophage subsets and fibrosis resolution following CCl_4 induced injury
- To determine the effect of antibody blockade of MFG-E8 on hepatic macrophage subsets and fibrosis resolution following CCl_4 induced injury
- To determine the effect of antibody blockade of integrin α_v (ITGAV) on hepatic macrophage subsets and fibrosis resolution following CCl_4 induced injury
- To determine the effect of liposome administration on hepatic macrophage subsets and fibrosis resolution following CCl_4 induced injury

RESULTS

Rosiglitazone administration has no detectable effect on hepatic macrophage subsets or resolution of fibrosis following CCl_4 injury

As shown in **Fig 8.1A** and described in detail in the legend, adult male C57BL/6 mice were administered 4 weeks of CCl_4 as before. At 24, 48 and 72 hrs following the final CCl_4

injection mice were given either rosiglitazone (10mg/kg) at a published dose (Genovese et al., 2005) or DMSO control. Animals were harvested at 96 hours, as shown.

Circulating monocytes were assessed by flow cytometry as before. As shown in **Fig 8.1B**, the administration of rosiglitazone showed a trend to reducing both subsets of circulating monocytes, that did not reach statistical significance (n=6-8). Hepatic macrophages and subsets were identified using flow cytometry on hepatic non-parenchymal cells as before (**Fig 3.8B, 3.12A and 3.12B**). As shown in **Fig 8.1C**, rosiglitazone administration did not change the relative contribution of macrophages to the hepatic leucocyte pool (n=4-8). Further analysis showed no change in the proportion of each of the 3 hepatic macrophage subsets in response to rosiglitazone (**Fig 8.1D**), indicating no increase in restorative macrophage number with drug treatment. Finally, as shown in **Fig 8.1E**, hepatic fibrosis, as assessed by PSR staining, was not altered by rosiglitazone therapy (n=6-8).

Figure 8.1 – Rosiglitazone does not affect Hepatic Macrophage Subsets

Adult male C57BL/6 mice were injured with 4 weeks of CCl_4 followed by administration of PPAR-γ agonist rosiglitazone (10mg/kg, IP) or DMSO (vehicle) control 24, 48 and 72 hrs after the final CCl_4 dose with harvest at 96 hrs as shown in (**A**). (**B**) Circulating monocytes ($CD11b^+$ $CD115^+$ Ly-$6G^-$ Ly-$6C^{hi}$ or Ly-$6C^{lo}$ cells) were identified using flow cytometry and quantified from mice treated with rosiglitazone or DMSO at time of harvest (96 hrs) (n=6-8). (**C**) Hepatic macrophages were identified by flow cytometry as before and expressed as a % of total hepatic CD45 positive cells (n=4-8). (**D**) Macrophage subsets were identified by flow cytometry as before and expressed as a % of total hepatic macrophages (n=4-8). (**E**) Hepatic fibrosis was assessed by PSR staining and morphometric pixel analysis (n=6-8; Expressed relative to mean % area for livers from DMSO-treated animals). All data expressed as Mean±SEM, NS=Not Significant.

Figure 8.1 - Rosiglitazone does not affect Hepatic Macrophage Subsets

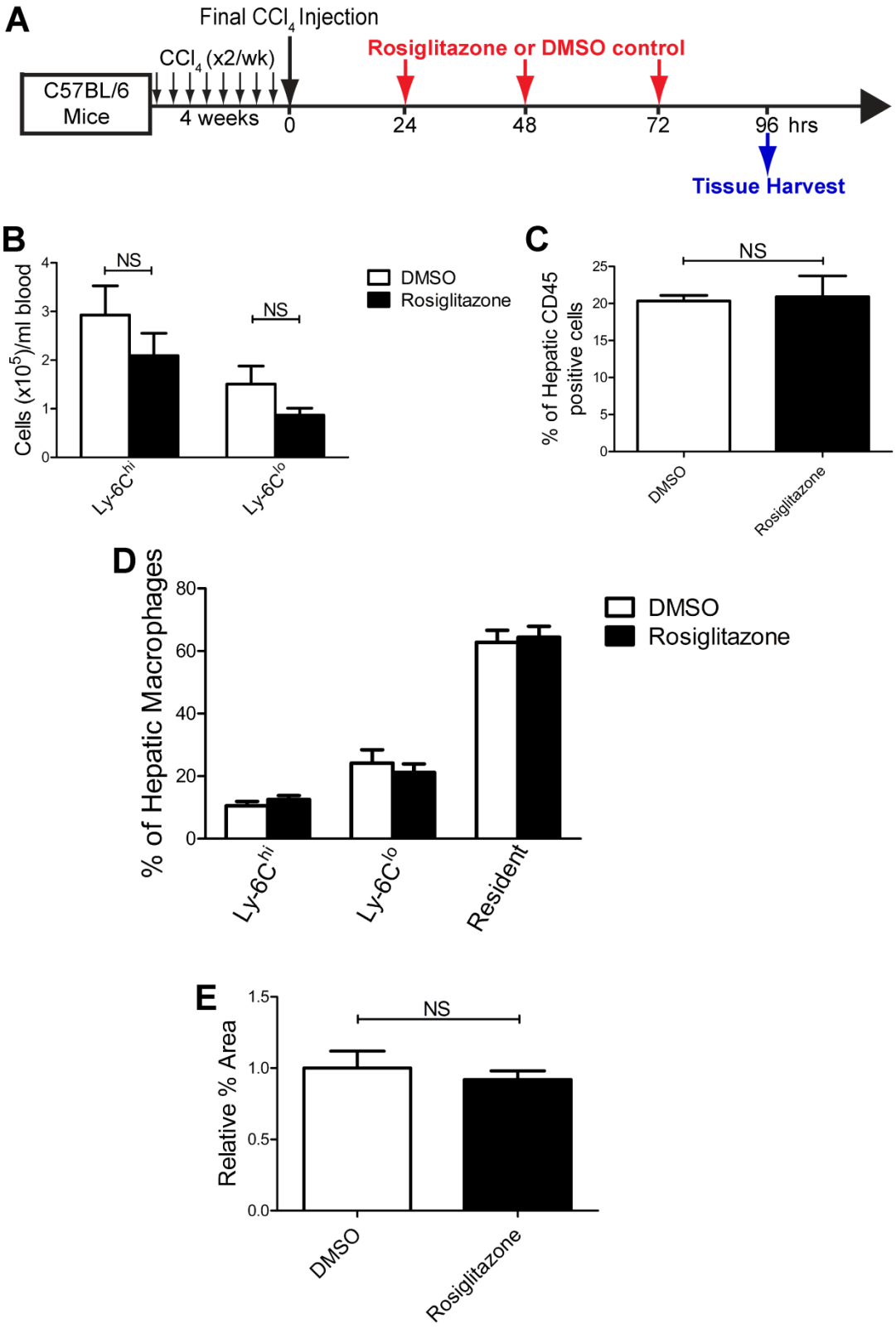

Antibody Blockade of MFG-E8 does not affect hepatic macrophage subsets or resolution of fibrosis following CCl_4 injury

To test the role of MFG-E8 in the generation of the restorative hepatic macrophage, I administered an Anti-MFG-E8 blocking antibody (or isotype control) at a published dose of 2mg/kg (Bu et al., 2007), to CCl_4-injured mice, 24, 48 and 72 hrs following the final CCl_4 injection with harvest at 96 hours (**Fig 8.2A**). I then proceeded to determine if this induced any changes in macrophage or fibrosis responses. Quantification of circulating monocytes as before, showed no difference in the number of either subset in response to the Anti-MFG-E8 antibody (**Fig 8.2B**, n=5-6). I proceeded to identify and quantify hepatic macrophages and subsets using flow cytometry of digested livers, as before. As shown, no difference was seen in the relative contribution of macrophages to the hepatic leucocyte pool (**Fig 8.2C**, n=5-6). Furthermore, the blocking antibody had no effect on relative proportion of each macrophage subset (**Fig 8.2D**, n=5-6). Finally, analysis of liver fibrosis by PSR staining showed no significant difference in fibrosis resolution following administration of the MFG-E8 blocking antibody when compared to the isotype control (**Fig 8.2E**, n=5-6).

Figure 8.2 – Anti-MFG-E8 does not affect Hepatic Macrophage Subsets or Fibrosis Resolution

Adult male C57BL/6 mice were injured with 4 weeks of CCl_4 followed by administration of Anti-MFG-E8 (2mg/kg i.p.) or Hamster IgG Isotype control antibody 24, 48 and 72 hrs after the final CCl_4 dose with harvest at 96 hrs as shown in (**A**). (**B**) Circulating monocytes ($CD11b^+$ $CD115^+$ Ly-$6G^-$ Ly-$6C^{hi}$ or Ly-$6C^{lo}$ cells) were identified using flow cytometry and quantified from mice treated with Anti-MFG-E8 or Isotype at time of harvest (96 hrs) (n=5-6). (**C**) Hepatic macrophages were identified by flow cytometry as before and expressed as a % of total hepatic CD45 positive cells (n=5-6). (**D**) Macrophage subsets were identified by flow cytometry as before and expressed as a % of total hepatic macrophages (n=5-6). (**E**) Hepatic fibrosis was assessed by PSR staining and morphometric pixel analysis (n=5-6; Expressed relative to mean % area for livers from Isotype-treated animals). All data expressed as Mean±SEM, NS=Not Significant.

Figure 8.2 - Anti-MFG-E8 does not affect Hepatic Macrophage Subsets or Fibrosis Resolution

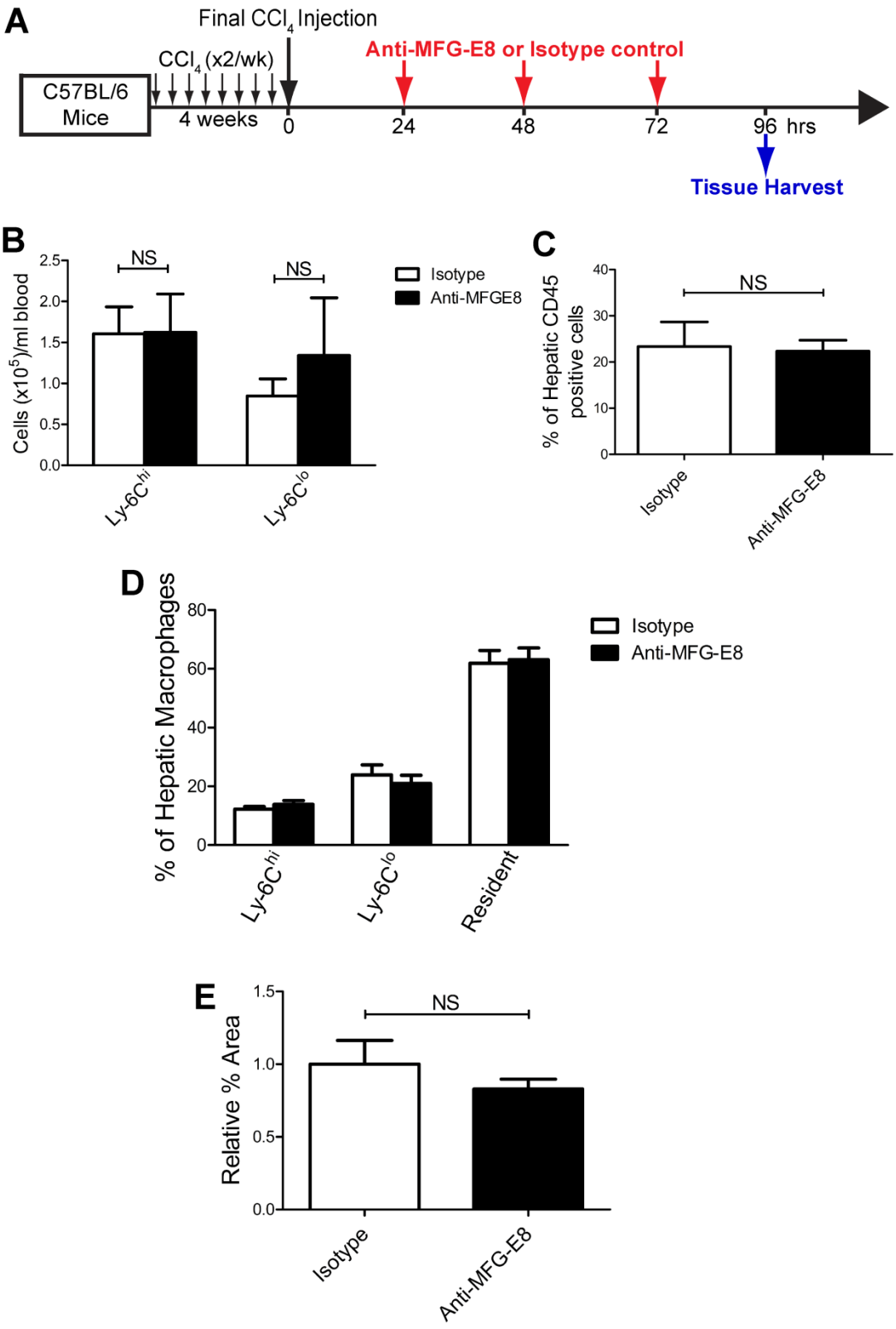

Antibody Blockade of Integrin α_v Reduces Hepatic Restorative Macrophages

I sought to determine whether blockade of the key phagocytic receptor ITGAV might alter hepatic macrophage subsets and affect liver fibrosis resolution. I utilised an Anti-ITGAV blocking antibody (RMV-7) or isotype control, at a previously published dose (Takahashi et al., 2001). Briefly, as shown in **Fig 8.3A**, adult male C57BL/6 mice were injured with 4 weeks of CCl_4 as before, followed by administration of Anti-ITGAV (200µg/mouse) or isotype control 24, 48 and 72 hrs following the final CCl_4 injection with harvest at 96 hrs.

As shown in **Fig 8.3B**, analysis of circulating monocyte subsets by flow cytometry at the time of harvest demonstrated no significant difference in the number of either monocyte subset, although there was a trend to a reduced number of Ly-6C^{lo} monocytes following treatment with anti-ITGAV (n=5). I proceeded to analyse the hepatic macrophages by flow cytometry as previously described. No difference was seen in the contribution of macrophages to the hepatic leucocyte pool (**Fig 8.3C**, n=5). However, as shown in **Fig 8.3D**, analysis of hepatic macrophage subsets demonstrated that Anti-ITGAV treatment did induce an alteration, with a significant reduction in the contribution of restorative Ly-6C^{lo} macrophages, whilst resident macrophages increased when compared to treatment with the isotype antibody (n=5). Analysis of liver fibrosis with PSR staining, on the other hand, did not show any significant difference with ITGAV blockade when compared to isotype control (**Fig 8.3D**, n=5).

Figure 8.3 - Anti-ITGAV reduces the Restorative Macrophage Population

Adult male C57BL/6 mice were injured with 4 weeks of CCl_4 followed by administration of Anti-ITGAV or Isotype control (200 µg/mouse i.p.) 24, 48 and 72 hrs after the final CCl_4 dose with harvest at 96 hrs as shown in (**A**). (**B**) Circulating monocytes ($CD11b^+$ $CD115^+$ $Ly\text{-}6G^-$ $Ly\text{-}6C^{hi}$ or $Ly\text{-}6C^{lo}$ cells) were identified using flow cytometry and quantified from mice treated with Anti-ITGAV or Isotype control at time of harvest (96 hrs) (n=5). (**C**) Hepatic macrophages were identified by flow cytometry as before and expressed as a % of total hepatic CD45 positive cells (n=5). (**D**) Macrophage subsets were identified by flow cytometry as before and expressed as a % of total hepatic macrophages (n=5). (**E**) Hepatic fibrosis was assessed by PSR staining and morphometric pixel analysis (n=5; Expressed relative to mean % area for livers from Isotype-treated animals). All data expressed as Mean±SEM; * $P<0.05$, ** $P<0.01$, NS=Not Significant.

Figure 8.3 - Anti-ITGAV reduces the Restorative Macrophage Population

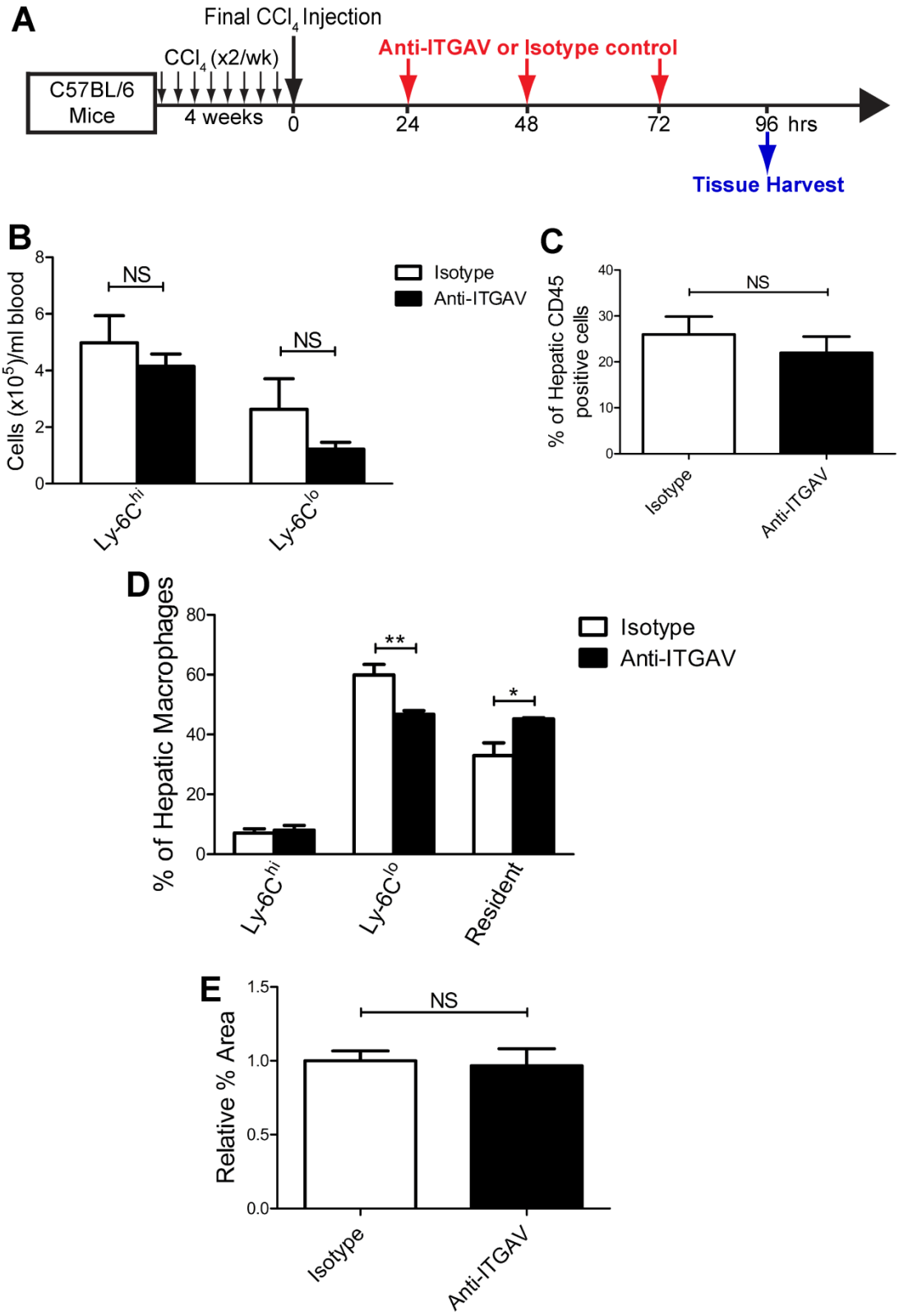

Administration of Liposomes during Fibrosis Resolution Increases Restorative Hepatic Macrophages

Given that the restorative macrophage phenotype could be partially recapitulated by the ingestion of liposomes *in vitro* (**Fig 7.5**), I sought to determine whether the administration of liposomes to mice could induce a similar change in macrophage phenotype *in vivo*.

Adult male C57BL/6 mice were injured with 4 weeks of CCl_4 followed by administration of 200µl of liposomal PBS (or PBS control) 48, 72 and 96 hrs after the final CCl_4 injection, with harvest at 120 hrs, according to the schedule shown (**Fig 8.4A**). As shown in **Fig 8.4B**, analysis of circulating monocyte subsets by flow cytometry at the time of harvest demonstrated that the administration of liposomes caused a significant increase in the number of circulating Ly-6C^{lo} monocytes, whilst no significant change was seen in the number of circulating Ly-6C^{hi} monocytes, albeit with a non-significant trend to reduction in this population (n=12-14).

I then proceeded to assess the effect of liposome administration on hepatic macrophages. As shown in **Fig 8.4C**, injection of liposomal PBS increased the relative contribution of macrophages to the hepatic leucocyte pool when compared to PBS alone (n=13-14). Macrophage subset analysis showed that this increase in hepatic macrophages was accompanied by a change in macrophage subsets, with a significant reduction in the contribution of Ly-6C^{hi} macrophages and a significant increase in the contribution of Ly-6C^{lo} macrophages following liposome administration (**Fig 8.4D**, n=13-14). Importantly, these changes were also observed when the absolute number of each macrophage subset was quantified (**Fig 8.4E**, n=13-14).

Figure 8.4 – Liposomes Increase the Restorative Macrophage Population

Adult male C57BL/6 mice were injured with 4 weeks of CCl_4 followed by administration of Lipsomal PBS or PBS control (200 µl/mouse i.v.) 48, 72 and 96 hrs after the final CCl_4 dose with harvest at 120 hrs as shown in (**A**). (**B**) Circulating monocytes ($CD11b^+$ $CD115^+$ Ly-$6G^-$ Ly-$6C^{hi}$ or Ly-$6C^{lo}$ cells) were identified using flow cytometry and quantified from mice treated with Lipsosomal PBS or PBS control at time of harvest (120 hrs) (n=12-14 from 2 independent experiments). (**C**) Hepatic macrophages were identified by flow cytometry as before and expressed as a % of total hepatic CD45 positive cells (n=13-14 from 2 independent experiments). (**D**) Macrophage subsets were identified by flow cytometry as before and expressed as a % of total hepatic macrophages (n=13-14 from 2 independent experiments). (**E**) Changes in hepatic macrophage subset number, identified by flow cytometry, following liposomal PBS or PBS administration (Relative to mean total macrophage number in PBS-treated livers; n=13-14 from 2 independent experiments). All data expressed as Mean±SEM; * $P<0.05$, ** $P<0.01$, *** $P<0.001$, NS=Not Significant.

Figure 8.4 - Liposomes Increase the Restorative Macrophage Population

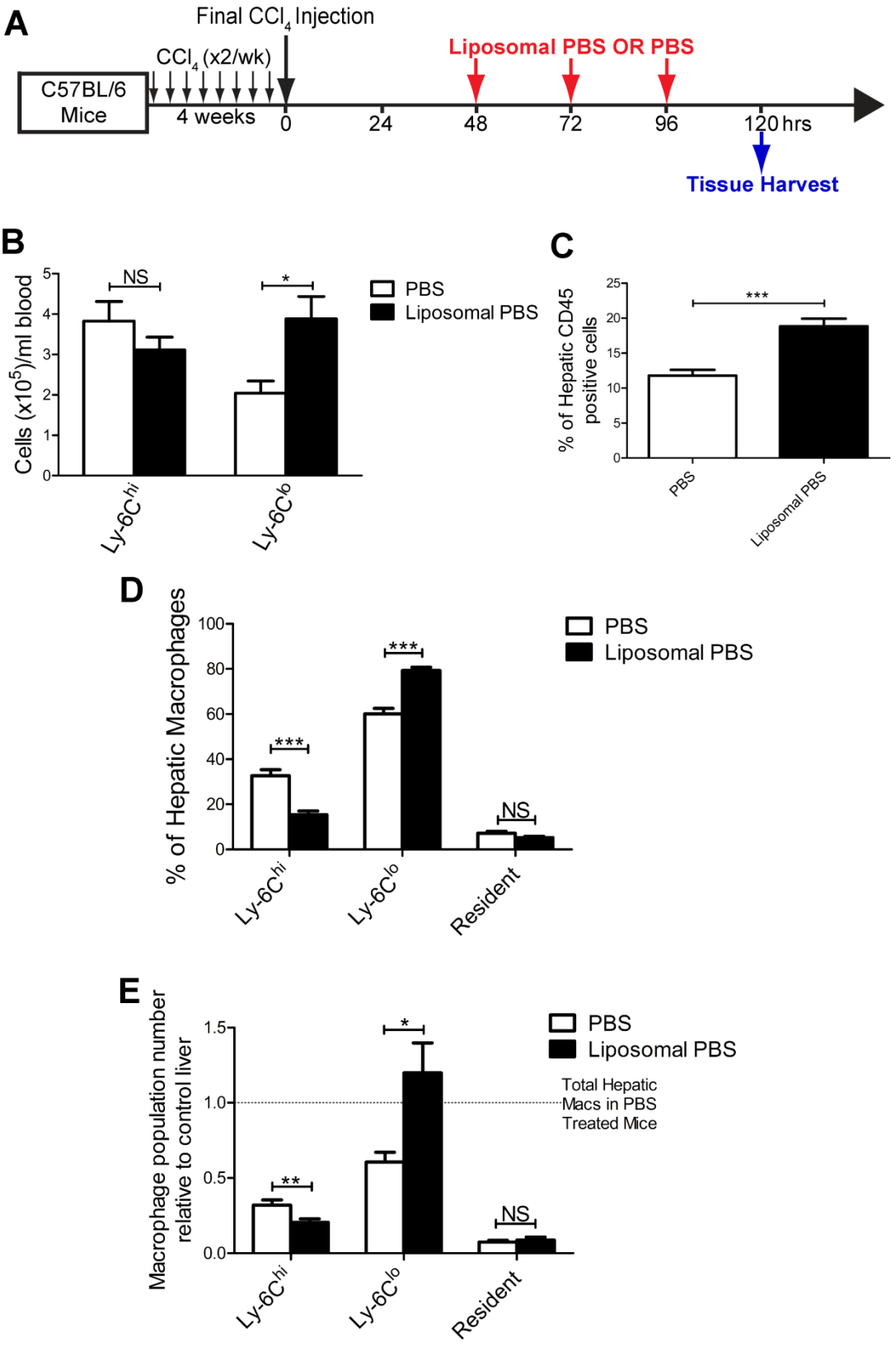

Liposome Administration Accelerates Hepatic Fibrosis Resolution

Having shown that liposome administration induced a change in hepatic macrophage phenotype, I sought to determine whether this could accelerate hepatic fibrosis resolution. As previously demonstrated, being post-phagocytic is a key feature of the restorative Ly-6C^{lo} macrophage subset. I therefore wished to confirm that hepatic macrophages showed evidence of liposome ingestion. To this end, liposomes were fluorescently labelled with membrane dye CM-DiI, prior to injection according to an identical schedule (**Fig 8.4A**). Hepatic macrophages were identified as before by flow cytometry. The percentage of each hepatic macrophage subset which was positive for CM-DiI, indicating ingestion of liposomes, was then defined using flow cytometry. As shown in **Fig 8.5A** , both Ly-6C^{lo} and "Resident" hepatic macrophages show a high degree of CM-DiI positivity, demonstrating a high level of phagocytosis of liposomes in these populations (n=8).

I then went on to assess the effect of liposomes on hepatic fibrosis resolution in the same model (**Fig 8.4A**). As shown in **Fig 8.5B and C**, liposome administration caused a reduction in hepatic PSR staining (n=6), indicating that this intervention accelerated the regression of liver fibrosis following chronic CCl_4 injury.

Figure 8.5 – Liposome Administration Accelerates Hepatic Fibrosis Resolution

Liposomal PBS or PBS control were administered to chronically injured C57BL/6 mice according to the schedule shown in Fig 8.4A. (**A**) Percentage of the stated hepatic macrophage subset containing fluorescently-labelled (CM-DiI) liposomes assessed by flow cytometry (n=8). (**B**) Fibrosis assessed by PSR staining following liposomal PBS (or PBS control) administration (Representative images shown; Scale bar=100μm) (**C**) Quantification of fibrosis by morphometric pixel analysis (Expressed relative to mean % area for liposome-treated liver; n=6). Data shown as Mean±S.E.M; **P*<0.05, ****P*<0.001.

Figure 8.5 - Liposome Administration Accelerates Hepatic Fibrosis Resolution

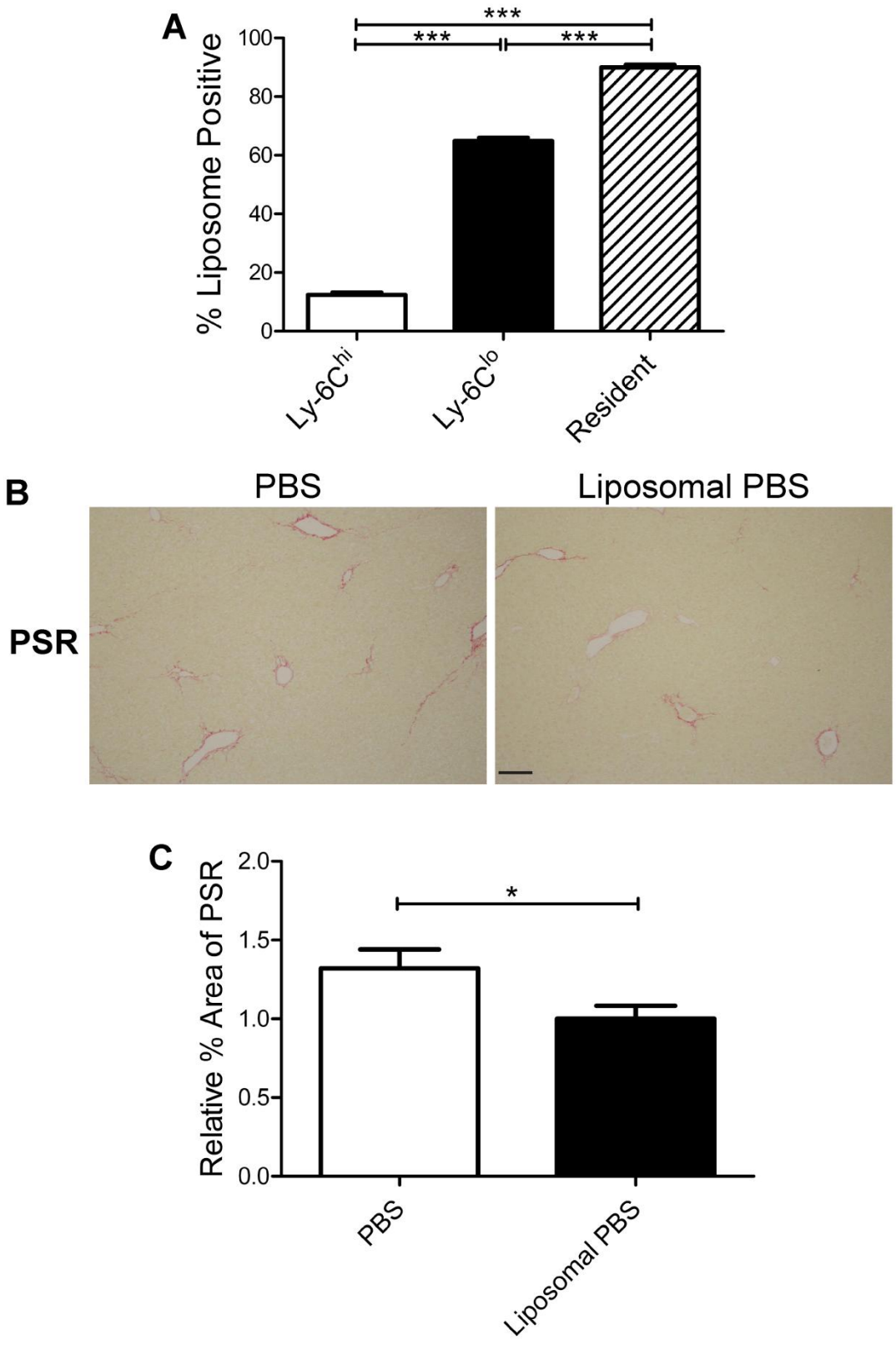

DISCUSSION

In this chapter I have sought to utilise the previous data to ascertain if the *in vivo* hepatic macrophage phenotype can be manipulated in the CCl_4 model. Ultimately, such studies are essential for translational purposes.

PPAR-γ signalling was an intriguing initial target. As previously demonstrated from the pathway analysis of genes upregulated in restorative macrophages, PPAR signalling was one of the enriched pathways (**Fig 6.3B**). It is known that PPAR-γ activation in macrophages plays an important role, being responsible for inflammatory gene expression, macrophage polarisation and promoting the resolution of inflammation (Bouhlel et al., 2007, Castrillo and Tontonoz, 2004, Gautier et al., 2012). Indeed, recent data using macrophage specific PPAR-γ knockout mice, has demonstrated that macrophage PPAR-γ expression has important anti-fibrotic properties in the liver (Moran-Salvador et al., 2013). Given the already well established clinical use of the PPAR-γ agonists pioglitazone and rosiglitazone in the management of diabetes, they would be potentially attractive anti-fibrotic drugs in liver fibrosis. Indeed, studies have already shown that pioglitazone may have an anti-fibrotic effect in the livers of non-diabetic NAFLD patients (Aithal et al., 2008). However, despite these data, there was no obvious effect of rosiglitazone administration on overall macrophage number, macrophage subsets or fibrosis regression in my CCl_4 model (**Fig 8.1**). Does this mean a genuine lack of effect? I'd suggest that the studies presented here are too preliminary to definitively state this. Whilst, I'd used a previously published dose of rosiglitazone, further studies are required to confirm that the drug was effective in activating PPAR-γ in the livers of mice *in vivo* at this dose. Secondly, the timing of drug administration may be too short to show a demonstrable effect. Future studies involving more protracted drug administration during fibrosis resolution would be useful. Thirdly, PPAR-γ activity is already evident in the restorative Ly-$6C^{lo}$ hepatic macrophage population *in vivo*. It is feasible that this pathway is already maximally activated in these cells and hence administration of a PPAR-γ agonist when this macrophage subset already predominates may have little overall effect. Hence, timing is likely to be crucial. Finally, PPAR-γ signalling is not specific to macrophages and indeed has effects on HSC activation (Marra et al., 2000) and hepatocyte function (Rogue et al., 2011). Thus, systemic treatment with PPAR-γ modulating drugs is likely to affect several hepatic cell types, making specific conclusions about the effect on macrophages difficult to draw.

I proceeded to try and inhibit the phagocytic process *in vivo* to determine whether this might alter macrophage phenotype and have consequent effects on hepatic fibrosis. Again, this is a

natural progression from my previous data, where I've shown that macrophage phagocytosis plays a key part in the generation of the restorative macrophage phenotype. I initially attempted to inactivate MFG-E8, a key molecule in the phagocytic process, *in vivo* using a blocking antibody (Bu et al., 2007) during fibrosis resolution following CCl_4 injury. Administration of this antibody had no demonstrable effect on circulating monocyte number, hepatic macrophage number, macrophage subsets or hepatic fibrosis resolution. As an alternative strategy for inhibiting phagocytosis, I administered the ITGAV blocking antibody RMV-7 to mice following CCl_4 injury, again at published doses that have been shown to be effective in mice *in vivo* (Takahashi et al., 2001). On this occasion, the ITGAV blocking antibody did induce a statistically significant reduction in the Ly-$6C^{lo}$ restorative macrophage subset (**Fig 8.3D**), suggesting that ITGAV activity and hence potentially phagocytosis are important for the generation of this macrophage population. However, no effect was seen on the overall levels of hepatic fibrosis. Whilst, in both of these blocking studies, published doses of antibody were used, further work is required to ascertain if the antibody was effective in inhibiting the relevant pathway and indeed inhibiting the phagocytic uptake of cell debris in the injured liver. Given that effective phagocytosis is such an innate protective immune and that the phagocytic process has such a range of receptors and pathways, it is likely that a degree of redundancy exists, such that even with the effective blockade of one pathway, effective clearance of cell debris may continue. This may also contribute to the overall lack of effect with these blockade strategies. A further caveat to interpretation of these data is the pleotropic functions of these molecules. Specifically, ITGAV also has an important role in the activation of latent TGF-β (Munger et al., 1999) and hence any global inhibition method such as a blocking antibody may also have effects outwith the role in phagocytosis.

The other strategy I employed to try and manipulate *in vivo* hepatic macrophage phenotype in my CCl_4 model was the administration of liposomes. As previously discussed, liposome uptake by macrophages has been shown to be a phagocytosis event and indeed as shown in **Fig 7.5**, liposome administration to macrophages *in vitro* induces a macrophage phenotype similar to that of the restorative hepatic Ly-$6C^{lo}$ macrophages *in vivo*. Furthermore, liposomes have been widely used in animal models as drug delivery vehicles to macrophages, most commonly for liposomal clodronate. Indeed liposomal drug delivery is also finding use in human disease (Chang and Yeh, 2012). Proof of principal that liposome administration per se can induce changes in macrophage phenotype *in vivo* with a consequent effect on tissue inflammation already exists in a rat model of acute myocardial infarction (Harel-Adar et al., 2011) and a model of inflammatory arthritis (Ma et al., 2011).

Furthermore, this effect may well be mediated by potentiation of macrophage ERK signalling (Ma et al., 2011), a pathway I've shown to be important in the matrix degrading properties of macrophages following phagocytosis (**Fig 7.3**). Hence, there is good scientific rationale to use liposomes as a means to manipulate hepatic macrophage phenotype *in vivo*, with the aim of enhancing the restorative macrophage population and accelerating fibrosis regression. It was therefore relevant to see that the administration of liposomes following 4 weeks of CCl_4 injury in my model, resulted in a striking change in hepatic macrophage phenotype, with a reduction in pro-fibrogenic Ly-6C^{hi} cells and an increase in restorative Ly-6C^{lo} macrophages (**Fig 8.4E**). Correspondingly, in keeping with this change in macrophage phenotype to favour scar resolution, liposome administration resulted in accelerated matrix degradation (**Fig 8.5B and C**). Overall, these findings demonstrate that the induction of phagocytosis in macrophages *in vivo* modifies macrophage phenotype, enhancing the restorative Ly-6C^{lo} subset, and accelerating the resolution of hepatic fibrosis.

SUMMARY

- Administration of the PPAR-γ agonist rosiglitazone to mice following CCl_4 injury, had no detectable effect on numbers of circulating monocytes or hepatic macrophage subsets and no obvious effect on liver fibrosis resolution in a short time frame.
- Antibody blockade of MFG-E8 *in vivo* following CCl_4 injury had no detectable effect on numbers of circulating monocytes or hepatic macrophage subsets and no obvious effect on liver fibrosis resolution.
- Antibody blockade of integrin α_v *in vivo* following CCl_4 injury, induced a change in hepatic macrophage phenotype with a reduction in restorative Ly-$6C^{lo}$ macrophage number, suggesting a role for this key phagocytosis receptor in the generation of this population.
- Antibody blockade of integrin α_v *in vivo* following CCl_4 injury had no detectable effect on liver fibrosis resolution in a short time frame.
- Administration of liposomal PBS to mice following CCl_4 injury induced a phenotypic switch in hepatic macrophages with a reduction in pro-fibrotic Ly-$6C^{hi}$ macrophage number and an increase in restorative Ly-$6C^{lo}$ hepatic macrophages.
- Lipsomal PBS administration resulted in accelerated resolution from liver fibrosis

CHAPTER 9 – DISCUSSION AND FUTURE WORK

In this thesis, I have established a reversible murine model of liver fibrosis using CCl_4 and have utilised this to identify and characterise the hitherto elusive restorative hepatic macrophage. This Ly-$6C^{lo}$ $CD11b^{hi}$ $F4/80^{int}$ macrophage population accumulates in the liver and is the main MMP-expressing macrophage subset during maximal fibrosis resolution, is necessary for degradation of tissue scar, is derived from infiltrating Ly-$6C^{hi}$ inflammatory monocytes, has a distinct pattern of gene expression including matrix degradation and phagocytic genes and is characterised by evidence of prior phagocytosis of dying cells. The restorative phenotype can be recapitulated *in vitro* by phagocytosis induced ERK signalling and can be induced *in vivo* by the administration of liposomes which accelerates scar resolution. Much of this data has been published (Ramachandran et al., 2012) and **Appendix 2**.

As discussed in detail in **Chapter 1**, there is a growing body evidence for a role of macrophages in inflammation and tissue fibrogenesis, not only in the liver, but also in other organs (Wynn and Barron, 2010). More recently, data is emerging to suggest a functional heterogeneity of macrophage subtypes *in vivo* and a potential role in fibrosis resolution (Duffield et al., 2005, Fallowfield et al., 2007, Ramachandran and Iredale, 2009, Gibbons et al., 2011). Given that tissue fibrosis is now estimated to contribute to up to 45% of deaths in the Western world (Hayden, 2011), a greater understanding of the processes involved is essential to develop badly needed anti-fibrotic therapies. The liver, with its well described fibrotic response to injury and potential reversibility, is the ideal organ to study the mechanisms of fibrogenesis and fibrosis regression (Ramachandran and Iredale, 2012a). Hence, I sought to use a reversible murine liver fibrosis model to identify the macrophage population responsible for the resolution of fibrosis: termed the restorative macrophage.

Initially, I needed to establish a robust and reproducible reversible liver fibrosis model. I utilised the widely-used CCl_4 model in mice. As shown in **Fig 3.1 to Fig 3.4**, 4 weeks of twice weekly CCl_4 treatment to male C57BL/6 mice induces significant hepatic fibrosis, which peaks 48-72 hours after the final CCl_4 injection, followed by fibrosis resolution. Importantly for subsequent experiments, this model enabled me to study a pro-fibrogenic timepoint (24 hrs after the final CCl_4 injection), and a pro-resolution timepoint (72 hrs after the final CCl_4 injection) at the time of initiation of maximal matrix degradation, when the liver is primed for scar breakdown.

Differential Ly-6C expression has been widely used to identify functionally distinct populations of circulating murine monocytes (Gordon and Taylor, 2005, Ingersoll et al., 2009) and more recently macrophage subpopulations in diseased tissue (Lin et al., 2009,

Arnold et al., 2007, Karlmark et al., 2009, Movahedi et al., 2010, Nahrendorf et al., 2007). Using this data, I was able to demonstrate that differential Ly-6C expression can be exploited to identify the macrophage subset responsible for fibrosis resolution. Specifically, in my CCl_4 model, a Ly-$6C^{lo}$ monocyte-derived macrophage subset accumulates maximally at the critical 72 hr timepoint (**Fig 3.9**) and represents the main MMP-expressing macrophage population in the liver at this time (**Fig 3.11**). Conversely, at the time of fibrogenesis (24 hrs) in this model a Ly-$6C^{hi}$ monocyte-derived macrophage population predominated (**Fig 3.9**). This mirrors another study in the liver where this subset has been shown to be pro-fibrogenic (Karlmark et al., 2009).

As a means of comparison I also sought to use a second model of liver murine liver fibrosis. Oral thioacetamide (TAA) induces a fibrotic response in rats (Jeong et al., 2001, Noda et al., 1996), but has only rarely been described in mice, with no robust data on reversibility. I established a murine TAA in male C57BL/6 mice model, demonstrating that significant fibrosis is induced by 8 weeks of treatment with cirrhosis by 52 weeks of therapy (**Fig 3.6**). This was a dose-response effect, with only the higher dose of TAA (600mg/l) causing this. However, in contrast to the CCl_4 model, no fibrosis reversibility was seen following TAA injury with recovery times of up to 8 weeks (**Fig 3.7**). Why this difference in reversibility between these 2 models? There are numerous potential explanations. From my data, the TAA model lacked the dynamic changes in monocyte-derived macrophages seen in the CCl_4 model. Specifically, no increase in Ly-$6C^{lo}$ or Ly-$6C^{hi}$ subsets was seen during treatment or following the cessation of TAA (**Fig 3.12**). This lack of accumulation of MMP-expressing restorative macrophages could explain the absence of matrix degradation I observed. This raises a wider question on fibrosis resolution – is tissue inflammation/damage and consequent recruitment of inflammatory cells, in particular macrophages, actually a pre-requisite for fibrosis resolution as well as fibrogenesis? Certainly, one of the features of non-resolving liver scars is hypocellularity, suggesting the absence of the intimate relationship between SAMs and fibrotic matrix may inhibit matrix degradation (Issa et al., 2004). Furthermore, a study by Mitchell and colleagues demonstrated that knockout of the monocyte chemokine receptor CCR2 in mice inhibits hepatic scar formation in response to CCl_4 injury but also attenuates scar resolution, indicating that CCR2-dependent monocyte recruitment is likely to be a pre-requisite for both fibrogenesis and fibrosis regression (Mitchell et al., 2009). This has important potential implications for the development of anti-fibrotic therapies. Some authors have suggested inhibiting the inflammatory process, in particular chemokines, as a potential anti-fibrotic therapy (Sahin et al., 2010, Vielhauer et al., 2010). However, this may also result in inhibition of fibrosis resolution and given that many

patients present with established liver fibrosis, a treatment that can manipulate the immune response to promote fibrosis regression is likely to be more useful. The TAA model I have described may provide a useful method for testing some of these theories. An interesting series of experiments would be to determine whether an established irreversible liver fibrosis induced by TAA could be made more reversible by inducing hepatic inflammation and monocyte recruitment, for example by giving a single injection of CCl_4 or perhaps even better by causing hepatic overexpression of CCL2 (MCP-1) by administration of an adenoviral vector.

Clearly, other factors may also contribute to the irreversibility seen with the TAA model. The composition of the scar tissue is likely to be different with liver fibrosis in TAA mice being rich in elastin (Pellicoro et al., 2011), which may be more resistant to degradation than the more typical collagens 1 and 3. The pattern of fibrosis is also different in TAA than CCl_4 injury, with a more biliary distribution evident in response to TAA (Jeong et al., 2001, Noda et al., 1996). This anatomical pattern may be more inherently resistant to scar breakdown, but also may result in preferential activation of portal myofibroblasts rather than HSCs, which may well have a different phenotype (Bosselut et al., 2010). Further light could be shed on this by isolating myofibroblasts from TAA and CCl_4 livers and comparing their phenotype and gene expression profiles.

Despite the obvious differences between the CCl_4 and TAA models, one similarity in terms of macrophages does exist; namely the loss of resident-type ($F4/80^{hi}$ $CD11b^{int}$) hepatic macrophages in response to injury and the progressive reaccumulation following the removal of the injurious stimulus (**Fig 3.9 and 3.12**). In depth study of this population was beyond the scope of this thesis. However, it would be intriguing to know the fate of these cells in response to injury (e.g. cell death, phenotypic change or migration to draining lymph nodes), the means of repopulation and their function during this repopulation phase. Complex lineage tracing experiments using inducible macrophage specific Cre mice would be required to unpick this, but is essential to our full understanding of the role of macrophages in hepatic fibrogenesis and resolution.

Following the initial characterisation of macrophage dynamics in my reversible CCl_4 model, I proceeded to obtain more functional data using macrophage depletion. I was able to show that in CD11b-DTR mice injured with CCl_4, DT administration during the resolution phase resulted in selective depletion of the predominant Ly-$6C^{lo}$ macrophage subset and consequently prevented fibrosis regression (**Fig 4.2 and 4.3**). The close correlation between the number of hepatic Ly-$6C^{lo}$ macrophages and the degree of fibrosis resolution (**Fig 4.4**)

emphasises their role as the restorative hepatic macrophage. The contrast between this CD11b-DTR model and macrophage depletion with liposomal clodronate, where no difference in fibrosis regression was observed (**Fig 4.6**), was striking. This is the first direct comparison of depletion, in the same disease model, between the liposomal clodronate and CD11b-DTR systems. What is clear from my data, is that liposomal clodronate induces a much more global depletion of different subpopulations of hepatic macrophage than CD11b-DTR (**Fig 4.6**). Additionally, liposomal clodronate seems to have more off target effects on other immune cell populations such as neutrophils or T cells (**Fig 4.6**). This is not withstanding the clear effects of liposome administration in itself (**Fig 8.4 and 8.5**). Thus, macrophage depletion with liposomal clodronate may miss more subtle functional effects, particularly when distinct subsets have opposing functions. Furthermore, experiments using liposomal clodronate should always also include 2 control arms, one with vehicle alone and one with liposomes alone.

Having identified the restorative hepatic macrophage as the Ly-6C^{lo} monocyte-derived population, I sought to characterise this subset further. A major question arising from studies regarding the divergent role of macrophages in fibrogenesis and recovery was whether these distinct functions were mediated by distinct cell populations or whether cells underwent a phenotypic switch *in situ* (Friedman, 2005, Wynn, 2011). Using a series of adoptive transfer and *in situ* labelling experiments (**Fig 5.1 to 5.4**), I have shown that the Ly-6C^{lo} population derives from Ly-6C^{hi} inflammatory monocytes, a common origin to the pro-fibrogenic Ly-6C^{hi} macrophages, and indicating that the restorative hepatic macrophage is formed by a switch in macrophage function *in vivo*. Additionally, this switch occurs after a significant amount of proliferative activity of these Ly-6C^{hi} macrophages (**Fig 5.5**), suggesting a combination of recruitment and local proliferation is needed to generate the restorative macrophage phenotype. These findings are certainly in keeping with the known ability of macrophages to change phenotype according to local environmental cues (Mosser and Edwards, 2008). My data is also analogous to that described for the role of macrophages in muscle regeneration (Arnold et al., 2007). Once again this highlights that a therapeutic strategy aimed at global inhibition of macrophage recruitment is unlikely to be entirely successful, as this would also diminish restorative macrophages. Hence a more subtle approach of trying to promote the formation of the pro-resolution phenotype is likely to be needed.

Having identified that pro-fibrotic Ly-6C^{hi} and pro-resolution Ly-6C^{lo} hepatic macrophages derive from a common origin, I proceeded to compare the gene expression profiles of these 2

populations to shed further light on the mechanisms of macrophage-induced fibrogenesis and fibrosis regression. I analysed these 2 populations using microarray whole trancriptome analysis, enabling unbiased comparisons to be made. This has highlighted a number of key features of the restorative macrophage subset. In particular, the upregulation of matrix-degrading MMPs such as MMP-12 and MMP-9, growth factors such as IGF-1, and other potentially anti-inflammatory molecules such as CX3CR1 (Karlmark et al., 2010) and CD74 (Heinrichs et al., 2011) was observed in the Ly-6C^{lo} cells (**Fig 6.2**). Expression of Arginase-1 was also increased in the restorative macrophage subset (**Fig 6.2**). This has recently been shown to have an anti-fibrotic role in the liver (Wynn and Barron, 2010). These microarray data also enabled me to identify specific markers of restorative macrophages, which could be utilised to identify them *in situ* in liver tissue using immunohistochemistry for MMP-12 and GPNMB. Importantly, I was also able to apply this to human liver tissue and identify subpopulations of macrophages which could represent the human restorative macrophage (**Fig 6.5**). This is useful, as the potential to perform multicolour flow cytometry on freshly isolated human liver is obviously much more limited. One of the other striking features of the restorative macrophage expression profile was the enrichment of genes associated with phagocytosis (**Fig 6.2 and 6.3**). As described in detail in **chapter 1**, phagocytosis is a key function of macrophages in inflammatory environments and has important consequences for macrophage phenotype. I therefore wondered whether phagocytosis of dead/dying cells in the inflamed liver might be a reason for the change in macrophage phenotype from one promoting fibrogenesis (Ly-6C^{hi}) to one promoting fibrosis resolution (Ly-6C^{lo}). Indeed, I was able to confirm definitively that the restorative Ly-6C^{lo} but not the Ly-6C^{hi} hepatic macrophage population had ingested apoptotic debris (**Fig 6.6**).

In addition to the information about the restorative macrophage, this dataset also provided valuable functional insights into the pro-fibrotic Ly-6C^{hi} macrophage subset. It should be borne in mind that whilst there is currently very limited characterisation of restorative macrophages in other organs, a macrophage population derived from Ly-6C^{hi} monocytes has been shown to be pro-fibrogenic in the liver (Karlmark et al., 2009), but also lung (Gibbons et al., 2011, Osterholzer et al., 2013) and kidney (Lin et al., 2009). However, the exact expression profile of these pro-fibrogenic macrophages had not previously been described. Expression of the key pro-fibrogenic cytokine TGF-β with resultant HSC activation has been the proposed mechanism of fibrosis promotion by hepatic macrophages (Wynn and Barron, 2010, Karlmark et al., 2009). Interestingly, I did not find a major difference in TGF-β expression between pro-fibrogenic and pro-resolution macrophage populations, arguing against this (**Fig 6.2**). However, pro-fibrotic Ly-6C^{hi} hepatic macrophages did show a

significantly higher level of expression of Thrombospondin 1 (Thbs1), a protein which in addition to having a role in phagocytosis is an important activator of latent TGF-β (Breitkopf et al., 2005, Crawford et al., 1998, Elpek et al., 2008, El-Youssef et al., 1999). Whether, this is an important functional observation linking hepatic macrophages and fibrogenesis should be further studied, ideally using macrophage-specific Thbs1 knockout mice. Ly-6C^{hi} hepatic macrophages also expressed other potentially pro-fibrogenic mediators. For example, Il-1β expression was higher in Ly-6C^{hi} macrophages (**Fig 6.4**), a cytokine which in addition to being pro-inflammatory has been shown to have a pro-fibrogenic role in the liver (Gieling et al., 2009), potentially via promoting HSC survival in an NF-κB dependent manner (Pradere et al., 2013). Additionally, Ly-6C^{hi} macrophages expressed higher levels of a number of chemokines, including CCL2 and CXCL10 (**Fig 6.2 and 6.4**). CCL2, in particular, has been shown to be pro-fibrotic in the liver (Imamura et al., 2005) and is likely to contribute to further recruitment of inflammatory monocytes and also have direct effects on hepatic stellate cell chemotaxis (Friedman, 2008). CXCL10 has also been shown to be a pro-fibrogenic chemokine in the liver (Hintermann et al., 2010). Chitinase 3-like 3 (Chi3l3 or YM-1) was another gene that was strikingly upregulated in the pro-fibrotic macrophage subset (**Fig 6.2 ad 6.4**) and indeed served as a marker for this population in immunohistochemical studies (**Fig 6.5**). Chi3l3 has also been shown to be a marker of the pro-fibrogenic marcrophage population in the lung (Gibbons et al., 2011). The exact function of Chi3l3 remains unknown, but chitinases themselves have been suggested to have a pro-fibrogenic function (Wynn and Barron, 2010) and indeed a human chitinase YKL-40 has been suggested as a serum marker of liver fibrosis (Johansen et al., 2000). Whether Chi3l3 is simply a marker of the pro-fibrotic hepatic macrophage or whether it has a functional role could be better defined using knockout mice.

The other thing that is clear from my extensive microarray dataset is that these *in vivo* hepatic macrophage subsets do not fit into the traditional M1/M2 macrophage paradigm (**Fig 6.2**). Whilst this has been a useful nomenclature to help understanding of the potential for macrophage polarisation, it clearly cannot represent the complex *in vivo* phenotypes observed and hence, should be avoided where possible, with a greater focus given to the functional role of the specific population.

Overall, these data enable development of a greater understanding of the functional role of liver macrophages in hepatic fibrogenesis and fibrosis resolution, summarised in the schematic diagram is shown in **Fig 9.1**.

Having characterised the pro-fibrotic and restorative hepatic macrophage subsets, I then wished to utilise these data to try and determine what causes the Ly-6C^{hi} macrophage population to change phenotype *in vivo* to develop pro-resolution features. Phagocytosis seems to play a major role in this switch and I was, hence able to model this *in vitro* (**Chapter 7**). Taking this 1 step further, my preliminary data suggests that phagocytosis-induced ERK signalling may well mediate the increase in matrix degrading enzymes expressed by restorative macrophages (**Fig 7.3**). If this could be confirmed *in vivo*, potentially using macrophage specific transgenic targeting or ERK inhibitors delivered in a macrophage specific manner perhaps via liposomes, this could offer a new means of manipulating *in vivo* macrophage phenotype.

I was, however, able to utilise my data showing that phagocytosis induces restorative macrophage phenotype to develop a novel therapeutic strategy. By administering liposomes to mice following CCl_4 injury, I was able to enhance the macrophage phenotypic switch *in vivo*, resulting in an increase in restorative hepatic macrophage number and reduction in pro-fibrotic macrophages (**Fig 8.4**) and hence accelerate fibrosis resolution (**Fig 8.5**). It would be intriguing to replicate these experiments in other models of liver fibrosis or indeed fibrosis in other organs to determine whether this could be developed as a genuine translational therapeutic strategy. An alternative would be to feed liposomes to macrophages *in vitro* to promote a matrix degrading properties and then to use these modified macrophages as a cell therapy.

It would be more readily translational if we could identify the specific pathway that links macrophage phagocytosis and the matrix degrading phenotype. Hopefully, this would yield a more druggable target to promote the phenotypic switch in macrophages and enhance fibrosis resolution. PPAR-γ was a potentially attractive pathway given the existence of drugs already in widespread clinical use. Unfortunately, my data did not demonstrate a significant effect of PPAR-γ agonism on macrophage phenotype or fibrosis regression (**Fig 8.1**). However, as described in **Chapter 8**, this may be experimental and certainly merits further study. I did show that blockade of integrin α_v does change the hepatic macrophage phenotype *in vivo*, albeit with no demonstrable effect on fibrosis regression in my initial studies (**Fig 8.3**). This again could be studied further, potentially using LysM-Cre mice crossed with mice with a floxed ITGAV gene. However, this highlights one of the key experimental problems in studying the role of specific pathways in fibrosis resolution. Namely, that fibrosis is a dynamic process and using transgenic mice with a relevant gene knocked out will result in a different level of peak inflammation/fibrosis following injury. This makes reliable

interpretation of the resolution phase almost impossible. Furthermore, global knockouts of molecules such as ITGAV or PPAR-γ will clearly have effects on cell types other than macrophages. Hence, what is badly needed is a series of inducible macrophage-specific cre mice, whereby tissue injury and fibrosis can be caused and then the gene of interest deleted solely in macrophages during the resolution phase, avoiding the confounding effects of differences in peak fibrosis. One such mouse line, Csf1r-Mer-iCre-Mer mice which enable inducible Cre expression in Csf1r-expressing monocytes in response to tamoxifen administration has recently been used to knockout Vegf expression in monocytes *in vivo* (Qian et al., 2011). Such mice could also be useful for more in depth lineage tracing experiments to study the fate of macrophages during fibrosis resolution.

How does the phenotype of the hepatic restorative macrophage compare to those described in the literature? In the context of murine peritoneal inflammation, a pro-resolution macrophage population has been identified (Bystrom et al., 2008). Analogous to my restorative macrophage subset, these macrophages show lower levels of expression of pro-inflammatory cytokines and chemokines than their pro-inflammatory counterparts, and importantly do not conform to the M1/M2 paradigm but rather represent hybrid cells (Bystrom et al., 2008). In muscle injury, the macrophage population responsible for promoting regeneration upregulates PPAR-γ (Arnold et al., 2007). However, extensive datasets on the phenotype of macrophages responsible for the resolution of tissue injury, such as that presented in thesis, do not currently exist for other organs. Further work characterising such populations would enable comparison to the liver and identification of pathways which might be targetable in several diseases.

What is the relevance of my data to human disease? I had deliberately focussed my attention on an early CCl_4-induced fibrosis in mice, which resolves rapidly. This was convenient as it enabled in depth analysis of macrophage dynamics on a day-by-day basis, and has provided robust and reproducible data. Reassuringly, I was also able to identify a subset of macrophages in human cirrhotic liver which expressed the same markers (MMP-12 and GPNMB) as the murine restorative macrophages. However, clearly much more work is required to translate my murine data to human disease, where liver fibrosis is generally formed over many years. Importantly, we do now have convincing evidence that human liver fibrosis is also reversible (Ramachandran and Iredale, 2009). Furthermore, our understanding of the heterogeneity of macrophages in the cirrhotic human liver is ever improving. In human livers, similar to my mouse model, 3 populations of macrophages could be identified by FACS (Zimmermann et al., 2010). These could be defined as $CD14^{hi}$ $CD16^{-}$, $CD14^{lo}$

$CD16^-$ and $CD14^+$ $CD16^+$. The $CD14^{lo}$ $CD16^-$ population was felt to represent the resident Kupffer cell population, analogous to the $F4/80^{hi}$ $CD11b^{int}$ population in murine livers. The $CD14^{hi}$ $CD16^-$ and $CD14^+$ $CD16^+$ were felt to represent monocyte-derived macrophage populations, with the $CD14^+$ $CD16^+$ subset accumulating maximally in the fibrotic/cirrhotic livers (Zimmermann et al., 2010). Interestingly, in my model, pro-inflammatory Ly-$6C^{hi}$ macrophages express higher levels of CD14 whilst restorative Ly-$6C^{lo}$ macrophages express higher levels of CD16/32, suggesting some similarities to the human data (**Fig 6.2B**). In a separate human study $CD14^{++}$ $CD16^+$ hepatic macrophages were confirmed to accumulate in diseased liver (Liaskou et al., 2012). Furthermore, this study demonstrated the capacity of human $CD14^{++}$ $CD16^-$ monocytes to change phenotype and acquire CD16 expression in response to IL-10 or TGF-β exposure. Analogous to the hepatic macrophages identified in my CCl_4 model, these $CD14^+$ $CD16^+$ hepatic macrophages show a significant phagocytic capacity and secrete a range of cytokines and chemokines (Liaskou et al., 2012). One might therefore assume that human hepatic $CD14^{++/hi}$ $CD16^-$ monocyte-derived macrophages correspond to Ly-$6C^{hi}$ cells in murine CCl_4–injured livers, whilst the $CD14^+$ $CD16^+$ population may well represent the restorative macrophage subset. However, the $CD14^+$ $CD16^+$ population expresses more CD80 and CD86 and also higher levels of cytokines and chemokines (including IL-1β and CCL2) than $CD14^{++}$ $CD16^-$ counterparts, which is more akin to Ly-$6C^{hi}$ macrophages in my model. In order to define these similarities more closely, further studies are required, potentially involving isolation of human hepatic macrophage subsets and microarray analysis with comparison to the gene expression profiles in my model. Even more useful would be to perform this study in human livers where fibrosis remodelling is actively occurring, for example in patients with chronic viral hepatitis who have received treatment or patients with alcohol-related liver disease who are now abstinent. Such studies would identification of common pathways in macrophages between human disease and murine models and are essential for the development of therapies which can manipulate macrophage phenotype and promote liver fibrosis resolution *in vivo*.

Figure 9.1 – Summary of the Proposed Role of Macrophages in Hepatic Fibrogenesis and Fibrosis Regression

Schematic showing the proposed role of macrophages in hepatic fibrogenesis and fibrosis regression, incorporating the data presented in this thesis. In response to hepatic injury, inflammatory monocytes are recruited to the liver. These proliferate *in situ* and form pro-fibrotic Ly-6C^{hi} macrophages in the liver, which show a number of features which can enhance fibrogenesis. Ly-6C^{hi} macrophages express high levels of thrombospondin-1, which can activate latent TGF-β, and hence promote transdifferentiation of quiescent hepatic stellate cells (HSCs) into a myofibroblast phenotype. These activated myofibroblasts proliferate and secrete ECM (resulting in scar formation) and TIMP-1, which inhibits both matrix-degradation by MMPs and HSC apoptosis. Hepatic Ly-6C^{hi} macrophages also express inflammatory cytokines IL-1β and TNF-α, which in addition to driving hepatic inflammation, promote myofibroblast survival. Pro-fibrotic macrophages produce high levels of chemokines such as CCL2 and CXCL10 which can further enhance recruitment of monocytes and other immune cells. Other molecules such as Chi3l3 show a high expression in Ly-6C^{hi} macrophages, but the exact function in fibrogenesis remains unknown. Within the liver these pro-fibrogenic macrophages then change phenotype, at least partly in response to phagocytosis of cellular debris and macrophage ERK signalling. This results in the generation of Ly-6C^{lo} restorative hepatic macrophages, which mediate fibrosis regression. These restorative macrophages upregulate opsonins and phagocytosis receptors, enhancing the clearance of cellular debris, and hence promoting the generation of further restorative macrophages. Ly-6C^{lo} macrophages downregulate thrombospondin-1 and pro-inflammatory cytokine expression, promoting myofibroblast apoptosis. They also upregulate matrix degrading enzymes such as MMP-12 and MMP-9, which in combination with falling TIMP-1 levels, results in increased hepatic matrix degrading activity and hence scar degradation. A number of other properties of the restorative macrophage are also shown, including expression of GPNMB, Arginase-1, anti-inflammatory receptors, activation of PPAR signalling and production of growth factors such as IGF-1 which may promote hepatocyte regeneration. The exact functional role of these pathways in macrophages remains to be defined and should be the focus of future studies.

Figure 9.1 - Summary of the Proposed Role of Macrophages in Hepatic Fibrogenesis and Fibrosis Regression

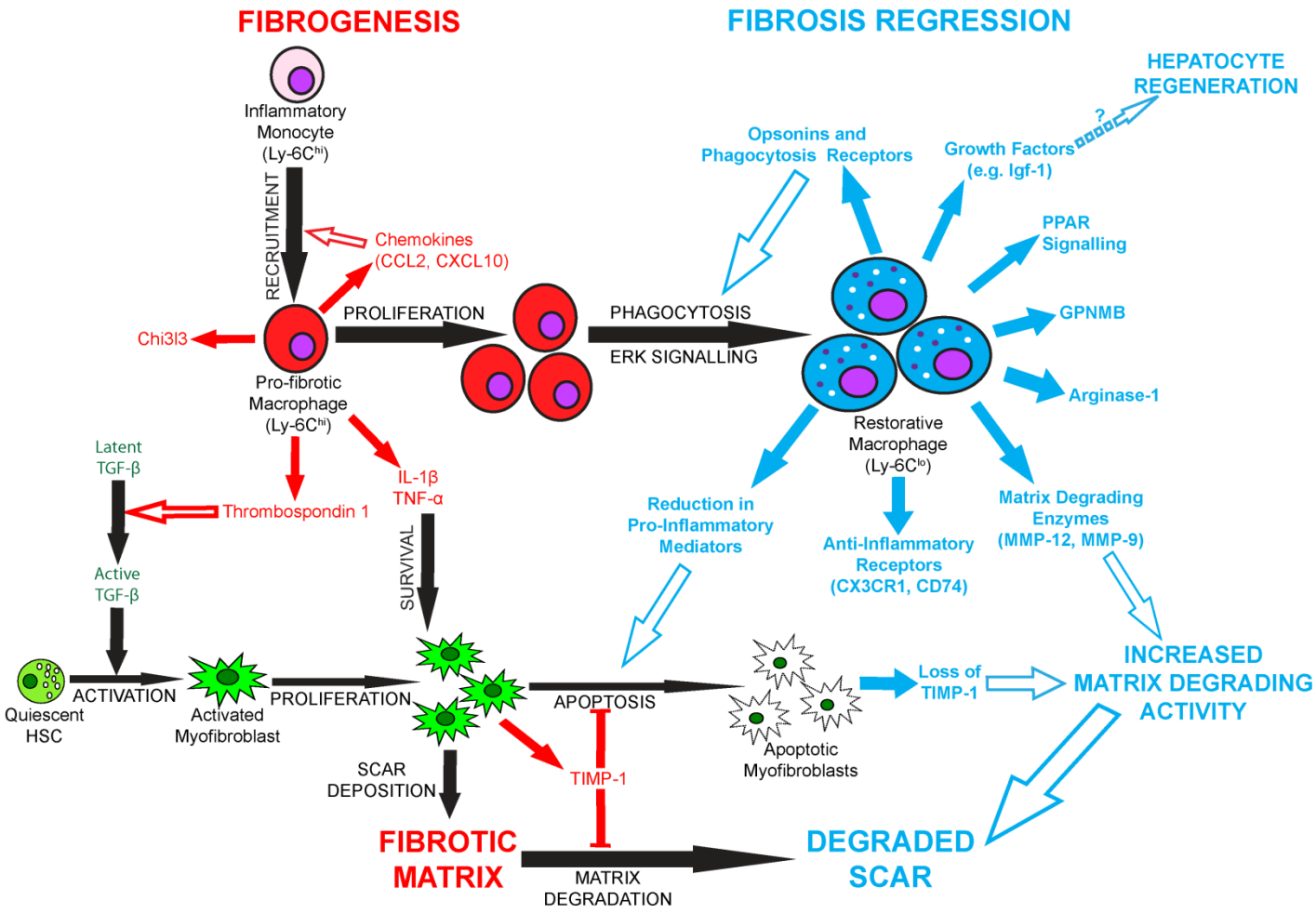

REFERENCES

AITHAL, G. P., THOMAS, J. A., KAYE, P. V., LAWSON, A., RYDER, S. D., SPENDLOVE, I., AUSTIN, A. S., FREEMAN, J. G., MORGAN, L. & WEBBER, J. 2008. Randomized, placebo-controlled trial of pioglitazone in nondiabetic subjects with nonalcoholic steatohepatitis. *Gastroenterology,* 135, 1176-84.

ALIKHAN, M. A. & RICARDO, S. D. 2013. Mononuclear phagocyte system in kidney disease and repair. *Nephrology (Carlton),* 18, 81-91.

ALTMANN, C., ANDRES-HERNANDO, A., MCMAHAN, R. H., AHUJA, N., HE, Z., RIVARD, C. J., EDELSTEIN, C. L., BARTHEL, L., JANSSEN, W. J. & FAUBEL, S. 2012. Macrophages mediate lung inflammation in a mouse model of ischemic acute kidney injury. *Am J Physiol Renal Physiol,* 302, F421-32.

ANSTEE, Q. M., WRIGHT, M., GOLDIN, R. & THURSZ, M. R. 2009. Parenchymal extinction: coagulation and hepatic fibrogenesis. *Clin Liver Dis,* 13, 117-26.

ANTHONY, B., ALLEN, J. T., LI, Y. S. & MCMANUS, D. P. 2010. Hepatic stellate cells and parasite-induced liver fibrosis. *Parasit Vectors,* 3, 60.

ANTHONY, P. P., ISHAK, K. G., NAYAK, N. C., POULSEN, H. E., SCHEUER, P. J. & SOBIN, L. H. 1977. The morphology of cirrhosis: definition, nomenclature, and classification. *Bull World Health Organ,* 55, 521-40.

AOKI, Y., MAENO, T., AOYAGI, K., UENO, M., AOKI, F., AOKI, N., NAKAGAWA, J., SANDO, Y., SHIMIZU, Y., SUGA, T., ARAI, M. & KURABAYASHI, M. 2009. Pioglitazone, a peroxisome proliferator-activated receptor gamma ligand, suppresses bleomycin-induced acute lung injury and fibrosis. *Respiration,* 77, 311-9.

AOYAMA, T., INOKUCHI, S., BRENNER, D. A. & SEKI, E. 2010. CX3CL1-CX3CR1 interaction prevents carbon tetrachloride-induced liver inflammation and fibrosis in mice. *Hepatology,* 52, 1390-400.

ARNOLD, L., HENRY, A., PORON, F., BABA-AMER, Y., VAN ROOIJEN, N., PLONQUET, A., GHERARDI, R. K. & CHAZAUD, B. 2007. Inflammatory monocytes recruited after skeletal muscle injury switch into antiinflammatory macrophages to support myogenesis. *J Exp Med,* 204, 1057-69.

ARTHUR, M. J., IREDALE, J. P. & MANN, D. A. 1999. Tissue inhibitors of metalloproteinases: role in liver fibrosis and alcoholic liver disease. *Alcohol Clin Exp Res,* 23, 940-3.

ARTHUR, M. J., MANN, D. A. & IREDALE, J. P. 1998. Tissue inhibitors of metalloproteinases, hepatic stellate cells and liver fibrosis. *J Gastroenterol Hepatol,* 13 Suppl, S33-8.

ATABAI, K., JAME, S., AZHAR, N., KUO, A., LAM, M., MCKLEROY, W., DEHART, G., RAHMAN, S., XIA, D. D., MELTON, A. C., WOLTERS, P., EMSON, C. L., TURNER, S. M., WERB, Z. & SHEPPARD, D. 2009. Mfge8 diminishes the severity of tissue fibrosis in mice by binding and targeting collagen for uptake by macrophages. *J Clin Invest,* 119, 3713-22.

AUFFRAY, C., FOGG, D., GARFA, M., ELAIN, G., JOIN-LAMBERT, O., KAYAL, S., SARNACKI, S., CUMANO, A., LAUVAU, G. & GEISSMANN, F. 2007. Monitoring of blood vessels and tissues by a population of monocytes with patrolling behavior. *Science,* 317, 666-70.

AUFFRAY, C., SIEWEKE, M. H. & GEISSMANN, F. 2009. Blood monocytes: development, heterogeneity, and relationship with dendritic cells. *Annu Rev Immunol,* 27, 669-92.

AZIZ, M., JACOB, A., MATSUDA, A. & WANG, P. 2011a. Review: milk fat globule-EGF factor 8 expression, function and plausible signal transduction in resolving inflammation. *Apoptosis,* 16, 1077-86.

AZIZ, M., JACOB, A., MATSUDA, A., WU, R., ZHOU, M., DONG, W., YANG, W. L. & WANG, P. 2011b. Pre-treatment of recombinant mouse MFG-E8 downregulates LPS-induced TNF-alpha production in macrophages via STAT3-mediated SOCS3 activation. *PLoS One,* 6, e27685.

BAMBOAT, Z. M., OCUIN, L. M., BALACHANDRAN, V. P., OBAID, H., PLITAS, G. & DEMATTEO, R. P. 2010. Conventional DCs reduce liver ischemia/reperfusion injury in mice via IL-10 secretion. *J Clin Invest,* 120, 559-69.

BATALLER, R. & BRENNER, D. A. 2005. Liver fibrosis. *J Clin Invest,* 115, 209-18.

BEAUSSIER, M., WENDUM, D., SCHIFFER, E., DUMONT, S., REY, C., LIENHART, A. & HOUSSET, C. 2007. Prominent contribution of portal mesenchymal cells to liver fibrosis in ischemic and obstructive cholestatic injuries. *Lab Invest,* 87, 292-303.

BEDORET, D., WALLEMACQ, H., MARICHAL, T., DESMET, C., QUESADA CALVO, F., HENRY, E., CLOSSET, R., DEWALS, B., THIELEN, C., GUSTIN, P., DE LEVAL, L., VAN ROOIJEN, N., LE MOINE, A., VANDERPLASSCHEN, A., CATALDO, D., DRION, P. V., MOSER, M., LEKEUX, P. & BUREAU, F. 2009. Lung interstitial macrophages alter dendritic cell functions to prevent airway allergy in mice. *J Clin Invest,* 119, 3723-38.

BEHAM-SCHMID, C., APFELBECK, U., SILL, H., TSYBROVSKY, O., HOFLER, G., HAAS, O. A. & LINKESCH, W. 2002. Treatment of chronic myelogenous leukemia with the tyrosine kinase inhibitor STI571 results in marked regression of bone marrow fibrosis. *Blood,* 99, 381-3.

BENYON, R. C. & ARTHUR, M. J. P. 2001. Extracellular matrix degradation and the role of hepatic stellate cells. *Seminars in Liver Disease,* 21, 373-384.

BENYON, R. C., IREDALE, J. P., GODDARD, S., WINWOOD, P. J. & ARTHUR, M. J. 1996. Expression of tissue inhibitor of metalloproteinases 1 and 2 is increased in fibrotic human liver. *Gastroenterology,* 110, 821-31.

BONEFELD, K. & MOLLER, S. 2011. Insulin-like growth factor-I and the liver. *Liver Int,* 31, 911-9.

BOSSELUT, N., HOUSSET, C., MARCELO, P., REY, C., BURMESTER, T., VINH, J., VAUBOURDOLLE, M., CADORET, A. & BAUDIN, B. 2010. Distinct proteomic features of two fibrogenic liver cell populations: hepatic stellate cells and portal myofibroblasts. *Proteomics,* 10, 1017-28.

BOUHLEL, M. A., DERUDAS, B., RIGAMONTI, E., DIEVART, R., BROZEK, J., HAULON, S., ZAWADZKI, C., JUDE, B., TORPIER, G., MARX, N., STAELS, B. & CHINETTI-GBAGUIDI, G. 2007. PPARgamma activation primes human monocytes into alternative M2 macrophages with anti-inflammatory properties. *Cell Metab,* 6, 137-43.

BOURNAZOU, I., POUND, J. D., DUFFIN, R., BOURNAZOS, S., MELVILLE, L. A., BROWN, S. B., ROSSI, A. G. & GREGORY, C. D. 2009. Apoptotic human cells inhibit migration of granulocytes via release of lactoferrin. *J Clin Invest,* 119, 20-32.

BOUWENS, L., BAEKELAND, M., DE ZANGER, R. & WISSE, E. 1986. Quantitation, tissue distribution and proliferation kinetics of Kupffer cells in normal rat liver. *Hepatology,* 6, 718-22.

BREITKOPF, K., SAWITZA, I., WESTHOFF, J. H., WICKERT, L., DOOLEY, S. & GRESSNER, A. M. 2005. Thrombospondin 1 acts as a strong promoter of transforming growth factor beta effects via two distinct mechanisms in hepatic stellate cells. *Gut,* 54, 673-81.

BRILLA, C. G., FUNCK, R. C. & RUPP, H. 2000. Lisinopril-mediated regression of myocardial fibrosis in patients with hypertensive heart disease. *Circulation,* 102, 1388-93.

BU, H. F., ZUO, X. L., WANG, X., ENSSLIN, M. A., KOTI, V., HSUEH, W., RAYMOND, A. S., SHUR, B. D. & TAN, X. D. 2007. Milk fat globule-EGF factor 8/lactadherin plays a crucial role in maintenance and repair of murine intestinal epithelium. *J Clin Invest,* 117, 3673-83.

BYSTROM, J., EVANS, I., NEWSON, J., STABLES, M., TOOR, I., VAN ROOIJEN, N., CRAWFORD, M., COLVILLE-NASH, P., FARROW, S. & GILROY, D. W. 2008. Resolution-phase macrophages possess a unique inflammatory phenotype that is controlled by cAMP. *Blood,* 112, 4117-27.

CAILHIER, J. F., PARTOLINA, M., VUTHOORI, S., WU, S., KO, K., WATSON, S., SAVILL, J., HUGHES, J. & LANG, R. A. 2005. Conditional macrophage ablation demonstrates that resident macrophages initiate acute peritoneal inflammation. *J Immunol,* 174, 2336-42.

CASTANO, A. P., LIN, S. L., SUROWY, T., NOWLIN, B. T., TURLAPATI, S. A., PATEL, T., SINGH, A., LI, S., LUPHER, M. L., JR. & DUFFIELD, J. S. 2009. Serum amyloid P inhibits fibrosis through Fc gamma R-dependent monocyte-macrophage regulation in vivo. *Sci Transl Med,* 1, 5ra13.

CASTRILLO, A. & TONTONOZ, P. 2004. Nuclear receptors in macrophage biology: at the crossroads of lipid metabolism and inflammation. *Annu Rev Cell Dev Biol,* 20, 455-80.

CHAN, M. F., LI, J., BERTRAND, A., CASBON, A. J., LIN, J. H., MALTSEVA, I. & WERB, Z. 2013. Protective effects of matrix metalloproteinase-12 following corneal injury. *J Cell Sci*.

CHANG, H. I. & YEH, M. K. 2012. Clinical development of liposome-based drugs: formulation, characterization, and therapeutic efficacy. *Int J Nanomedicine,* 7, 49-60.

CHEN, H., HE, Y. W., LIU, W. Q. & ZHANG, J. H. 2008. Rosiglitazone prevents murine hepatic fibrosis induced by Schistosoma japonicum. *World J Gastroenterol,* 14, 2905-11.

CHEONG, C., MATOS, I., CHOI, J. H., DANDAMUDI, D. B., SHRESTHA, E., LONGHI, M. P., JEFFREY, K. L., ANTHONY, R. M., KLUGER, C., NCHINDA, G., KOH, H., RODRIGUEZ, A., IDOYAGA, J., PACK, M., VELINZON, K., PARK, C. G. & STEINMAN, R. M. 2010. Microbial stimulation fully differentiates monocytes to DC-SIGN/CD209(+) dendritic cells for immune T cell areas. *Cell,* 143, 416-29.

CHI, H., BARRY, S. P., ROTH, R. J., WU, J. J., JONES, E. A., BENNETT, A. M. & FLAVELL, R. A. 2006. Dynamic regulation of pro- and anti-inflammatory cytokines by MAPK phosphatase 1 (MKP-1) in innate immune responses. *Proc Natl Acad Sci U S A,* 103, 2274-9.

CHOW, A., BROWN, B. & MERAD, M. 2011. Studying the mononuclear phagocyte system in the molecular age. *Nature reviews. Immunology,* 11.

CHUNG, E. Y., LIU, J., HOMMA, Y., ZHANG, Y., BRENDOLAN, A., SAGGESE, M., HAN, J., SILVERSTEIN, R., SELLERI, L. & MA, X. 2007. Interleukin-10 expression in macrophages during phagocytosis of apoptotic cells is mediated by homeodomain proteins Pbx1 and Prep-1. *Immunity,* 27, 952-64.

COLNOT, S. & PERRET, C. 2011. Liver Zonation. *In:* MONGA, S. P. S. (ed.) *Molecular Pathology of Liver Diseases.* Springer US.

CONCHILLO, M., DE KNEGT, R. J., PAYERAS, M., QUIROGA, J., SANGRO, B., HERRERO, J. I., CASTILLA-CORTAZAR, I., FRYSTYK, J., FLYVBJERG, A., YOSHIZAWA, C., JANSEN, P. L., SCHARSCHMIDT, B. & PRIETO, J. 2005. Insulin-like growth factor I (IGF-I) replacement therapy increases albumin concentration in liver cirrhosis: results of a pilot randomized controlled clinical trial. *J Hepatol,* 43, 630-6.

CONWAY, B. & HUGHES, J. 2012. Cellular orchestrators of renal fibrosis. *QJM,* 105, 611-5.

CORTEZ-RETAMOZO, V., SWIRSKI, F. K., WATERMAN, P., YUAN, H., FIGUEIREDO, J. L., NEWTON, A. P., UPADHYAY, R., VINEGONI, C., KOHLER, R., BLOIS, J., SMITH, A., NAHRENDORF, M., JOSEPHSON, L., WEISSLEDER, R. & PITTET, M. J. 2008. Real-

time assessment of inflammation and treatment response in a mouse model of allergic airway inflammation. *J Clin Invest,* 118, 4058-66.

CRAWFORD, S. E., STELLMACH, V., MURPHY-ULLRICH, J. E., RIBEIRO, S. M., LAWLER, J., HYNES, R. O., BOIVIN, G. P. & BOUCK, N. 1998. Thrombospondin-1 is a major activator of TGF-beta1 in vivo. *Cell,* 93, 1159-70.

CROFTON, R. W., DIESSELHOFF-DEN DULK, M. M. & VAN FURTH, R. 1978. The origin, kinetics, and characteristics of the Kupffer cells in the normal steady state. *J Exp Med,* 148, 1-17.

DAI, X. M., RYAN, G. R., HAPEL, A. J., DOMINGUEZ, M. G., RUSSELL, R. G., KAPP, S., SYLVESTRE, V. & STANLEY, E. R. 2002. Targeted disruption of the mouse colony-stimulating factor 1 receptor gene results in osteopetrosis, mononuclear phagocyte deficiency, increased primitive progenitor cell frequencies, and reproductive defects. *Blood,* 99, 111-20.

DEAN, R. A., COX, J. H., BELLAC, C. L., DOUCET, A., STARR, A. E. & OVERALL, C. M. 2008. Macrophage-specific metalloelastase (MMP-12) truncates and inactivates ELR+ CXC chemokines and generates CCL2, -7, -8, and -13 antagonists: potential role of the macrophage in terminating polymorphonuclear leukocyte influx. *Blood,* 112, 3455-64.

DENNIS, G., JR., SHERMAN, B. T., HOSACK, D. A., YANG, J., GAO, W., LANE, H. C. & LEMPICKI, R. A. 2003. DAVID: Database for Annotation, Visualization, and Integrated Discovery. *Genome Biol,* 4, P3.

DESBOIS-MOUTHON, C., WENDUM, D., CADORET, A., REY, C., LENEUVE, P., BLAISE, A., HOUSSET, C., TRONCHE, F., LE BOUC, Y. & HOLZENBERGER, M. 2006. Hepatocyte proliferation during liver regeneration is impaired in mice with liver-specific IGF-1R knockout. *FASEB J,* 20, 773-5.

DEVEY, L., FERENBACH, D., MOHR, E., SANGSTER, K., BELLAMY, C. O., HUGHES, J. & WIGMORE, S. J. 2009. Tissue-resident macrophages protect the liver from ischemia reperfusion injury via a heme oxygenase-1-dependent mechanism. *Mol Ther,* 17, 65-72.

DEVITT, A. & MARSHALL, L. J. 2011. The innate immune system and the clearance of apoptotic cells. *J Leukoc Biol,* 90, 447-57.

DIENSTAG, J. L., GOLDIN, R. D., HEATHCOTE, E. J., HANN, H. W., WOESSNER, M., STEPHENSON, S. L., GARDNER, S., GRAY, D. F. & SCHIFF, E. R. 2003. Histological outcome during long-term lamivudine therapy. *Gastroenterology,* 124, 105-17.

DIEZ, J., QUEREJETA, R., LOPEZ, B., GONZALEZ, A., LARMAN, M. & MARTINEZ UBAGO, J. L. 2002. Losartan-dependent regression of myocardial fibrosis is associated with reduction of left ventricular chamber stiffness in hypertensive patients. *Circulation,* 105, 2512-7.

DIXON, J. B., BHATHAL, P. S. & O'BRIEN, P. E. 2006. Weight loss and non-alcoholic fatty liver disease: falls in gamma-glutamyl transferase concentrations are associated with histologic improvement. *Obes Surg,* 16, 1278-86.

DUFFIELD, J. S., FORBES, S. J., CONSTANDINOU, C. M., CLAY, S., PARTOLINA, M., VUTHOORI, S., WU, S., LANG, R. & IREDALE, J. P. 2005. Selective depletion of macrophages reveals distinct, opposing roles during liver injury and repair. *J Clin Invest,* 115, 56-65.

DUFOUR, J. F., DELELLIS, R. & KAPLAN, M. M. 1997. Reversibility of hepatic fibrosis in autoimmune hepatitis. *Ann Intern Med,* 127, 981-5.

EL-YOUSSEF, M., MU, Y., HUANG, L., STELLMACH, V. & CRAWFORD, S. E. 1999. Increased expression of transforming growth factor-beta1 and thrombospondin-1 in

congenital hepatic fibrosis: possible role of the hepatic stellate cell. *J Pediatr Gastroenterol Nutr,* 28, 386-92.

ELPEK, G. O., GOKHAN, G. A. & BOZOVA, S. 2008. Thrombospondin-1 expression correlates with angiogenesis in experimental cirrhosis. *World J Gastroenterol,* 14, 2213-7.

ELSHARKAWY, A. M., OAKLEY, F. & MANN, D. A. 2005. The role and regulation of hepatic stellate cell apoptosis in reversal of liver fibrosis. *Apoptosis,* 10, 927-939.

ERWIG, L. P. & HENSON, P. M. 2007. Immunological consequences of apoptotic cell phagocytosis. *Am J Pathol,* 171, 2-8.

FALIZE, L., GUILLYGOMARC'H, A., PERRIN, M., LAINE, F., GUYADER, D., BRISSOT, P., TURLIN, B. & DEUGNIER, Y. 2006. Reversibility of hepatic fibrosis in treated genetic hemochromatosis: a study of 36 cases. *Hepatology,* 44, 472-7.

FALLOWFIELD, J. A., MIZUNO, M., KENDALL, T. J., CONSTANDINOU, C. M., BENYON, R. C., DUFFIELD, J. S. & IREDALE, J. P. 2007. Scar-associated macrophages are a major source of hepatic matrix metalloproteinase-13 and facilitate the resolution of murine hepatic fibrosis. *J Immunol,* 178, 5288-95.

FERENBACH, D. A., RAMDAS, V., SPENCER, N., MARSON, L., ANEGON, I., HUGHES, J. & KLUTH, D. C. 2010. Macrophages expressing heme oxygenase-1 improve renal function in ischemia/reperfusion injury. *Mol Ther,* 18, 1706-13.

FIORETTO, P., STEFFES, M. W., SUTHERLAND, D. E., GOETZ, F. C. & MAUER, M. 1998. Reversal of lesions of diabetic nephropathy after pancreas transplantation. *N Engl J Med,* 339, 69-75.

FISCHER, R., CARIERS, A., REINEHR, R. & HAUSSINGER, D. 2002. Caspase 9-dependent killing of hepatic stellate cells by activated Kupffer cells. *Gastroenterology,* 123, 845-61.

FORBES, S. J., RUSSO, F. P., REY, V., BURRA, P., RUGGE, M., WRIGHT, N. A. & ALISON, M. R. 2004. A significant proportion of myofibroblasts are of bone marrow origin in human liver fibrosis. *Gastroenterology,* 126, 955-63.

FRANCESCHINI, B., RUSSO, C., DIOGUARDI, N. & GRIZZI, F. 2007. Increased liver mast cell recruitment in patients with chronic C virus-related hepatitis and histologically documented steatosis. *J Viral Hepat,* 14, 549-55.

FRIEDMAN, S. L. 2000. Molecular regulation of hepatic fibrosis, an integrated cellular response to tissue injury. *J Biol Chem,* 275, 2247-50.

FRIEDMAN, S. L. 2005. Mac the knife? Macrophages- the double-edged sword of hepatic fibrosis. *J Clin Invest,* 115, 29-32.

FRIEDMAN, S. L. 2008. Hepatic stellate cells: protean, multifunctional, and enigmatic cells of the liver. *Physiol Rev,* 88, 125-72.

FRIEDMAN, S. L. & ARTHUR, M. J. 1989. Activation of cultured rat hepatic lipocytes by Kupffer cell conditioned medium. Direct enhancement of matrix synthesis and stimulation of cell proliferation via induction of platelet-derived growth factor receptors. *J Clin Invest,* 84, 1780-5.

FRIEDMAN, S. L., ROCKEY, D. C., MCGUIRE, R. F., MAHER, J. J., BOYLES, J. K. & YAMASAKI, G. 1992. ISOLATED HEPATIC LIPOCYTES AND KUPFFER CELLS FROM NORMAL HUMAN LIVER - MORPHOLOGICAL AND FUNCTIONAL-CHARACTERISTICS IN PRIMARY CULTURE. *Hepatology,* 15, 234-243.

FRIEDMAN, S. L., ROLL, F. J., BOYLES, J. & BISSELL, D. M. 1985. Hepatic lipocytes: the principal collagen-producing cells of normal rat liver. *Proc Natl Acad Sci U S A,* 82, 8681-5.

GAO, B. & RADAEVA, S. 2012. Natural killer and natural killer T cells in liver fibrosis. *Biochim Biophys Acta*.

GARCIA-TSAO, G., FRIEDMAN, S., IREDALE, J. & PINZANI, M. 2010. Now there are many (stages) where before there was one: In search of a pathophysiological classification of cirrhosis. *Hepatology,* 51, 1445-9.

GAUTIER, E. L., CHOW, A., SPANBROEK, R., MARCELIN, G., GRETER, M., JAKUBZICK, C., BOGUNOVIC, M., LEBOEUF, M., VAN ROOIJEN, N., HABENICHT, A. J., MERAD, M. & RANDOLPH, G. J. 2012. Systemic Analysis of PPARgamma in Mouse Macrophage Populations Reveals Marked Diversity in Expression with Critical Roles in Resolution of Inflammation and Airway Immunity. *J Immunol,* 189, 2614-24.

GEISSMANN, F., AUFFRAY, C., PALFRAMAN, R., WIRRIG, C., CIOCCA, A., CAMPISI, L., NARNI-MANCINELLI, E. & LAUVAU, G. 2008. Blood monocytes: distinct subsets, how they relate to dendritic cells, and their possible roles in the regulation of T-cell responses. *Immunol Cell Biol,* 86, 398-408.

GEISSMANN, F., MANZ, M. G., JUNG, S., SIEWEKE, M. H., MERAD, M. & LEY, K. 2010. Development of monocytes, macrophages, and dendritic cells. *Science,* 327, 656-61.

GENOVESE, T., CUZZOCREA, S., DI PAOLA, R., MAZZON, E., MASTRUZZO, C., CATALANO, P., SORTINO, M., CRIMI, N., CAPUTI, A. P., THIEMERMANN, C. & VANCHERI, C. 2005. Effect of rosiglitazone and 15-deoxy-Delta12,14-prostaglandin J2 on bleomycin-induced lung injury. *Eur Respir J,* 25, 225-34.

GENTLEMAN, R. C., CAREY, V. J., BATES, D. M., BOLSTAD, B., DETTLING, M., DUDOIT, S., ELLIS, B., GAUTIER, L., GE, Y., GENTRY, J., HORNIK, K., HOTHORN, T., HUBER, W., IACUS, S., IRIZARRY, R., LEISCH, F., LI, C., MAECHLER, M., ROSSINI, A. J., SAWITZKI, G., SMITH, C., SMYTH, G., TIERNEY, L., YANG, J. Y. & ZHANG, J. 2004. Bioconductor: open software development for computational biology and bioinformatics. *Genome Biol,* 5, R80.

GETTS, D. R., TERRY, R. L., GETTS, M. T., MULLER, M., RANA, S., SHRESTHA, B., RADFORD, J., VAN ROOIJEN, N., CAMPBELL, I. L. & KING, N. J. 2008. Ly6c+ "inflammatory monocytes" are microglial precursors recruited in a pathogenic manner in West Nile virus encephalitis. *J Exp Med,* 205, 2319-37.

GIBBONS, M. A., MACKINNON, A. C., RAMACHANDRAN, P., DHALIWAL, K., DUFFIN, R., PHYTHIAN-ADAMS, A. T., VAN ROOIJEN, N., HASLETT, C., HOWIE, S. E., SIMPSON, A. J., HIRANI, N., GAULDIE, J., IREDALE, J. P., SETHI, T. & FORBES, S. J. 2011. Ly6Chi Monocytes Direct Alternatively Activated Pro-fibrotic Macrophage Regulation of Lung Fibrosis. *Am J Respir Crit Care Med*.

GIELING, R. G., WALLACE, K. & HAN, Y. P. 2009. Interleukin-1 participates in the progression from liver injury to fibrosis. *Am J Physiol Gastrointest Liver Physiol,* 296, G1324-31.

GINHOUX, F., GRETER, M., LEBOEUF, M., NANDI, S., SEE, P., GOKHAN, S., MEHLER, M. F., CONWAY, S. J., NG, L. G., STANLEY, E. R., SAMOKHVALOV, I. M. & MERAD, M. 2010. Fate mapping analysis reveals that adult microglia derive from primitive macrophages. *Science,* 330, 841-5.

GORDON, S. 2003. Alternative activation of macrophages. *Nat Rev Immunol,* 3, 23-35.

GORDON, S. & TAYLOR, P. R. 2005. Monocyte and macrophage heterogeneity. *Nat Rev Immunol,* 5, 953-64.

GU, K., ZHAO, J. D., REN, Z. G., MA, N. Y., LAI, S. T., WANG, J., LIU, J. & JIANG, G. L. 2011. A natural process of cirrhosis resolution and deceleration of liver regeneration after thioacetamide withdrawal in a rat model. *Mol Biol Rep,* 38, 1687-96.

HAMMEL, P., COUVELARD, A., O'TOOLE, D., RATOUIS, A., SAUVANET, A., FLEJOU, J. F., DEGOTT, C., BELGHITI, J., BERNADES, P., VALLA, D., RUSZNIEWSKI, P. & LEVY, P. 2001. Regression of liver fibrosis after biliary drainage in patients with chronic pancreatitis and stenosis of the common bile duct. *N Engl J Med,* 344, 418-23.

HAREL-ADAR, T., BEN MORDECHAI, T., AMSALEM, Y., FEINBERG, M. S., LEOR, J. & COHEN, S. 2011. Modulation of cardiac macrophages by phosphatidylserine-presenting liposomes improves infarct repair. *Proc Natl Acad Sci U S A,* 108, 1827-32.

HARTY, M. W., MURATORE, C. S., PAPA, E. F., GART, M. S., RAMM, G. A., GREGORY, S. H. & TRACY, T. F., JR. 2010. Neutrophil depletion blocks early collagen degradation in repairing cholestatic rat livers. *Am J Pathol,* 176, 1271-81.

HARTY, M. W., PAPA, E. F., HUDDLESTON, H. M., YOUNG, E., NAZARETH, S., RILEY, C. A., RAMM, G. A., GREGORY, S. H. & TRACY, T. F., JR. 2008. Hepatic macrophages promote the neutrophil-dependent resolution of fibrosis in repairing cholestatic rat livers. *Surgery,* 143, 667-78.

HASEGAWA-MORIYAMA, M., OHNOU, T., GODAI, K., KURIMOTO, T., NAKAMA, M. & KANMURA, Y. 2012. Peroxisome proliferator-activated receptor-gamma agonist rosiglitazone attenuates postincisional pain by regulating macrophage polarization. *Biochem Biophys Res Commun,* 426, 76-82.

HASHIMOTO, D., MILLER, J. & MERAD, M. 2011. Dendritic cell and macrophage heterogeneity in vivo. *Immunity,* 35, 323-35.

HAYASHIDANI, S., TSUTSUI, H., SHIOMI, T., IKEUCHI, M., MATSUSAKA, H., SUEMATSU, N., WEN, J., EGASHIRA, K. & TAKESHITA, A. 2003. Anti-monocyte chemoattractant protein-1 gene therapy attenuates left ventricular remodeling and failure after experimental myocardial infarction. *Circulation,* 108, 2134-40.

HAYDEN, T. 2011. Scarred by disease. *Nat Med,* 17, 18-20.

HEINRICHS, D., KNAUEL, M., OFFERMANNS, C., BERRES, M.-L., NELLEN, A., LENG, L., SCHMITZ, P., BUCALA, R., TRAUTWEIN, C., WEBER, C., BERNHAGEN, J. & WASMUTH, H. 2011. Macrophage migration inhibitory factor (MIF) exerts antifibrotic effects in experimental liver fibrosis via CD74. *Proceedings of the National Academy of Sciences of the United States of America,* 108, 17444-17453.

HEMMANN, S., GRAF, J., RODERFELD, M. & ROEB, E. 2007. Expression of MMPs and TIMPs in liver fibrosis - a systematic review with special emphasis on anti-fibrotic strategies. *J Hepatol,* 46, 955-75.

HENDERSON, N. C., MACKINNON, A. C., FARNWORTH, S. L., KIPARI, T., HASLETT, C., IREDALE, J. P., LIU, F. T., HUGHES, J. & SETHI, T. 2008. Galectin-3 expression and secretion links macrophages to the promotion of renal fibrosis. *Am J Pathol,* 172, 288-98.

HENDERSON, N. C., MACKINNON, A. C., FARNWORTH, S. L., POIRIER, F., RUSSO, F. P., IREDALE, J. P., HASLETT, C., SIMPSON, K. J. & SETHI, T. 2006. Galectin-3 regulates myofibroblast activation and hepatic fibrosis. *Proc Natl Acad Sci U S A,* 103, 5060-5.

HENSON, P. M. 2005. Dampening inflammation. *Nat Immunol,* 6, 1179-81.

HERNANDEZ-GEA, V. & FRIEDMAN, S. L. 2011. Pathogenesis of liver fibrosis. *Annu Rev Pathol,* 6, 425-56.

HIGASHI, K., ODA, T., KUSHIYAMA, T., HYODO, T., YAMADA, M., SUZUKI, S., SAKURAI, Y., MIURA, S. & KUMAGAI, H. Additive antifibrotic effects of pioglitazone and candesartan on experimental renal fibrosis in mice. *Nephrology (Carlton),* 15, 327-35.

HINTERMANN, E., BAYER, M., PFEILSCHIFTER, J. M., LUSTER, A. D. & CHRISTEN, U. 2010. CXCL10 promotes liver fibrosis by prevention of NK cell mediated hepatic stellate cell inactivation. *J Autoimmun,* 35, 424-35.

HOCHREITER-HUFFORD, A. & RAVICHANDRAN, K. S. 2013. Clearing the dead: apoptotic cell sensing, recognition, engulfment, and digestion. *Cold Spring Harb Perspect Biol,* 5, a008748.

HOLT, M. P., CHENG, L. & JU, C. 2008. Identification and characterization of infiltrating macrophages in acetaminophen-induced liver injury. *J Leukoc Biol,* 84, 1410-21.

HU, B., PUNTURIERI, A., TODT, J., SONSTEIN, J., POLAK, T. & CURTIS, J. L. 2002. Recognition and phagocytosis of apoptotic T cells by resident murine tissue macrophages require multiple signal transduction events. *J Leukoc Biol,* 71, 881-9.

HUANG DA, W., SHERMAN, B. T. & LEMPICKI, R. A. 2009a. Bioinformatics enrichment tools: paths toward the comprehensive functional analysis of large gene lists. *Nucleic Acids Res,* 37, 1-13.

HUANG DA, W., SHERMAN, B. T. & LEMPICKI, R. A. 2009b. Systematic and integrative analysis of large gene lists using DAVID bioinformatics resources. *Nat Protoc,* 4, 44-57.

HUME, D. A. 2008. Macrophages as APC and the dendritic cell myth. *J Immunol,* 181, 5829-35.

HUNG, K. S., LEE, T. H., CHOU, W. Y., WU, C. L., CHO, C. L., LU, C. N., JAWAN, B. & WANG, C. H. 2005. Interleukin-10 gene therapy reverses thioacetamide-induced liver fibrosis in mice. *Biochem Biophys Res Commun,* 336, 324-31.

HUYNH, M. L., FADOK, V. A. & HENSON, P. M. 2002. Phosphatidylserine-dependent ingestion of apoptotic cells promotes TGF-beta1 secretion and the resolution of inflammation. *J Clin Invest,* 109, 41-50.

IDE, M., KUWAMURA, M., KOTANI, T., SAWAMOTO, O. & YAMATE, J. 2005. Effects of gadolinium chloride (GdCl(3)) on the appearance of macrophage populations and fibrogenesis in thioacetamide-induced rat hepatic lesions. *J Comp Pathol,* 133, 92-102.

IHM, S. H., CHANG, K., KIM, H. Y., BAEK, S. H., YOUN, H. J., SEUNG, K. B. & KIM, J. H. Peroxisome proliferator-activated receptor-gamma activation attenuates cardiac fibrosis in type 2 diabetic rats: the effect of rosiglitazone on myocardial expression of receptor for advanced glycation end products and of connective tissue growth factor. *Basic Res Cardiol,* 105, 399-407.

IKEGAMI, T., ZHANG, Y. & MATSUZAKI, Y. 2007. Liver fibrosis: possible involvement of EMT. *Cells Tissues Organs,* 185, 213-21.

IMAMURA, M., OGAWA, T., SASAGURI, Y., CHAYAMA, K. & UENO, H. 2005. Suppression of macrophage infiltration inhibits activation of hepatic stellate cells and liver fibrogenesis in rats. *Gastroenterology,* 128, 138-46.

INGERSOLL, M. A., PLATT, A. M., POTTEAUX, S. & RANDOLPH, G. J. 2011. Monocyte trafficking in acute and chronic inflammation. *Trends Immunol,* 32, 470-7.

INGERSOLL, M. A., SPANBROEK, R., LOTTAZ, C., GAUTIER, E. L., FRANKENBERGER, M., HOFFMANN, R., LANG, R., HANIFFA, M., COLLIN, M., TACKE, F., HABENICHT, A. J., ZIEGLER-HEITBROCK, L. & RANDOLPH, G. J. 2009. Comparison of gene expression profiles between human and mouse monocyte subsets. *Blood,* 115, e10-9.

INUZUKA, S., UENO, T. & TANIKAWA, K. 1994. Fibrogenesis in acute liver injuries. *Pathol Res Pract,* 190, 903-9.

IREDALE, J. 2008. Defining therapeutic targets for liver fibrosis: exploiting the biology of inflammation and repair. *Pharmacol Res,* 58, 129-36.

IREDALE, J. P. 2001. Hepatic stellate cell behavior during resolution of liver injury. *Semin Liver Dis,* 21, 427-36.

IREDALE, J. P. 2007. Models of liver fibrosis: exploring the dynamic nature of inflammation and repair in a solid organ. *J Clin Invest,* 117, 539-48.

IREDALE, J. P., BENYON, R. C., ARTHUR, M. J., FERRIS, W. F., ALCOLADO, R., WINWOOD, P. J., CLARK, N. & MURPHY, G. 1996. Tissue inhibitor of metalloproteinase-1 messenger

RNA expression is enhanced relative to interstitial collagenase messenger RNA in experimental liver injury and fibrosis. *Hepatology,* 24, 176-84.

IREDALE, J. P., BENYON, R. C., PICKERING, J., MCCULLEN, M., NORTHROP, M., PAWLEY, S., HOVELL, C. & ARTHUR, M. J. 1998. Mechanisms of spontaneous resolution of rat liver fibrosis. Hepatic stellate cell apoptosis and reduced hepatic expression of metalloproteinase inhibitors. *J Clin Invest,* 102, 538-49.

IREDALE, J. P., MURPHY, G., HEMBRY, R. M., FRIEDMAN, S. L. & ARTHUR, M. J. 1992. Human hepatic lipocytes synthesize tissue inhibitor of metalloproteinases-1. Implications for regulation of matrix degradation in liver. *J Clin Invest,* 90, 282-7.

ISSA, R., WILLIAMS, E., TRIM, N., KENDALL, T., ARTHUR, M. J., REICHEN, J., BENYON, R. C. & IREDALE, J. P. 2001. Apoptosis of hepatic stellate cells: involvement in resolution of biliary fibrosis and regulation by soluble growth factors. *Gut,* 48, 548-57.

ISSA, R., ZHOU, X., CONSTANDINOU, C. M., FALLOWFIELD, J., MILLWARD-SADLER, H., GACA, M. D., SANDS, E., SULIMAN, I., TRIM, N., KNORR, A., ARTHUR, M. J., BENYON, R. C. & IREDALE, J. P. 2004. Spontaneous recovery from micronodular cirrhosis: evidence for incomplete resolution associated with matrix cross-linking. *Gastroenterology,* 126, 1795-808.

ISSA, R., ZHOU, X., TRIM, N., MILLWARD-SADLER, H., KRANE, S., BENYON, C. & IREDALE, J. 2003. Mutation in collagen-1 that confers resistance to the action of collagenase results in failure of recovery from CCl4-induced liver fibrosis, persistence of activated hepatic stellate cells, and diminished hepatocyte regeneration. *FASEB J,* 17, 47-9.

JEHLE, A. W., GARDAI, S. J., LI, S., LINSEL-NITSCHKE, P., MORIMOTO, K., JANSSEN, W. J., VANDIVIER, R. W., WANG, N., GREENBERG, S., DALE, B. M., QIN, C., HENSON, P. M. & TALL, A. R. 2006. ATP-binding cassette transporter A7 enhances phagocytosis of apoptotic cells and associated ERK signaling in macrophages. *J Cell Biol,* 174, 547-56.

JENKINS, S. J., RUCKERL, D., COOK, P. C., JONES, L. H., FINKELMAN, F. D., VAN ROOIJEN, N., MACDONALD, A. S. & ALLEN, J. E. 2011. Local macrophage proliferation, rather than recruitment from the blood, is a signature of TH2 inflammation. *Science,* 332, 1284-8.

JEONG, D. H., JANG, J. J., LEE, S. J., LEE, J. H., LIM, I. K., LEE, M. J. & LEE, Y. S. 2001. Expression patterns of cell cycle-related proteins in a rat cirrhotic model induced by CCl4 or thioacetamide. *J Gastroenterol,* 36, 24-32.

JEONG, W. I., LEE, C. S., PARK, S. J., CHUNG, J. Y. & JEONG, K. S. 2002. Kinetics of macrophages, myofibroblasts and mast cells in carbon tetrachloride-induced rat liver cirrhosis. *Anticancer Res,* 22, 869-77.

JIAO, J., SASTRE, D., FIEL, M. I., LEE, U. E., GHIASSI-NEJAD, Z., GINHOUX, F., VIVIER, E., FRIEDMAN, S. L., MERAD, M. & ALOMAN, C. 2012. Dendritic cell regulation of carbon tetrachloride-induced murine liver fibrosis regression. *Hepatology,* 55, 244-55.

JOHANSEN, J. S., CHRISTOFFERSEN, P., MOLLER, S., PRICE, P. A., HENRIKSEN, J. H., GARBARSCH, C. & BENDTSEN, F. 2000. Serum YKL-40 is increased in patients with hepatic fibrosis. *J Hepatol,* 32, 911-20.

KAIMORI, A., POTTER, J., KAIMORI, J. Y., WANG, C., MEZEY, E. & KOTEISH, A. 2007. Transforming growth factor-beta1 induces an epithelial-to-mesenchymal transition state in mouse hepatocytes in vitro. *J Biol Chem,* 282, 22089-101.

KARLMARK, K., ZIMMERMANN, H., RODERBURG, C., GASSLER, N., WASMUTH, H., LUEDDE, T., TRAUTWEIN, C. & TACKE, F. 2010. The fractalkine receptor CX_3CR1 protects

against liver fibrosis by controlling differentiation and survival of infiltrating hepatic monocytes. *Hepatology (Baltimore, Md.),* 52, 1769-1851.

KARLMARK, K. R., WEISKIRCHEN, R., ZIMMERMANN, H. W., GASSLER, N., GINHOUX, F., WEBER, C., MERAD, M., LUEDDE, T., TRAUTWEIN, C. & TACKE, F. 2009. Hepatic recruitment of the inflammatory Gr1+ monocyte subset upon liver injury promotes hepatic fibrosis. *Hepatology,* 50, 261-74.

KENDALL, T. J., HENNEDIGE, S., AUCOTT, R. L., HARTLAND, S. N., VERNON, M. A., BENYON, R. C. & IREDALE, J. P. 2009. p75 Neurotrophin receptor signaling regulates hepatic myofibroblast proliferation and apoptosis in recovery from rodent liver fibrosis. *Hepatology,* 49, 901-10.

KINNMAN, N. & HOUSSET, C. 2002. Peribiliary myofibroblasts in biliary type liver fibrosis. *Front Biosci,* 7, d496-503.

KISS, E., POPOVIC, Z. V., BEDKE, J., ADAMS, J., BONROUHI, M., BABELOVA, A., SCHMIDT, C., EDENHOFER, F., ZSCHIEDRICH, I., DOMHAN, S., ABDOLLAHI, A., SCHAFER, L., GRETZ, N., PORUBSKY, S. & GRONE, H. J. Peroxisome proliferator-activated receptor (PPAR)gamma can inhibit chronic renal allograft damage. *Am J Pathol,* 176, 2150-62.

KISSELEVA, T. & BRENNER, D. A. 2012. The phenotypic fate and functional role for bone marrow-derived stem cells in liver fibrosis. *J Hepatol,* 56, 965-72.

KISSELEVA, T., CONG, M., PAIK, Y., SCHOLTEN, D., JIANG, C., BENNER, C., IWAISAKO, K., MOORE-MORRIS, T., SCOTT, B., TSUKAMOTO, H., EVANS, S. M., DILLMANN, W., GLASS, C. K. & BRENNER, D. A. 2012. Myofibroblasts revert to an inactive phenotype during regression of liver fibrosis. *Proc Natl Acad Sci U S A,* 109, 9448-53.

KISSELEVA, T., UCHINAMI, H., FEIRT, N., QUINTANA-BUSTAMANTE, O., SEGOVIA, J. C., SCHWABE, R. F. & BRENNER, D. A. 2006. Bone marrow-derived fibrocytes participate in pathogenesis of liver fibrosis. *J Hepatol,* 45, 429-38.

KNITTEL, T., KOBOLD, D., SAILE, B., GRUNDMANN, A., NEUBAUER, K., PISCAGLIA, F. & RAMADORI, G. 1999. Rat liver myofibroblasts and hepatic stellate cells: different cell populations of the fibroblast lineage with fibrogenic potential. *Gastroenterology,* 117, 1205-21.

KRIZHANOVSKY, V., YON, M., DICKINS, R. A., HEARN, S., SIMON, J., MIETHING, C., YEE, H., ZENDER, L. & LOWE, S. W. 2008. Senescence of activated stellate cells limits liver fibrosis. *Cell,* 134, 657-67.

KUBES, P. & MEHAL, W. Z. 2012. Sterile inflammation in the liver. *Gastroenterology,* 143, 1158-72.

KUNDU, A. K., NAGAOKA, M., CHOWDHURY, E. H., HIROSE, S., SASAGAWA, T. & AKAIKE, T. 2003. IGF-1 induces growth, survival and morphological change of primary hepatocytes on a galactose-bared polymer through both MAPK and beta-catenin pathways. *Cell Struct Funct,* 28, 255-63.

KUROSAKA, K., TAKAHASHI, M. & KOBAYASHI, Y. 2003. Activation of extracellular signal-regulated kinase 1/2 is involved in production of CXC-chemokine by macrophages during phagocytosis of late apoptotic cells. *Biochem Biophys Res Commun,* 306, 1070-4.

LANDSMAN, L., VAROL, C. & JUNG, S. 2007. Distinct differentiation potential of blood monocyte subsets in the lung. *J Immunol,* 178, 2000-7.

LAWRENCE, T. & NATOLI, G. 2011. Transcriptional regulation of macrophage polarization: enabling diversity with identity. *Nat Rev Immunol,* 11, 750-61.

LEASK, A. & ABRAHAM, D. J. 2004. TGF-beta signaling and the fibrotic response. *FASEB J,* 18, 816-27.

LEON, D. A. & MCCAMBRIDGE, J. 2006. Liver cirrhosis mortality rates in Britain from 1950 to 2002: an analysis of routine data. *Lancet,* 367, 52-6.

LI, C. Y. & BAEK, J. Y. 2002. Mastocytosis and fibrosis: role of cytokines. *Int Arch Allergy Immunol,* 127, 123-6.

LI, H., SORENSON, A. L., POCZOBUTT, J., AMIN, J., JOYAL, T., SULLIVAN, T., CROSSNO, J. T., JR., WEISER-EVANS, M. C. & NEMENOFF, R. A. 2011. Activation of PPARgamma in myeloid cells promotes lung cancer progression and metastasis. *PLoS One,* 6, e28133.

LIASKOU, E., ZIMMERMANN, H. W., LI, K. K., HTUN OO, Y., SURESH, S., STAMATAKI, Z., QURESHI, O., LALOR, P. F., SHAW, J., SYN, W. K., CURBISHLEY, S. M. & ADAMS, D. H. 2012. Monocyte subsets in human liver disease show distinct phenotypic and functional characteristics. *Hepatology*.

LIEBER, C. S. 2004. CYP2E1: from ASH to NASH. *Hepatol Res,* 28, 1-11.

LIM, A., MA, F., NIKOLIC-PATERSON, D., THOMAS, M., HURST, L. & TESCH, G. 2009. Antibody blockade of c-fms suppresses the progression of inflammation and injury in early diabetic nephropathy in obese db/db mice. *Diabetologia,* 52, 1669-1748.

LIN, S. L., CASTANO, A. P., NOWLIN, B. T., LUPHER, M. L., JR. & DUFFIELD, J. S. 2009. Bone marrow Ly6Chigh monocytes are selectively recruited to injured kidney and differentiate into functionally distinct populations. *J Immunol,* 183, 6733-43.

LIN, Y. F., DENG, M. C., TSENG, L. P., JIANG, P. R., JAN, T. R., HSIEH, F. I. & LIU, D. Z. 2011. Adjuvant effect of liposome in chicken result from induction of nitric oxide. *Biomed Mater,* 6, 015011.

LUCAS, T., WAISMAN, A., RANJAN, R., ROES, J., KRIEG, T., MULLER, W., ROERS, A. & EMING, S. A. 2010. Differential roles of macrophages in diverse phases of skin repair. *J Immunol,* 184, 3964-77.

MA, F., LIU, J., KITCHING, A., MANTHEY, C. & NIKOLIC-PATERSON, D. 2009. Targeting renal macrophage accumulation via c-fms kinase reduces tubular apoptosis but fails to modify progressive fibrosis in the obstructed rat kidney. *American journal of physiology. Renal physiology,* 296, 85.

MA, H. M., WU, Z. & NAKANISHI, H. 2011. Phosphatidylserine-containing liposomes suppress inflammatory bone loss by ameliorating the cytokine imbalance provoked by infiltrated macrophages. *Lab Invest,* 91, 921-31.

MACDONALD, K. P., PALMER, J. S., CRONAU, S., SEPPANEN, E., OLVER, S., RAFFELT, N. C., KUNS, R., PETTIT, A. R., CLOUSTON, A., WAINWRIGHT, B., BRANSTETTER, D., SMITH, J., PAXTON, R. J., CERRETTI, D. P., BONHAM, L., HILL, G. R. & HUME, D. A. 2010. An antibody against the colony-stimulating factor 1 receptor depletes the resident subset of monocytes and tissue- and tumor-associated macrophages but does not inhibit inflammation. *Blood,* 116, 3955-63.

MAHDAVIAN DELAVARY, B., VAN DER VEER, W. M., VAN EGMOND, M., NIESSEN, F. B. & BEELEN, R. H. 2011. Macrophages in skin injury and repair. *Immunobiology,* 216, 753-62.

MAHER, J. J., BISSELL, D. M., FRIEDMAN, S. L. & ROLL, F. J. 1988. COLLAGEN MEASURED IN PRIMARY CULTURES OF NORMAL RAT HEPATOCYTES DERIVES FROM LIPOCYTES WITHIN THE MONOLAYER. *Journal of Clinical Investigation,* 82, 450-459.

MAHER, J. J. & MCGUIRE, R. F. 1990. EXTRACELLULAR-MATRIX GENE-EXPRESSION INCREASES PREFERENTIALLY IN RAT LIPOCYTES AND SINUSOIDAL ENDOTHELIAL-CELLS DURING HEPATIC-FIBROSIS INVIVO. *Journal of Clinical Investigation,* 86, 1641-1648.

MANIBUSAN, M. K., ODIN, M. & EASTMOND, D. A. 2007. Postulated carbon tetrachloride mode of action: a review. *J Environ Sci Health C Environ Carcinog Ecotoxicol Rev,* 25, 185-209.

MANTOVANI, A., BISWAS, S. K., GALDIERO, M. R., SICA, A. & LOCATI, M. 2013. Macrophage plasticity and polarization in tissue repair and remodelling. *J Pathol,* 229, 176-85.

MANTOVANI, A., SICA, A., SOZZANI, S., ALLAVENA, P., VECCHI, A. & LOCATI, M. 2004. The chemokine system in diverse forms of macrophage activation and polarization. *Trends Immunol,* 25, 677-86.

MARCELLIN, P., GANE, E., BUTI, M., AFDHAL, N., SIEVERT, W., JACOBSON, I. M., WASHINGTON, M. K., GERMANIDIS, G., FLAHERTY, J. F., SCHALL, R. A., BORNSTEIN, J. D., KITRINOS, K. M., SUBRAMANIAN, G. M., MCHUTCHISON, J. G. & HEATHCOTE, E. J. 2013. Regression of cirrhosis during treatment with tenofovir disoproxil fumarate for chronic hepatitis B: a 5-year open-label follow-up study. *Lancet,* 381, 468-75.

MARIM, F. M., SILVEIRA, T. N., LIMA, D. S., JR. & ZAMBONI, D. S. 2010. A method for generation of bone marrow-derived macrophages from cryopreserved mouse bone marrow cells. *PLoS One,* 5, e15263.

MARRA, F. 1999. Hepatic stellate cells and the regulation of liver inflammation. *Journal of Hepatology,* 31, 1106-1119.

MARRA, F., EFSEN, E., ROMANELLI, R. G., CALIGIURI, A., PASTACALDI, S., BATIGNANI, G., BONACCHI, A., CAPORALE, R., LAFFI, G., PINZANI, M. & GENTILINI, P. 2000. Ligands of peroxisome proliferator-activated receptor gamma modulate profibrogenic and proinflammatory actions in hepatic stellate cells. *Gastroenterology,* 119, 466-78.

MCELROY, M. K. & PETERSON, M. R. 2011. Number of portal tract macrophages correlates with the modified hepatic activity index in chronic hepatitis C infection. *Ann Diagn Pathol,* 15, 103-7.

MEHAL, W. Z., IREDALE, J. & FRIEDMAN, S. L. 2011. Scraping fibrosis: expressway to the core of fibrosis. *Nat Med,* 17, 552-3.

MELHEM, A., MUHANNA, N., BISHARA, A., ALVAREZ, C. E., ILAN, Y., BISHARA, T., HORANI, A., NASSAR, M., FRIEDMAN, S. L. & SAFADI, R. 2006. Anti-fibrotic activity of NK cells in experimental liver injury through killing of activated HSC. *J Hepatol,* 45, 60-71.

MIRCESCU, M. M., LIPUMA, L., VAN ROOIJEN, N., PAMER, E. G. & HOHL, T. M. 2009. Essential role for neutrophils but not alveolar macrophages at early time points following Aspergillus fumigatus infection. *J Infect Dis,* 200, 647-56.

MITCHELL, C., COUTON, D., COUTY, J. P., ANSON, M., CRAIN, A. M., BIZET, V., RENIA, L., POL, S., MALLET, V. & GILGENKRANTZ, H. 2009. Dual role of CCR2 in the constitution and the resolution of liver fibrosis in mice. *Am J Pathol,* 174, 1766-75.

MORAN-SALVADOR, E., TITOS, E., RIUS, B., GONZALEZ-PERIZ, A., GARCIA-ALONSO, V., LOPEZ-VICARIO, C., MIQUEL, R., BARAK, Y., ARROYO, V. & CLARIA, J. 2013. Cell-specific PPARgamma deficiency establishes anti-inflammatory and anti-fibrogenic properties for this nuclear receptor in non-parenchymal liver cells. *J Hepatol*.

MOSSER, D. M. & EDWARDS, J. P. 2008. Exploring the full spectrum of macrophage activation. *Nat Rev Immunol,* 8, 958-69.

MOVAHEDI, K., LAOUI, D., GYSEMANS, C., BAETEN, M., STANGE, G., VAN DEN BOSSCHE, J., MACK, M., PIPELEERS, D., IN'T VELD, P., DE BAETSELIER, P. & VAN GINDERACHTER, J. A. 2010. Different tumor microenvironments contain functionally distinct subsets of macrophages derived from Ly6C(high) monocytes. *Cancer Res,* 70, 5728-39.

MUNGER, J. S., HUANG, X., KAWAKATSU, H., GRIFFITHS, M. J., DALTON, S. L., WU, J., PITTET, J. F., KAMINSKI, N., GARAT, C., MATTHAY, M. A., RIFKIN, D. B. & SHEPPARD, D.

1999. The integrin alpha v beta 6 binds and activates latent TGF beta 1: a mechanism for regulating pulmonary inflammation and fibrosis. *Cell,* 96, 319-28.

MURPHY-ULLRICH, J. E. & POCZATEK, M. 2000. Activation of latent TGF-beta by thrombospondin-1: mechanisms and physiology. *Cytokine Growth Factor Rev,* 11, 59-69.

MURPHY, F., WAUNG, J., COLLINS, J., ARTHUR, M. J., NAGASE, H., MANN, D., BENYON, R. C. & IREDALE, J. P. 2004. N-Cadherin cleavage during activated hepatic stellate cell apoptosis is inhibited by tissue inhibitor of metalloproteinase-1. *Comp Hepatol,* 3 Suppl 1, S8.

NAHRENDORF, M., SWIRSKI, F. K., AIKAWA, E., STANGENBERG, L., WURDINGER, T., FIGUEIREDO, J. L., LIBBY, P., WEISSLEDER, R. & PITTET, M. J. 2007. The healing myocardium sequentially mobilizes two monocyte subsets with divergent and complementary functions. *J Exp Med,* 204, 3037-47.

NODA, S., MASUMI, S., MORIYAMA, M., KANNAN, Y., OHTA, M., SUGANO, T. & YAMATE, J. 1996. Population of hepatic macrophages and response of perfused liver to platelet-activating factor during production of thioacetamide-induced cirrhosis in rats. *Hepatology,* 24, 412-8.

NOVOBRANTSEVA, T. I., MAJEAU, G. R., AMATUCCI, A., KOGAN, S., BRENNER, I., CASOLA, S., SHLOMCHIK, M. J., KOTELIANSKY, V., HOCHMAN, P. S. & IBRAGHIMOV, A. 2005. Attenuated liver fibrosis in the absence of B cells. *J Clin Invest,* 115, 3072-82.

O'CONNOR, R. A., LEECH, M. D., SUFFNER, J., HAMMERLING, G. J. & ANDERTON, S. M. 2010. Myelin-reactive, TGF-beta-induced regulatory T cells can be programmed to develop Th1-like effector function but remain less proinflammatory than myelin-reactive Th1 effectors and can suppress pathogenic T cell clonal expansion in vivo. *J Immunol,* 185, 7235-43.

OAKLEY, F., TRIM, N., CONSTANDINOU, C. M., YE, W., GRAY, A. M., FRANTZ, G., HILLAN, K., KENDALL, T., BENYON, R. C., MANN, D. A. & IREDALE, J. P. 2003. Hepatocytes express nerve growth factor during liver injury: evidence for paracrine regulation of hepatic stellate cell apoptosis. *Am J Pathol,* 163, 1849-58.

OKAZAKI, T., HIROTA, S., XU, Z. D., MAEYAMA, K., NAKAMA, A., KAWANO, S., HORI, M. & KITAMURA, Y. 1998. Increase of mast cells in the liver and lung may be associated with but not a cause of fibrosis: demonstration using mast cell-deficient Ws/Ws rats. *Lab Invest,* 78, 1431-8.

OSTERHOLZER, J. J., OLSZEWSKI, M. A., MURDOCK, B. J., CHEN, G. H., ERB-DOWNWARD, J. R., SUBBOTINA, N., BROWNING, K., LIN, Y., MOREY, R. E., DAYRIT, J. K., HOROWITZ, J. C., SIMON, R. H. & SISSON, T. H. 2013. Implicating Exudate Macrophages and Ly-6Chigh Monocytes in CCR2-Dependent Lung Fibrosis following Gene-Targeted Alveolar Injury. *J Immunol,* 190, 3447-57.

OSTERREICHER, C. H., PENZ-OSTERREICHER, M., GRIVENNIKOV, S. I., GUMA, M., KOLTSOVA, E. K., DATZ, C., SASIK, R., HARDIMAN, G., KARIN, M. & BRENNER, D. A. 2011. Fibroblast-specific protein 1 identifies an inflammatory subpopulation of macrophages in the liver. *Proc Natl Acad Sci U S A,* 108, 308-13.

OTTO, D. A. & VEECH, R. L. 1980. Isolation of a lipocyte-rich fraction from rat liver nonparenchymal cells. *Adv Exp Med Biol,* 132, 509-17.

PARES, A., CABALLERIA, J., BRUGUERA, M., TORRES, M. & RODES, J. 1986. Histological course of alcoholic hepatitis. Influence of abstinence, sex and extent of hepatic damage. *J Hepatol,* 2, 33-42.

PARSONS, C. J., BRADFORD, B. U., PAN, C. Q., CHEUNG, E., SCHAUER, M., KNORR, A., KREBS, B., KRAFT, S., ZAHN, S., BROCKS, B., FEIRT, N., MEI, B., CHO, M. S., RAMAMOORTHI, R., ROLDAN, G., NG, P., LUM, P., HIRTH-DIETRICH, C.,

TOMKINSON, A. & BRENNER, D. A. 2004. Antifibrotic effects of a tissue inhibitor of metalloproteinase-1 antibody on established liver fibrosis in rats. *Hepatology,* 40, 1106-15.

PATEL, K., GORDON, S. C., JACOBSON, I., HEZODE, C., OH, E., SMITH, K. M., PAWLOTSKY, J. M. & MCHUTCHISON, J. G. 2004. Evaluation of a panel of non-invasive serum markers to differentiate mild from moderate-to-advanced liver fibrosis in chronic hepatitis C patients. *Journal of Hepatology,* 41, 935-942.

PELLICORO, A., AUCOTT, R. L., RAMACHANDRAN, P., ROBSON, A. J., FALLOWFIELD, J. A., SNOWDON, V. K., HARTLAND, S. N., VERNON, M., DUFFIELD, J. S., BENYON, R. C., FORBES, S. J. & IREDALE, J. P. 2011. Elastin accumulation is regulated at the level of degradation by macrophage metalloelastase (MMP-12) during experimental liver fibrosis. *Hepatology*.

PEREZ TAMAYO, R. 1983. Is cirrhosis of the liver experimentally produced by CCl4 and adequate model of human cirrhosis? *Hepatology,* 3, 112-20.

PERRY, D. G. & MARTIN, W. J., 2ND 1995. Fluorescent liposomes as quantitative markers of phagocytosis by alveolar macrophages. *J Immunol Methods,* 181, 269-85.

PHYTHIAN-ADAMS, A. T., COOK, P. C., LUNDIE, R. J., JONES, L. H., SMITH, K. A., BARR, T. A., HOCHWELLER, K., ANDERTON, S. M., HAMMERLING, G. J., MAIZELS, R. M. & MACDONALD, A. S. 2010. CD11c depletion severely disrupts Th2 induction and development in vivo. *J Exp Med,* 207, 2089-96.

PINZANI, M. & ROMBOUTS, K. 2004. Liver fibrosis: from the bench to clinical targets. *Dig Liver Dis,* 36, 231-42.

PIZANO-MARTINEZ, O., YANEZ-SANCHEZ, I., ALATORRE-CARRANZA, P., MIRANDA-DIAZ, A., ORTIZ-LAZARENO, P. C., GARCIA-IGLESIAS, T., DANERI-NAVARRO, A., VAZQUEZ-DEL MERCADO, M., FAFUTIS-MORRIS, M. & DELGADO-RIZO, V. 2011. YKL-40 expression in CD14(+) liver cells in acute and chronic injury. *World J Gastroenterol,* 17, 3830-5.

POPOV, Y., SVERDLOV, D. Y., BHASKAR, K. R., SHARMA, A. K., MILLONIG, G., PATSENKER, E., KRAHENBUHL, S., KRAHENBUHL, L. & SCHUPPAN, D. 2010. Macrophage-mediated phagocytosis of apoptotic cholangiocytes contributes to reversal of experimental biliary fibrosis. *Am J Physiol Gastrointest Liver Physiol,* 298, G323-34.

POPOV, Y., SVERDLOV, D. Y., SHARMA, A. K., BHASKAR, K. R., LI, S., FREITAG, T. L., LEE, J., DIETERICH, W., MELINO, G. & SCHUPPAN, D. 2011. Tissue transglutaminase does not affect fibrotic matrix stability or regression of liver fibrosis in mice. *Gastroenterology,* 140, 1642-52.

POPPELMANN, M., BECKER, W. M. & PETERSEN, A. 2002. Combination of zymography and immunodetection to analyze proteins in complex culture supernatants. *Electrophoresis,* 23, 993-7.

POYNARD, T., MCHUTCHISON, J., MANNS, M., TREPO, C., LINDSAY, K., GOODMAN, Z., LING, M. H. & ALBRECHT, J. 2002. Impact of pegylated interferon alfa-2b and ribavirin on liver fibrosis in patients with chronic hepatitis C. *Gastroenterology,* 122, 1303-13.

PRADERE, J. P., KLUWE, J., DE MINICIS, S., JIAO, J. J., GWAK, G. Y., DAPITO, D. H., JANG, M. K., GUENTHER, N. D., MEDERACKE, I., FRIEDMAN, R., DRAGOMIR, A. C., ALOMAN, C. & SCHWABE, R. F. 2013. Hepatic macrophages but not dendritic cells contribute to liver fibrosis by promoting the survival of activated hepatic stellate cells. *Hepatology*.

QIAN, B. Z., LI, J., ZHANG, H., KITAMURA, T., ZHANG, J., CAMPION, L. R., KAISER, E. A., SNYDER, L. A. & POLLARD, J. W. 2011. CCL2 recruits inflammatory monocytes to facilitate breast-tumour metastasis. *Nature,* 475, 222-5.

RADAEVA, S., SUN, R., JARUGA, B., NGUYEN, V. T., TIAN, Z. & GAO, B. 2006. Natural killer cells ameliorate liver fibrosis by killing activated stellate cells in NKG2D-dependent and tumor necrosis factor-related apoptosis-inducing ligand-dependent manners. *Gastroenterology,* 130, 435-52.

RAMACHANDRAN, P. & IREDALE, J. P. 2009. Reversibility of liver fibrosis. *Ann Hepatol,* 8, 283-91.

RAMACHANDRAN, P. & IREDALE, J. P. 2012a. Liver fibrosis: a bidirectional model of fibrogenesis and resolution. *QJM,* 105, 813-7.

RAMACHANDRAN, P. & IREDALE, J. P. 2012b. Macrophages: central regulators of hepatic fibrogenesis and fibrosis resolution. *J Hepatol,* 56, 1417-9.

RAMACHANDRAN, P., PELLICORO, A., VERNON, M. A., BOULTER, L., AUCOTT, R. L., ALI, A., HARTLAND, S. N., SNOWDON, V. K., CAPPON, A., GORDON-WALKER, T. T., WILLIAMS, M. J., DUNBAR, D. R., MANNING, J. R., VAN ROOIJEN, N., FALLOWFIELD, J. A., FORBES, S. J. & IREDALE, J. P. 2012. Differential Ly-6C expression identifies the recruited macrophage phenotype, which orchestrates the regression of murine liver fibrosis. *Proc Natl Acad Sci U S A,* 109, E3186-95.

RAVICHANDRAN, K. S. & LORENZ, U. 2007. Engulfment of apoptotic cells: signals for a good meal. *Nat Rev Immunol,* 7, 964-74.

RAZA, S. L., NEHRING, L. C., SHAPIRO, S. D. & CORNELIUS, L. A. 2000. Proteinase-activated receptor-1 regulation of macrophage elastase (MMP-12) secretion by serine proteinases. *J Biol Chem,* 275, 41243-50.

RICARDO, S. D., VAN GOOR, H. & EDDY, A. A. 2008. Macrophage diversity in renal injury and repair. *J Clin Invest,* 118, 3522-30.

RICKARD, A. J., MORGAN, J., TESCH, G., FUNDER, J. W., FULLER, P. J. & YOUNG, M. J. 2009. Deletion of mineralocorticoid receptors from macrophages protects against deoxycorticosterone/salt-induced cardiac fibrosis and increased blood pressure. *Hypertension,* 54, 537-43.

RODERFELD, M., WEISKIRCHEN, R., WAGNER, S., BERRES, M. L., HENKEL, C., GROTZINGER, J., GRESSNER, A. M., MATERN, S. & ROEB, E. 2006. Inhibition of hepatic fibrogenesis by matrix metalloproteinase-9 mutants in mice. *FASEB J,* 20, 444-54.

ROEB, E., BEHRMANN, I., GROTZINGER, J., BREUER, B. & MATERN, S. 2000. An MMP-9 mutant without gelatinolytic activity as a novel TIMP-1-antagonist. *FASEB J,* 14, 1671-3.

ROGUE, A., LAMBERT, C., JOSSE, R., ANTHERIEU, S., SPIRE, C., CLAUDE, N. & GUILLOUZO, A. 2011. Comparative gene expression profiles induced by PPARgamma and PPARalpha/gamma agonists in human hepatocytes. *PLoS One,* 6, e18816.

ROJKIND, M. & MARTINEZ-PALOMO, A. 1976. Increase in type I and type III collagens in human alcoholic liver cirrhosis. *Proc Natl Acad Sci U S A,* 73, 539-43.

RUSSO, F. P., ALISON, M. R., BIGGER, B. W., AMOFAH, E., FLOROU, A., AMIN, F., BOU-GHARIOS, G., JEFFERY, R., IREDALE, J. P. & FORBES, S. J. 2006. The bone marrow functionally contributes to liver fibrosis. *Gastroenterology,* 130, 1807-21.

RYGIEL, K. A., ROBERTSON, H., MARSHALL, H. L., PEKALSKI, M., ZHAO, L., BOOTH, T. A., JONES, D. E., BURT, A. D. & KIRBY, J. A. 2008. Epithelial-mesenchymal transition contributes to portal tract fibrogenesis during human chronic liver disease. *Lab Invest,* 88, 112-23.

SAFADI, R., OHTA, M., ALVAREZ, C. E., FIEL, M. I., BANSAL, M., MEHAL, W. Z. & FRIEDMAN, S. L. 2004. Immune stimulation of hepatic fibrogenesis by CD8 cells and attenuation by transgenic interleukin-10 from hepatocytes. *Gastroenterology,* 127, 870-82.

SAHIN, H., TRAUTWEIN, C. & WASMUTH, H. E. 2010. Functional role of chemokines in liver disease models. *Nat Rev Gastroenterol Hepatol,* 7, 682-90.

SAITO, J. M., BOSTICK, M. K., CAMPE, C. B., XU, J. & MAHER, J. J. 2003. Infiltrating neutrophils in bile duct-ligated livers do not promote hepatic fibrosis. *Hepatol Res,* 25, 180-191.

SAKAIDA, I., HIRONAKA, K., TERAI, S. & OKITA, K. 2003. Gadolinium chloride reverses dimethylnitrosamine (DMN)-induced rat liver fibrosis with increased matrix metalloproteinases (MMPs) of Kupffer cells. *Life Sci,* 72, 943-59.

SALGUERO PALACIOS, R., RODERFELD, M., HEMMANN, S., RATH, T., ATANASOVA, S., TSCHUSCHNER, A., GRESSNER, O. A., WEISKIRCHEN, R., GRAF, J. & ROEB, E. 2008. Activation of hepatic stellate cells is associated with cytokine expression in thioacetamide-induced hepatic fibrosis in mice. *Lab Invest,* 88, 1192-203.

SANZ, S., PUCILOWSKA, J. B., LIU, S., RODRIGUEZ-ORTIGOSA, C. M., LUND, P. K., BRENNER, D. A., FULLER, C. R., SIMMONS, J. G., PARDO, A., MARTINEZ-CHANTAR, M. L., FAGIN, J. A. & PRIETO, J. 2005. Expression of insulin-like growth factor I by activated hepatic stellate cells reduces fibrogenesis and enhances regeneration after liver injury. *Gut,* 54, 134-41.

SARMA, N. J., TIRIVEEDHI, V., SUBRAMANIAN, V., SHENOY, S., CRIPPIN, J. S., CHAPMAN, W. C. & MOHANAKUMAR, T. 2012. Hepatitis C virus mediated changes in miRNA-449a modulates inflammatory biomarker YKL40 through components of the NOTCH signaling pathway. *PLoS One,* 7, e50826.

SAVILL, J., DRANSFIELD, I., GREGORY, C. & HASLETT, C. 2002. A blast from the past: clearance of apoptotic cells regulates immune responses. *Nat Rev Immunol,* 2, 965-75.

SAVILL, J., DRANSFIELD, I., HOGG, N. & HASLETT, C. 1990. Vitronectin receptor-mediated phagocytosis of cells undergoing apoptosis. *Nature,* 343, 170-3.

SERBINA, N. V., SALAZAR-MATHER, T. P., BIRON, C. A., KUZIEL, W. A. & PAMER, E. G. 2003. TNF/iNOS-producing dendritic cells mediate innate immune defense against bacterial infection. *Immunity,* 19, 59-70.

SERPAGGI, J., CARNOT, F., NALPAS, B., CANIONI, D., GUECHOT, J., LEBRAY, P., VALLET-PICHARD, A., FONTAINE, H., BEDOSSA, P. & POL, S. 2006. Direct and indirect evidence for the reversibility of cirrhosis. *Hum Pathol,* 37, 1519-26.

SHECHTER, R., LONDON, A., VAROL, C., RAPOSO, C., CUSIMANO, M., YOVEL, G., ROLLS, A., MACK, M., PLUCHINO, S., MARTINO, G., JUNG, S. & SCHWARTZ, M. 2009. Infiltrating blood-derived macrophages are vital cells playing an anti-inflammatory role in recovery from spinal cord injury in mice. *PLoS Med,* 6, e1000113.

SHI, J., AISAKI, K., IKAWA, Y. & WAKE, K. 1998. Evidence of hepatocyte apoptosis in rat liver after the administration of carbon tetrachloride. *Am J Pathol,* 153, 515-25.

SHI, Z., WAKIL, A. E. & ROCKEY, D. C. 1997. Strain-specific differences in mouse hepatic wound healing are mediated by divergent T helper cytokine responses. *Proc Natl Acad Sci U S A,* 94, 10663-8.

SHIKATA, T. & SKAI, T. 1974. Elastogenesis in the liver. *Acta Pathol Jpn,* 24, 21-31.

SHIN, D. M., YANG, C. S., YUK, J. M., LEE, J. Y., KIM, K. H., SHIN, S. J., TAKAHARA, K., LEE, S. J. & JO, E. K. 2008. Mycobacterium abscessus activates the macrophage innate immune response via a physical and functional interaction between TLR2 and dectin-1. *Cell Microbiol,* 10, 1608-21.

SILLER-LOPEZ, F., SANDOVAL, A., SALGADO, S., SALAZAR, A., BUENO, M., GARCIA, J., VERA, J., GALVEZ, J., HERNANDEZ, I., RAMOS, M., AGUILAR-CORDOVA, E. & ARMENDARIZ-BORUNDA, J. 2004. Treatment with human metalloproteinase-8

gene delivery ameliorates experimental rat liver cirrhosis. *Gastroenterology,* 126, 1122-33; discussion 949.

SMYTH, G. K. 2004. Linear models and empirical bayes methods for assessing differential expression in microarray experiments. *Stat Appl Genet Mol Biol,* 3, Article3.

SOBREVALS, L., RODRIGUEZ, C., ROMERO-TREVEJO, J. L., GONDI, G., MONREAL, I., PANEDA, A., JUANARENA, N., ARCELUS, S., RAZQUIN, N., GUEMBE, L., GONZALEZ-ASEGUINOLAZA, G., PRIETO, J. & FORTES, P. 2010. Insulin-like growth factor I gene transfer to cirrhotic liver induces fibrolysis and reduces fibrogenesis leading to cirrhosis reversion in rats. *Hepatology,* 51, 912-21.

SOUZA-TARLA, C. D., UZUELLI, J. A., MACHADO, A. A., GERLACH, R. F. & TANUS-SANTOS, J. E. 2005. Methodological issues affecting the determination of plasma matrix metalloproteinase (MMP)-2 and MMP-9 activities. *Clin Biochem,* 38, 410-4.

STABLES, M. J., SHAH, S., CAMON, E. B., LOVERING, R. C., NEWSON, J., BYSTROM, J., FARROW, S. & GILROY, D. W. 2011. Transcriptomic analyses of murine resolution-phase macrophages. *Blood,* 118, e192-208.

STIENSTRA, R., DUVAL, C., KESHTKAR, S., VAN DER LAAK, J., KERSTEN, S. & MULLER, M. 2008. Peroxisome proliferator-activated receptor gamma activation promotes infiltration of alternatively activated macrophages into adipose tissue. *J Biol Chem,* 283, 22620-7.

STONEMAN, V., BRAGANZA, D., FIGG, N., MERCER, J., LANG, R., GODDARD, M. & BENNETT, M. 2007. Monocyte/macrophage suppression in CD11b diphtheria toxin receptor transgenic mice differentially affects atherogenesis and established plaques. *Circ Res,* 100, 884-93.

STOUT, R. D., JIANG, C., MATTA, B., TIETZEL, I., WATKINS, S. K. & SUTTLES, J. 2005. Macrophages sequentially change their functional phenotype in response to changes in microenvironmental influences. *J Immunol,* 175, 342-9.

SUGIHARA, A., TSUJIMURA, T., FUJITA, Y., NAKATA, Y. & TERADA, N. 1999. Evaluation of role of mast cells in the development of liver fibrosis using mast cell-deficient rats and mice. *J Hepatol,* 30, 859-67.

SUNAMI, Y., LEITHAUSER, F., GUL, S., FIEDLER, K., GULDIKEN, N., ESPENLAUB, S., HOLZMANN, K. H., HIPP, N., SINDRILARU, A., LUEDDE, T., BAUMANN, B., WISSEL, S., KREPPEL, F., SCHNEIDER, M., SCHARFFETTER-KOCHANEK, K., KOCHANEK, S., STRNAD, P. & WIRTH, T. 2012. Hepatic activation of IKK/NFkappaB signaling induces liver fibrosis via macrophage-mediated chronic inflammation. *Hepatology,* 56, 1117-28.

SUNDERKOTTER, C., NIKOLIC, T., DILLON, M. J., VAN ROOIJEN, N., STEHLING, M., DREVETS, D. A. & LEENEN, P. J. 2004. Subpopulations of mouse blood monocytes differ in maturation stage and inflammatory response. *J Immunol,* 172, 4410-7.

TACKE, F., ALVAREZ, D., KAPLAN, T. J., JAKUBZICK, C., SPANBROEK, R., LLODRA, J., GARIN, A., LIU, J., MACK, M., VAN ROOIJEN, N., LIRA, S. A., HABENICHT, A. J. & RANDOLPH, G. J. 2007. Monocyte subsets differentially employ CCR2, CCR5, and CX3CR1 to accumulate within atherosclerotic plaques. *J Clin Invest,* 117, 185-94.

TACKE, F., GINHOUX, F., JAKUBZICK, C., VAN ROOIJEN, N., MERAD, M. & RANDOLPH, G. J. 2006. Immature monocytes acquire antigens from other cells in the bone marrow and present them to T cells after maturing in the periphery. *J Exp Med,* 203, 583-97.

TAKAHASHI, F., TAKAHASHI, K., OKAZAKI, T., MAEDA, K., IENAGA, H., MAEDA, M., KON, S., UEDE, T. & FUKUCHI, Y. 2001. Role of osteopontin in the pathogenesis of bleomycin-induced pulmonary fibrosis. *Am J Respir Cell Mol Biol,* 24, 264-71.

TAYLOR, P. R., MARTINEZ-POMARES, L., STACEY, M., LIN, H. H., BROWN, G. D. & GORDON, S. 2005. Macrophage receptors and immune recognition. *Annu Rev Immunol,* 23, 901-44.

THOMAS, J. A., POPE, C., WOJTACHA, D., ROBSON, A. J., GORDON-WALKER, T. T., HARTLAND, S., RAMACHANDRAN, P., VAN DEEMTER, M., HUME, D. A., IREDALE, J. P. & FORBES, S. J. 2011. Macrophage therapy for murine liver fibrosis recruits host effector cells improving fibrosis, regeneration, and function. *Hepatology,* 53, 2003-15.

TODA, S., HANAYAMA, R. & NAGATA, S. 2012. Two-step engulfment of apoptotic cells. *Mol Cell Biol,* 32, 118-25.

TRIM, N., MORGAN, S., EVANS, M., ISSA, R., FINE, D., AFFORD, S., WILKINS, B. & IREDALE, J. 2000. Hepatic stellate cells express the low affinity nerve growth factor receptor p75 and undergo apoptosis in response to nerve growth factor stimulation. *Am J Pathol,* 156, 1235-43.

TROEGER, J. S., MEDERACKE, I., GWAK, G. Y., DAPITO, D. H., MU, X., HSU, C. C., PRADERE, J. P., FRIEDMAN, R. A. & SCHWABE, R. F. 2012. Deactivation of hepatic stellate cells during liver fibrosis resolution in mice. *Gastroenterology,* 143, 1073-83 e22.

TUCHWEBER, B., DESMOULIERE, A., BOCHATON-PIALLAT, M. L., RUBBIA-BRANDT, L. & GABBIANI, G. 1996. Proliferation and phenotypic modulation of portal fibroblasts in the early stages of cholestatic fibrosis in the rat. *Lab Invest,* 74, 265-78.

VALLEDOR, A. F., COMALADA, M., XAUS, J. & CELADA, A. 2000. The differential time-course of extracellular-regulated kinase activity correlates with the macrophage response toward proliferation or activation. *J Biol Chem,* 275, 7403-9.

VAN ROOIJEN, N. & SANDERS, A. 1994. Liposome mediated depletion of macrophages: mechanism of action, preparation of liposomes and applications. *J Immunol Methods,* 174, 83-93.

VERA, M., SOBREVALS, L., ZARATIEGUI, M., MARTINEZ, L., PALENCIA, B., RODRIGUEZ, C. M., PRIETO, J. & FORTES, P. 2007. Liver transduction with a simian virus 40 vector encoding insulin-like growth factor I reduces hepatic damage and the development of liver cirrhosis. *Gene Ther,* 14, 203-10.

VERNON, M. A., MYLONAS, K. J. & HUGHES, J. 2010. Macrophages and renal fibrosis. *Semin Nephrol,* 30, 302-17.

VIELHAUER, V., KULKARNI, O., REICHEL, C. A. & ANDERS, H. J. 2010. Targeting the recruitment of monocytes and macrophages in renal disease. *Semin Nephrol,* 30, 318-33.

VOS, C. M., VAN HAASTERT, E. S., DE GROOT, C. J., VAN DER VALK, P. & DE VRIES, H. E. 2003. Matrix metalloproteinase-12 is expressed in phagocytotic macrophages in active multiple sclerosis lesions. *J Neuroimmunol,* 138, 106-14.

WALLACE, W. A., FITCH, P. M., SIMPSON, A. J. & HOWIE, S. E. 2007. Inflammation-associated remodelling and fibrosis in the lung - a process and an end point. *Int J Exp Pathol,* 88, 103-10.

WANG, C. H., SHEN, Y. C., HSIEH, J. J., YEH, K. Y. & CHANG, J. W. 2006. Clodronate alleviates cachexia and prolongs survival in nude mice xenografted with an anaplastic thyroid carcinoma cell line. *J Endocrinol,* 190, 415-23.

WANLESS, I. R., NAKASHIMA, E. & SHERMAN, M. 2000. Regression of human cirrhosis. Morphologic features and the genesis of incomplete septal cirrhosis. *Arch Pathol Lab Med,* 124, 1599-607.

WATSON, M. R., WALLACE, K., GIELING, R. G., MANAS, D. M., JAFFRAY, E., HAY, R. T., MANN, D. A. & OAKLEY, F. 2008. NF-kappaB is a critical regulator of the survival of rodent and human hepatic myofibroblasts. *J Hepatol,* 48, 589-97.

WEIGERT, A., JOHANN, A. M., VON KNETHEN, A., SCHMIDT, H., GEISSLINGER, G. & BRUNE, B. 2006. Apoptotic cells promote macrophage survival by releasing the antiapoptotic mediator sphingosine-1-phosphate. *Blood,* 108, 1635-42.

WU, Y., SINGH, S., GEORGESCU, M. M. & BIRGE, R. B. 2005. A role for Mer tyrosine kinase in alphavbeta5 integrin-mediated phagocytosis of apoptotic cells. *J Cell Sci,* 118, 539-53.

WYNN, T. A. 2008. Cellular and molecular mechanisms of fibrosis. *J Pathol,* 214, 199-210.

WYNN, T. A. 2011. Integrating mechanisms of pulmonary fibrosis. *J Exp Med,* 208, 1339-50.

WYNN, T. A. & BARRON, L. 2010. Macrophages: master regulators of inflammation and fibrosis. *Semin Liver Dis,* 30, 245-57.

XU, J., LEE, G., WANG, H., VIERLING, J. M. & MAHER, J. J. 2004. Limited role for CXC chemokines in the pathogenesis of alpha-naphthylisothiocyanate-induced liver injury. *Am J Physiol Gastrointest Liver Physiol,* 287, G734-41.

YAMAMOTO, M., SUMIYOSHI, H., NAKAGAMI, K. & TAHARA, E. 1984. Distribution of collagen types I, III, and V in fibrotic and neoplastic human liver. *Acta Pathol Jpn,* 34, 77-86.

YONA, S., KIM, K. W., WOLF, Y., MILDNER, A., VAROL, D., BREKER, M., STRAUSS-AYALI, D., VIUKOV, S., GUILLIAMS, M., MISHARIN, A., HUME, D. A., PERLMAN, H., MALISSEN, B., ZELZER, E. & JUNG, S. 2013. Fate mapping reveals origins and dynamics of monocytes and tissue macrophages under homeostasis. *Immunity,* 38, 79-91.

YOSHIJI, H., KURIYAMA, S., MIYAMOTO, Y., THORGEIRSSON, U. P., GOMEZ, D. E., KAWATA, M., YOSHII, J., IKENAKA, Y., NOGUCHI, R., TSUJINOUE, H., NAKATANI, T., THORGEIRSSON, S. S. & FUKUI, H. 2000. Tissue inhibitor of metalloproteinases-1 promotes liver fibrosis development in a transgenic mouse model. *Hepatology,* 32, 1248-1254.

YOSHIJI, H., KURIYAMA, S., YOSHII, J., IKENAKA, Y., NOGUCHI, R., NAKATANI, T., TSUJINOUE, H., YANASE, K., NAMISAKI, T., IMAZU, H. & FUKUI, H. 2002. Tissue inhibitor of metalloproteinases-1 attenuates spontaneous liver fibrosis resolution in the transgenic mouse. *Hepatology,* 36, 850-60.

ZHOU, X., MURPHY, F. R., GEHDU, N., ZHANG, J., IREDALE, J. P. & BENYON, R. C. 2004. Engagement of alphavbeta3 integrin regulates proliferation and apoptosis of hepatic stellate cells. *J Biol Chem,* 279, 23996-4006.

ZIMMERMANN, H. W., SEIDLER, S., NATTERMANN, J., GASSLER, N., HELLERBRAND, C., ZERNECKE, A., TISCHENDORF, J. J., LUEDDE, T., WEISKIRCHEN, R., TRAUTWEIN, C. & TACKE, F. 2010. Functional contribution of elevated circulating and hepatic non-classical CD14CD16 monocytes to inflammation and human liver fibrosis. *PLoS One,* 5, e11049.

APPENDIX 1 – TABLE OF GENE NAMES

Abbreviation	Gene Name
Plau	Plasminogen activator, urokinase
Mmp13	matrix metallopeptidase 13
Mmp2	matrix metallopeptidase 2
Mmp9	matrix metallopeptidase 9
Mmp12	matrix metallopeptidase 12
Hgf	hepatocyte growth factor
Igf1	insulin-like growth factor 1
Mif	macrophage migration inhibitory factor
Cd74	CD74 antigen (invariant polypeptide of major histocompatibility complex, class II antigen-associated)
Cx3cr1	chemokine (C-X3-C motif) receptor 1
Ccr2	chemokine (C-C motif) receptor 2
Ccr1	chemokine (C-C motif) receptor 1
Sell	selectin, lymphocyte
Thbs1	thrombospondin 1
Tgf-β1	transforming growth factor, beta 1
Cxcl10	chemokine (C-X-C motif) ligand 10 (IP10)
Cxcl3	chemokine (C-X-C motif) ligand 3
Cxcl2	chemokine (C-X-C motif) ligand 2 (MIP-2)
Ccl4	chemokine (C-C motif) ligand 4 (MIP-1B)
Ccl3	chemokine (C-C motif) ligand 3 (MIP-1a)
Ccl2	chemokine (C-C motif) ligand 2 (MCP-1)
Il-10	interleukin 10
Il-12β	interleukin 12b
Il-12α	interleukin 12a
Il-6	interleukin 6
Il-1β	interleukin 1 beta
Tnf-α	tumor necrosis factor
Scarb1	scavenger receptor class B, member 1
Ech1	enoyl coenzyme A hydratase 1, peroxisomal
Abca1	ATP-binding cassette, sub-family A (ABC1), member 1
Lpl	lipoprotein lipase
Cd36	CD36 antigen (Scarb3)
Marco	macrophage receptor with collagenous structure
Trem2	triggering receptor expressed on myeloid cells 2
Axl	AXL receptor tyrosine kinase
Mertk	c-mer proto-oncogene tyrosine kinase
Gpnmb	glycoprotein (transmembrane) nmb
Cd81	CD81 antigen
Cd5l	CD5 antigen-like
Fcrls	Fc receptor-like S, scavenger receptor

Mfge8	milk fat globule-EGF factor 8 protein
Gas6	growth arrest specific 6
C1qb	complement component 1, q subcomponent, beta polypeptide
C1qa	complement component 1, q subcomponent, alpha polypeptide
Mrc1	mannose receptor, C type 1
Arg1	arginase, liver
Retnla	resistin like alpha
Kdm6b	KDM1 lysine (K)-specific demethylase 6B
Chi3l3	chitinase-like 3
Il1rn	interleukin 1 receptor antagonist
Ciita	class II transactivator
Cd32	Fc receptor, IgG, low affinity IIb
Cd16	Fc receptor, IgG, low affinity III
Serpine1	serine (or cysteine) peptidase inhibitor, clade E, member 1
Cd86	CD86 antigen
Cd80	CD80 antigen
Cd14	CD14 antigen

APPENDIX 2 – PUBLISHED PAPER

Differential Ly-6C expression identifies the recruited macrophage phenotype, which orchestrates the regression of murine liver fibrosis

Prakash Ramachandran[a], Antonella Pellicoro[a], Madeleine A. Vernon[a], Luke Boulter[a], Rebecca L. Aucott[a], Aysha Ali[a], Stephen N. Hartland[a], Victoria K. Snowdon[a], Andrea Cappon[a,b], Timothy T. Gordon-Walker[a], Mike J. Williams[a], Donald R. Dunbar[c], Jonathan R. Manning[c], Nico van Rooijen[d], Jonathan A. Fallowfield[a], Stuart J. Forbes[a], and John P. Iredale[a,1]

[a]University of Edinburgh/Medical Research Council Centre for Inflammation Research and [c]University of Edinburgh Bioinformatics Core, Centre for Cardiovascular Sciences, The Queen's Medical Research Institute, Edinburgh EH16 4TJ, United Kingdom; [b]Department of Surgical, Oncological and Gastroenterological Sciences, Padova University Hospital, 35128 Padova, Italy; and [d]Department of Molecular Cell Biology, Vrije Universiteit, 1081 BT, Amsterdam, The Netherlands

Edited by Mina J Bissell, E. O. Lawrence Berkeley National Laboratory, Berkeley, CA, and approved September 24, 2012 (received for review December 29, 2011)

Although macrophages are widely recognized to have a profibrotic role in inflammation, we have used a highly tractable CCl_4-induced model of reversible hepatic fibrosis to identify and characterize the macrophage phenotype responsible for tissue remodeling: the hitherto elusive restorative macrophage. This CD11B^{hi} F4/80^{int} Ly-6C^{lo} macrophage subset was most abundant in livers during maximal fibrosis resolution and represented the principle matrix metalloproteinase (MMP) -expressing subset. Depletion of this population in *CD11B* promoter–diphtheria toxin receptor (CD11B-DTR) transgenic mice caused a failure of scar remodeling. Adoptive transfer and in situ labeling experiments showed that these restorative macrophages derive from recruited Ly-6C^{hi} monocytes, a common origin with profibrotic Ly-6C^{hi} macrophages, indicative of a phenotypic switch in vivo conferring proresolution properties. Microarray profiling of the Ly-6C^{lo} subset, compared with Ly-6C^{hi} macrophages, showed a phenotype outside the M1/M2 classification, with increased expression of MMPs, growth factors, and phagocytosis-related genes, including Mmp9, Mmp12, insulin-like growth factor 1 (Igf1), and Glycoprotein (transmembrane) nmb (Gpnmb). Confocal microscopy confirmed the postphagocytic nature of restorative macrophages. Furthermore, the restorative macrophage phenotype was recapitulated in vitro by the phagocytosis of cellular debris with associated activation of the ERK signaling cascade. Critically, induced phagocytic behavior in vivo, through administration of liposomes, increased restorative macrophage number and accelerated fibrosis resolution, offering a therapeutic strategy to this orphan pathological process.

Kupffer Cell | collagen | degradation | myofibroblast | proliferation

As the generic and common pathological endpoint to chronic injury, fibrosis has been estimated to contribute to 45% of all deaths in industrialized nations (1, 2). Currently, no direct antifibrotic therapeutic interventions exist. Long thought of as inexorably progressive, recent evidence, particularly in the liver (3) but also the kidney (4), lung (5, 6), and heart (7), indicates that some reversibility exists, even in advanced disease. Therefore, a more detailed understanding of the specific mechanisms governing fibrosis regression will likely inform therapeutic approaches.

Macrophages have long been implicated in promoting tissue fibrosis (8–10). However, it has recently been shown that they also play a pivotal role in fibrosis regression (6, 11), in part through expression of matrix-degrading metalloproteinase enzymes (MMPs) (12). Macrophages are capable of distinct activation states and functions, which in vitro, can be broadly classified as M1 (classical) or M2 (alternative) (13, 14). It is generally postulated that M1 macrophages are proinflammatory, whereas M2 macrophages are responsible for immunomodulation and wound-healing responses (14). However, it is increasingly clear that this binary classification does not address the more complex heterogeneity in vivo, where macrophages adopt distinct phenotypes and even switch between phenotypes in response to the myriad of stimuli to which they are exposed (13). These in vivo macrophage phenotypes are impossible to recapitulate exactly in tissue culture models, emphasizing the importance of the characterization of macrophages on the basis of function (13).

Ly-6C is a cell surface glycoprotein that is widely used to identify functionally discrete murine circulating monocyte populations: Ly-6C^{hi} monocytes (analogous to CD14^{hi} CD16^{lo} human monocytes) are recruited early to inflammatory environments and thought to be proinflammatory, whereas Ly-6C^{lo} monocytes (analogous to CD14^{lo} CD16^{hi} human monocytes) are a more patrolling cell type and can replenish resident tissue macrophages (15, 16). Differential Ly-6C expression in diseased tissues has identified functionally distinct macrophage populations (17–20). Indeed, an Ly-6C^{hi} intrahepatic macrophage population, derived from recruitment of circulating Ly-6C^{hi} monocytes, is critical for fibrogenesis (21). However, the nature, origin, and phenotype of the macrophage subset responsible for mediating fibrosis resolution have not been defined.

In this study, we have exploited differential Ly-6C expression in a tractable and reproducible model of reversible murine hepatic fibrosis to identify the specific macrophage population responsible for fibrosis resolution: the restorative macrophage. We have gone on to characterize this cell, and we have shown categorically that it is derived from recruited inflammatory monocytes after a phenotypic switch mediated by the ingestion of cellular debris and that it represents a newly identified phenotype distinct from the M1/M2 paradigm. Finally, we have established this mechanism to manipulate macrophage phenotype in vivo and accelerate fibrosis resolution.

Author contributions: P.R., A.P., M.A.V., L.B., S.N.H., S.J.F., and J.P.I. designed research; P.R., A.P., M.A.V., L.B., R.L.A., A.A., S.N.H., V.K.S., A.C., T.T.G.-W., and M.J.W. performed research; N.v.R. contributed new reagents/analytic tools; P.R., A.P., D.R.D., and J.R.M. analyzed data; and P.R., J.A.F., S.J.F., and J.P.I. wrote the paper.

The authors declare no conflict of interest.

This article is a PNAS Direct Submission.

Freely available online through the PNAS open access option.

Data deposition: The microarray data reported in the paper have been deposited in the ArrayExpress database, www.ebi.ac.uk/arrayexpress (accession no. E-MEXP-3177).

[1]To whom correspondence should be addressed. E-mail: john.iredale@ed.ac.uk.

See Author Summary on page 18649 (volume 109, number 46).

This article contains supporting information online at www.pnas.org/lookup/suppl/doi:10.1073/pnas.1119964109/-/DCSupplemental.

Results

Experimental Liver Fibrosis Shows Distinct Phases of Fibrogenesis and Resolution. We established a model of liver fibrosis reversal from which macrophage populations could be isolated on a day-to-day basis. C57BL/6 mice were administered two times weekly i.p. carbon tetrachloride (CCl_4) for 4 wk followed by tissue harvests 24, 48, 72, 96, 168, and 256 h after the final CCl_4 injection (Fig. 1*A*). Comparison was made with age-matched uninjured (control) animals. Hepatic fibrosis and myofibroblast activation were assessed by immunohistochemistry and morphometric analysis of picrosirius red (PSR), collagen 1, collagen 3, and α-smooth muscle actin (α-SMA). Liver fibrosis and myofibroblast activation (α-SMA) peaked at 48–72 h, identifying 24 h as a time of active fibrogenesis, whereas maximal scar resolution and reduction in myofibroblast area occurred between 72 and 96 h and was followed by a more protracted regression of the residual fibrosis (96–256 h) (Fig. 1 *B* and *C*). Scar resolution occurred after reduction in overall hepatic damage as assessed by serum alanine aminotransferase (ALT) and aspartate aminotransferase (AST) levels (Fig. 1*D*). Additionally, at the initiation of scar resolution, there was a significant reduction in hepatic levels of Il-1β, Ccl2, Ccl3, and Cxcl2, suggesting an overall change in macrophage phenotype (Fig. 1*E*). As we have previously shown (3), loss of liver Timp-1 at a gene and protein level preceded fibrosis regression (Fig. S1 *A* and *B*).

Ly-6C^{lo} Monocyte-Derived Macrophages Predominate During Maximal Fibrosis Resolution and Represent the Principle MMP-Expressing Subset. Having identified the time of early and maximal fibrosis resolution (72 h), we determined whether there were associated changes in specific hepatic macrophage subsets. Total hepatic macrophages were identified on flow cytometry as viable CD45+ Ly-6G− NK1.1− CD3− B220− CD11B+ F4/80+ cells from the nonparenchymal cell fraction of digested livers (Fig. S2 *A*–*E*). Importantly, coinciding with maximal fibrosis resolution, total hepatic macrophage number peaked at 72 h (Fig. 2*A*), and macrophages closely associated with hepatic scars topographically (Fig. 2*B*).

Flow cytometric analysis of hepatic macrophages enabled identification of distinct subsets. F4/80^{hi} CD11B^{intermediate} macrophages predominated in the control (uninjured) liver and represent the resident Kupffer cell population (22) (Fig. 2*C*). The proportion of resident macrophages was reduced during active inflammation/fibrogenesis (24 h) and progressively increased during resolution (Fig. 2 *C* and *E*). The CD11B^{hi} F4/80^{intermediate} subset represents a recruited monocyte-derived macrophage population (22). Analysis of Ly-6C expression on this subset identified two clearly distinct hepatic recruited macrophage populations: Ly-6C^{hi} and Ly-6C^{lo} (Fig. 2*D*). Dynamic changes in these macrophage populations were seen during fibrogenesis and resolution (Fig. 2 *D* and *E*). Whereas during fibrogenesis (24 h), Ly-6C^{hi} (profibrotic) macrophages were the predominant subset (21) (Fig. 2*E*), at maximal scar resolution (72 h), when macrophage number peaked, there was a reduction in the Ly-6C^{hi} population and a dramatic and significant increase in Ly-6C^{lo} macrophages, which became the dominant population (Fig. 2*E*). Overall, these changes were also evident when absolute macrophage numbers were quantified (Fig. 2*F*). Therefore, Ly-6C^{lo} monocyte-derived macrophages at the time of maximal scar resolution represented the most numerous macrophage population seen throughout the injury and recovery phases (4.13 ± 0.5-fold more than the total number of macrophages in the undamaged liver).

During late resolution (168 h), the relative proportions of macrophage subsets returned to control liver, although there remained an increase in the proportion of the Ly-6C^{lo} subset (Fig. 2*E*). We have previously shown that macrophage MMP expression is critical for fibrosis regression (12). To identify the principle hepatic MMP-expressing macrophage subset, we used a pan-MMP substrate (MMPsense), which becomes fluorescent after cleavage by active MMPs in vivo (23), enabling us to identify a population of MMPsense-positive hepatic macrophages by flow cytometry (Fig.

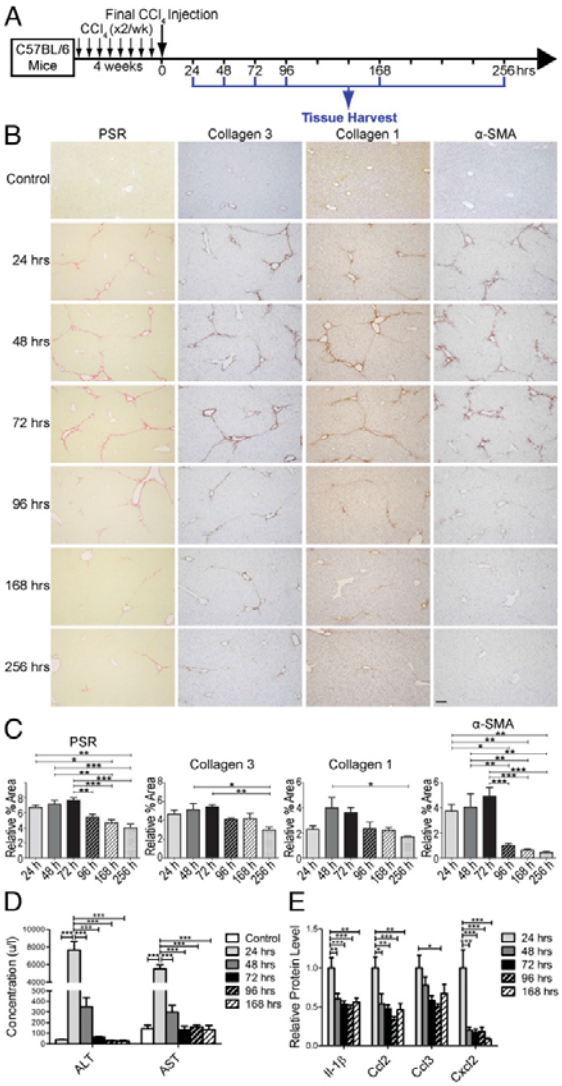

Fig. 1. Experimental liver fibrosis shows distinct phases of fibrogenesis and resolution. (*A*) Schematic representation of the model of reversible hepatic fibrosis in C57BL/6 mice by 4 wk of two times per week i.p. CCl_4 followed by harvest at serial time points after the final injection. Comparisons were made with control (uninjured) animals. (*B* and *C*) Histological characterization of hepatic fibrosis and myofibroblast activation by PSR, collagen 1, collagen 3, and α-SMA immunohistochemistry. (*B*) Representative images are shown for control animals and each time point. (Scale bar: 100 μm.) (*C*) Quantification of histological changes by morphometric pixel analysis expressed relative to mean percent area of control animals (n = 4 per time point; representative of three independent experiments). (*D*) Serum ALT and AST levels in control mice and at stated time point after the final CCl_4 dose (n = 5–6 per time point from two independent experiments). (*E*) Whole-liver protein levels of Il-1β, Ccl2, Ccl3, and Cxcl2 measured by multiplex cytokine assay expressed relative to mean protein concentration at the 24-h time point for each (n = 7–9 per time point from two independent experiments). All data shown as mean ± SEM. *P < 0.05, **P < 0.01, ***P < 0.001.

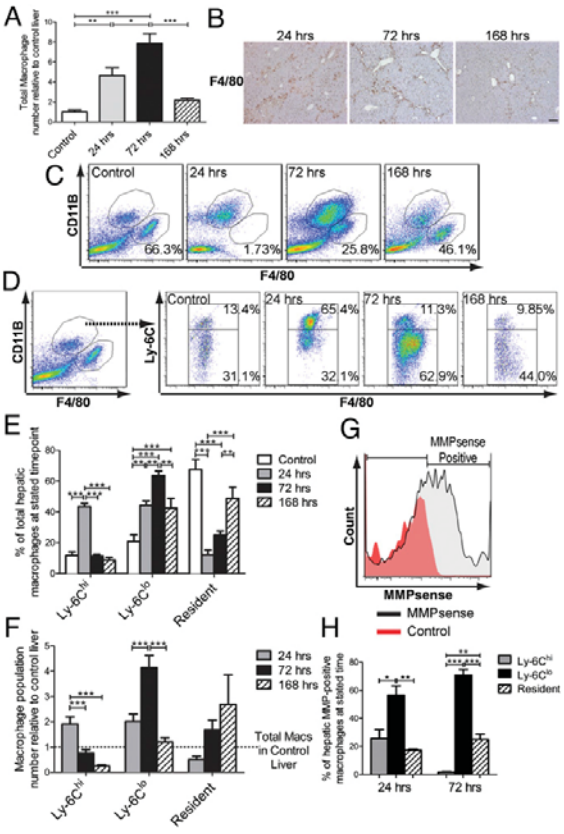

Fig. 2. Ly-6C^{lo} macrophages predominate during maximal fibrosis resolution and represent the principle MMP expressing subset. (*A*–*G*) Analysis of hepatic macrophages at 24 (inflammation/fibrogenesis), 72 (early and maximal scar resolution), and 168 h (late resolution) after the final CCl_4 injection. Comparison was made to control (uninjured) mice. (*A*) Total hepatic macrophage number quantified by flow cytometry expressed relative to the mean number of macrophages in control liver (n = 8–12 per time point from two independent experiments). (*B*) F4/80 immunohistochemistry indicates that macrophages localize around areas of scar at 72 h. (Scale bar: 100 μm.) (*C*) F4/80^{hi} CD11B^{int} resident Kupffer cells during injury and resolution (representative percentages indicate F4/80^{hi} CD11B^{int} cells as a proportion of total macrophages). (*D*) Subset analysis of CD11B^{hi} F4/80^{int} monocyte-derived macrophages on the basis of differential Ly-6C expression identifies two distinct populations: Ly-6C^{hi} and Ly-6C^{lo} with dynamic changes during injury and resolution (representative percentages indicate each subset as a proportion of total hepatic macrophages). (*E*) Quantification of Ly-6C^{hi}, Ly-6C^{lo}, and resident macrophage subsets as a proportion of total hepatic macrophage number (n = 10–17 per time point from four independent experiments). (*F*) Relative number per liver of each macrophage subset at each time point expressed relative to mean total macrophage number in control liver (n = 12–17 per time point from four independent experiments). (*G* and *H*) After 4 wk of CCl_4, mice were given fluorescent MMP substrate (MMPsense) or vehicle control at 0 or 48 h with harvest at 24 or 72 h, respectively. (*G*) Identification of MMPsense-positive macrophages at 24 and 72 h by flow cytometry. (*H*) Macrophage subset analysis of MMPsense-positive macrophage population at 24 and 72 h (n = 3–4). All data shown as mean ± SEM. $^*P < 0.05$, $^{**}P < 0.01$, $^{***}P < 0.001$. Representative flow cytometry plots, histograms, and images are shown.

2*G*). Subset analysis of these cells during both fibrogenesis (24 h) and maximal matrix degradation (72 h) showed that the predominant active MMP-expressing macrophage population at both time points was the Ly-6C^{lo} macrophage (Fig. 2*H*). Therefore, Ly-6C^{lo} monocyte-derived macrophages accumulate maximally during the most rapid phase of fibrosis resolution. Furthermore, they represent the principle MMP-expressing population during both fibrogenesis and fibrosis regression.

Depletion of CD11B-Positive Macrophages Defines Ly-6C^{lo} Cells as Being Critical for Scar Resolution. To define the functional role of distinct macrophage subsets in mediating scar resolution, a well-described selective in vivo macrophage depletion strategy was used (11). *CD11B* promoter - diphtheria toxin receptor (CD11B-DTR) transgenic mice were given CCl_4 for 4 wk. To ensure maximal macrophage depletion throughout the rapid phase of scar resolution, i.v. diphtheria toxin (DT) (or PBS control) was administered 48, 72, and 96 h after the final CCl_4 injection followed by harvest at 120 h (Fig. 3*A*). In concordance with previous data (17), administration of DT was effective in depleting both populations of circulating monocytes (Ly-6C^{hi} and Ly-6C^{lo}) (Fig. S3 *A* and *B*). The degree of depletion was more profound for the Ly-6C^{lo} monocytes in keeping with them being a more mature cell type forming from differentiation of Ly-6C^{hi} monocytes (15) and thus, taking longer to replenish after depletion (24).

We proceeded to analyze hepatic macrophage subsets in CD11B-DTR mice (Fig. 3 *B* and *C*). Importantly, administration of DT during maximal fibrosis resolution, when Ly-6C^{lo} intrahepatic macrophages predominate, induced significant depletion of this subset until harvest, causing a 76.7 ± 3.16% reduction in relative number at 120 h (Fig. 3 *B* and *C*). No depletion of the smaller population of hepatic Ly-6C^{hi} macrophages was seen, whereas there was a minor increase in the resident macrophage number (Fig. 3*C*). For comparison, we depleted macrophages during the inflammatory/fibrogenic phase when both Ly-6C^{hi} and Ly-6C^{lo} hepatic macrophages are present in large numbers. DT was administered to CD11B-DTR mice 8 h after final CCl_4, with harvest at 24 h. Using this strategy, we observed a more general depletion of both Ly-6C^{hi} and Ly-6C^{lo} monocyte-derived macrophage subsets (Fig. S3*C*). Thus, timing depletion for when an individual population predominates is critical for selectivity. What is also apparent from these data is that the Ly-6C^{lo} hepatic macrophage subset is more susceptible to depletion after DT than the Ly-6C^{hi} subset. This result is likely to reflect the higher level of CD11B expression in Ly-6C^{lo} macrophages than the Ly-6C^{hi} subset (Fig. S3*D*). Importantly, DT administration during fibrosis regression did not induce a change in the number of hepatic neutrophils or CD3-positive cells (Fig. S3 *E* and *F*). Furthermore, this depletion strategy caused persistent fibrosis, indicating a failure to remodel the hepatic scar (Fig. 3 *D* and *E*). No difference was detected in the α-SMA area after macrophage depletion, suggesting that the observed phenotype was a result of reduced matrix degradation rather than increased myofibroblast activation (Fig. 3 *D* and *E*). To confirm the specificity of these findings, we administered DT (or PBS control) to WT mice according to the same schedule (Fig. 3*A*). DT administration to WT mice had no effect on macrophage subsets or hepatic fibrosis (Fig. S3 *G* and *H*). To further show the specific effect of hepatic Ly-6C^{lo} macrophages on fibrosis regression, we identified a statistically significant inverse correlation between the number of Ly-6C^{lo} macrophages and the degree of fibrosis (Fig. 3*F*), indicating that the degree of depletion of this subset directly relates to the amount of residual scar. Critically, no significant correlations were seen between the number of Ly-6C^{hi} or resident macrophages and the degree of fibrosis (Fig. S3 *I* and *J*).

These findings indicate that Ly-6C^{lo} macrophages are critical for the resolution of hepatic fibrosis and the restoration of normal tissue architecture. Furthermore, given the temporal and numerical association of the Ly-6C^{lo} subset with the time of maximal scar degradation (Fig. 2 *D*–*F*) and the fact that they are the principle MMP-expressing population (Fig. 2*H*), we postulated that these represent the elusive restorative macrophages.

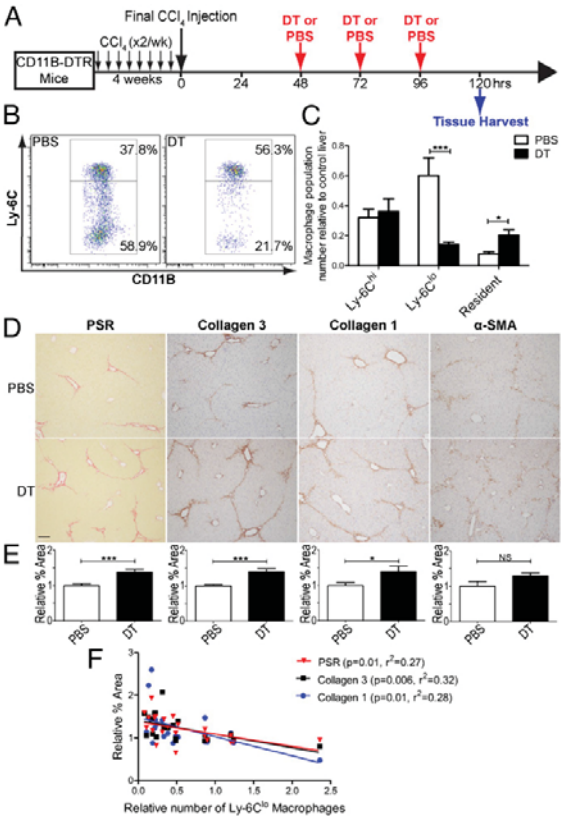

Fig. 3. Depletion of CD11B-positive macrophages defines Ly-6C^{lo} cells as being critical for scar resolution. (*A*) Schematic representation of model of macrophage depletion during fibrosis resolution in CD11B-DTR mice by administration of DT (or PBS control). (*B*) Flow cytometry data from livers of PBS and DT-treated mice gated on viable CD45+ Ly-6G− CD11B^{hi} F4/80^{int} hepatic macrophages (representative percentages of each subset as a proportion of total macrophage number shown). (*C*) Quantification of relative number of each macrophage subset expressed relative to mean total macrophage number in PBS-treated livers (n = 11–13 from two independent experiments). (*D*) Representative PSR staining and immunohistochemistry of collagen 1, collagen 3, and α-SMA after macrophage depletion or control. (Scale bar: 100 μm.) (*E*) Quantification of histological changes by pixel analysis expressed relative to mean percent area in PBS-treated liver (n = 10–12 from two independent experiments). (*F*) Correlation of degree of fibrosis assessed by PSR, collagen 1, and collagen 3 area with the relative number of Ly-6C^{lo} macrophages (n = 22 from two independent experiments). All data shown as mean ± SEM. *P < 0.05, ***P < 0.001. NS, nonsignificant. Representative flow cytometry plots and images are shown.

CD11c+ dendritic cells (DCs) have been associated with resolution of liver injury (25, 26) and share a number of cell surface markers with macrophages (27). The restorative macrophage subset at 72 h expressed only intermediate levels of CD11c (Fig. S4*A*). Furthermore, administration of DT to chronically injured CD11c-DOG mice at a dose known to deplete hepatic DCs (28) had no effect on the identified hepatic macrophage subsets (Fig. S4 *B* and *C*), indicating no significant contribution of hepatic DCs to these populations.

Ly-6C^{lo} Macrophages Derive from an in Situ Phenotypic Switch of Recruited Ly-6C^{hi} Monocytes. The profibrotic Ly-6C^{hi} macrophage subset has been shown to derive from a Chemokine (C-C motif) receptor 2 (CCR2)-dependent recruitment of circulating Ly-6C^{hi} monocytes (21). Given that hepatic Ly-6C^{lo} macrophages are also monocyte-derived (Fig. 2*D*), restorative macrophages must have an origin from recruited Ly-6C^{hi} or Ly-6C^{lo} monocytes. Blood analysis showed that, during active fibrogenesis (24 h), there was an increased number of both populations of circulating monocytes, whereas during maximal resolution (72 h), only the Ly-6C^{hi} monocytes remained elevated (Fig. S5 *A*–*C*).

To determine which of the circulating monocyte populations contributed to the formation of the restorative macrophages, adoptive transfer and in vivo labeling experiments were performed. For adoptive transfer, hepatic fibrosis was induced in C57BL/6 mice (CD45.2+); 4 h after the final CCl_4 injection, we injected 9×10^5 FACS-sorted bone marrow-derived CD45.1+ Ly-6C^{hi} monocytes (Ly-6G− CD115+ CD11B+ Ly-6C^{hi} cells) (Fig. S5*D*) or vehicle control through the tail vein, with harvests at 24, 72, and 168 h (Fig. 4*A*). Adoptively transferred CD45.1+ Ly-6C^{hi} monocytes could be detected in livers during active fibrogenesis (24 h) and early resolution (72 h) but not during late resolution (Fig. 4*B*). Even at 24 h, these monocytes had differentiated into Ly-6C^{lo} macrophages (Fig. 4 *C*–*E*). This population remained the predominant macrophage population formed from the adoptively transferred monocytes at 72 h (Fig. 4 *C*–*E*). To determine the relative contribution of Ly-6C^{lo} monocytes to the hepatic macrophage subsets, we used a well-validated in vivo labeling technique (29, 30). After chronic injury with 4 wk of CCl_4, mice were given 200 μL fluorescent latex beads (which selectively label circulating Ly-6C^{lo} monocytes) through the tail vein 4 h after the final CCl_4 injection. Animals were harvested at 24, 72, and 168 h (Fig. 4*F*). This technique caused selective labeling of circulating Ly-6C^{lo} monocytes (Fig. S5 *E* and *F*) as previously shown (29, 30). Latex-positive cells could not be identified in livers at 24 or 72 h, despite concurrent positive circulating Ly-6C^{lo} monocytes (Fig. 4*G*). However, a population of intrahepatic latex-positive cells emerged during late resolution (168 h) (Fig. 4*H*), predominantly in the resident macrophage population (Fig. 4 *H* and *I*).

Recent work has also shown a key role for local proliferation in the accumulation of macrophages during chronic inflammation (31). Given the dramatic increase in the number of Ly-6C^{lo} macrophages at maximal resolution (Fig. 2*F*), we determined the contribution of local macrophage proliferation to this population. Using flow cytometric K_i-67 staining on hepatic nonparenchymal cells after 4 wk of CCl_4, we could identify proliferative hepatic macrophages (Fig. 4*J*). Interestingly, the recruited proinflammatory Ly-6C^{hi} macrophage population represented the most proliferative macrophage subset at 24, 72, and 120 h after the final CCl_4 injection (Fig. 4*K*). The fact that the number of Ly-6C^{hi} macrophages rapidly declines (Fig. 2 *E* and *F*) in the context of active proliferation emphasizes that this population undergoes a switch in phenotype in vivo.

These data show that restorative Ly-6C^{lo} macrophages derive from circulating Ly-6C^{hi} monocytes, a common origin to profibrotic macrophages, and that an in vivo phenotypic switch leads to fibrosis-modifying capabilities. Furthermore, Ly-6C^{lo} monocytes make no contribution to the proresolution population but contribute to repopulating the resident macrophage pool during late resolution.

Ly-6C^{lo} Macrophages Show a Characteristic Gene Expression Profile Favoring Scar Resolution. Having identified that Ly-6C^{lo} macrophages, derived from a phenotypic switch of Ly-6C^{hi} monocytes, are critical for regression of hepatic fibrosis, we sought to define the mediators produced by this newly identified macrophage subset that confer its restorative properties. Affymetrix mouse gene microarrays were performed on FACS-sorted restorative 72-h Ly-6C^{lo} macrophages and compared with the profibrotic 24-h Ly-6C^{hi} macrophages given their common origin, distinct functional roles, and relative predominance at critical time points in

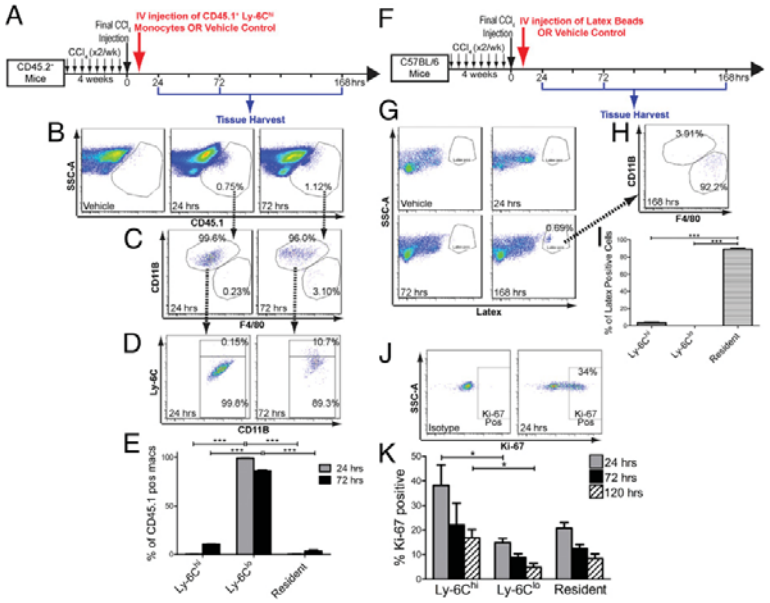

Fig. 4. Ly-6C^{lo} hepatic macrophages derive from recruited Ly-6C^{hi} monocytes. (*A*) Schematic representation of the model of adoptive transfer of CD45.1+ Ly-6C^{hi} monocytes (or vehicle control) into C57BL/6 mice (CD45.2+) 4 h after the final CCl_4 injection, with livers harvested at 24, 72, and 168 h. (*B*) Identification of injected CD45.1+ cells in digested livers at 24 and 72 h time points (gating on viable CD45.2− cells). (*C*) Hepatic CD45.1+ cells have predominantly differentiated into CD11B^{hi} F4/80^{int} monocyte-derived macrophages. (*D*) CD45.1+ monocytes have largely formed the restorative Ly-6C^{lo} macrophage subset. (*E*) Quantification of the proportion of identified CD45.1+ hepatic macrophages forming each of the macrophage subsets (n = 3 per time point). (*F*) Schematic representation of the model of in situ labeling of circulating Ly-6C^{lo} monocytes by injection of fluorescent latex beads (or vehicle control) 4 h after the final CCl_4 injection. (*G*) Latex-positive macrophages are identified in the liver only at 168 h (gating on viable CD45+ Ly-6G− hepatic macrophages). (*H*) Latex-positive cells have formed the resident CD11b^{int} F4/80^{hi} macrophage population. (*I*) Quantification of the proportion of latex-positive cells forming each of the hepatic macrophage subsets at 168 h (expressed as a percent of latex-positive cells; n = 4). (*J* and *K*) K_i-67 staining of hepatic macrophages 24, 72, and 120 h after final CCl_4 dose after 4 wk of injury. (*J*) K_i-67–positive macrophages identified by flow cytometry. (*K*) Percentage of the stated macrophage subset at the indicated time point identified as K_i-67–positive (n = 3–6). All data shown as mean ± SEM. $^*P < 0.05$, $^{***}P < 0.001$. Representative flow cytometry plots and proportions are shown.

the fibrogenesis resolution model. Specific microarray hits were confirmed by quantitative PCR.

A number of differentially regulated genes were identified, and the full list is available in Tables S1 and S2. In keeping with the critical role of macrophage MMP expression in fibrosis resolution (12), the switch to a proresolution macrophage phenotype was associated with an up-regulation of MMPs (Fig. 5*A*). Furthermore, a number of proinflammatory cytokines and chemokines were down-regulated, and concurrently, genes associated with an antiinflammatory macrophage program [e.g. Chemokine (C-X3-C) receptor 1 (CX3CR1)] (32) or antifibrotic effects (e.g. Macrophage migration inhibitory factor (MIF) and CD74) (33) were increased (Fig. 5*A*). Expression of TGF-β, the archetypal profibrotic cytokine, was reduced in the restorative macrophage population along with Thrombospondin-1 (Thbs1), a potent activator of latent TGF-β (34). We also identified additional proresolution mechanisms, such as a strong increase in expression of insulin-like growth factor 1 (Igf1), which has been implicated as being antifibrotic (35) (Fig. 5*A*). Thus, the switch to a restorative macrophage phenotype confers a number of proresolution features, highlighting the importance of a cellular mechanism for tissue fibrosis regression.

We performed pathway enrichment analysis on the differentially regulated genes from the two macrophage populations using the DAVID bioinformatics tool (36, 37). The proinflammatory macrophage population was enriched for pathways, including response to wounding, coagulation cascade, and chemotaxis (Fig. S6*A*), which are important for fibrogenesis (38, 39). Analysis of the restorative macrophages showed enrichment for pathways, such as lysosomes, endocytosis, scavenger receptors, and antigen presentation, which are implicated in phagocytosis (Fig. S6*B*). We also identified enhancement of pathways implicated in fatty acid metabolism and peroxisome proliferator activated receptor (PPAR) signaling (Fig. S6*B*). The enrichment of phagocytosis-related genes was confirmed individually, where a number of opsonins, receptors, and genes involved in the recognition, binding, and clearance of apoptotic cells were up-regulated in the restorative macrophage population (Fig. 5*B*). Similarly, a number of PPAR-γ target genes was up-regulated in these proresolution macrophages (Fig. 5*B*). We also assessed the degree of expression of a number of previously described M1 and M2 macrophage markers to determine how hepatic inflammatory and restorative macrophages fit into the traditional paradigm (Fig. 5 *A* and *B*). Although Ly-6C^{lo} restorative macrophages show increased expression of some M2 genes, such as Macrophage Mannose receptor 1 (Mrc1), Arginase-1 (Arg1), and Retnla (Fizz-1), they also down-regulate other characteristic M2 genes, including Chi3l3 (YM-1), Il-1 receptor antagonist (Il1rn), Kdm6b (Jmjd3), Ccl24, Il-10, and TGF-β (14, 40). Simultaneously, these Ly-6C^{lo} macrophages up-regulate traditional M1 genes, such as Ciita (MHC class II transactivator), CD16, CD32, and Serpine1 (plasminogen activator inhibitor type 1) (14, 40, 41). Therefore, these hepatic macrophage populations do not fit into the M1/M2 classification and represent newly identified macrophage phenotypes (Fig. 5*B*).

We proceeded to confirm a number of the gene expression changes at a protein level using flow cytometry (Fig. 5*C*). Additionally, by administering MMPsense 24 h before harvest, we showed that the switch from inflammatory to restorative macrophage phenotype resulted in an increase in active MMP expression (Fig. 5*C*). Our microarray data also enabled us to identify the functionally distinct macrophage subsets in situ using immunohistochemistry for Chi3l3, MMP-12, and Glycoprotein (transmembrane) nmb (Gpnmb) (Fig. 5*D*). We confirmed the specificity of these markers in our CD11B-DTR depletion model, where the administration of DT causes a significant reduction in the number of MMP-12–positive cells histologically (Fig. S6*C*), whereas there was no significant difference in the number of Chi3l3-positive cells (Fig. S6*D*), mirroring the changes seen on flow cytometry (Fig. 3 *B* and *C*). We went on to show the presence of similar MMP-12– and GPNMB-expressing cells associated with scars in cirrhotic human livers (Fig. 5*D*) and have identified them as a subpopulation of human CD68-positive macrophages (Fig. S6 *E* and *F*).

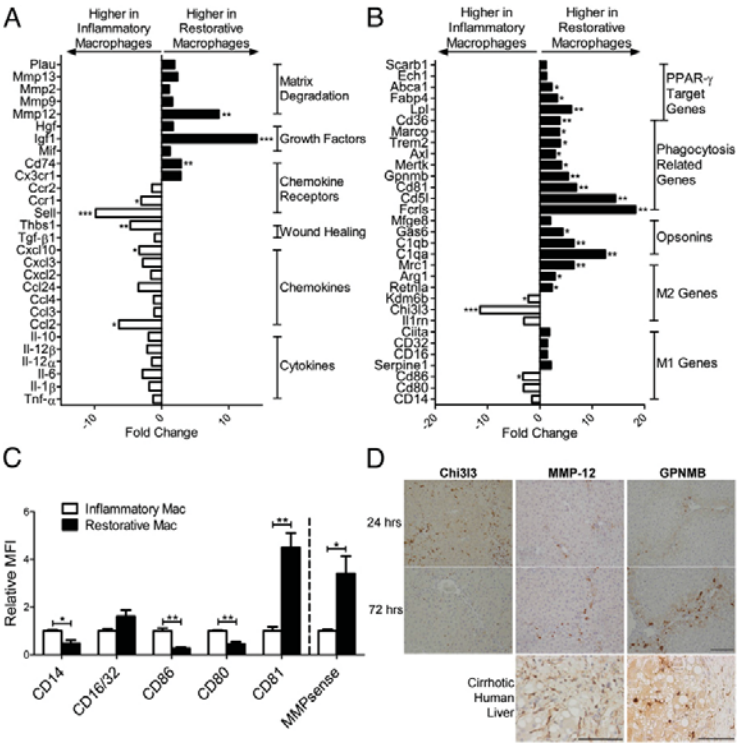

Fig. 5. Ly-6C^{lo} macrophages show a gene expression profile favoring scar resolution. (*A* and *B*) Microarray analysis of inflammatory Ly-6C^{hi} and restorative Ly-6C^{lo} hepatic macrophage populations isolated by FACS sorting from livers 24 and 72 h after the final CCl_4 injection, respectively. (*A*) Differential regulation of cytokines, chemokines, chemokine receptors, growth factors, and matrix-degrading enzymes between the inflammatory and restorative macrophage populations (expressed as fold change between the two macrophage subsets). (*B*) Differential expression of opsonins, phagocytosis-related genes, PPAR-γ target genes, and macrophage phenotype markers (M1, classical; M2, alternative) between the macrophage subsets on microarray (expressed as fold change between the two macrophage populations). All microarray data based on $n = 3$ per group taken from two independent experiments. $^*P < 0.05$, $^{**}P < 0.01$, $^{***}P < 0.001$. (*C*) Flow cytometric analysis comparing expression of stated marker between inflammatory Ly-6C^{hi} and restorative Ly-6C^{lo} hepatic macrophages. MMPsense was administered 24 h before the time of harvest to compare MMP activity between macrophage subsets expressed relative to average MFI for inflammatory macrophage subset ($n = 3$–6). MFI, mean fluorescence intensity. $^*P < 0.05$, $^{**}P < 0.01$. (*D*) Immunohistochemistry for genes differentially regulated on microarray in murine liver at 24 and 72 h time points and cirrhotic human liver (representative images shown). (Scale bars: 100 μm.)

These data indicate that the phenotypic switch to the restorative macrophage population results in a loss of proinflammatory gene expression, increased expression of matrix-degrading enzymes, and enrichment of phagocytosis-related genes. Furthermore, the identified macrophage phenotypes fall outside the M1/M2 paradigm, highlighting the limitations of this classification in an in vivo setting.

Restorative Ly-6C^{lo} Macrophages Are Postphagocytic. Having identified up-regulation of phagocytosis-related pathways, we determined if restorative macrophages were postphagocytic. It is recognized that ingestion of cellular debris can influence macrophage phenotype (42). Furthermore, the switch to fibrosis resolution in our model followed a reduction in hepatocyte death as assessed by serum ALT and AST (Fig. 1*D*), indicating that the increase in the restorative Ly-6C^{lo} population (Fig. 2 *E* and *F*) occurred after the clearance of cellular debris.

Flow cytometric and immunohistochemical analysis showed that, compared with the proinflammatory 24-h Ly-6C^{hi} macrophages, restorative 72-h Ly-6C^{lo} macrophages were larger [forward scatter area (FSC-A)], were more complex [side scatter area (SSC-A)], and showed features of being postingestion (Fig. 6 *A* and *B*). We FACS sorted these two macrophage subsets and TUNEL stained each to quantify the presence of intra- or extracellular apoptotic debris using confocal microscopy (Fig. 6*C*). No difference was seen in the percentage of each macrophage subset associated with TUNEL-positive debris (Fig. 6*D*). However, in the proinflammatory macrophages, apoptotic debris was predominantly bound to the cell surface, whereas in the restorative macrophage subset, the debris had been ingested (Fig. 6 *C* and *E*), confirming the postphagocytic phenotype of the Ly-6C^{lo} macrophage population. These findings are consistent with the known ability of monocytes to bind apoptotic debris, but a delayed capacity to ingest until differentiation into a more mature macrophage subtype has occurred (43, 44).

Macrophage Phagocytosis in Vitro Induces a Matrix-Degrading Phenotype Through ERK Signaling. Having identified evidence of prior phagocytosis as a key feature of the restorative macrophage population, we sought to model this phenotype in vitro. Given that the predominant cellular debris in the CCl_4 model is hepatocyte-derived, we determined whether ingestion of hepatocyte debris might induce a similar change in macrophage phenotype. Primary bone marrow-derived macrophages (BMDMs), widely used to study macrophage biology in vitro (45), were cultured in the presence and absence of cell debris generated from strain-matched primary murine hepatocytes. Macrophage morphology changed significantly after coculture in keeping with ingestion of hepatocyte debris (Fig. 7*A*). Hepatocyte debris alone did not attach to the wells. After ingestion, BMDMs up-regulated Mmp12, Mmp9, and Igf1 and down-regulated Thbs1 and Chi3l3 (Fig. 7*B*), mirroring the phenotypic switch seen in vivo (Fig. 5 *A* and *B*). To confirm the active secretion of MMPs and determine if this effect was a general effect of phagocytosis on macrophages independent of the type of debris, we used the well-described model of phagocytosis of apoptotic thymocytes (46). Culture supernatants from BMDMs fed with apoptotic thymocytes for 12 h showed a robust increase in active MMP-9 and MMP-12 secretion detected by gelatin zymography and Western blotting, respectively (Fig. 7 *C* and *D*).

We then sought to determine which signaling pathways might link macrophage phagocytosis with the increase in matrix-degrading activity. MAPK signaling, specifically the ERK and p38 cascades, is activated in macrophages after phagocytosis, and it has been reported to regulate a number of macrophage responses (47, 48). Using immunohistochemistry, we could identify nuclear phos-

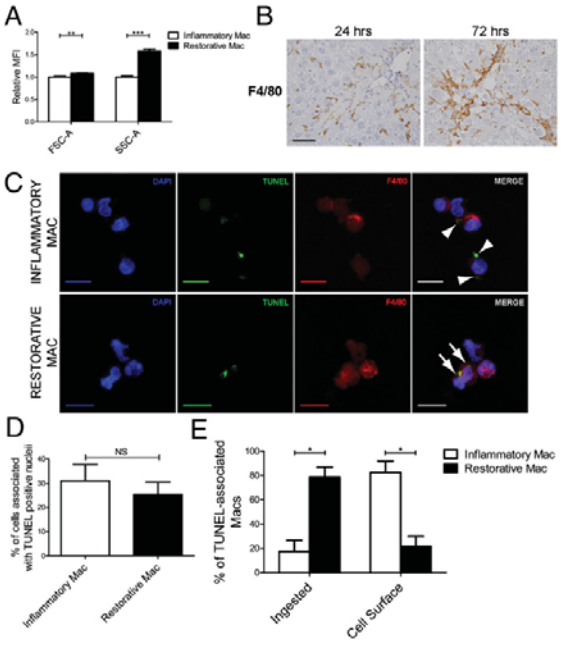

Fig. 6. Restorative Ly-6C^{lo} macrophages are postphagocytic. Comparison of inflammatory (24 h Ly-6C^{hi}) and restorative (72 h Ly-6C^{lo}) macrophage subsets after 4 wk of CCl_4. (*A*) Size [forward scatter area (FSC-A)] and complexity [side scatter area (SSC-A)] of macrophage subsets assessed by flow cytometry expressed relative to average MFI for inflammatory macrophages (n = 13 from three independent experiments). (*B*) F4/80 immunohistochemistry shows larger scar-associated macrophages at 72 h. (Scale bar: 50 μm.) (*C*–*E*) TUNEL staining and confocal microscopy of FACS-sorted subsets. (*C*) Stained DAPI, TUNEL, F4/80, and merged image for macrophage subsets. (Scale bars: 10 μm.) Arrowheads, cell-surface debris; arrows, ingested debris. (*D*) Percentage of each subset associated with TUNEL-positive nuclei by cell counting (n = 3–4). (*E*) Percentage of TUNEL-associated macrophages with ingested or cell-surface debris (n = 3–4). Data shown as mean ± SEM. $^*P < 0.05$, $^{**}P < 0.01$, $^{***}P < 0.001$. NS, nonsignificant. Representative images are shown.

pho-ERK staining in macrophages at the 72-h time point (Fig. 7*E*), indicating activation of the ERK signaling pathway in scar-associated macrophages during maximal fibrosis resolution. To show a functional role for ERK signaling in the observed macrophage phenotype, we administered the specific ERK kinase [mitogen-activated protein kinase kinase 1 and 2 (MEK1/2)] inhibitor PD98059 (50 μM) or vehicle control to BMDMs at published doses (49, 50) for 1 h before and during feeding with hepatocyte debris in vitro. Administration of PD98059 significantly inhibited macrophage up-regulation of Mmp9, Mmp12, and Igf1 in response to the ingestion of hepatocyte debris (Fig. 7*F*). Furthermore, casein zymography on culture supernatants showed that ERK inhibition abrogated the increase in active MMP-9 and MMP-12 secretion observed after phagocytosis (Fig. 7*G*), indicating a critical role for MEK1/2 activation in the increased matrix-degrading activity in macrophages in response to phagocytosis. MEK1/2 inhibition had no effect on the down-regulation of Thbs1 and Chi3l3 in response to phagocytosis (Fig. S7*A*), suggesting that cross-talk between signaling pathways is required for generating the complex overall phenotype of the restorative macrophage. We confirmed the role of MEK1/2 in macrophage Mmp12 up-regulation in response to phagocytosis using a second specific inhibitor UO126 (20 μM) (Fig. S7*B*). Administration of a p38 MAPK inhibitor (SB203580; 10 μM) at a published dose (51) had no effect on macrophage expression of Mmp9, Mmp12, or Igf1 in response to phagocytosis (Fig. S7*C*).

These data show that the matrix-degrading phenotype of the proresolution macrophage can be modeled in vitro by the phagocytosis of cellular debris, and this phenotypic switch is, at least in part, mediated by phagocytosis-related MEK1/2 activation and ERK signaling in macrophages.

Induction of Phagocytic Behavior Using Liposomes Enhances the Restorative Macrophage Phenotype in Vivo and Accelerates Fibrosis Resolution. Having conclusively identified macrophage phagocytosis as a key determinant of the proresolution matrix-degrading phenotype, we wished to use this information to manipulate

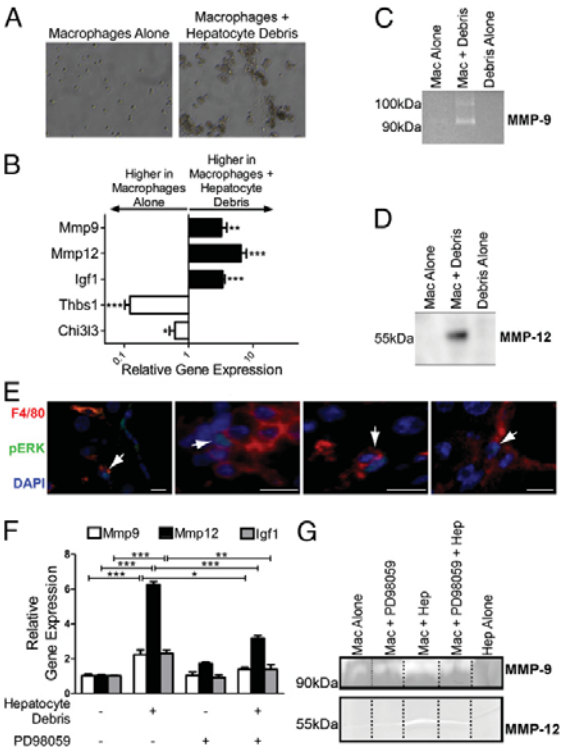

Fig. 7. Macrophage phagocytosis in vitro induces a matrix-degrading phenotype through ERK signaling. (*A* and *B*) Coculture of BMDMs with hepatocyte debris. (*A*) Changes in macrophage morphology on phase-contrast microscopy. Hepatocyte debris alone was nonadherent. (*B*) Changes in macrophage gene expression after coculture expressed relative to mean expression of macrophages alone (n = 11–12 from two independent experiments). (*C* and *D*) Coculture of BMDMs with apoptotic thymocytes. (*C*) Gelatin zymography of culture supernatants equalized for protein content showing active MMP-9 (representative zymogram from n = 4 from two independent experiments). (*D*) Western blot for MMP-12 on culture supernatants equalized for protein content (representative blot from n = 4 from two independent experiments). (*E*) Dual immunofluorescence for F4/80 and phospho-ERK in mouse liver 72 h after final CCl_4 dose after 4 wk of injury. Arrows, nuclear pERK and F4/80 dual positive cells. (Scale bars: 10 μm.) (*F* and *G*). Culture of BMDMs ± MEK1/2 inhibitor (PD98059; 50 μM) ± hepatocyte debris. (*F*) Changes in macrophage gene expression after coculture expressed relative to mean expression of macrophages alone (n = 6). (*G*) Casein zymography of culture supernatants equalized for protein content showing active MMP-9 and MMP-12 (representative zymogram from n = 3 shown). Data shown as mean ± SEM. $^*P < 0.05$, $^{**}P < 0.01$, $^{***}P < 0.001$. Representative images are shown.

macrophage phenotype in vivo with a therapeutic benefit in accelerating fibrosis resolution. The systemic administration of cellular debris is likely to have significant confounding off-target effects. Liposome uptake by macrophages represents a genuine phagocytosis event (52), and it has been widely used to target macrophages in vivo. Furthermore, recent studies have shown that liposome administration can alter macrophage phenotype in vivo in part by induction of ERK signaling after ingestion (53, 54). We proceeded to feed BMDMs with liposomes in vitro, which induced a change in macrophage phenotype (Fig. 8*A*) analogous to the change that we observed in vivo (Fig. 5 *A* and *B*) and similar to the tissue culture models after the ingestion of cellular debris (Fig. 7*B*). Thus, ingestion of liposomes models the phagocytosis of cellular debris and the generation of restorative macrophages. We went on to administer liposomes (or vehicle control) to chronically injured mice during maximal fibrosis resolution for 48, 72, and 96 h after the final CCl_4 injection, with harvest at 120 h (Fig. 8*B*). In keeping with an induction of phagocytic behavior, liposome administration caused a reduction in proinflammatory Ly-6C^{hi} macrophages and an increase in restorative Ly-6C^{lo} hepatic macrophages during fibrosis resolution (Fig. 8*C*). Liposomes, when fluorescently labeled, were rarely detected in Ly-6C^{hi} macrophages but frequently seen in Ly-6C^{lo} macrophages, indicative of a postphagocytic phenotype (Fig. 8*D*). Critically, this manipulation accelerated the regression of liver fibrosis (Fig. 8 *E* and *F*), indicating that, by inducing phagocytosis, macrophages could be switched to a phenotype promoting fibrosis resolution in vivo.

Discussion

In a murine model of reversible hepatic fibrosis, we have used differential Ly-6C expression to identify and characterize the hitherto elusive restorative macrophage. This Ly-6C^{lo} CD11B^{hi} F4/80^{int} macrophage population accumulates in the liver, and it is the main MMP-expressing macrophage subset during maximal fibrosis resolution, is necessary for degradation of tissue scar, is derived from infiltrating Ly-6C^{hi} inflammatory monocytes, has a distinct pattern of gene expression, including matrix degradation and phagocytic and growth factors, and is characterized by evidence of prior phagocytosis of dying cells. The restorative phenotype can be recapitulated in vitro by phagocytosis-induced ERK signaling and can be induced in vivo by the administration of liposomes, which accelerates scar resolution.

Although evidence for a central role for macrophages in inflammation and tissue fibrogenesis has been described across organ systems (8), data have recently emerged to suggest a functional heterogeneity of subtypes in vivo and a role in fibrosis resolution (3, 6, 11, 12). Differential Ly-6C expression has been widely used to identify functionally distinct populations of circulating murine monocytes (15, 16) and macrophage populations in pathology (17–21). Our data show that Ly-6C expression can be exploited to identify the macrophage subset responsible for fibrosis resolution. Key questions arising from studies regarding the divergent role of macrophages in fibrogenesis and recovery were whether these distinct functions were mediated by resident or recruited cells and whether those cells underwent a phenotypic switch in situ (55, 56). Herein, we have shown conclusively that the proresolution Ly-6C^{lo} macrophage population derives from recruited Ly-6C^{hi} monocytes, a common origin to the profibrotic Ly-6C^{hi} macrophage, indicating a switch in macrophage function in vivo. This finding is in keeping with the known ability of monocytes and macrophages to change phenotype in situ depending on local environmental cues (13). These findings have implications for development of antifibrotic therapies, where targeting inflammatory monocyte recruitment might adversely impact on the population of restorative Ly-6C^{lo} macrophages (39, 57). This finding provides an explanation for the apparently counterintuitive observation made in the work by Mitchell et al. (58): that decreased CCR2-dependent recruitment of Ly-6C^{hi} monocytes retards fibrosis resolution (58). A more detailed study of the signals controlling macrophage dynamics and phenotype during fibrosis resolution now depends on the development of monocyte/macrophage-specific chemokine receptor KO transgenic mice, in which key genes can be inducibly deleted without the confounding variable of differences in peak fibrosis that complicates noninducible transgenic models.

The contribution of local macrophage proliferation during hepatic fibrogenesis or fibrosis resolution has not previously been defined. We have shown a high level of proliferation of proinflammatory hepatic Ly-6C^{hi} monocyte-derived macrophages, suggesting that a combination of recruitment and local proliferation is required for the generation of restorative Ly-6C^{lo} macrophages. This finding initially seems to contrast with findings in work by Jenkins et al. (31), where resident F4/80^{hi} pleural macrophages proliferated during chronic parasitic infection. However, using classical inflammatory stimuli, the work by Jenkins et al. (31) also showed the capacity of recruited monocyte-derived macrophages to proliferate in the context of Il-4 stimulation (31). Our work is, therefore, complementary to this study, highlighting that the relative contribution of recruitment and

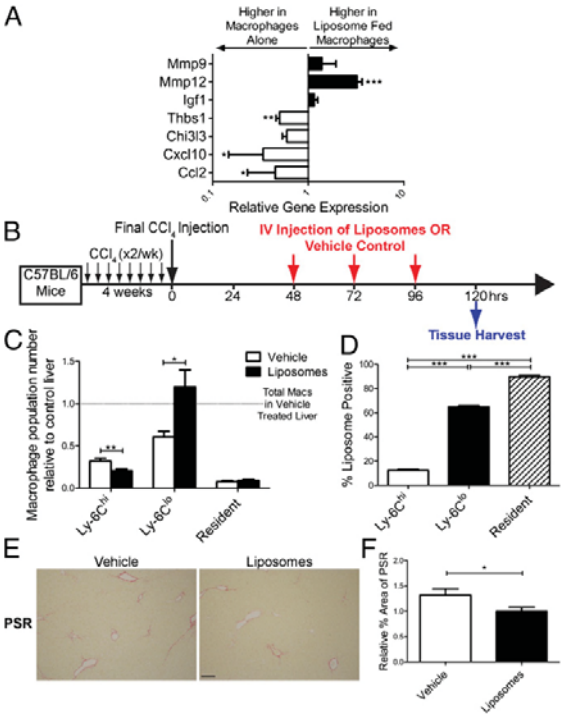

Fig. 8. Induction of phagocytic behavior using liposomes enhances the restorative macrophage phenotype in vivo and accelerates fibrosis resolution. (*A*) Changes in macrophage gene expression after in vitro feeding with liposomes expressed relative to mean expression of unfed macrophages ($n = 6$). (*B*) Schematic representation of the model of liposome (or vehicle) administration during resolution phase after 4 wk of CCl_4 injury. (*C*) Changes in hepatic macrophage subsets after liposome administration relative to mean total macrophage number in vehicle-treated livers ($n = 13$–14). (*D*) Percentage of each hepatic macrophage subset containing fluorescently labeled liposomes assessed by flow cytometry ($n = 8$). (*E*) Fibrosis assessed by PSR staining after liposome (or vehicle) administration. Representative images are shown. (Scale bar: 100 μm.) (*F*) Quantification of fibrosis by morphometric pixel analysis expressed relative to mean percent area for liposome-treated liver ($n = 6$). Data shown as mean ± SEM. $^*P < 0.05$, $^{**}P < 0.01$, $^{***}P < 0.001$.

local proliferation to tissue macrophage expansion during inflammation is critically dependent on the nature of injury and organ involved. Investigators should consider this information in future studies on macrophage dynamics.

A major difficulty in studying macrophage heterogeneity in vivo is the lack of defined specific markers for functionally distinct populations, necessitating the use of flow cytometry on freshly isolated tissue to recognize subsets. Thus, existing strategies for macrophage depletion are unable to specifically select for functionally distinct subsets. In this work, we used the widely used CD11B-DTR system (11, 17). This transgenic strategy shows selectivity for $CD11B^{hi}$ $F4/80^{lo}$ monocytes and monocyte-derived macrophages compared with $CD11B^{lo}$ $F4/80^{hi}$ resident tissue macrophages. We have gone on to show that specific depletion of subsets of $CD11B^{hi}$ $F4/80^{lo}$ cells is critically dependent on timing. Furthermore, our data indicate an increased susceptibility of Ly-$6C^{lo}$ macrophages to depletion with DT, which is likely to be a result of higher levels of CD11B expression in this population. We have discovered a number of genes that are differentially expressed by the functionally distinct populations. These findings could inform transgenic studies, where individual macrophage subsets could be specifically depleted or labeled in vivo. Using these data, we could identify distinct macrophages in situ using immunohistochemistry, enabling more easy translation to studying human tissue. Our findings are based on the highly tractable and predictable CCl_4 model of reversible hepatic fibrosis. To study macrophage dynamics and phenotype on a day-by-day basis, we deliberately focused on an early fibrosis, which resolves rapidly and completely. A future goal is the more detailed analysis of hepatic macrophage subsets in cirrhotic human liver to identify analogous populations to those populations described in this study; until this analysis is undertaken, extrapolation of our findings to human models must be guarded.

The data presented also show that the switch to a proresolution macrophage population confers a number of potential antifibrotic properties. Principally, there is a change from expression of proinflammatory cytokines, chemokines, and profibrotic genes, such as thrombospondin-1 (34), to a profile incorporating genes responsible for scar degradation, such as Mmp12 and Mmp9, genes critical for the clearance of cellular debris, and a number of potential antifibrotic pathways, such as Igf1 (35) and CD74/MIF (33). Furthermore, our data expose the limitations of categorizing macrophage populations from an in vivo setting into the widely used but restrictive M1/M2 paradigm. Moving forward, we suggest that a more functional classification of macrophage subsets should be used to better represent their biology.

Phagocytosis can elicit significant effects on macrophage phenotype and function (19, 42). By showing that the proresolution macrophage phenotype can be promoted by ingestion of debris and that the increase in matrix-degrading activity is mediated by phagocytosis-induced ERK signaling, we have identified a potential therapeutic approach to manipulate these cells in situ. Crucially, our data showing that the in vivo phenotypic switch can be induced through phagocytosis of administered liposomes with a beneficial effect on fibrosis resolution identify a possible translational strategy for the treatment of tissue fibrosis. An attractive alternative therapeutic strategy would be the use of macrophages modified in vitro by feeding with liposomes to generate proresolution features as a cell therapy to induce fibrosis regression. This use would require modification of the macrophages to ensure adequate trafficking to the fibrotic liver after peripheral injection, but it remains an intriguing area for additional study.

In conclusion, we have identified and characterized a specific macrophage phenotype responsible for the resolution of tissue fibrosis. In addition to the value in studying macrophage biology, this study has important implications for fibrosis research and the future development of antifibrotic therapies aimed at targeting macrophages in vivo.

Materials and Methods

Mice. C57BL/6 mice ($CD45.2^+$) were purchased from Harlan. CD11B-DTR mice, originally obtained from R. Lang, Children's Hospital Research Foundation, Cincinnati, OH and as previously described (11), were maintained as heterozygotes on a C57BL/6 background. $CD45.1^+$ C57BL/6 mice (59) were provided by S. M. Anderton, University of Edinburgh. CD11C-DOG mice (28) were provided by A. S. MacDonald, University of Edinburgh. Mice were bred under specific pathogen-free conditions at the University of Edinburgh. All experiments had local ethical approval and were conducted under UK Home Office Legislation.

Liver Fibrosis Models. Adult male mice at least 6 wk of age were used. Hepatic fibrosis was induced by two times per week i.p. CCl_4 (0.4 μL/g; Sigma) diluted 1:3 in olive oil (Sigma) for 4 wk (nine injections). Animals were culled at stated time points after the final CCl_4 injection. For depletion studies, DT (10 ng/g in PBS; List Biological Laboratories) or PBS control was administered to fibrotic CD11B-DTR or WT mice i.v. through the tail vein at the stated time points. DC depletion in fibrotic CD11C-DOG mice was performed by administration of DT (12 ng/g) or PBS control i.p. at the stated time points. Adoptive transfer experiments were performed through the tail vein at stated time points using (*i*) 9×10^5 FACS-sorted $CD45.1^+$ Ly-$6C^{hi}$ monocytes from bone marrow in RPMI 1640 or vehicle control; (*ii*) 250 μL fluorescent latex beads [0.5 μm Fluoresbrite polychromatic red microspheres; 2.5% solids (wt/vol) diluted 1:25 in PBS for injection; Polysciences Inc] or vehicle control; and (*iii*) 250 μL liposomes (60) (provided by N.v.R.), CM-DiI–labeled (Invitrogen) liposomes (labeled according to the manufacturer's protocol), or PBS control.

Flow Cytometry and FACS Sorting. Flow cytometry (using BD LSR Fortessa II) and FACS sorting (using BD FACSAria II) were performed on hepatic nonparenchymal cells containing the total hepatic leukocyte population (*SI Materials and Methods*). FACS sorting routinely yielded cell purity levels of over 95%.

Detection of in Vivo MMP Activity. To detect in vivo MMP activity, 2 nmol MMPsense 680 (Perkin-Elmer) (or vehicle control) were administered to animals through the tail vein 24 h before harvest according to the manufacturer's protocol. Hepatic macrophages were identified using flow cytometry followed by identification of MMPsense-positive macrophages with excitation laser at 635 nm (23).

Microarray Analysis. Fifty nanograms RNA from FACS-sorted cells was processed using the Ovation Pico WTA system (NuGen) according to the manufacturer's protocol ($n = 3$ per group). Processed RNAs were hybridized to Affymetrix GeneChip Mouse Gene 1.0 ST Arrays. RNA/microarray processing was carried out by ARK Genomics (Roslin Institute). Data analysis was performed as described (*SI Materials and Methods*). Fold change > 2 with adjusted $P < 0.05$ was considered significant for individual gene changes. Gene ontology and Kyoto Encyclopedia of Genes and Genomes (KEGG) pathway enrichment analysis was done with the DAVID tool (36, 37) on genes that were significantly differentially expressed. Microarray data are available in the ArrayExpress database (www.ebi.ac.uk/arrayexpress) under accession number E-MEXP-3177.

In Vitro Phagocytosis Assay. BMDMs, primary murine hepatocyte debris, and apoptotic thymocytes were prepared as described (*SI Materials and Methods*); 2×10^5 BMDMs were seeded per well in 12-well plates followed by the addition of 5×10^5 washed dead hepatocytes (or control medium) and 1×10^6 washed dead thymocytes or liposomes at 1:10 dilution by volume (or PBS control) cultured for 16 h (or 12 h for thymocytes) at 37 °C 5% (vol/vol) CO_2 in DMEM/F12 Glutamax (Gibco) medium with 10% FCS. Where stated, inhibitors PD98059 (50 μM; Cayman Chemical), UO126 (20 μM; New England Biolabs), SB203580 (10 μM; Cayman Chemical), or DMSO control were added to the plated BMDMs for 1 h before and maintained throughout the 16-h incubation with hepatocyte debris. Supernatants were then harvested and stored at −80 °C, noningested hepatocytes or liposomes were removed by vigorous washing three times with PBS, and residual adherent macrophages were used for additional analysis. In control wells containing hepatocyte debris alone, no adherent cells were detected.

Statistical Analysis. All data are expressed as mean ± SEM. Statistical analysis was performed using GraphPad Prism 5 software. Statistical evaluation of multiple groups was performed using a one-way ANOVA with posthoc Tukey test. Statistical evaluation of two groups was performed using Student *t* test or Mann–Whitney test if data were not normally distributed. A value of $P < 0.05$ was considered statistically significant.

Additional Methods. Additional methods are shown in *SI Materials and Methods*.

ACKNOWLEDGMENTS. We thank Prof. S. M. Anderton for providing the CD45.1 mice and Dr. A. S. MacDonald for providing CD11c-DOG mice. P.R., M.A.V., and V.K.S. were supported by Wellcome Trust Research Training Fellowships. A.P., R.L.A., S.N.H., and J.P.I. were supported by a Medical Research Council Programme grant. L.B. was supported by a Medical Research Council PhD studentship. A.A. was supported by the Royal College of Surgeons of Edinburgh. T.T.G.-W. and M.J.W. were supported by Medical Research Council Research Training Fellowships. D.R.D. and J.R.M. were supported in part by the Edinburgh British Heart Foundation Centre of Research Excellence. J.A.F. was supported by the Academy of Medical Sciences and the Health Foundation. S.J.F. was supported by the Sir Jules Thorn Trust.

1. Hayden T (2011) Scarred by disease. *Nat Med* 17(1):18–20.
2. Wynn TA (2008) Cellular and molecular mechanisms of fibrosis. *J Pathol* 214(2): 199–210.
3. Ramachandran P, Iredale JP (2009) Reversibility of liver fibrosis. *Ann Hepatol* 8(4): 283–291.
4. Eddy AA (2005) Can renal fibrosis be reversed? *Pediatr Nephrol* 20(10):1369–1375.
5. Pickrell JA, Diel JH, Slauson DO, Halliwell WH, Mauderly JL (1983) Radiation-induced pulmonary fibrosis resolves spontaneously if dense scars are not formed. *Exp Mol Pathol* 38(1):22–32.
6. Gibbons MA, et al. (2011) Ly6Chi monocytes direct alternatively activated profibrotic macrophage regulation of lung fibrosis. *Am J Respir Crit Care Med* 184(5):569–581.
7. Tyralla K, et al. (2011) High-dose enalapril treatment reverses myocardial fibrosis in experimental uremic cardiomyopathy. *PLoS One* 6(1):e15287.
8. Wynn TA, Barron L (2010) Macrophages: Master regulators of inflammation and fibrosis. *Semin Liver Dis* 30(3):245–257.
9. Vernon MA, Mylonas KJ, Hughes J (2010) Macrophages and renal fibrosis. *Semin Nephrol* 30(3):302–317.
10. Hardie WD, Glasser SW, Hagood JS (2009) Emerging concepts in the pathogenesis of lung fibrosis. *Am J Pathol* 175(1):3–16.
11. Duffield JS, et al. (2005) Selective depletion of macrophages reveals distinct, opposing roles during liver injury and repair. *J Clin Invest* 115(1):56–65.
12. Fallowfield JA, et al. (2007) Scar-associated macrophages are a major source of hepatic matrix metalloproteinase-13 and facilitate the resolution of murine hepatic fibrosis. *J Immunol* 178(8):5288–5295.
13. Mosser DM, Edwards JP (2008) Exploring the full spectrum of macrophage activation. *Nat Rev Immunol* 8(12):958–969.
14. Mantovani A, et al. (2004) The chemokine system in diverse forms of macrophage activation and polarization. *Trends Immunol* 25(12):677–686.
15. Gordon S, Taylor PR (2005) Monocyte and macrophage heterogeneity. *Nat Rev Immunol* 5(12):953–964.
16. Ingersoll MA, et al. (2010) Comparison of gene expression profiles between human and mouse monocyte subsets. *Blood* 115(3):e10–e19.
17. Lin SL, Castaño AP, Nowlin BT, Lupher ML, Jr., Duffield JS (2009) Bone marrow Ly6Chigh monocytes are selectively recruited to injured kidney and differentiate into functionally distinct populations. *J Immunol* 183(10):6733–6743.
18. Nahrendorf M, et al. (2007) The healing myocardium sequentially mobilizes two monocyte subsets with divergent and complementary functions. *J Exp Med* 204(12): 3037–3047.
19. Arnold L, et al. (2007) Inflammatory monocytes recruited after skeletal muscle injury switch into antiinflammatory macrophages to support myogenesis. *J Exp Med* 204(5): 1057–1069.
20. Movahedi K, et al. (2010) Different tumor microenvironments contain functionally distinct subsets of macrophages derived from Ly6C(high) monocytes. *Cancer Res* 70(14):5728–5739.
21. Karlmark KR, et al. (2009) Hepatic recruitment of the inflammatory Gr1+ monocyte subset upon liver injury promotes hepatic fibrosis. *Hepatology* 50(1):261–274.
22. Holt MP, Cheng L, Ju C (2008) Identification and characterization of infiltrating macrophages in acetaminophen-induced liver injury. *J Leukoc Biol* 84(6):1410–1421.
23. Cortez-Retamozo V, et al. (2008) Real-time assessment of inflammation and treatment response in a mouse model of allergic airway inflammation. *J Clin Invest* 118(12):4058–4066.
24. Sunderkötter C, et al. (2004) Subpopulations of mouse blood monocytes differ in maturation stage and inflammatory response. *J Immunol* 172(7):4410–4417.
25. Bamboat ZM, et al. (2010) Conventional DCs reduce liver ischemia/reperfusion injury in mice via IL-10 secretion. *J Clin Invest* 120(2):559–569.
26. Jiao J, et al. (2012) Dendritic cell regulation of carbon tetrachloride-induced murine liver fibrosis regression. *Hepatology* 55(1):244–255.
27. Hume DA (2008) Macrophages as APC and the dendritic cell myth. *J Immunol* 181(9): 5829–5835.
28. Phythian-Adams AT, et al. (2010) CD11c depletion severely disrupts Th2 induction and development in vivo. *J Exp Med* 207(10):2089–2096.
29. Tacke F, et al. (2006) Immature monocytes acquire antigens from other cells in the bone marrow and present them to T cells after maturing in the periphery. *J Exp Med* 203(3):583–597.
30. Tacke F, et al. (2007) Monocyte subsets differentially employ CCR2, CCR5, and CX3CR1 to accumulate within atherosclerotic plaques. *J Clin Invest* 117(1):185–194.
31. Jenkins SJ, et al. (2011) Local macrophage proliferation, rather than recruitment from the blood, is a signature of TH2 inflammation. *Science* 332(6035):1284–1288.
32. Karlmark KR, et al. (2010) The fractalkine receptor CX_3CR1 protects against liver fibrosis by controlling differentiation and survival of infiltrating hepatic monocytes. *Hepatology* 52(5):1769–1782.
33. Heinrichs D, et al. (2011) Macrophage migration inhibitory factor (MIF) exerts antifibrotic effects in experimental liver fibrosis via CD74. *Proc Natl Acad Sci USA* 108 (42):17444–17449.
34. Breitkopf K, et al. (2005) Thrombospondin 1 acts as a strong promoter of transforming growth factor beta effects via two distinct mechanisms in hepatic stellate cells. *Gut* 54(5):673–681.
35. Sobrevals L, et al. (2010) Insulin-like growth factor I gene transfer to cirrhotic liver induces fibrolysis and reduces fibrogenesis leading to cirrhosis reversion in rats. *Hepatology* 51(3):912–921.
36. Dennis G, Jr., et al. (2003) DAVID: Database for Annotation, Visualization, and Integrated Discovery. *Genome Biol* 4(5):3.
37. Huang W, Sherman BT, Lempicki RA (2009) Systematic and integrative analysis of large gene lists using DAVID bioinformatics resources. *Nat Protoc* 4(1):44–57.
38. Anstee QM, Wright M, Goldin R, Thursz MR (2009) Parenchymal extinction: Coagulation and hepatic fibrogenesis. *Clin Liver Dis* 13(1):117–126.
39. Sahin H, Trautwein C, Wasmuth HE (2010) Functional role of chemokines in liver disease models. *Nat Rev Gastroenterol Hepatol* 7(12):682–690.
40. Lawrence T, Natoli G (2011) Transcriptional regulation of macrophage polarization: Enabling diversity with identity. *Nat Rev Immunol* 11(11):750–761.
41. Martinez FO, Gordon S, Locati M, Mantovani A (2006) Transcriptional profiling of the human monocyte-to-macrophage differentiation and polarization: New molecules and patterns of gene expression. *J Immunol* 177(10):7303–7311.
42. Savill J, Dransfield I, Gregory C, Haslett C (2002) A blast from the past: Clearance of apoptotic cells regulates immune responses. *Nat Rev Immunol* 2(12):965–975.
43. Henson PM, Bratton DL, Fadok VA (2001) Apoptotic cell removal. *Curr Biol* 11(19): R795–R805.
44. Newman SL, Henson JE, Henson PM (1982) Phagocytosis of senescent neutrophils by human monocyte-derived macrophages and rabbit inflammatory macrophages. *J Exp Med* 156(2):430–442.
45. Marim FM, Silveira TN, Lima DS, Jr., Zamboni DS (2010) A method for generation of bone marrow-derived macrophages from cryopreserved mouse bone marrow cells. *PLoS One* 5(12):e15263.
46. Ferenbach DA, et al. (2010) Macrophages expressing heme oxygenase-1 improve renal function in ischemia/reperfusion injury. *Mol Ther* 18(9):1706–1713.
47. Kurosaka K, Takahashi M, Kobayashi Y (2003) Activation of extracellular signal-regulated kinase 1/2 is involved in production of CXC-chemokine by macrophages during phagocytosis of late apoptotic cells. *Biochem Biophys Res Commun* 306(4):1070–1074.
48. Chung EY, et al. (2007) Interleukin-10 expression in macrophages during phagocytosis of apoptotic cells is mediated by homeodomain proteins Pbx1 and Prep-1. *Immunity* 27(6):952–964.
49. Raza SL, Nehring LC, Shapiro SD, Cornelius LA (2000) Proteinase-activated receptor-1 regulation of macrophage elastase (MMP-12) secretion by serine proteinases. *J Biol Chem* 275(52):41243–41250.
50. Valledor AF, Comalada M, Xaus J, Celada A (2000) The differential time-course of extracellular-regulated kinase activity correlates with the macrophage response toward proliferation or activation. *J Biol Chem* 275(10):7403–7409.
51. Chi H, et al. (2006) Dynamic regulation of pro- and anti-inflammatory cytokines by MAPK phosphatase 1 (MKP-1) in innate immune responses. *Proc Natl Acad Sci USA* 103(7):2274–2279.
52. Perry DG, Martin WJ, 2nd (1995) Fluorescent liposomes as quantitative markers of phagocytosis by alveolar macrophages. *J Immunol Methods* 181(2):269–285.
53. Ma HM, Wu Z, Nakanishi H (2011) Phosphatidylserine-containing liposomes suppress inflammatory bone loss by ameliorating the cytokine imbalance provoked by infiltrated macrophages. *Lab Invest* 91(6):921–931.
54. Harel-Adar T, et al. (2011) Modulation of cardiac macrophages by phosphatidylserine-presenting liposomes improves infarct repair. *Proc Natl Acad Sci USA* 108(5): 1827–1832.
55. Friedman SL (2005) Mac the knife? Macrophages—the double-edged sword of hepatic fibrosis. *J Clin Invest* 115(1):29–32.
56. Wynn TA (2011) Integrating mechanisms of pulmonary fibrosis. *J Exp Med* 208(7): 1339–1350.
57. Vielhauer V, Kulkarni O, Reichel CA, Anders HJ (2010) Targeting the recruitment of monocytes and macrophages in renal disease. *Semin Nephrol* 30(3):318–333.
58. Mitchell C, et al. (2009) Dual role of CCR2 in the constitution and the resolution of liver fibrosis in mice. *Am J Pathol* 174(5):1766–1775.
59. O'Connor RA, Leech MD, Suffner J, Hämmerling GJ, Anderton SM (2010) Myelin-reactive, TGF-β-induced regulatory T cells can be programmed to develop Th1-like effector function but remain less proinflammatory than myelin-reactive Th1 effectors and can suppress pathogenic T cell clonal expansion in vivo. *J Immunol* 185(12): 7235–7243.
60. Van Rooijen N, Sanders A (1994) Liposome mediated depletion of macrophages: Mechanism of action, preparation of liposomes and applications. *J Immunol Methods* 174(1–2):83–93.

Supporting Information

Ramachandran et al. 10.1073/pnas.1119964109

SI Materials and Methods

Hepatic Nonparenchymal Cell Isolation. Isolation of hepatic nonparenchymal cell (NPC) fraction was performed using a modified MACS protocol (http://www.miltenyibiotec.com/download/protocols_gentlemacs_en/1105/gentleMACS-Liver-04.pdf) from Miltenyi Biotech. Briefly, mouse livers in situ were perfused with 10 mL 0.9% NaCl solution through the inferior vena cava followed by cutting of the portal vein to remove circulating cells. Livers were then harvested and weighed; either the whole liver or the right lobe was homogenized using a scalpel and digested in RPMI 1640 containing Collagenase B (1.6 mg/mL; Roche) and DNase I (100 μg/mL; Roche) for 45 min at 37 °C. Digested livers were passed through 40-μm cell strainers, and enzymes were inactivated by the addition of RPMI 1640 with 10% FCS. Contaminating hepatocytes were removed by two-time centrifugation at 50,000 × *g* for 5 min followed by red cell lysis with lysis buffer (0.15 M NH_4Cl, 10 mM $KHCO_3$, 0.1 mM EDTA in H_2O) for 5 min on ice. The remaining nonparenchymal cell fraction containing hepatic macrophages was then harvested by centrifugation at 300,000 × *g* for 10 min, counted, and used for flow cytometry and FACS sorting.

Flow Cytometry and FACS Sorting. Nonspecific antibody binding was blocked by incubating cells with 10% mouse serum for 20 min at 4 °C followed by incubation with combinations of primary antibodies (each used at 1/100 dilution unless stated) for 30 min at 4 °C. The following preconjugated antibodies were used: CD11B (clone M1/70; Ebioscience), CD11C (clone N418; Ebioscience), Ly-6C (clone HK1.4; Ebioscience), CD45.2 (clone 104; Ebioscience), CD45.1 (clone A20; Ebioscience), CD115 (clone AFS98; Ebioscience), CD36 (clone 72–1; Ebioscience), F4/80 (dilution 1:50; clone BM8; Invitrogen), Ly-6G (clone 1A8; Biolegend), CD3 (clone 17A2; Biolegend), NK1.1 (clone PK136; Biolegend), B220 (clone RA3-6B2; Biolegend), CD14 (clone Sa14-2; Biolegend), CD16/32 (dilution 1:200; clone 93; Biolegend), CD80 (clone 16–10A1; Biolegend), CD86 (clone GL-1; Biolegend), and CD81 (clone Eat-1; Biolegend). Cell viability was assessed with Propidium Iodide (Sigma) or Fixable Viability Dye eFluor780 (Ebioscience) according to manufacturers' protocols. K_i-67 staining for flow cytometric analysis was performed as described (1) using the K_i-67 staining kit (clone B56; BD) and the Fix and Perm Kit (Ebioscience). After antibody staining, samples were either analyzed immediately or fixed with 10% buffered formalin. Data were analyzed using FlowJo7.5 software (Treestar).

Hepatic macrophages were defined as viable $CD45^+$ Ly-$6G^-$ $CD3^-$ $NK1.1^-$ $B220^-$ $CD11B^+$ $F4/80^+$ cells from NPC fraction of digested livers and used to identify macrophage subsets. Subsets were expressed as proportions of total hepatic macrophages or $CD45^+$ cells. Quantification of absolute numbers of cells per liver was performed by expressing each subset as a proportion of NPCs, counting total number of NPCs in the digested portion of liver, calculating the total number of NPCs in the whole liver by weight differential, and thus, calculating the total number of each subset. Where stated, these values were expressed relative to the mean of the control liver, which was assigned a value of one.

Circulating monocytes (from whole blood diluted 1:1 in 4.8% sodium citrate buffer) were stained and fixed using BD FACSlyse (BD) before analysis. Monocytes were identified as $CD45^+$ $CD115^+$ $CD11B^+$ Ly-$6G^-$ Ly-$6C^{hi}$ and Ly-$6C^{lo}$ cells from whole blood and expressed as a percentage of total peripheral mononuclear cells or a number of cells per 1 mL blood using counting beads.

FACS-sorted viable $CD45.1^+$ Ly-$6G^-$ $CD115^+$ $CD11B^+$ Ly-$6C^{hi}$ monocytes from whole bone marrow were used for adoptive transfer experiments.

Microarray Data Analysis. Data were extracted through the GCOS software, and CEL files were used for additional data processing. CEL files were imported into Bioconductor (2), normalized by robust multi-array average (RMA) in the Oligo (http://www.bioconductor.org/packages/2.0/bioc/html/oligo.html) module, and statistically analyzed with the Limma (3).

RNA Extraction and Quantitative RT-PCR. For whole liver, the caudate lobe was snap frozen in liquid nitrogen and stored at −80 °C. RNA was extracted using TRIzol reagent (Invitrogen) and RNeasy mini columns (Qiagen) according to the manufacturer's protocol, followed by quantification using the Nanodrop Spectrophotometer (Thermo Scientific); 1 μg RNA was reverse-transcribed using SuperScript III (Invitrogen) according to the manufacturer's protocol. Gene expression was calculated using the $\Delta\Delta C_T$ method relative to housekeeping gene 18S.

For FACS-sorted cells, RNA was extracted using the RNeasy Micro Plus Kit (Qiagen) according to the manufacturer's protocol; 10 ng RNA were reverse-transcribed and amplified using the Whole Transcriptome Kit (Qiagen). Gene expression was calculated using the $\Delta\Delta C_T$ method relative to housekeeping gene β2M.

For the in vitro phagocytosis assay, RNA was extracted using the Rneasy Micro Plus Kit (Qiagen), and 100 ng RNA were reverse-transcribed using SuperScript III (Invitrogen). Gene expression was calculated using the $\Delta\Delta C_T$ method relative to housekeeping gene β2M.

Where stated, relative gene expression was calculated by normalizing to the mean expression of one group, which was assigned a value of one.

The following primer sets were purchased—18S, B2M, Chi3l3, Chemokine (C-C motif) receptor 2 (Ccr2), and Chemokine (C-X3-C) receptor 1 (Cx3cr1) from Applied Biosystems and insulin-like growth factor 1 (Igf1), Thbs1, Il-1β, and Cxcl10 from Qiagen. The remaining primer sequences were designed using primer express software, and the sequences are available. Genes were analyzed using either TaqMan Express qPCR Supermix (Invitrogen) or Quantifast SYBR Green PCR Kit (Qiagen) on an ABI 7500 Fast Real-Time System according to the manufacturers' instructions.

Immunohistochemistry and Immunofluorescence. After harvest, liver tissue was fixed overnight in 10% neutral buffered formalin or Methacarn solution followed by paraffin embedding. Human cirrhotic liver was fixed in formalin; 4-μm tissue sections were dewaxed and rehydrated in decreasing concentrations of ethanol. Where stated, antigen retrieval was performed by boiling for 15 min in 10 mM sodium citrate buffer, pH 6. Endogenous peroxidize activity was inhibited with 3% hydrogen peroxide, and nonspecific binding was minimized using protein block solution (Dako). All primary antibodies were incubated overnight at 4 °C. Appropriate biotinylated secondary antibodies were used at 1/300 dilution at room temperature for 1 h. Immunostaining was developed using 3,3′-diaminobenzidine (Dako). The following primary antibodies and conditions were used: collagen 1 (1310–08; 1/100 dilution; formalin-fixed; antigen retrieval; Southern Biotech), collagen 3 (1310–01; 1/100 dilution; formalin-fixed; antigen retrieval; Southern Biotech), α-smooth muscle actin (α-SMA; clone 1A4; 1/4,000 dilution; formalin-fixed; antigen retrieval; Sigma-Aldrich), F4/80 (ab6640; 1/200 dilution; formalin-fixed; no antigen

retrieval; Abcam), Chi3l3 (01404; 1/100 dilution; formalin-fixed; antigen retrieval; Stemcell Technologies), metalloproteinase enzyme 12 (MMP-12; sc-8839; 1/240 dilution; formalin-fixed; 20 min antigen retrieval; Santa Cruz), murine and human Glycoprotein (transmembrane) nmb (Gpnmb) (sc-47006; 1/200 dilution; formalin-fixed; 15 min antigen retrieval; Santa Cruz), and human MMP-12 (AB52897; 1/400 dilution; 20 min antigen retrieval by boiling in Tris·EDTA, pH 9; Abcam). Picrosirius red staining was performed according to standard protocols. Where stated, morphometric pixel analysis to quantify histological staining was performed. Briefly, sections were blinded, and a minimum of 20 nonoverlapping fields per section were photographed at 100× magnification using a Nikon Eclipse E600 microscope and NIS-Elements D3.1 Software. Pixel counts of positive staining were performed in Adobe Photoshop CS2 and expressed as a percentage of the total pixel count. Where stated, relative percent area was calculated by normalizing to the mean the percent area of one group, which was assigned a value of one. Where stated, cell counts were performed at 200× magnification on blinded slides, with a minimum of 20 fields counted per mouse.

Dual immunofluorescence for F4/80 and phospho-ERK was performed on formalin-fixed paraffin-embedded sections, sequentially incubated with F4/80 (ab6640; Abcam) at 1:100 for 2 h, and rinsed; then, rabbit anti-rat HRP (P0450; Dako) was added followed by the TSAT Plus Cyanine 3 System (NEL744B001KT; PerkinElmer). Sections were then antigen-retrieved for 10 min with 10 mM sodium citrate buffer and blocked again. The second primary antibody pERK (4370; Cell Signaling) was incubated at 1:100 overnight followed by donkey anti-rabbit Alexa 488 (A21206; Invitrogen). Sections were mounted in DAPI hard-set mounting medium (H1500; Vector Labs).

For dual immunofluorescence on human tissue for CD68 and MMP-12, antigen retrieval (20 min; Tris·EDTA, pH 9) was followed by protein block (X0909; Dako), sequential incubation with anti–MMP-12 (ab52897; 1/100 dilution; overnight; Abcam) and donkey anti-rabbit Alexa 488 (A21206; Invitrogen), protein block, anti-CD68 (M0867; 1/50 dilution; 2 h; Dako), and donkey anti-mouse Alexa 555 (A31570; Invitrogen). For CD68 and GPNMB, antigen retrieval (15 min; Tris·EDTA, pH 9) was followed by protein block (X0909; Dako), sequential incubation of GPNMB (sc47006; 1/100 dilution; overnight; Santa Cruz), donkey anti-goat Alexa 488 (A11055; Invitrogen), protein block, anti-CD68 (M0867; 1/50 dilution; 2 h; Dako), and donkey anti-mouse Alexa 555 (A31570; Invitrogen). For both, sections were then blocked with 0.1% Sudan Black B (Sigma) and mounted with DAPI hard-set mounting medium (H1500; Vector Labs).

Immunocytochemistry. TUNEL staining of FACS-sorted Ly-6C^{hi} and Ly-6C^{int} macrophage subsets was performed using TACS TdT-Fluor in Situ Apoptosis Detection Kit—Fluorescein (R&D Systems) according to the manufacturer's protocol. The association between apoptotic debris and macrophages was assessed using a Leica SP5 Confocal microscope with z-stacks on each field. Images were blinded and analyzed using ImageJ software for the presence of cell surface or intracellular apoptotic debris. A minimum of 25 macrophages was counted per slide. The percentage of macrophages associated with TUNEL-positive nuclei was quantified followed by quantification of the localization of the apoptotic debris.

Western Blotting, Zymography, and ELISA. For tissue inhibitor of metalloproteinase 1 (TIMP-1) Western blotting, whole-tissue protein extracts were made by homogenization of samples in lysis buffer (50 mM Hepes, 1mM DTT, 0.1 mM EDTA, 0.1% CHAPS, pH 7.4). Protein concentration was determined by Bradford Assay, and equal amounts (20 μg protein/well) were subjected to SDS/PAGE on 12% gels. After electrophoresis, samples were transferred onto nitrocellulose membranes and blocked for 2 h at room temperature in 5% nonfat dry milk in Tris-buffered saline and 0.1% Tween (TBST). Membranes were incubated overnight at 4 °C with primary antibody in TBST containing 5% BSA (TIMP-1 at 1:500 dilution; 7–6C1; Calbiochem). Membranes were then washed (three times for 15 min each) in TBST before the addition of an HRP-conjugated secondary antibody (1:2,000 dilution) in TBST containing 5% nonfat dry milk for 1 h at room temperature. After incubation, membranes were washed again (three times) in TBST for 15 min each followed by development using enhanced chemiluminescence (ECLplus; Amersham) and visualization on a VersaDoc.

For Western blotting and zymography on in vitro phagocytosis assays, culture supernatants were harvested. Protein levels were quantified using Bradford reagent (Sigma-Aldrich) and equalized with PBS to ensure equal protein loading. Gelatin zymography was performed as previously described (4). Briefly, samples were subjected to electrophoresis on a 10% SDS/PAGE gel copolymerized with 1% gelatin substrate. After electrophoresis, gels were renatured in 2.5% Triton X-100 for 30 min before incubation in activity buffer [50 mM Tris, 200 mM NaCl, 5 mM CaCl2 (anhydrous), 0.02% Brij-35, pH 7.5] at 37 °C for 16–24 h. Gels were then stained with 0.5% Coomassie Brilliant Blue before destaining in 40% methanol and 10% acetic acid. MMP-9 gelatinolytic activity was detected as destained bands against a background of Coomassie-stained gelatin. The active form of MMP-9 was detected at 92 kDa. Casein zymography was performed as previously described (5) with minor modifications. Equalized culture supernatants were subjected to electrophoresis on a 12% SDS/PAGE gel containing 0.25% skimmed milk powder. After electrophoresis, gels were rinsed in deionized water and renatured in 2.5% Triton X-100 for 1 h before incubation in activity buffer (50 mM Tris, 200 mM NaCl, 5 mM $CaCl_2$, 0.02% Brij-35, pH 7.5) at 37 °C for 72 h. Subsequently, the gel was stained with SimplyBlue Safe Stain (Life Technologies) before destaining in water. Proteolytic activity was detected as destained bands against a background of Coomassie-stained casein. For MMP-12 Western blotting, media from the phagocytosis assay were freeze-dried, and equalized resuspended samples were subjected to SDS/PAGE on a 10% gels. After electrophoresis, samples were transferred onto nitrocellulose membranes and blocked for 2 h at room temperature in 3% BSA (Sigma-Aldrich) in TBST. Membranes were incubated overnight at 4 °C with primary antibody in TBST containing 3% BSA (MMP-12 at 1:1,000 dilution; SA453-0100; Biomol). Membranes were then washed (three times for 10 min each) in TBST before the addition of an HRP-conjugated secondary antibody (1:2,000 dilution) in TBST containing 5% nonfat dry milk for 1 h at room temperature. After incubation, membranes were washed again (three times) in TBST for 10 min each followed by development using Immobilon Western Chemiluminescent HRP Substrate (Millipore) and visualization on a VersaDoc Imaging system (BioRad).

For tissue cytokine ELISA, whole-tissue protein extracts were made in Tissue Protein Extraction Reagent (T-PER; Thermo Scientific), containing protease inhibitors aprotinin, leupeptin, and PMSF. A Bradford assay was performed, and samples were equalized to a total protein concentration of 50 μg/μL. These samples were then assayed using Bio-plex mouse cytokine assay (Bio-Rad) according to the manufacturer's protocol.

Serum Analysis. At the time of harvest, whole blood was collected from the inferior vena cava, and serum was isolated by centrifugation at 7,000 × *g* for 5 min and analyzed for alanine aminotransferase and aspartate aminotransferase levels using a standard bioanalyser.

In Vitro Phagocytosis Assay. Bone marrow-derived macrophages (BMDMs) were prepared as described (6) from adult male C57BL/6 mice by differentiating whole bone marrow for 7 d at 37 °C

5% CO_2 in DMEM/F12 Glutamax (Gibco) medium with 10% FCS and 20% L929 conditioned medium under nonadherent conditions using Ultra Low Adherence Flasks (Corning). This process routinely yielded a macrophage population of >90% purity as assessed by flow cytometry for CD11B and F4/80.

Primary murine hepatocytes were prepared using a modified two-stage perfusion technique (http://tools.invitrogen.com/content/sfs/manuals/3736.pdf). Briefly, adult male C57BL/6 mice were anesthetized with i.p. ketamine and medetomidine. After cannulation of the portal vein, livers were perfused with 50 mL Liver Perfusion Medium (Gibco) followed by 50 mL Liver Digestion Medium (Gibco). Livers were dissociated, and hepatocytes were washed three times in hepatocyte wash medium (Gibco) and cultured overnight at 37 °C 5% CO_2 on collagen-coated (10 μg/cm^2 rat tail collagen; Sigma) tissue culture flasks in Williams E medium (Gibco) supplemented with 10% FCS and 1% Pen/Strep solution. For preparation of hepatocyte debris, adherent viable hepatocytes were detached using trypsin, washed, and cultured in suspension in serum-free Williams E medium containing anti-mouse CD95 (1/500 dilution; Clone Jo-2; BD Pharmingen) at 37 °C for 8 h. This preparation yielded a population of >95% trypan blue-positive hepatocytes.

Apoptotic thymocytes were prepared as previously described (7). Briefly, thymuses were removed from C57BL/6 mice, ages 3–5 wk, homogenized in RPMI medium, and incubated with dexamethasone (1 μM; Mayne Pharma) and 1% FCS at 37 °C 5% CO_2 for 16 h. This process routinely yielded a population of dead thymocytes with over 90% trypan blue-positive.

1. Jenkins SJ, et al. (2011) Local macrophage proliferation, rather than recruitment from the blood, is a signature of TH2 inflammation. *Science* 332(6035):1284–1288.
2. Gentleman RC, et al. (2004) Bioconductor: Open software development for computational biology and bioinformatics. *Genome Biol* 5(10):R80.
3. Smyth GK (2004) Linear models and empirical bayes methods for assessing differential expression in microarray experiments. *Stat Appl Genet Mol Biol* 3:Article3.
4. Souza-Tarla CD, Uzuelli JA, Machado AA, Gerlach RF, Tanus-Santos JE (2005) Methodological issues affecting the determination of plasma matrix metalloproteinase (MMP)-2 and MMP-9 activities. *Clin Biochem* 38(5):410–414.
5. Pöppelmann M, Becker WM, Petersen A (2002) Combination of zymography and immunodetection to analyze proteins in complex culture supernatants. *Electrophoresis* 23(7–8):993–997.
6. Henderson NC, et al. (2008) Galectin-3 expression and secretion links macrophages to the promotion of renal fibrosis. *Am J Pathol* 172(2):288–298.
7. Ferenbach DA, et al. (2010) Macrophages expressing heme oxygenase-1 improve renal function in ischemia/reperfusion injury. *Mol Ther* 18(9):1706–1713.

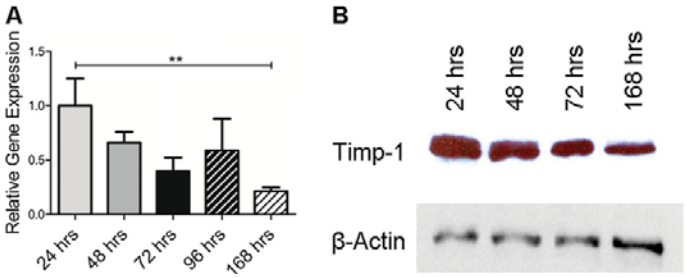

Fig. S1. Fibrosis regression follows a reduction in hepatic TIMP-1. Whole-liver Timp-1 levels were measured at stated time points after the final CCl_4 injection after 4 wk of chronic injury. (*A*) Gene expression by quantitative PCR expressed relative to mean expression at the 24-h time point (n = 4–8 from two independent experiments). (*B*) TIMP-1 protein expression by Western blot (representative blot shown). All data shown as mean ± SEM. $^{**}P < 0.01$.

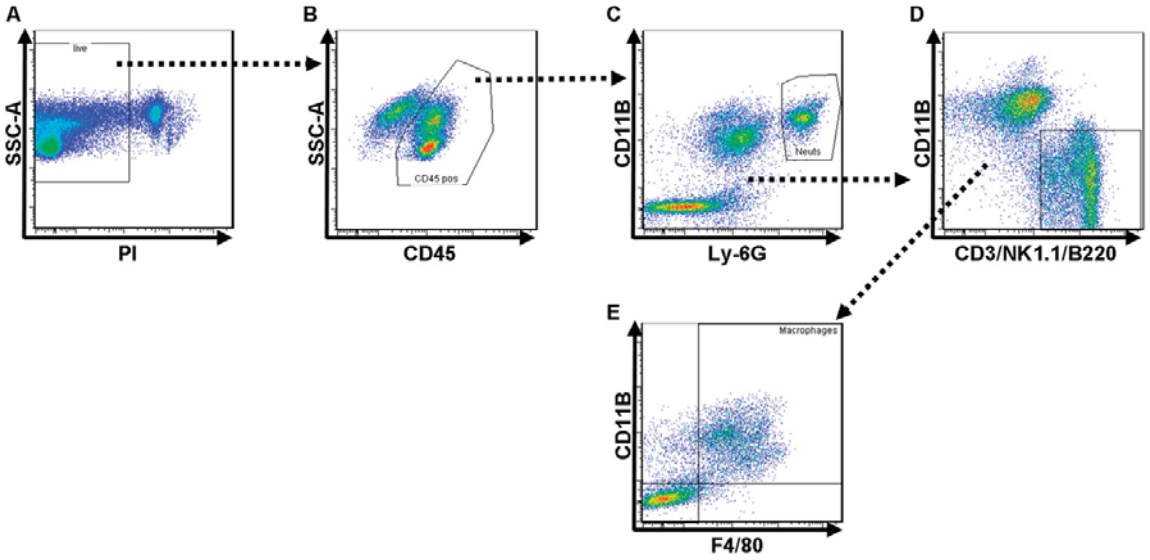

Fig. S2. Gating strategy for identification of hepatic macrophages. The hepatic nonparenchymal cell fraction was isolated as detailed in *Materials and Methods*. (*A*) Viable cells were selected by propidium iodide (PI) exclusion. (*B*) CD45-positive viable cells were gated. (*C*) Neutrophils were identified as viable CD45+ CD11b+ and Ly-6G+ cells, and they were excluded from subsequent macrophage gating. (*D*) Cells positive for CD3, B220, or NK1.1 were excluded from subsequent macrophage gating. (*E*) Macrophages were selected as viable CD45+ Ly-6G− NK1.1− B220− CD3− and dual-positive CD11B+ F4/80+ cells. Representative flow cytometry plots are shown.

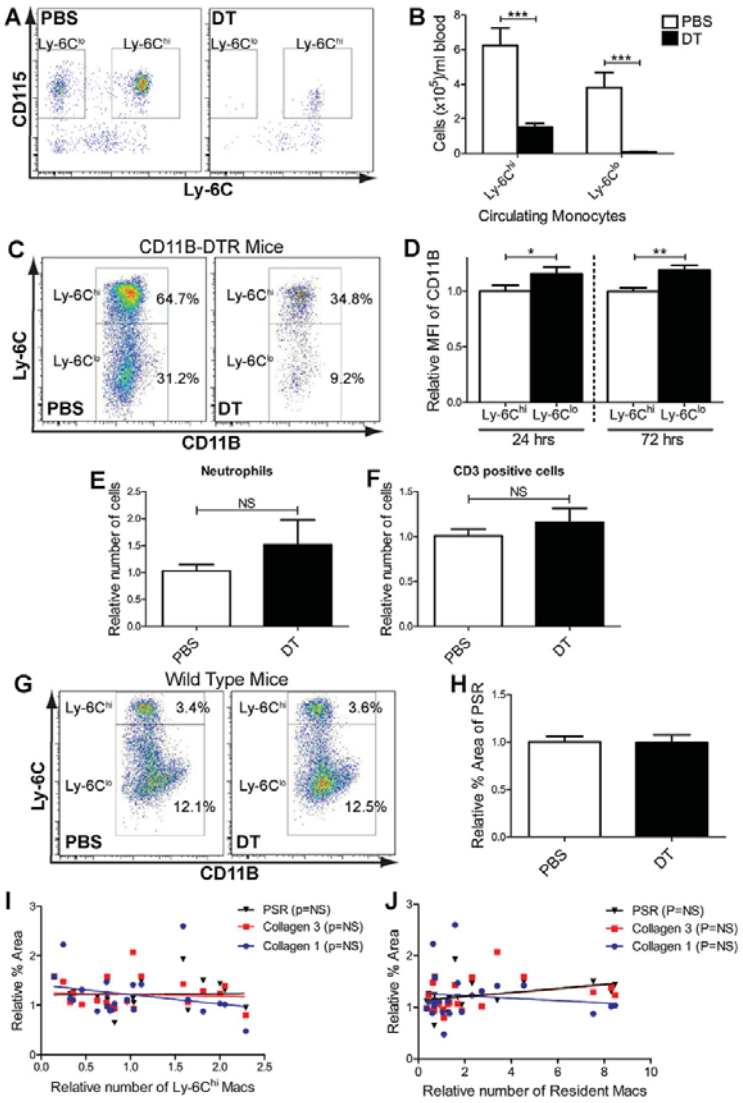

Fig. S3. Macrophage depletion in *CD11B* promoter–diphtheria toxin receptor (CD11B-DTR) transgenic mice is selective. (*A*, *B*, *E*, *F*, *I*, and *J*) Model of macrophage depletion during fibrosis resolution in CD11B-DTR mice after 4 wk of injury by administration of diphtheria toxin (DT; or PBS control) 48. 72, and 96 h after the final CCl_4 injection with harvest at 120 h. (*A*) Analysis of circulating monocytes by flow cytometry. Ly-6C^{hi} and Ly-6C^{lo} circulating monocytes were identified in blood gating on CD11B+ Ly-6G− CD115+ Ly-6C^{hi} and Ly-6C^{lo} cells. (*B*) Ly-6C^{hi} and Ly-6C^{lo} circulating monocyte number per 1 ml blood in CD11B-DTR mice given DT or PBS control (n = 11–13 from two independent experiments). (*C*) Macrophage depletion during inflammation/fibrogenesis phase. CD11B-DTR mice were injured with CCl_4 followed by administration of DT (or PBS control) 8 h after the final CCl_4 injection with harvest at 24 h. Analysis of hepatic macrophage subsets after DT or PBS administration (data shown as percentage of mean total hepatic macrophage number in PBS-treated animals; n = 2). (*D*) CD11B expression of Ly-6C^{hi} and Ly-6C^{lo} hepatic macrophages in WT mice after 4 wk of CCl_4 was assessed 24 and 72 h after the final CCl_4 injection by flow cytometry expressed as mean fluorescence intensity (MFI) of CD11B relative to mean CD11B MFI of Ly-6C^{hi} macrophages at the stated time point (n = 14–15). (*E*) Quantification of the number of hepatic neutrophils in DT- and PBS-treated mice expressed relative to total neutrophil number in PBS-treated livers (n = 11–13 from two independent experiments). (*F*) Quantification of the number of hepatic CD3-positive cells in DT- and PBS-treated mice expressed relative to total CD3 cell number in PBS-treated livers (n = 11–13 from two independent experiments). (*G* and *H*) Administration of DT or PBS to WT mice after 4 wk of injury at 48, 72, and 96 h after the final CCl_4 injection with harvest at 120 h. (*G*) Analysis of hepatic macrophage subsets in WT mice receiving DT or PBS. (*H*) Quantification of fibrosis in WT mice receiving DT or PBS by picrosirius red staining and morphometric pixel analysis expressed relative to mean percentage area for PBS-treated liver (n = 2). (*I*) Correlation of the degree of fibrosis assessed by picrosirius red staining, collagen 1, and collagen 3 percent area with the relative number of hepatic Ly-6C^{hi} macrophages in CD11B-DTR mice (n = 22 from two independent experiments). (*J*) Correlation of degree of fibrosis assessed by picrosirius red staining, collagen 1, and collagen 3 percent area with the relative number of resident hepatic macrophages in CD11B-DTR mice (n = 22 from two independent experiments). All data shown as mean ± SEM. *P < 0.05, **P < 0.01, ***P < 0.001. NS, nonsignificant. Representative flow cytometry plots and percentages are shown.

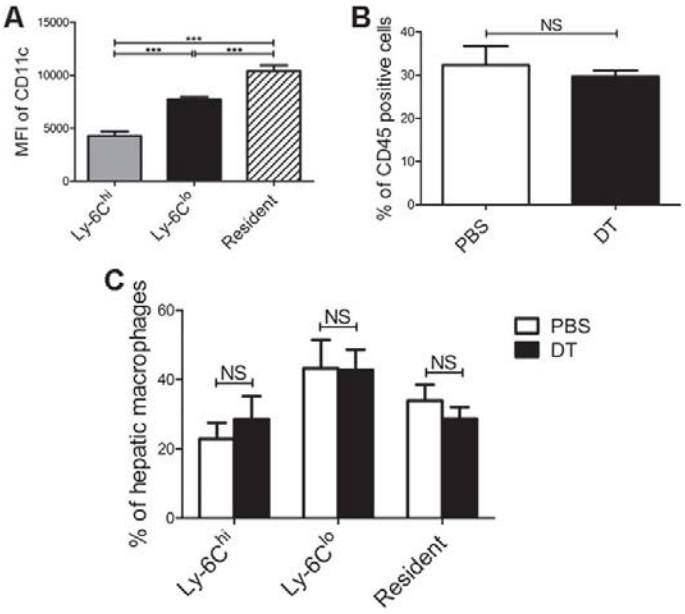

Fig. S4. Minimal contribution of dendritic cells to macrophage subsets. (*A*) CD11c expression of each macrophage subset 72 h after the final CCl_4 injection after 4 wk of injury expressed as MFI of CD11c assessed by flow cytometry (n = 5). Data indicate intermediate CD11c expression of proresolution Ly-6C^{lo} macrophage subsets. (*B* and *C*) Adult male CD11c.DOG mice were administered two time per week i.p. CCl_4 for 4 wk followed by 12 ng/g diphtheria toxin (or PBS control) 48 and 72 h after the final CCl_4 injection. Mice were harvested at 96 h. (*B*) Quantification of total hepatic macrophage number as a proportion of CD45-positive hepatic nonparenchymal cells after DT or PBS control (n = 7). Data indicate no depletion of hepatic macrophages by administering DT to CD11c.DOG mice. (*C*) Quantification of the number of each macrophage subset as a proportion of total hepatic macrophages after DT or PBS control (n = 7). Data indicate no depletion of macrophage subsets after DT administration to CD11c.DOG mice. All data shown as mean ± SEM. ***$P < 0.001$.

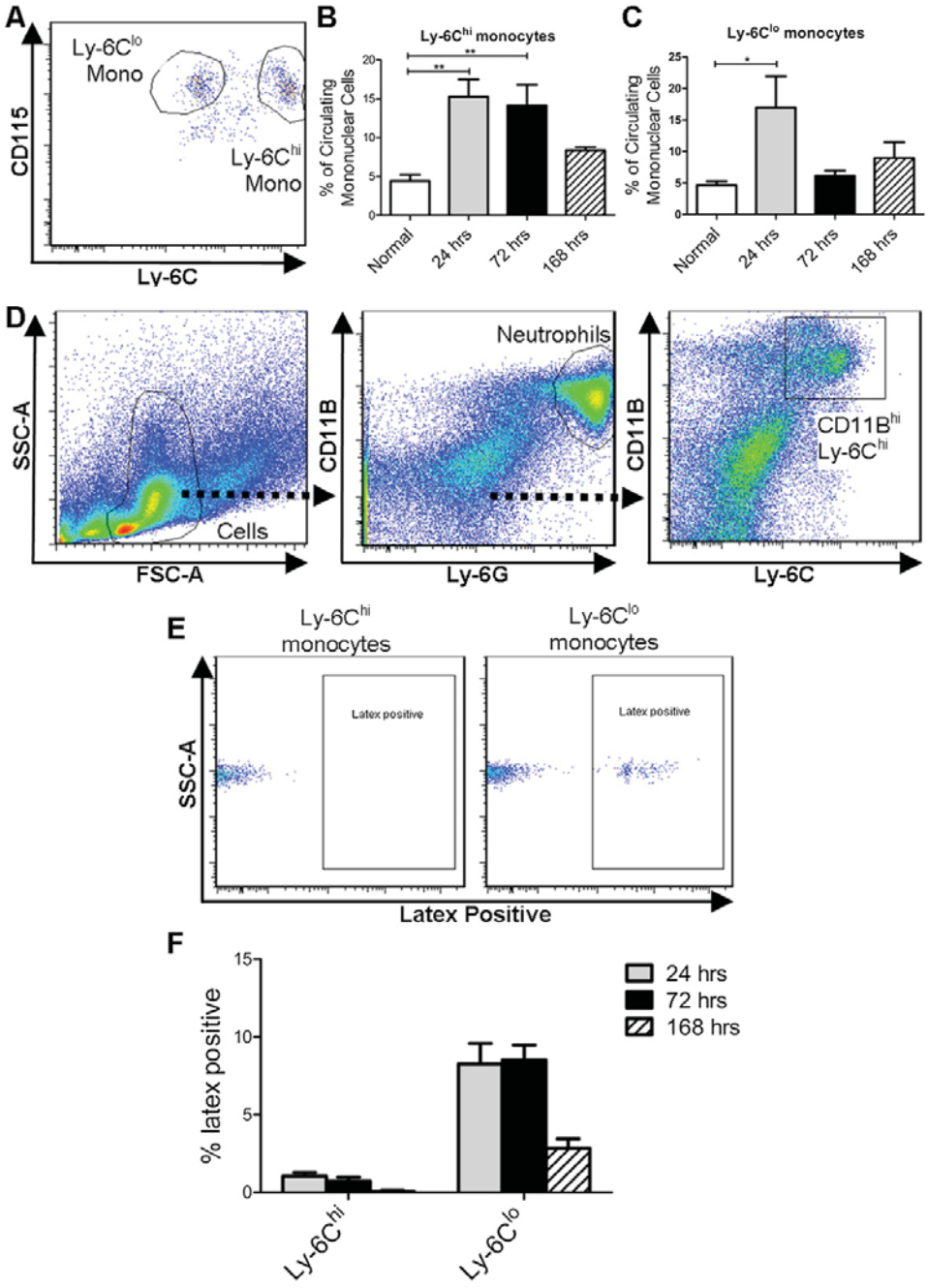

Fig. S5. Contribution of circulating monocytes to restorative macrophage population. (*A*) Ly-6C^{hi} and Ly-6C^{lo} circulating monocytes were identified in blood gating on CD11B+ Ly-6G– CD115+ Ly-6C^{hi} and Ly-6C^{lo} cells. (*B*) Ly-6C^{hi} monocytes were quantified as a proportion of total circulating mononuclear cells at stated time points during injury and resolution after chronic CCl_4 administration and normal (uninjured control) mice ($n = 5$). (*C*) Ly-6C^{lo} monocytes were quantified as a proportion of total circulating mononuclear cells during injury and resolution after chronic CCl_4 administration and normal (uninjured control) mice ($n = 5$). (*D*) Ly-6C^{hi} monocytes for adoptive transfer were isolated by FACS sorting of whole bone marrow from male CD45.1+ C57BL/6 mice gating on the cells [excluding the neutrophils (CD11B+ Ly-6G+) and selecting CD115+ CD11B+ Ly-6C^{hi} cells]. (*E* and *F*) Administration of fluorescent latex beads through the tail vein 4 h after the final CCl_4 injection after 4 wk of injury, with harvest of peripheral blood at 24, 72, and 168 h. (*E*) Flow cytometry analysis of Ly-6C^{hi} and Ly-6C^{lo} monocytes (monocyte populations identified as in *A*) showed fluorescent latex beads predominantly in circulating Ly-6C^{lo} monocytes. (*F*) Quantification of the proportion of circulating Ly-6C^{hi} and Ly-6C^{lo} monocytes containing latex beads as assessed by flow cytometry at the stated time points after the final CCl_4 injection. All data are expressed as mean ± SEM. $^*P < 0.05$, $^{**}P < 0.01$. Representative flow cytometry plots are shown.

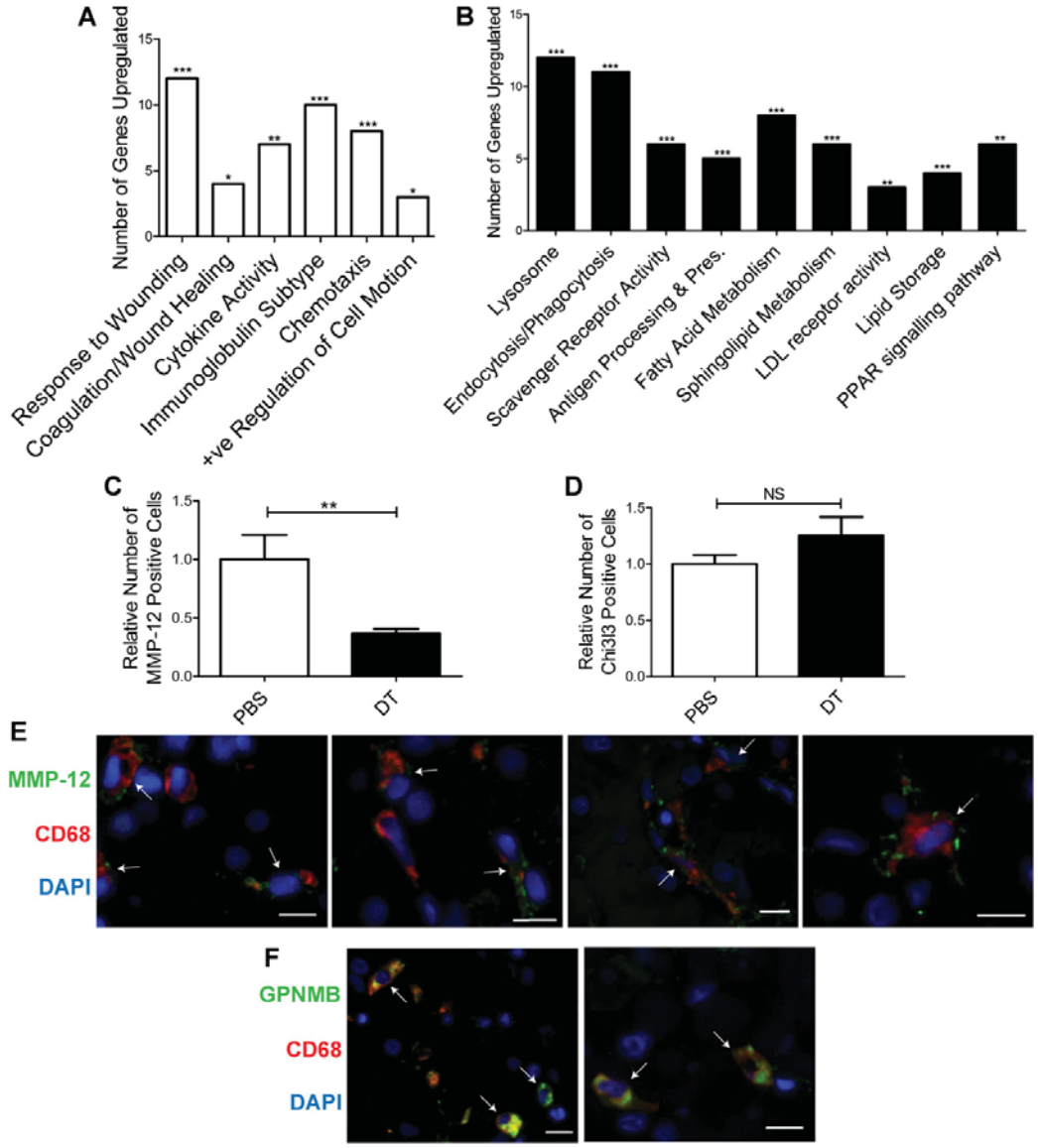

Fig. S6. Pathway analysis and specific markers of inflammatory and restorative macrophages. Microarray analysis of inflammatory Ly-6C^{hi} and restorative Ly-6C^{lo} hepatic macrophage populations isolated by FACS sorting from livers 24 and 72 h after the final CCl_4 injection, respectively. Pathway analysis of genes up-regulated in each macrophage subset using the DAVID tool expressed as the number of up-regulated genes in the stated pathway. (*A*) Pathways enriched in proinflammatory macrophage subset. (*B*) Pathways enriched in the restorative macrophage subset. All microarray data are based on $n = 3$ per group taken from two independent experiments. (*C* and *D*) CD11B-DTR mice were injured for 4 wk with CCl_4 followed by administration of DT or PBS 48, 72, and 96 h after the final CCl_4 injection with harvest at 120 h. Immunohistochemistry for MMP-12 and Chi3l3 was performed. (*C*) Average cell counts of MMP-12–positive cells per 200× field expressed relative to the average count from PBS-treated mice ($n = 5$–6). (*D*) Average cell counts of Chi3l3-positive cells per 200× field expressed relative to the average count from PBS-treated mice ($n = 5$–6). (*E*) Dual immunofluorescence for CD68 (red), MMP-12 (green), and DAPI (blue) in cirrhotic human liver. (Scale bar: 10 μm.) Arrows indicate cells with colocalization. (*F*) Dual immunofluorescence for CD68 (red), GPNMB (green), and DAPI (blue) in cirrhotic human liver (arrows indicate cells with colocalization). (Scale bar: 10 μm.) Representative images are shown. All data expressed as mean ± SEM. *$P <$ 0.05, **$P < 0.01$, ***$P < 0.001$. NS, nonsignificant.

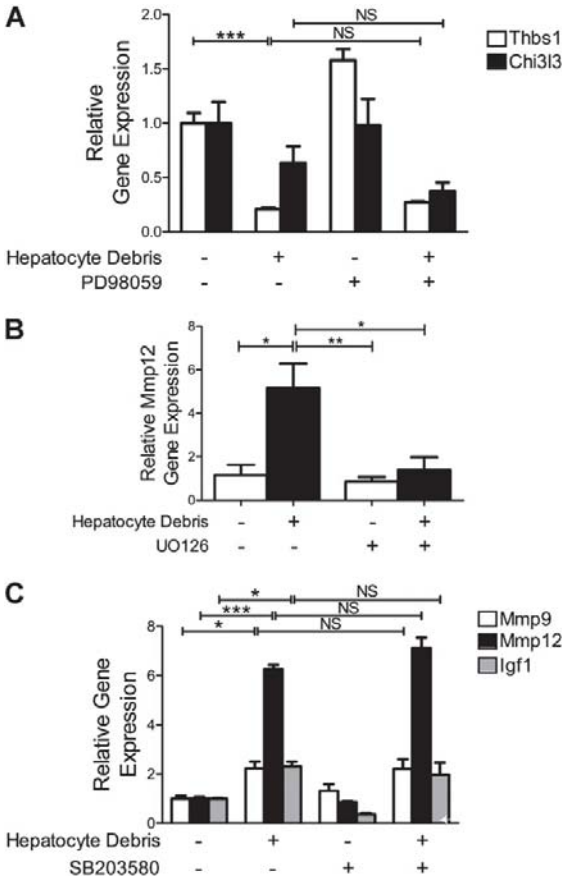

Fig. S7. Inhibition of ERK or p38 signaling cascades during macrophage phagocytosis of hepatocyte debris . (*A*) Coculture of BMDMs ± mitogen-activated protein kinase kinase 1 and 2 (MEK1/2) inhibitor (PD98059; 50 μM) ± hepatocyte debris. Changes in macrophage gene expression after coculture (data are shown relative to mean expression of macrophages alone; $n = 6$). (*B*) Coculture of BMDMs ± MEK1/2 inhibitor (UO126; 20 μM) ± hepatocyte debris. Changes in macrophage Mmp12 gene expression after coculture (data are shown relative to mean Mmp12 expression of macrophages alone; $n = 3$). (*C*) Coculture of BMDMs ± p38 MAPK inhibitor (SB203580; 10 μM) ± hepatocyte debris. Changes in macrophage gene expression after coculture (data are shown relative to mean expression of macrophages alone; $n = 6$). All data expressed as mean ± SEM. $^{*}P < 0.05$, $^{**}P < 0.01$, $^{***}P < 0.001$. NS, nonsignificant.

Table S1. Genes more highly expressed in inflammatory macrophages

Table S1

List of genes more highly expressed in inflammatory 24 h Ly-6C^{hi} macrophages compared with restorative 72 h Ly-6C^{lo} hepatic macrophages on microarray analysis of FACS-sorted populations. Fold change shown is based on average expression level in restorative macrophages compared with average expression level in inflammatory macrophages. Genes are shown with fold difference > 2 and $P < 0.05$. Based on $n = 3$ for each macrophage subset from two independent experiments.

Table S2. Genes more highly expressed in restorative macrophages

Table S2

List of genes more highly expressed in restorative 72 h Ly-6C^{lo} macrophages compared with inflammatory 24 h Ly-6C^{hi} hepatic macrophages on microarray analysis of FACS-sorted populations. Fold change shown is based on average expression level in restorative macrophages compared with average expression level in inflammatory macrophages. Genes are shown with fold difference > 2 and $P < 0.05$. Based on $n = 3$ for each macrophage subset from two independent experiments.

TABLE S1 - Genes more highly expressed in inflammatory macrophages

EntrezGene ID	Gene Name	Description	Mean Expression Inflammatory Macs	Mean expression Restorative Macs	Adjusted P Value	Fold Change (Resolution_v_Inflammatory)
13003	Vcan	versican	1915.03	69.4984	0.00432356	-27.5549
17067	Ly6c1	lymphocyte antigen 6 complex; locus C1	1640.79	74.2268	0.000264531	-22.1051
100041546	Ly6c2	lymphocyte antigen 6 complex; locus C2	2140.26	118.703	0.000362377	-18.0303
16178	Il1r2	interleukin 1 receptor; type II	784.185	48.9239	0.00668119	-16.0287
16819	Lcn2	lipocalin 2	1417.82	103.953	0.0114523	-13.639
12655	Chi3l3	chitinase 3-like 3	4828.28	422.54	9.57E-05	-11.4268
20343	Sell	selectin; lymphocyte	816.171	83.0061	0.00054082	-9.83266
108105	B3gnt5	UDP-GlcNAc:betaGal beta-1;3-N-acetylglucosaminyltransferase 5	286.62	29.4557	0.00951475	-9.73055
245126	Tarm1	T cell-interacting; activating receptor on myeloid cells 1	1292.92	152.212	0.00840112	-8.49419
20558	Slfn4	schlafen 4	248.619	33.5841	0.0329009	-7.40289
80914	Uck2	uridine-cytidine kinase 2	851.972	116.708	0.0125672	-7.30001
751864	Gm9733	predicted gene 9733	628.956	98.1827	0.0207107	-6.40597
20296	Ccl2	chemokine (C-C motif) ligand 2	2537.48	399.523	0.018883	-6.35129
68891	Cd177	CD177 antigen	287.273	50.4782	0.00102528	-5.69104
320790	Chd7	chromodomain helicase DNA binding protein 7	376.212	66.4435	0.0085149	-5.66214
231507	Plac8	placenta-specific 8	5267.19	943.952	0.00068115	-5.57993
74145	F13a1	coagulation factor XIII; A1 subunit	2686.16	504.477	0.00054082	-5.32465
66107	1100001G20Rik	RIKEN cDNA 1100001G20 gene	871.888	174.264	0.0085149	-5.00327
17394	Mmp8	matrix metallopeptidase 8	973.341	199.43	0.0198999	-4.88062
17295	Met	met proto-oncogene	378.562	78.941	0.0089083	-4.79551
16612	Klk1	kallikrein 1	134.644	28.6736	0.0431947	-4.69573
21825	Thbs1	thrombospondin 1	6153.3	1314.35	0.00692015	-4.68164
227929	Cytip	cytohesin 1 interacting protein	1360.93	305.315	0.00840112	-4.45747
213002	Ifitm6	interferon induced transmembrane protein 6	1637.76	379.873	0.00917856	-4.31133
58223	Mmp19	matrix metallopeptidase 19	429.544	100.254	0.0202155	-4.28456
320790	Chd7	chromodomain helicase DNA binding protein 7	382.891	90.4338	0.00764526	-4.23393
56089	Ramp3	receptor (calcitonin) activity modifying protein 3	305.089	73.8202	0.0275618	-4.13287
64380	Ms4a4c	membrane-spanning 4-domains; subfamily A; member 4C	2079.08	513.298	0.00068115	-4.05044
68713	Ifitm1	interferon induced transmembrane protein 1	1386.85	344.847	0.0109339	-4.02164
68713	Ifitm1	interferon induced transmembrane protein 1	1155.62	288.063	0.016853	-4.01168
18795	Plcb1	phospholipase C; beta 1	205.445	52.0212	0.0116831	-3.94925
241197	Serpinb10-ps	serine (or cysteine) peptidase inhibitor; clade B (ovalbumin); member 10; pseudogene	74.1314	19.0958	0.0188603	-3.88207
58218	Trem3	triggering receptor expressed on myeloid cells 3	434.828	115.21	0.0218954	-3.77422
353346	Gpr141	G protein-coupled receptor 141	565.986	152.875	0.0205853	-3.70229
54483	Mefv	Mediterranean fever	432.089	119.631	0.00879388	-3.61184
320790	Chd7	chromodomain helicase DNA binding protein 7	356.811	99.4798	0.033098	-3.58677
320790	Chd7	chromodomain helicase DNA binding protein 7	299.849	83.9685	0.0164859	-3.57097
14782	Gsr	glutathione reductase	1085.94	305.037	0.016389	-3.56005
21930	Tnfaip6	tumor necrosis factor alpha induced protein 6	87.0077	24.467	0.0196243	-3.55612
225372	Apbb3	amyloid beta (A4) precursor protein-binding; family B; member 3	188.384	53.1761	0.0160986	-3.54264
20555	Slfn1	schlafen 1	1306.83	369.508	0.0158063	-3.53669
246746	Cd300lf	CD300 antigen like family member F	437.661	124.32	0.0074295	-3.52043
320790	Chd7	chromodomain helicase DNA binding protein 7	504.137	143.213	0.0451961	-3.52019
18227	Nr4a2	nuclear receptor subfamily 4; group A; member 2	776.934	225.264	0.0347453	-3.449
228608	Smox	spermine oxidase	339.96	99.4361	0.0136084	-3.41888
17858	Mx2	myxovirus (influenza virus) resistance 2	89.6739	26.2426	0.027088	-3.41711

18106	Cd244	CD244 natural killer cell receptor 2B4	439.779	129.39	0.0047493	-3.39886
226695	Ifi205	interferon activated gene 205	706.387	208.977	0.0116831	-3.38022
15945	Cxcl10	chemokine (C-X-C motif) ligand 10	1231.71	368.68	0.0307801	-3.34085
16541	Napsa	napsin A aspartic peptidase	580.105	174.607	0.00161077	-3.32234
217151	Arl5c	ADP-ribosylation factor-like 5C	392.918	118.339	0.021191	-3.32028
320790	Chd7	chromodomain helicase DNA binding protein 7	226.845	68.9333	0.0162885	-3.29079
102442	Dennd4a	DENN/MADD domain containing 4A	219.207	66.8915	0.0460454	-3.27705
320790	Chd7	chromodomain helicase DNA binding protein 7	67.2003	20.595	0.0320739	-3.26295
171285	Havcr2	hepatitis A virus cellular receptor 2	662.085	206.37	0.0036594	-3.20824
12524	Cd86	CD86 antigen	750.058	233.897	0.0193961	-3.20678
56532	Ripk3	receptor-interacting serine-threonine kinase 3	220.243	69.1413	0.00432356	-3.18541
666907	Ms4a4a	membrane-spanning 4-domains; subfamily A; member 4A	1092.8	343.708	0.00194296	-3.17945
12795	Plk3	polo-like kinase 3 (Drosophila)	381.325	121.813	0.0205093	-3.1304
18793	Plaur	plasminogen activator; urokinase receptor	1429.51	459.066	0.0271519	-3.11395
58185	Rsad2	radical S-adenosyl methionine domain containing 2	373.452	120.128	0.00951475	-3.10878
68836	Mrpl52	mitochondrial ribosomal protein L52	1029.66	332.038	0.0286471	-3.10103
320790	Chd7	chromodomain helicase DNA binding protein 7	461.973	149.161	0.0450635	-3.09714
57444	Isg20	interferon-stimulated protein	332.875	107.682	0.0047493	-3.09129
100038882	Isg15	ISG15 ubiquitin-like modifier	1028.42	333.305	0.00194296	-3.08552
12484	Cd24a	CD24a antigen	972.455	316.252	0.0314445	-3.07494
320790	Chd7	chromodomain helicase DNA binding protein 7	343.988	111.887	0.00730403	-3.07443
12768	Ccr1	chemokine (C-C motif) receptor 1	410.077	134.761	0.0135864	-3.043
320790	Chd7	chromodomain helicase DNA binding protein 7	328.317	108.019	0.0121681	-3.03944
320790	Chd7	chromodomain helicase DNA binding protein 7	208.893	68.9739	0.0333219	-3.02858
76905	Lrg1	leucine-rich alpha-2-glycoprotein 1	278.739	92.0627	0.0139141	-3.02771
320790	Chd7	chromodomain helicase DNA binding protein 7	343.287	115.91	0.0214939	-2.96168
58203	Zbp1	Z-DNA binding protein 1	989.064	335.532	0.0047493	-2.94775
13723	Emb	embigin	1516.36	514.615	0.00658815	-2.9466
16421	Itgb7	integrin beta 7	201.247	68.3589	0.00746563	-2.94397
110175	Ggct	gamma-glutamyl cyclotransferase	580.245	198.914	0.0109939	-2.91706
16906	Lmnb1	lamin B1	476.906	163.908	0.0286269	-2.9096
320790	Chd7	chromodomain helicase DNA binding protein 7	100.659	35.2856	0.0329009	-2.85268
26921	Map4k4	mitogen-activated protein kinase kinase kinase kinase 4	759.492	267.56	0.0147885	-2.83858
14067	F5	coagulation factor V	117.784	41.6865	0.00274086	-2.82548
18726	Lilra6	leukocyte immunoglobulin-like receptor; subfamily A (with TM domain); member 6	222.202	78.7486	0.0279051	-2.82167
70021	Nt5dc2	5'-nucleotidase domain containing 2	293.19	104.08	0.0102601	-2.81697
67800	Dgat2	diacylglycerol O-acyltransferase 2	194.161	68.9741	0.0366246	-2.81498
57248	Ly6i	lymphocyte antigen 6 complex; locus I	167.109	59.5051	0.00799656	-2.80832
17119	Mxd1	MAX dimerization protein 1	500.841	179.568	0.0328719	-2.78914
320790	Chd7	chromodomain helicase DNA binding protein 7	313.565	112.52	0.0242675	-2.78674
66222	Serpinb1a	serine (or cysteine) peptidase inhibitor; clade B; member 1a	90.0778	32.4971	0.0188603	-2.77188
320790	Chd7	chromodomain helicase DNA binding protein 7	676.799	245.686	0.0193961	-2.75474
19652	Rbm3	RNA binding motif protein 3	4427.68	1632.09	0.0125672	-2.71289
15186	Hdc	histidine decarboxylase	234.747	87.2201	0.049212	-2.69143
14718	Got1	glutamate oxaloacetate transaminase 1; soluble	865.002	322.649	0.0438692	-2.68094
14134	Fcnb	ficolin B	94.296	35.1942	0.0196243	-2.67931
14058	F10	coagulation factor X	4403.54	1648.87	0.0497144	-2.67063
12502	Cd3g	CD3 antigen; gamma polypeptide	111.496	42.0709	0.0331413	-2.6502
18413	Osm	oncostatin M	1115.26	424.67	0.0251637	-2.62618
60361	Ms4a4b	membrane-spanning 4-domains; subfamily A; member 4B	160.113	61.047	0.00730403	-2.62277

21810	Tgfbi	transforming growth factor; beta induced	5046.01	1964.71	0.0111743	-2.56832
102442	Dennd4a	DENN/MADD domain containing 4A	270.051	105.16	0.0347453	-2.56801
14538	Gcnt2	glucosaminyl (N-acetyl) transferase 2; I-branching enzyme	239.775	93.716	0.0125965	-2.55853
16012	Igfbp6	insulin-like growth factor binding protein 6	255.802	100.104	0.0442229	-2.55537
193385	Fam65b	family with sequence similarity 65; member B	177.688	69.9693	0.00730403	-2.53952
320790	Chd7	chromodomain helicase DNA binding protein 7	115.181	45.8119	0.0181157	-2.5142
74116	Pi16	peptidase inhibitor 16	109.658	43.6238	0.0085149	-2.51371
100217453	Snord16a	small nucleolar RNA; C/D box 16A	42.1458	16.7903	0.035492	-2.51013
320790	Chd7	chromodomain helicase DNA binding protein 7	156.78	62.6598	0.0463354	-2.50208
320790	Chd7	chromodomain helicase DNA binding protein 7	324.063	130.496	0.0438692	-2.48332
270152	Amica1	adhesion molecule; interacts with CXADR antigen 1	99.2848	40.3049	0.0275032	-2.46334
16468	Jarid2	jumonji; AT rich interactive domain 2	708.106	288.65	0.0324977	-2.45317
20660	Sorl1	sortilin-related receptor; LDLR class A repeats-containing	591.323	241.067	0.0136424	-2.45295
13350	Dgat1	diacylglycerol O-acyltransferase 1	234.429	95.8359	0.0125993	-2.44615
57905	Isy1	ISY1 splicing factor homolog (S. cerevisiae)	391.562	160.319	0.0407616	-2.44239
12399	Runx3	runt related transcription factor 3	294.889	120.867	0.0310488	-2.43978
72462	Rrp1b	ribosomal RNA processing 1 homolog B (S. cerevisiae)	132.303	54.3632	0.0226492	-2.43368
19652	Rbm3	RNA binding motif protein 3	4285.07	1771.63	0.0188603	-2.41871
11758	Prdx6	peroxiredoxin 6	1104.46	458.906	0.0148611	-2.40673
68133	Gcsh	glycine cleavage system protein H (aminomethyl carrier)	594.23	247.352	0.0333178	-2.40236
71302	Arhgap26	Rho GTPase activating protein 26	503.787	210.302	0.0167442	-2.39554
11931	Atp1b1	ATPase; Na+/K+ transporting; beta 1 polypeptide	76.3797	32.265	0.0286471	-2.36726
16995	Ltb4r1	leukotriene B4 receptor 1	252.478	106.724	0.0178973	-2.3657
104183	Chi3l4	chitinase 3-like 4	36.3517	15.4214	0.0250706	-2.35723
74155	Errfi1	ERBB receptor feedback inhibitor 1	279.436	121.433	0.0479384	-2.30115
19652	Rbm3	RNA binding motif protein 3	3736.54	1638.54	0.0183914	-2.2804
56696	Gpr132	G protein-coupled receptor 132	432.136	189.592	0.0295618	-2.27929
20849	Stat4	signal transducer and activator of transcription 4	88.5878	38.95	0.00692015	-2.2744
80879	Slc16a3	solute carrier family 16 (monocarboxylic acid transporters); member 3	1021.52	449.728	0.0427538	-2.27142
12721	Coro1a	coronin; actin binding protein 1A	2592.66	1144.94	0.00636412	-2.26446
20725	Serpinb8	serine (or cysteine) peptidase inhibitor; clade B; member 8	412.736	182.614	0.0135232	-2.26016
74178	Stk40	serine/threonine kinase 40	210.366	93.3374	0.0203225	-2.25382
14571	Gpd2	glycerol phosphate dehydrogenase 2; mitochondrial	545.955	242.623	0.049212	-2.25022
246696	Slc25a28	solute carrier family 25; member 28	224.507	99.8052	0.00612777	-2.24945
13860	Eps8	epidermal growth factor receptor pathway substrate 8	264.97	118.12	0.0193961	-2.24322
13723	Emb	embigin	138.689	63.0836	0.00274086	-2.19849
93725	Ear10	eosinophil-associated; ribonuclease A family; member 10	1109.1	506.002	0.0317247	-2.19188
217431	Nol10	nucleolar protein 10	88.96	40.6486	0.0184615	-2.18851
216850	Kdm6b	KDM1 lysine (K)-specific demethylase 6B	413.472	189.633	0.0445669	-2.18038
22337	Vdr	vitamin D receptor	94.2077	43.2166	0.0415157	-2.1799
71914	Antxr2	anthrax toxin receptor 2	198.74	91.9462	0.0176003	-2.16148
57778	Fmnl1	formin-like 1	351.846	162.952	0.0463923	-2.1592
384009	Glipr2	GLI pathogenesis-related 2	186.254	86.8837	0.0449904	-2.14372
16978	Lrrfip1	leucine rich repeat (in FLII) interacting protein 1	315.157	147.759	0.0462926	-2.13291
12363	Casp4	caspase 4; apoptosis-related cysteine peptidase	562.985	264.259	0.0251637	-2.13043
320790	Chd7	chromodomain helicase DNA binding protein 7	645.733	304.57	0.0109939	-2.12015
320790	Chd7	chromodomain helicase DNA binding protein 7	167.504	79.072	0.0202237	-2.11837
320790	Chd7	chromodomain helicase DNA binding protein 7	425.33	201.377	0.0335927	-2.11211
381650	Thap6	THAP domain containing 6	200.959	95.2379	0.00701715	-2.11008
93725	Ear10	eosinophil-associated; ribonuclease A family; member 10	1002.62	477.161	0.0339356	-2.10123

433926	Lrrc8b	leucine rich repeat containing 8 family; member B	110.395	52.6503	0.0116831	-2.09676
12393	Runx2	runt related transcription factor 2	225.902	108.138	0.0259188	-2.08901
18712	Pim1	proviral integration site 1	565.723	271.115	0.0378565	-2.08665
434341	Nlrc5	NLR family; CARD domain containing 5	93.9608	45.0596	0.0378565	-2.08526
17936	Nab1	Ngfi-A binding protein 1	604.109	291.13	0.0190513	-2.07505
14011	Etv6	ets variant gene 6 (TEL oncogene)	816.709	394.243	0.0190513	-2.07159
20556	Slfn2	schlafen 2	2684.83	1297.54	0.0125672	-2.06916
12696	Cirbp	cold inducible RNA binding protein	332.928	161.868	0.0196243	-2.05679
24074	Taf7	TAF7 RNA polymerase II; TATA box binding protein (TBP)-associated factor	187.888	91.3677	0.0358713	-2.05639
13586	Ear1	eosinophil-associated; ribonuclease A family; member 1	963.762	469.815	0.0426328	-2.05136
72075	Ogfr	opioid growth factor receptor	243.715	118.913	0.0120003	-2.04953
20230	Satb1	special AT-rich sequence binding protein 1	132.836	65.4663	0.021191	-2.02908
13587	Ear2	eosinophil-associated; ribonuclease A family; member 2	1008.21	499.615	0.0450635	-2.01797
64381	Ms4a8a	membrane-spanning 4-domains; subfamily A; member 8A	504.924	250.563	0.0294476	-2.01516
66665	5730528L13Rik	RIKEN cDNA 5730528L13 gene	66.077	32.887	0.0235665	-2.00922
12983	Csf2rb	colony stimulating factor 2 receptor; beta; low-affinity (granulocyte-macrophage)	1078.06	536.593	0.0378355	-2.00908
66645	Pspc1	paraspeckle protein 1	353.613	176.541	0.0418192	-2.003
209239	Gan	giant axonal neuropathy	110.43	55.151	0.0274921	-2.00232

TABLE S2 - Genes more highly expressed in restorative macrophages

EntrezGene ID	Gene Name	Description	Mean Expression Inflammatory Mac	Mean Expression Restorative Mac	Adjusted P value	Fold Change (Resolution_v_Inflammatory)
242341	Atp6v0d2	ATPase; H+ transporting; lysosomal V0 subunit D2	30.6364	779.78	0.00151635	25.4527
278180	Vsig4	V-set and immunoglobulin domain containing 4	58.5147	1270.9	0.0102601	21.7194
80891	Fcrls	Fc receptor-like S; scavenger receptor	13.8606	253.795	0.00126278	18.3105
53945	Slc40a1	solute carrier family 40 (iron-regulated transporter); member 1	31.901	548.37	0.00692015	17.1897
11801	Cd5l	CD5 antigen-like	56.0734	810.427	0.0102601	14.453
16000	Igf1	insulin-like growth factor 1	105.725	1500.51	0.000734109	14.1926
12259	C1qa	complement component 1; q subcomponent; alpha polypeptide	335.548	4194.59	0.00161077	12.5007
79362	Bhlhe41	basic helix-loop-helix family; member e41	19.8688	230.842	0.00159236	11.6183
109225	Ms4a7	membrane-spanning 4-domains; subfamily A; member 7	125.944	1357.26	0.00138361	10.7767
20719	Serpinb6a	serine (or cysteine) peptidase inhibitor; clade B; member 6a	87.5744	796.84	0.00730403	9.099
14276	Folr2	folate receptor 2 (fetal)	23.0849	209.516	0.0109939	9.0759
19224	Ptgs1	prostaglandin-endoperoxide synthase 1	59.7842	526.126	0.0072974	8.80041
17381	Mmp12	matrix metallopeptidase 12	201.619	1720.75	0.00658815	8.53468
12262	C1qc	complement component 1; q subcomponent; C chain	432.781	3683.59	0.00692015	8.51146
69068	1810011O10Rik	RIKEN cDNA 1810011O10 gene	31.5771	257.972	0.0438692	8.1696
269823	Pon3	paraoxonase 3	46.3144	365.441	0.00018332	7.89044
12517	Cd72	CD72 antigen	72.6845	565.29	0.00280743	7.77732
15446	Hpgd	hydroxyprostaglandin dehydrogenase 15 (NAD)	225.919	1740.37	0.00951475	7.70352
17110	Lyz1	lysozyme 1	287.98	2182.55	0.0142169	7.57881
54725	Cadm1	cell adhesion molecule 1	63.6155	481.686	0.00791889	7.57184
17060	Blnk	B-cell linker	70.1185	503.998	0.00054082	7.18779
54486	Hpgds	hematopoietic prostaglandin D synthase	70.8113	498.449	0.00658815	7.03911
12520	Cd81	CD81 antigen	216.144	1508.27	0.0047493	6.9781
18830	Pltp	phospholipid transfer protein	319.474	2089.76	0.00653543	6.54127
12260	C1qb	complement component 1; q subcomponent; beta polypeptide	369.829	2393.27	0.00410287	6.4713
17533	Mrc1	mannose receptor; C type 1	196.449	1270.5	0.00272217	6.46733
21858	Timp2	tissue inhibitor of metalloproteinase 2	217.408	1325.29	0.00692015	6.09587
16956	Lpl	lipoprotein lipase	390.725	2348.92	0.00151635	6.01169
227671	Gbgt1	globoside alpha-1;3-N-acetylgalactosaminyltransferase 1	41.8452	245.643	0.0223829	5.87029
100043125	Gm11711	predicted gene 11711	203.507	1189.96	0.0135232	5.84725
67092	Gatm	glycine amidinotransferase (L-arginine:glycine amidinotransferase)	107.132	624.531	0.00917856	5.82955
100043125	Gm11711	predicted gene 11711	193.96	1113.34	0.0135232	5.74006
67448	Plxdc2	plexin domain containing 2	42.922	242.517	0.00054082	5.65018
99543	Olfml3	olfactomedin-like 3	100.626	560.813	0.0188603	5.57323
93695	Gpnmb	glycoprotein (transmembrane) nmb	741.027	4019.44	0.00917856	5.42415
11853	Rhoc	ras homolog gene family; member C	90.826	477.39	0.00658815	5.25609
15199	Hebp1	heme binding protein 1	34.3509	173.755	0.00840112	5.05824
11988	Slc7a2	solute carrier family 7 (cationic amino acid transporter; y+ system); member 2	53.3254	261.212	0.0109939	4.89845
16403	Itga6	integrin alpha 6	58.1039	284.504	0.019044	4.89646
12140	Fabp7	fatty acid binding protein 7; brain	373.115	1825.29	0.016389	4.89204
70564	5730469M10Rik	RIKEN cDNA 5730469M10 gene	37.0685	179.503	0.0125672	4.84246

20702	Serpina1c	serine (or cysteine) peptidase inhibitor; clade A; member 1C	48.1782	227.227	0.0335927	4.71639
69810	Clec4b1	C-type lectin domain family 4; member b1	74.1517	341.849	0.00194296	4.61012
12709	Ckb	creatine kinase; brain	221.673	1020.93	0.00956631	4.60556
56043	Akr1e1	aldo-keto reductase family 1; member E1	47.5009	213.96	0.00692015	4.50434
107568	Wwp1	WW domain containing E3 ubiquitin protein ligase 1	117.465	528.275	0.00274086	4.49728
214459	Fnbp1l	formin binding protein 1-like	99.81	445.563	0.0047493	4.46412
233016	Blvrb	biliverdin reductase B (flavin reductase (NADPH))	154.56	686.98	0.00432356	4.44475
16790	Anpep	alanyl (membrane) aminopeptidase	250.151	1111.12	0.00054082	4.44181
14456	Gas6	growth arrest specific 6	65.3214	285.496	0.0286471	4.37063
109711	Actn1	actinin; alpha 1	66.6662	291.048	0.00432356	4.36575
170786	Cd209a	CD209a antigen	49.8979	216.313	0.00138361	4.33511
76267	Fads1	fatty acid desaturase 1	34.7595	149.769	0.026142	4.30873
242248	Bank1	B-cell scaffold protein with ankyrin repeats 1	41.6168	178.616	0.0147885	4.29191
16068	Il18bp	interleukin 18 binding protein	151.756	641.091	0.0136424	4.22447
12389	Cav1	caveolin 1; caveolae protein	45.9581	191.682	0.00528017	4.1708
56744	Pf4	platelet factor 4	503.931	2091.31	0.0242159	4.14999
17289	Mertk	c-mer proto-oncogene tyrosine kinase	152.588	623.674	0.0196243	4.0873
20612	Siglec1	sialic acid binding Ig-like lectin 1; sialoadhesin	92.6964	375.376	0.019952	4.04952
21973	Top2a	topoisomerase (DNA) II alpha	54.9489	221.778	0.0427538	4.03609
12353	Car6	carbonic anhydrase 6	33.6846	132.427	0.0440426	3.93139
74202	Fblim1	filamin binding LIM protein 1	47.7239	187.119	0.0159202	3.92087
94275	Maged1	melanoma antigen; family D; 1	41.3257	160.375	0.00194296	3.88075
83433	Trem2	triggering receptor expressed on myeloid cells 2	158.522	613.74	0.0160986	3.87165
381524	AI427809	expressed sequence AI427809	55.3229	213.56	0.00239787	3.86026
12443	Ccnd1	cyclin D1	74.6937	285.739	0.0142169	3.82548
192187	Stab1	stabilin 1	148.454	567.425	0.0256615	3.82224
194590	Reps2	RALBP1 associated Eps domain containing protein 2	15.2363	58.1001	0.014754	3.81328
12491	Cd36	CD36 antigen	717.531	2709.95	0.00509619	3.77677
66889	Rnf128	ring finger protein 128	47.0411	176.108	0.0113641	3.7437
17167	Marco	macrophage receptor with collagenous structure	118.705	443.032	0.0314445	3.73221
54635	Pdgfc	platelet-derived growth factor; C polypeptide	25.2977	94.413	0.00912612	3.73208
77976	Nuak1	NUAK family; SNF1-like kinase; 1	15.7263	58.6542	0.0214277	3.72968
20148	Dhrs3	dehydrogenase/reductase (SDR family) member 3	625.573	2294.84	0.0089083	3.66837
232801	Lilra5	leukocyte immunoglobulin-like receptor; subfamily A (with TM domain); member 5	39.7031	144.844	0.0085149	3.64817
331004	Slc9a9	solute carrier family 9 (sodium/hydrogen exchanger); member 9	136.262	492.282	0.0295618	3.61277
17001	Ltc4s	leukotriene C4 synthase	42.5305	152.698	0.00280743	3.59031
54598	Calcrl	calcitonin receptor-like	123.65	443.656	0.00730403	3.58801
12972	Cryz	crystallin; zeta	42.8332	153.512	0.00658815	3.58396
17219	Mcm6	minichromosome maintenance deficient 6 (MIS5 homolog; S. pombe) (S. cerevisiae)	63.7234	227.827	0.0286471	3.57525
64540	Tspan4	tetraspanin 4	67.6029	240.982	0.031447	3.56466
100434	Slc44a1	solute carrier family 44; member 1	276.02	945.461	0.0109339	3.42533
71602	Myo1e	myosin IE	152.17	512.647	0.00430425	3.36892
18186	Nrp1	neuropilin 1	239.652	803.552	0.0333219	3.35299
30794	Pdlim4	PDZ and LIM domain 4	59.6651	199.982	0.00487876	3.35174
14132	Fcgrt	Fc receptor; IgG; alpha chain transporter	251.356	837.386	0.0318646	3.33148
11770	Fabp4	fatty acid binding protein 4; adipocyte	149.321	495.246	0.0134867	3.31665
14211	Smc2	structural maintenance of chromosomes 2	41.7539	138.014	0.0295618	3.30542
66140	Fam33a	family with sequence similarity 33; member A	39.0184	128.615	0.0251637	3.29626

71085	Arhgap19	Rho GTPase activating protein 19	24.7634	80.9093	0.0335841	3.26729
140742	Sesn1	sestrin 1	99.664	325.556	0.0274921	3.26653
66569	Gdpd1	glycerophosphodiester phosphodiesterase domain containing 1	63.6519	205.943	0.026087	3.23546
18858	Pmp22	peripheral myelin protein 22	206.309	666.187	0.0301271	3.22907
21391	Tbxas1	thromboxane A synthase 1; platelet	171.708	552.629	0.0167442	3.21842
104099	Itga9	integrin alpha 9	99.3854	316.211	0.0256359	3.18167
26886	Cenph	centromere protein H	25.9041	82.3258	0.0386505	3.1781
12390	Cav2	caveolin 2	49.3895	156.679	0.00054082	3.17231
52276	Cdca8	cell division cycle associated 8	32.303	102.446	0.0214089	3.17139
218215	Rnf144b	ring finger protein 144B	37.4731	118.043	0.0431947	3.15008
207818	Smagp	small cell adhesion glycoprotein	138.63	434.319	0.0135232	3.13293
232288	Frmd4b	FERM domain containing 4B	142.215	445.41	0.0284265	3.13194
17909	Myo10	myosin X	94.3184	293.779	0.0284265	3.11476
26879	B3galnt1	UDP-GalNAc:betaGlcNAc beta 1;3-galactosaminyltransferase; polypeptide 1	33.813	104.744	0.0250231	3.09774
14187	Akr1b8	aldo-keto reductase family 1; member B8	91.7979	282.539	0.0262866	3.07784
14158	Fert2	fer (fms/fps related) protein kinase; testis specific 2	26.9681	82.9279	0.00701274	3.07503
72297	B3gnt3	UDP-GlcNAc:betaGal beta-1;3-N-acetylglucosaminyltransferase 3	46.9122	144.063	0.0394702	3.07092
11745	Anxa3	annexin A3	558.705	1710.88	0.0196243	3.06222
229841	Cenpe	centromere protein E	22.2135	67.9806	0.0196243	3.06033
74096	Hvcn1	hydrogen voltage-gated channel 1	58.885	180.043	0.0196191	3.05754
27973	Vkorc1	vitamin K epoxide reductase complex; subunit 1	80.0936	244.731	0.00749678	3.05557
19075	Prim1	DNA primase; p49 subunit	31.3243	95.5091	0.0109939	3.04904
71706	Slc46a3	solute carrier family 46; member 3	63.0018	191.242	0.0142169	3.0355
12534	Cdk1	cyclin-dependent kinase 1	54.5732	161.908	0.0435182	2.9668
68487	Tmem140	transmembrane protein 140	91.3987	270.374	0.0389495	2.95818
16889	Lipa	lysosomal acid lipase A	819.311	2413.15	0.0113811	2.94533
26362	Axl	AXL receptor tyrosine kinase	232.471	681.449	0.0193961	2.93133
23890	Gpr34	G protein-coupled receptor 34	13.4101	39.1806	0.0221549	2.92171
99899	Ifi44	interferon-induced protein 44	62.7102	183.063	0.0378565	2.91919
16149	Cd74	CD74 antigen (invariant polypeptide of major histocompatibility complex; class II antigen-associated)	1196.63	3489.55	0.00658815	2.91613
11846	Arg1	arginase; liver	1509.28	4393.63	0.0378559	2.91108
98365	Slamf9	SLAM family member 9	117.818	342.765	0.00951475	2.90928
16443	Itsn1	intersectin 1 (SH3 domain protein 1A)	43.6525	126.479	0.00151635	2.8974
16644	Kng1	kininogen 1	24.1833	69.1718	0.0494453	2.86031
66881	Pcyox1	prenylcysteine oxidase 1	200.986	573.595	0.0348882	2.8539
14969	H2-Eb1	histocompatibility 2; class II antigen E beta	938.14	2677.33	0.000827136	2.85387
20133	Rrm1	ribonucleotide reductase M1	89.2254	253.049	0.0331373	2.83606
67150	Rnf141	ring finger protein 141	99.6778	282.404	0.00280743	2.83317
83768	Dpp7	dipeptidylpeptidase 7	109.625	309.335	0.0195961	2.82176
67893	Tmem86a	transmembrane protein 86A	149.381	419.977	0.0323452	2.81145
74760	Rab3il1	RAB3A interacting protein (rabin3)-like 1	95.9871	269.832	0.0335927	2.81113
12874	Cpd	carboxypeptidase D	228.229	641.482	0.0109339	2.8107
15505	Hsph1	heat shock 105kDa/110kDa protein 1	173.701	486.876	0.00194296	2.80296
218772	Rarb	retinoic acid receptor; beta	32.0245	88.8996	0.0347453	2.77599
19361	Rad51	RAD51 homolog (S. cerevisiae)	15.4953	42.9915	0.0214277	2.77449
15366	Hmmr	hyaluronan mediated motility receptor (RHAMM)	18.5794	51.0741	0.0133886	2.74896
15473	Hrsp12	heat-responsive protein 12	40.4132	110.944	0.0310906	2.74524

246278	Cd207	CD207 antigen	22.3964	60.7668	0.0135232	2.71324
67150	Rnf141	ring finger protein 141	110.344	299.02	0.00138361	2.70989
20363	Sepp1	selenoprotein P; plasma; 1	1539.79	4154.95	0.0085149	2.69838
102866	Pls3	plastin 3 (T-isoform)	38.7037	104.226	0.0375828	2.69292
233406	Prc1	protein regulator of cytokinesis 1	20.7612	55.1364	0.045774	2.65574
13733	Emr1	EGF-like module containing; mucin-like; hormone receptor-like sequence 1	609.815	1615.58	0.0121681	2.6493
319934	Sbf2	SET binding factor 2	91.3683	241.606	0.00138361	2.64431
106581	Itfg3	integrin alpha FG-GAP repeat containing 3	70.7169	184.905	0.0491071	2.61472
12606	Cebpa	CCAAT/enhancer binding protein (C/EBP); alpha	406.414	1059.92	0.0431947	2.60797
76901	Phf15	PHD finger protein 15	35.9519	92.4685	0.0188603	2.57201
67861	Akr1b10	aldo-keto reductase family 1; member B10 (aldose reductase)	35.1746	90.2846	0.0085149	2.56676
56490	Zbtb20	zinc finger and BTB domain containing 20	43.1605	110.701	0.0125672	2.56487
79221	Hdac9	histone deacetylase 9	49.3822	126.294	0.0202004	2.55749
54381	Pgcp	plasma glutamate carboxypeptidase	84.292	215.48	0.0483571	2.55635
211401	Mtss1	metastasis suppressor 1	90.9513	231.76	0.00668119	2.54818
16974	Lrp6	low density lipoprotein receptor-related protein 6	114.34	289.518	0.0137448	2.53208
15212	Hexb	hexosaminidase B	743.497	1880.33	0.00305422	2.52904
20503	Slc16a7	solute carrier family 16 (monocarboxylic acid transporters); member 7	44.1926	111.292	0.026142	2.51835
16948	Lox	lysyl oxidase	18.8056	47.1752	0.0324977	2.50858
20972	Syngr1	synaptogyrin 1	60.3725	151.164	0.0250706	2.50385
22154	Tubb5	tubulin; beta 5	638.926	1599.63	0.0193961	2.50362
11689	Alox5	arachidonate 5-lipoxygenase	47.5892	119.099	0.0198901	2.50264
69270	Gins1	GINS complex subunit 1 (Psf1 homolog)	34.986	87.426	0.0158063	2.49888
70984	4931406C07Rik	RIKEN cDNA 4931406C07 gene	139.155	346.876	0.0419083	2.49272
69633	2310014D11Rik	RIKEN cDNA 2310014D11 gene	68.0207	168.853	0.0085149	2.48237
13435	Dnmt3a	DNA methyltransferase 3A	208.836	517.71	0.0102601	2.47902
15213	Hey1	hairy/enhancer-of-split related with YRPW motif 1	58.2007	144.047	0.0208466	2.47501
74136	Sec14l1	SEC14-like 1 (S. cerevisiae)	133.303	329.369	0.0237925	2.47082
16592	Fabp5	fatty acid binding protein 5; epidermal	1040.68	2568.27	0.0368642	2.46789
108907	Nusap1	nucleolar and spindle associated protein 1	38.7199	95.2421	0.0347699	2.45977
63959	Slc29a1	solute carrier family 29 (nucleoside transporters); member 1	56.6763	139.382	0.0303626	2.45927
18968	Pola1	polymerase (DNA directed); alpha 1	35.5033	87.238	0.0386298	2.45718
217166	Nr1d1	nuclear receptor subfamily 1; group D; member 1	40.8287	99.8512	0.0274617	2.44561
51944	D2Ertd750e	DNA segment; Chr 2; ERATO Doi 750; expressed	30.285	73.7418	0.0347453	2.43493
67460	Decr1	2;4-dienoyl CoA reductase 1; mitochondrial	111.003	269.828	0.00951475	2.43081
12359	Cat	catalase	268.891	653.338	0.00701274	2.42975
100434	Slc44a1	solute carrier family 44; member 1	110.716	268.719	0.0124764	2.4271
69632	Arhgef12	Rho guanine nucleotide exchange factor (GEF) 12	55.8701	134.406	0.0112768	2.40569
237052	Tceal1	transcription elongation factor A (SII)-like 1	27.1552	65.2249	0.0167442	2.40193
29869	Ulk2	Unc-51 like kinase 2 (C. elegans)	83.9947	201.584	0.0329009	2.39997
107350	AW112010	expressed sequence AW112010	158.559	380.006	0.00658815	2.39662
100039968	Gm12942	predicted gene 12942	44.4894	106.309	0.0196243	2.38954
71710	Lrrcc1	leucine rich repeat and coiled-coil domain containing 1	39.5021	94.2262	0.0167442	2.38534
108723	Card11	caspase recruitment domain family; member 11	40.0741	95.467	0.0142899	2.38226
76192	Abhd12	abhydrolase domain containing 12	399.736	949.617	0.026777	2.37561
18611	Pea15a	phosphoprotein enriched in astrocytes 15A	353.753	839.655	0.0109939	2.37357
22619	Siae	sialic acid acetylesterase	92.21	218.85	0.0434047	2.37338

11787	Apbb2	amyloid beta (A4) precursor protein-binding; family B; member 2	32.6407	77.4654	0.0162885	2.37328
56386	B4galt6	UDP-Gal:betaGlcNAc beta 1;4-galactosyltransferase; polypeptide 6	94.057	223.047	0.0038818	2.37141
12235	Bub1	budding uninhibited by benzimidazoles 1 homolog (S. cerevisiae)	17.4967	41.2868	0.016853	2.35969
142980	Tlr3	toll-like receptor 3	44.1158	103.587	0.0274921	2.34807
104923	Adi1	acireductone dioxygenase 1	68.7502	161.39	0.0345541	2.34748
22041	Trf	transferrin	759.024	1777.96	0.0370027	2.34244
12388	Ctnnd1	catenin (cadherin associated protein); delta 1	155.31	363.447	0.0118032	2.34015
52668	Ifi27l1	interferon; alpha-inducible protein 27 like 1	294.741	688.402	0.00951475	2.33562
68024	Hist1h2bc	histone cluster 1; H2bc	514.103	1199.75	0.0310138	2.33368
15000	H2-DMb2	histocompatibility 2; class II; locus Mb2	217.173	506.459	0.00912612	2.33205
433375	Creg1	cellular repressor of E1A-stimulated genes 1	634.864	1476.64	0.0109939	2.32592
11676	Aldoc	aldolase C; fructose-bisphosphate	32.7418	76.085	0.0338695	2.32379
57262	Retnla	resistin like alpha	15.8595	36.7558	0.0404864	2.31759
16592	Fabp5	fatty acid binding protein 5; epidermal	1292.26	2994.23	0.0370027	2.31706
17220	Mcm7	minichromosome maintenance deficient 7 (S. cerevisiae)	29.4094	68.1338	0.0295618	2.31673
15211	Hexa	hexosaminidase A	628.648	1454.6	0.0196243	2.31385
192654	Pla2g15	phospholipase A2; group XV	127.876	293.973	0.0344318	2.2989
50883	Chek2	CHK2 checkpoint homolog (S. pombe)	42.5997	97.8402	0.0435209	2.29673
20410	Sorbs3	sorbin and SH3 domain containing 3	49.1421	112.523	0.0334193	2.28975
11303	Abca1	ATP-binding cassette; sub-family A (ABC1); member 1	416.345	951.06	0.0102601	2.28431
67008	1600012F09Rik	RIKEN cDNA 1600012F09 gene	82.4944	187.953	0.0329219	2.27837
67008	1600012F09Rik	RIKEN cDNA 1600012F09 gene	82.4944	187.953	0.0329219	2.27837
110391	Qdpr	quinoid dihydropteridine reductase	78.851	179.641	0.0152473	2.27824
232413	Clec12a	C-type lectin domain family 12; member a	575.027	1305.64	0.0139539	2.27057
66447	Mgst3	microsomal glutathione S-transferase 3	127.721	289.906	0.0243907	2.26984
77619	Prelid2	PRELI domain containing 2	38.5341	86.9876	0.00730403	2.25742
68170	B230118H07Rik	RIKEN cDNA B230118H07 gene	43.2357	97.6011	0.0206655	2.25742
69716	Trip13	thyroid hormone receptor interactor 13	38.1613	86.0577	0.0245269	2.25511
15064	Mr1	major histocompatibility complex; class I-related	39.4391	88.7181	0.0250706	2.2495
54447	Asah2	N-acylsphingosine amidohydrolase 2	77.7327	174.365	0.0348882	2.24314
14865	Gstm4	glutathione S-transferase; mu 4	26.9033	60.1291	0.0461864	2.23501
75578	Fggy	FGGY carbohydrate kinase domain containing	36.8034	82.0656	0.0176573	2.22984
15985	Cd79b	CD79B antigen	89.1166	198.491	0.034692	2.22732
65962	Slc9a3r2	solute carrier family 9 (sodium/hydrogen exchanger); member 3 regulator 2	73.3575	163.336	0.0440488	2.22657
72273	2210404O07Rik	RIKEN cDNA 2210404O07 gene	63.846	141.604	0.0116831	2.21791
67249	Tbc1d19	TBC1 domain family; member 19	30.3445	67.0644	0.0195133	2.2101
20307	Ccl8	chemokine (C-C motif) ligand 8	17.3925	38.2712	0.0338695	2.20044
210126	Lpp	LIM domain containing preferred translocation partner in lipoma	86.0456	189.133	0.0196243	2.19806
76781	Mettl4	methyltransferase like 4	30.8393	67.7693	0.0089083	2.1975
16950	Loxl3	lysyl oxidase-like 3	59.5605	130.808	0.047353	2.19622
14263	Fmo5	flavin containing monooxygenase 5	46.2348	101.32	0.0386298	2.19142
20970	Sdc3	syndecan 3	228.766	498.753	0.0143923	2.18019
14645	Glul	glutamate-ammonia ligase (glutamine synthetase)	1019.59	2221.86	0.0104846	2.17917
67008	1600012F09Rik	RIKEN cDNA 1600012F09 gene	122.743	266.695	0.0368313	2.17279
381236	AI747699	expressed sequence AI747699	111.538	241.956	0.035009	2.16926
66422	Dctpp1	dCTP pyrophosphatase 1	293.383	636.211	0.028399	2.16853

16568	Kif3a	kinesin family member 3A	58.8119	127.437	0.01006	2.16686
330662	Dock1	dedicator of cytokinesis 1	74.9603	162.284	0.0198998	2.16493
27999	Fam3c	family with sequence similarity 3; member C	223.011	480.486	0.0251637	2.15454
69634	Clybl	citrate lyase beta like	75.1275	161.745	0.00737692	2.15294
16881	Lig1	ligase I; DNA; ATP-dependent	64.4586	138.677	0.00321515	2.15142
52065	Mfhas1	malignant fibrous histiocytoma amplified sequence 1	56.3931	121.052	0.0374851	2.14658
52163	Camk1	calcium/calmodulin-dependent protein kinase I	155.901	334.59	0.0440714	2.14617
71566	9030425E11Rik	RIKEN cDNA 9030425E11 gene	29.5615	63.4035	0.0188603	2.1448
12483	Cd22	CD22 antigen	37.3169	79.7282	0.0167442	2.13651
234353	Psd3	pleckstrin and Sec7 domain containing 3	18.8615	40.2396	0.0279038	2.13342
12934	Dpysl2	dihydropyrimidinase-like 2	255.069	543.658	0.0493658	2.13141
67849	Cdca5	cell division cycle associated 5	20.228	42.8671	0.0324977	2.1192
96875	Prg4	proteoglycan 4 (megakaryocyte stimulating factor; articular superficial zone protein)	51.1178	108.241	0.0167442	2.11747
210544	Wdr67	WD repeat domain 67	64.2872	135.19	0.0242159	2.10291
16168	Il15	interleukin 15	41.9049	87.7843	0.0310458	2.09484
14960	H2-Aa	histocompatibility 2; class II antigen A; alpha	2415.99	5042.96	0.00658815	2.08733
52626	Cdkn2aipnl	CDKN2A interacting protein N-terminal like	111.679	232.516	0.0494815	2.082
22129	Ttc3	tetratricopeptide repeat domain 3	59.1796	123.094	0.0116831	2.08001
207425	Wdr11	WD repeat domain 11	95.6132	198.658	0.0196274	2.07773
270160	Rab39	RAB39; member RAS oncogene family	38.4281	79.7929	0.0295618	2.07642
57266	Cxcl14	chemokine (C-X-C motif) ligand 14	150.409	311.921	0.0483571	2.07382
216848	Chd3	chromodomain helicase DNA binding protein 3	1066.31	2204.61	0.0085149	2.06751
70974	Pgm2l1	phosphoglucomutase 2-like 1	80.6545	166.458	0.0100211	2.06384
16579	Kifap3	kinesin-associated protein 3	40.4567	83.4244	0.0288962	2.06206
14961	H2-Ab1	histocompatibility 2; class II antigen A; beta 1	1781.53	3668.04	0.00951475	2.05893
14645	Glul	glutamate-ammonia ligase (glutamine synthetase)	164.832	339.056	0.0250231	2.05698
209334	Gen1	Gen homolog 1; endonuclease (Drosophila)	17.8924	36.7807	0.0313836	2.05566
73724	Mcee	methylmalonyl CoA epimerase	219.034	450.171	0.00668119	2.05526
11975	Atp6v0a1	ATPase; H+ transporting; lysosomal V0 subunit A1	232.853	475.927	0.0438692	2.0439
56358	Copz2	coatomer protein complex; subunit zeta 2	69.0136	141.028	0.0467524	2.04348
12580	Cdkn2c	cyclin-dependent kinase inhibitor 2C (p18; inhibits CDK4)	29.3522	59.9302	0.0380401	2.04176
76561	Snx7	sorting nexin 7	35.5008	72.4077	0.0047493	2.03961
11593	Aga	aspartylglucosaminidase	146.545	298.869	0.0186581	2.03944
18974	Pole2	polymerase (DNA directed); epsilon 2 (p59 subunit)	23.7147	48.3592	0.0294025	2.03921
14420	Galc	galactosylceramidase	159.914	325.569	0.0259188	2.0359
15116	Has1	hyaluronan synthase1	20.3935	41.4732	0.0335841	2.03365
75415	Arhgap12	Rho GTPase activating protein 12	127.235	258.477	0.0261433	2.03149
77864	Ypel2	yippee-like 2 (Drosophila)	35.1769	71.4073	0.0312965	2.02995
56278	Gkap1	G kinase anchoring protein 1	27.618	55.9385	0.0102601	2.02544
226971	Plekhb2	pleckstrin homology domain containing; family B (evectins) member 2	112.937	227.18	0.0409382	2.01156
229445	Ctso	cathepsin O	147.685	296.86	0.016369	2.01008
320506	Lmbrd2	LMBR1 domain containing 2	139.601	280.519	0.0167442	2.00943
56217	Mpp5	membrane protein; palmitoylated 5 (MAGUK p55 subfamily member 5)	115.915	232.773	0.0085149	2.00813
17085	Ly9	lymphocyte antigen 9	538.459	1081.25	0.00764526	2.00805